SINGLE-WALLED CARBON NANOTUBES AS NOVEL NIR FLUORESCENT PROBES FOR BIOMEDICAL OPTICAL IMAGING

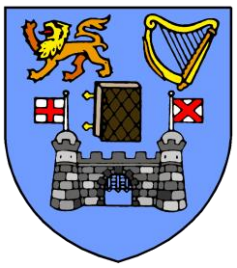

A thesis submitted to University of Dublin, Trinity College
for the degree of Doctor of Philosophy.

by

Dania Movia

School of Chemistry
December 2011
University of Dublin
Trinity College

To Mum and Dad

“E' questo, che le hanno
insegnato, mamma e
papa', nel suo passato.
Non puo' scordarlo.”

DECLARATION

This thesis is submitted by the undersigned to the University of Dublin, Trinity College for the examination of Doctorate of Philosophy.

I declare that this thesis has not been submitted as an exercise for a degree at this or any other university and it is entirely my own work. Due acknowledgements and references are given to the work of others where appropriate.

I agree to deposit this thesis in the University's open access institutional repository or allow the library to do so on my behalf, subject to Irish Copyright Legislation and Trinity College Library conditions of use and acknowledgement.

_____

Dania Movia

ACKNOWLEDGMENTS

I wish to thank my supervisor Dr. Silvia Giordani for her precious advices and supervision and all Giordani's research group (former and present members) for help and support during these years. In particular, I would like to thank Dr. Elisa Del Canto for the AFM images and Raman measurements shown in this thesis, Dr. Kevin Flavin for his invaluable help during these years, Dr. Manuel Natali for the synthesis of spiropyrans and finally Dr. Laura Soldi for the fruitful discussions.

I am particularly thankful to Prof. Yuri Volkov for giving me the opportunity to include toxicological studies in my research project, to Dr. Adriele Prina-Mello for the scientific support during these years and to Dr. Despina Bazou for the experiments carried out with the USWT. I also would like to acknowledge Dr. Manuel Ruther for all the instrumental trainings and Prof. Yuri Rakovich for the 2D FLIM measurements.

A particular thank goes to my parents, who have always supported me and thought me to do my best in anything I was involved in, and of course to Moreno, who really believes that I am the smarter scientist in the world. Thanks for being always on my side. Thanks to all the friends I met during these years: Elisa, Manuel, Kevin, Laura, Ana and Stefano for the wonderful time spent together; Adriele, Guido, Simone, Giovanni, Elena and Andrea for the fantastic "salamate" and being "my little Italy"; Despina for the real Xmas tree and the most enjoyable time in our D4; Daniela, Rohit, Niall, David McGovern, David Meehan, Elisabetta, Ruggero, Mauro, Jason, Michael and Darragh for making my days in CRANN happy and cheerful. A special thank goes to all my friends back home who cheered me up anytime I needed it: Francesca, Luca, Elisa, Alice, Sharon, Matteo, Veronica, Francesco, Enrico, Alice Melpignano e Andrea. Thanks to all you guys, you are simply fantastic!

Finally, I am really grateful to Science Foundation Ireland and IRCSET for the financial support.

SUMMARY

Synthetic carbon allotropes, such as SWNTs, represent a growing family of fascinating nanomaterials with outstanding properties that are relevant in many potential applications, ranging from synthetic materials to drug delivery systems and imaging probes. These novel technologies are very exciting but they require considerable development and precaution before they can be translated into realistic, clinical-relevant tools. In fact, all the studies employing SWNTs in life science are at a very early, proof-of-concept stage, as systematic preclinical therapeutic data are completely lacking.

The main aim of this work involves the development of novel single-walled carbon nanotubes (SWNTs)-based near-infrared (NIR) fluorescent probes with reduced toxicological impact on human health. These novel NIR probes are expected to find application in *in vitro* and *in vivo* optical imaging as biomedical diagnostic tools.

Chapter I illustrates (1) the application of optical imaging in biomedical diagnostics, with particular emphasis on the NIR fluorescence imaging, (2) the current impact of nanotechnology on biomedicine and biomedical imaging, (3) SWNTs chemical reactivity and the current state-of-the-art in the non-covalent/covalent functionalisation of SWNTs for biomedical applications, (4) a description of the main biomedical applications of SWNTs scaffolds, and finally (5) the biodistribution of SWNTs and their translocation across biological membranes. This chapter also includes a section describing the aims of this research project.

In Chapter II, the preparation and the full optical characterization of NIR probes based on covalently functionalised SWNTs are reported. The two-step oxidation procedure employed as functionalisation method results in SWNTs (1) free from toxic metal impurities, (2) characterised by small aspect ratio, (3) decorated with functional oxygenated groups that enable potential further functionalisation, and (4) able to emit efficiently in the NIR. These results establish for the first time the potential use of covalently modified SWNTs as NIR fluorescent agents for *in vitro*/*in vivo* optical imaging.

Since SWNTs' unique properties (such as size, shape, and composition) have raised safety concerns on their potential human toxicity and on the techniques that need to be used to assess such toxicity, Chapter III assesses the cytotoxicity of the SWNTs-based

NIR probes previously developed using for the first time three-dimensional (3D) cellular, tissue-mimetic models. The data, showing that no cytotoxicity was detectable in the 3D cellular model, (1) clearly underlines the importance of incorporating 3D tissue-mimetic cell models in the assessment of SWNTs toxicity, (2) it strongly leads to the redefinition of the conventional nanotoxicology protocols, and finally (3) it establishes the potential employment of the SWNTs probes developed in these research project in biological systems.

Finally, Chapter IV provides a detailed description of the general methods and experimental procedures that have been used in this research project, while Chapter V reports conclusions and future outlook for the research project.

Chapter VI reports the statistical analysis of the *in vitro* cytotoxicity studies described in Chapter III.

CONTENTS

LIST OF ABBREVIATIONS

$\times g$	Units of gravity (times gravity)
1D	One-dimensional
2D	Two-dimensional
3D	Three-dimensional
Ab	Antibody
AFM	Atomic force microscopy
CNTs	Carbon nanotubes
CDs	Cyclodextrins
CO	Carbon monoxide
DNA	Deoxyribonucleic acid
DOS	Density of states
FDA	Food and Drug Administration
FLIM	Fluorescence lifetime imaging microscopy
*f*NIRS	Functional NIR spectroscopy
FT-IR	Fourier transform infrared spectroscopy
h	Hours
HCSA	High Content Screening and Analysis
HiPCO	High pressure CO
HR-TEM	High-resolution transmission electron microscopy
IC_{50}	Half-maximum inhibitory concentration
ICG	Indocyanine Green
IL-6	Interleukin-6
min	Minutes
N_2	Nitrogen
NIR	Near-infrared
NIR II	Second NIR window (1000-1400 nm)
NIRFs	NIR fluorophores
NMs	Nanomaterials
NTFET	Carbon nanotubes field effect transistor
o-SWNTs	Oxidised SWNTs

PEG	Polylysine-polyethylene glycol
PL	Photoluminescence
p-SWNTs	Purified SWNTs
RES	Reticuloendothelial system
RGD	Arginine-Glycine-Aspartic acid sequence
RPM	Revolutions per minute
RNA	Ribonucleic acid
r-SWNTs	Raw SWNTs
s	Seconds
SDBS	Sodium dodecylbenzene sulphonate
siRNA	Small interfering RNA
SWNTs	Single-walled carbon nanotubes
TGA	Thermal gravimetric analysis
TNF-α	Tumour necrosis factor-alpha
THP-1	Human monocytic leukemia cell line
USWT	Ultrasound standing wave trap
UV	Ultraviolet
Vis	Visible

LIST OF TABLES

LIST OF FIGURES

CHAPTER II

Figure 2.5. (a) Raman spectra of r- (black line), p- (grey line) and o-SWNTs (light grey line) (λ_{exc} = 633 nm) normalized on the G-band. (b) Radial breathing modes (RBMs) of r- (black line), p- (grey line), and o-SWNTs (light grey line). (c) ATR/Fourier transform IR (ATR/FT-IR) spectra of r- (black line), p- (grey line) and o-SWNTs (light grey line). Raman and ATR/FT-IR measurements were carried out by Elisa Del Canto.

Figure 2.6. (a-c) NIR-PL spectra of r- (black line), p- (grey line) and o-SWNTs (light grey line) dispersed in SDBS aqueous solution at λ_{exc} of (a) 638 nm, (b) 683 nm and (c) 785 nm. $[SWNTs]_i = 8\times10^{-2}$ mg/ml; SWNTs:SDBS weight ratio = 1:25. (d) Histogram of the average NIR-PL efficiency of r-, p- and o-SWNTs dispersed in SDBS aqueous solution. $[SWNTs]_i = 8\times10^{-2}$ mg/ml; SWNTs:SDBS weight ratio = 1:25. The data are expressed as average ($n_{\lambda exc}$ = 3; $n_{measurements}$ = 3) ± standard deviation and normalized to the NIR-PL efficiency of r-SWNTs.

Figure 2.7. (a-f) Comparison of the NIR-PL spectra of (a, d) r-, (b, e) p- and (c, f) o-SWNTs collected with the NS1 NanoSpectralyzer® (black line) and the Fluorolog-3 (grey line) at (a-c) 683 nm and (d-f) 785 nm excitation wavelength. The emission intensities of the spectra are not compared. $[SWNTs]_i = 4.2\times10^{-2}$ mg/ml; SWNTs:SDBS weight ratio of 1:25.

Figure 2.8. Vis emission spectra of r- (black line), p- (grey line) and o-SWNTs (light grey line) dispersed in SDBS aqueous solution at λ_{exc} of (a) 638 nm, (b) 683 nm, (c) 785 nm and (d) 420 nm. $[SWNTs]_i = 8\times10^{-2}$ mg/ml; SWNTs:SDBS weight ratio = 1:25.

Figure 2.9. UV-Vis/NIR absorption spectra of r- (black line), p- (grey line) and o-SWNTs (light grey line) in SDBS aqueous solution. $[SWNTs]_i = 2.1\times10^{-2}$ mg/ml; SWNTs:SDBS weight ratio = 1:25.

Figure 2.10. (a, c) FLIM images (80 µm × 80 µm) of large aggregates of (a) p- and (c) o-SWNTs dispersed in DMF. Optical window: 670 nm - 1000 nm; λ_{exc} = 630 nm. (b, d) Histograms of the lifetime distribution of the large aggregates of (b) p- and (d) o-SWNTs imaged.

CHAPTER III

activation of THP-1 cells in 3D aggregates after 24 h. (e, f) Arrows point out the punctate F-actin staining. Scale bars: 20 μm (50× magnification).

Figure 3.6. Representative (a-c) confocal and (d, e) epifluorescent microscopy images of (a, d) non-treated and (b, c, e) PMA-treated 3D cell aggregates stained with Phalloidin-Alexa 488 conjugate after 24 h incubation. (a, b) Different F-actin organization is evident between the two aggregates. (c) Z-stack image of the PMA-treated 3D cell aggregate shown in (b) illustrating the cells in direct contact with the substrate. Redistribution of F-actin into intensely staining punctate foci is evident (arrows). (e) Large cell aggregates are seen in PMA-treated samples. (a-c) Scale bar: 20 μm (63× magnification); (d, e) scale bars: 40 μm (10× magnification).

Figure 3.7. (a, b) Percentage (%) of cell death quantified by Trypan Blue exclusion assay and (c, d) % of live and dead cells detected by flow cytometry in 3D cell aggregates in culture exposed to (a, c) p- and (b, d) o-SWNTs at 1.2×10^{-4} μg/cell for 24 h.

Figure 3.8. Representative flow cytometry graphs (single cells gated) of 3D aggregates in culture: (a) negative control; (b) Paclitaxel 1.7 μM; (c, d, e) exposed to p-SWNTs; (f, g, h) exposed to o-SWNTs. (c, f) DMSO-, (d, g) BSA-, and (f, h) Pluronic F68-stabilised dispersions were tested.

Figure 3.9. (a, b) Representative confocal images of (a) non-treated (negative control) and (b) SWNTs-treated 3D cell aggregates in culture after 24 h. (c, d) Gallery of stack images of (c) non-treated and (d) SWNTs-treated 3D cell aggregates. Micrographs in (c) and (d) are of the same 3D cell aggregate shown in (a) and (b) respectively. Live cells are seen in green, red indicates dead cells. SWNTs sample: p-SWNTs BSA-stabilised dispersion. Scale bars: 20 μm (20× magnification).

Figure 3.10. Release of (a-c, g-i) TNF-α and (d-f, j-l) IL-6 from 2D cell cultures after 24 and 72 h exposure to (a-f) p- and (g-l) o-SWNTs at various concentrations: (a, d, g, j) 12×10^{-4}, (b, e, h, k) 6×10^{-4} and (c, f, i, l) 1.2×10^{-4} μg/cell.

CHAPTER V

CHAPTER VI

DMSO-stabilised (grey), BSA-stabilised (red), and Pluronic F68-stabilised (light blue) dispersions were tested for each concentration.

LIST OF SCHEMES

CHAPTER I.
INTRODUCTION AND OVERVIEW

CONTENTS

1. OPTICAL IMAGING IN BIOMEDICAL DIAGNOSTICS

Imaging with light combines a variety of different diagnostic modalities that, if supported by the design of efficient imaging agents, can allow identifying and characterizing fundamental processes at the organ, tissue, cellular and molecular level. As *in vivo* optical imaging techniques are currently characterised by limited depth penetration through human tissues, their clinical application is at the moment limited to surface (*i.e.*, skin) or ocular imaging.[1] In particular, only Indocyanine Green (ICG) angiography is applied nowadays on a regular basis for the ophthalmologic diagnosis of ocular diseases.[2]

Although optical imaging is not currently employed in many clinical diagnostics techniques, there is increasing interest in its application to all avenues of biomedical diagnostics.[1] Optical imaging requires in fact a rather simple, inexpensive instrumentation, is easy to handle and, as opposed to radioactive radiation, this technique permits imaging regimes that are more flexible with respect to the needs of medical diagnosis (*i.e.*, several analysis can be carried out in close sequence).[2] Additionally, in the field of drug delivery, optical imaging can provide a valuable tool for tracking the administered drug through the body to ascertain whether successful delivery to the desired organ or tissue structure has been achieved.[2]

Optical imaging can be divided into two modalities.[2] The first modality requires administration of a fluorescent probe and external light to generate fluorescent emission.[2,3] In the second modality (called bioluminescence), visible (Vis) light is generated by an *in vivo* enzyme-mediated process when a substrate is degradated.[2]

Depending on the light wavelength used, different penetration depths can be achieved by optical imaging.[2,3] Photons of the ultraviolet (UV)-Vis spectral range (up to 650 nm) are strongly absorbed within one millimeter of tissue thickness by deoxy- and oxy-hemoglobin (*i.e.*, blood). Therefore, UV-Vis fluorescent probes and bioluminescence can be used only for imaging tissue surfaces or *in vitro*. In contrast, near-infrared (NIR) radiation allows the higher tissue penetration, due to minimal absorbency of the tissues. The NIR window is primarily limited by the light absorption of blood components at short wavelengths (670-700 nm) and water at long wavelengths (1400-1600 nm). The establishment and validation of suitable NIR probes is therefore a prerequisite for the reliable exploitation of optical imaging as an *in vivo* diagnostic tool playing an essential role in both the clinic practice and basic research.

1.1. Near-Infrared (NIR) Fluorescence Imaging

In vivo NIR fluorescence imaging holds enormous potential for its quantitative sensitivity, inherent biological safety and relative ease of use. For these reasons, it has been increasingly employed in research,[3-6] and there is a substantial interest in the translation of this novel optical technique into a widespread clinic diagnostic tool. For example, functional NIR spectroscopy (*f*NIRS) is an emerging functional neuroimaging technology that has been FDA approved for clinical applications since it offers a relatively non-invasive, safe and portable methodology for monitoring brain activity and for studying brain disorders.[7]

Effective deep-tissue fluorescence imaging requires the application of exogenously administrated NIR-emissive contrast agents. NIR fluorophores (NIRFs) can be categorized according to their mechanism of contrast generation (non-specific, targeted or activatable)[3] or according to their chemical composition (organic or inorganic).[5]

Mechanism of contrast generation Non-specific probes are fluorescent dyes which achieve contrast by distributing differentially in healthy and diseased tissues, while targeted fluorescent probes are constituted by a targeting biomolecule (such as antibodies, antibody fragments, proteins, peptides, nucleic acids, polysaccharides or small molecules) conjugated with a fluorescent dye. Finally, in activatable probes the fluorescent dye molecules are coupled in close proximity to each other, thereby quenching their fluorescence (Figure 1.1a). The fluorescence is recovered by enzyme-mediated cleavage, which liberates the dye molecules (Figure 1.1a). Since no background fluorescence is detectable in the quenched state, activatable probes allow to achieve the highest sensitivity.

Chemical composition The list of suitable organic NIRFs includes mainly cyanine dyes, lanthanide chelates and tetrapyrrole-based dyes.[3] In particular, cyanine dyes, such as ICG (Figure 1.1b), can be used as fluorescent probes for imaging vascular disorders.[3,8] Owing to their short circulation half-lives, low photo-bleaching thresholds and lack of strong NIR emission in the second near-infrared window (called NIR II)[4] (1000 – 1400 nm), organic fluorophores cannot be used at tissue depths greater than 1-2 cm. In contrast, inorganic fluorophores (namely, semiconductor quantum dots (QDs)) possess vastly superior optical characteristics when compared to traditional organic fluorophores (*i.e.*, they strongly emit in the NIR II region), but at the cost of decreased safety, as their composite materials are toxic in their elemental form. As a result, there

is currently no available NIR-fluorescent agent that possesses the ideal properties for human application as deep-tissue imaging probe. Lots of efforts have been placed in the development of the first generation of organic NIRFs capable of deep-tissue optical imaging.[5] Among them, nanomaterials such as polymersomes (50 nm to 50 μm diameter polymer vesicles incorporating organic NIRFs)[5,9] and SWNTs[4,10-14] have been extensively studied to engineer new NIR-fluorescent probes.

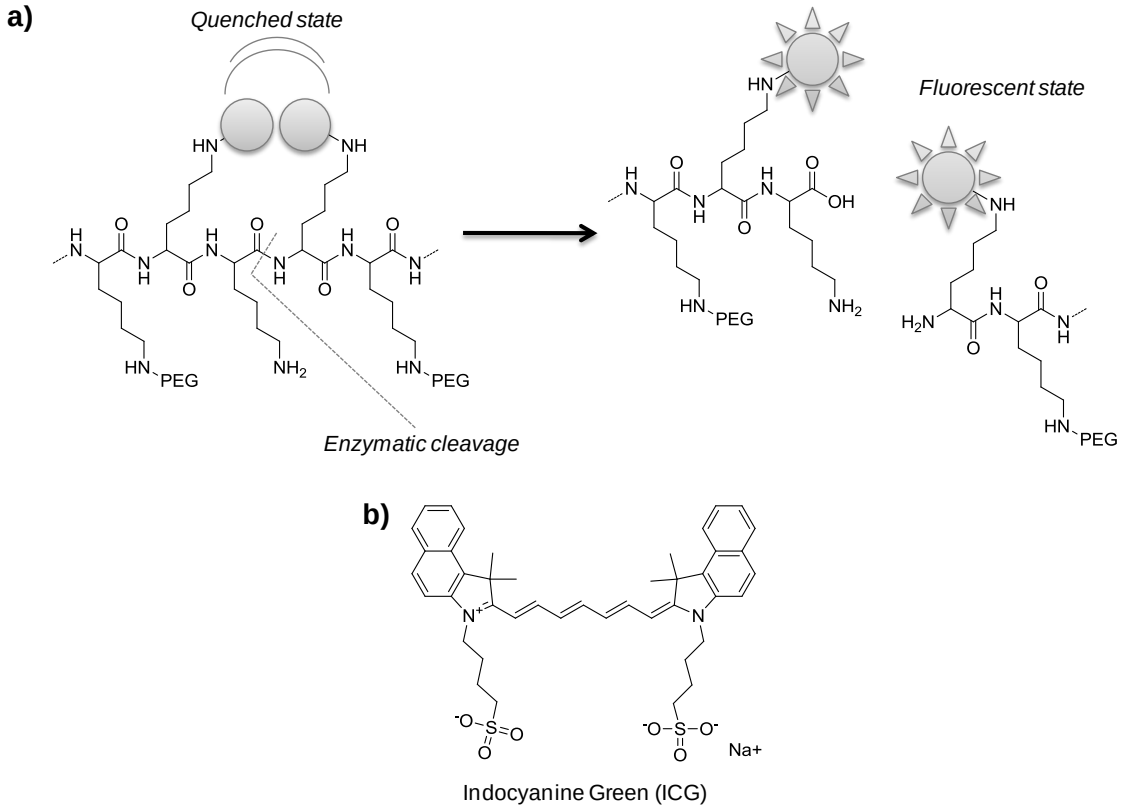

Figure 1.1. (a) Example of the mechanism of activation of an activatable probe. The fluorescent molecules are grafted in close proximity onto a polylysine-polyethylene glycol (PEG) chain (fluorescence quenching). After enzymatic cleavage of the polymeric backbone, fluorescence is recovered. (b) Example of NIR fluorescent cyanine dye. Chemical structure of Indocyanine Green (ICG), a clinically approved NIR fluorescent probe used in ophthalmology.

2. NANOTECHNOLOGY AND BIOMEDICINE

Nanotechnology has the potential to affect almost every area of society. Biomedicine is one particular area in which revolutionary new nanotechnologies hold promise of great benefits for humanity in the future.[15] Over the coming years, biomedical

nanodevices will have a variety of uses and they will potentially save a great number of lives. Nanotechnologies could aid for example in the formation of molecular structures for the regeneration or replacement of body tissues damaged/lost by infection, accident and disease, or in the development of targeted drug therapies that have fewer side effects and that are more effective ('smart drugs'). These predictions for the future have great significance not only in encouraging nanotechnology research but also in determining a means of oversight. The National Cancer Institute, for example, has created the Alliance for Nanotechnology in Cancer with the hope that investments in this field could lead to breakthroughs in terms of diagnostics and treatment of cancer.

As pointed out by "The Project on Emerging Nanotechnologies", the inventory of nanotechnology products that are publicly available has grown by nearly 621% (from 212 to 1317 products) since 2006, with the largest increase allocated in health and fitness products (from roughly 150 to 738 products).[16] Many of these commercialised products are not available directly to the consumer but they are employed by researchers and physicians to treat specific diseases in hospitals (including appetite disorders and cancer) (Table 1.1).

Table 1.1. Medical applications of current nanotechnology products. The products listed are commercially available but not always accessible directly to the consumer.

Nanomaterial	**Application**			
	Drug delivery system†		**Medical tools†**	
	Commercial name	**Target**	**Commercial name**	**Target**
Nanocrystals	Megace® ES	Appetite control	Acticoat®	Antimicrobial barrier protection
	Rapamune®	Immunosuppressant		
	Emend®	Cancer	TriLite™ Technology	Imaging
	TriCor®	Cholesterol		
Nanoparticles	Doxil®	Cancer	Orthovita	Bone replacement
	Abraxane®	Cancer	Vitoss	Bone replacement
	Neowater™	Chemical substitute	Zirconium Oxide	Dental devices
	Estrasorb™	Hormone therapy	EnSeal System	Surgery
Quantum dots	---	---	Qdot Nanocrystals	Imaging

† Source: www.nanotechproject.org/inventories/medicine/apps

2.1. NANOMATERIALS AND BIOMEDICAL IMAGING

Dedicated nanomaterials (NMs) could be used in the future as optical imaging probes to monitor the progress of a therapy or disease.[17-19] The use of NMs as probes has two major advantages:[18] (1) they can merge multiple modalities on one probe, enabling higher imaging sensitivity and (2) NMs may be engineered in order to combine imaging and drug-delivery, thus leading to synergistic medical effectiveness and enabling the development of a new generation of theranostics. In particular, the potential combination of imaging and treatment is an exclusive feature of NMs and has the potential to change the current medical paradigm of "see and treat"[17] to "detect and prevent"[17]. Therefore, there is an emerging rush to commercialize NMs for diagnostic imaging purposes. So far, Trylite™ (nanoclusters of 8-12 individual nanocrystals)[20] and Qdot Nanocrystals (clusters of a semiconductor material)[21] are the only two NMs that have achieved FDA approval for use in biomedical optical imaging.

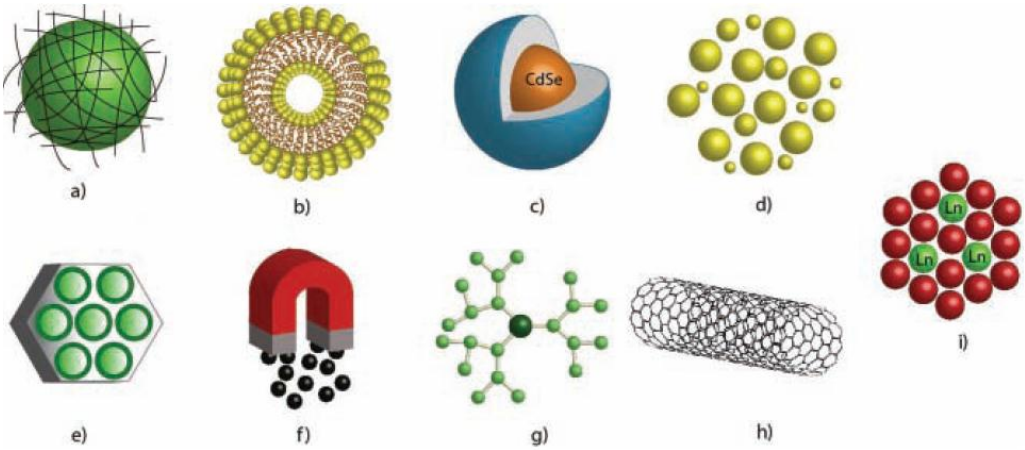

Figure 1.2. Schematic representation of NMs that might be used as imaging probes: (a) polymeric nanoparticles; (b) liposomes; (c) QDs with a CdSe core; (d) gold nanoparticles; (e) zeolite L; (f) magnetic nanoparticles; (g) dendrimers; (h) carbon nanotubes (CNTs); (i) upconverting nanophosphors (adapted from an image by Barreto *et al.*[22]).

A wide range of NMs might be used as imaging probes.[19,22] As for NIR fluorophores, NMs-based probes can be categorised into organic (*i.e.*, liposomes, dendrimers and carbon nanotubes) and inorganic materials (*i.e.*, QDs, metallic nanostructures and metal oxides) (Figure 1.2). After functionalisation with various chemical moieties, NMs can be employed in a variety of molecular imaging techniques, such as computed

tomography (CT), magnetic resonance imaging (MRI), single-photon emission tomography (SPECT), positron emission tomography (PET), ultrasound imaging and Vis/NIR optical imaging methods.[23]

Most NMs are easily cleared by the reticuloendothelial system (RES).[24] The RES consists of phagocytic cells (*i.e.*, monocytes and macrophages) located in the spleen, lymph nodes and in the liver (Kupffer cells) with the main function of removing senescent cells and external agents from the bloodstream. In particular, the smaller the NM is, the longer its retention time in the bloodstream is. [25,26] The mechanism used by the body to recognize and clear NMs by RES involves three steps: (1) opsonization, (2) phagocytosis and (3) clearance.[27] In the opsonization, the NM is enveloped by proteins called opsonins, which allow recognition of the foreign agent by phagocytic cells.[27,28] Recognition and attachment of phagocytes to the surface-bound opsonins results in ingestion of the particle by endocytocis and degradation by enzymatic/oxidative processes. If not biodegradable, depending on its size and molecular weight, the NM will be removed by the renal system or stored in one of the RES organs.[27] Opsonization is influenced by the hydrophilicity of NMs. This process is faster when the material is hydrophobic, due to the enhanced affinity of blood serum proteins for their surface.[27,29,30]

In order to reduce their opsonization (and to avoid their premature clearance by the RES), shielding groups have been attached onto NMs' surface. PEGylation is one of the main methods employed.[24,27,31] PEGylation refers to the process of grafting, adsorbing or covalently binding polyethylene glycol (PEG) or its derivatives onto the NMs surface. Covering the surface of NMs with PEG sterically prevents the efficient binding of opsonins onto their surface, thereby hindering phagocytosis.[27] Recently, Choi *et al.* demonstrated that the biodistribution of NIR fluorescent PEGylated QDs is a function of the length of the PEG employed: only QDs coated with long PEG chains (n = 22) remained in fact in the bloodstream for 4 h post-injection.[32] Additionally, PEGylation increases NMs' hydrophilicity.

3. SINGLE-WALLED CARBON NANOTUBES AND BIOMEDICINE

3.1. DEFINING SWNTS

Carbon nanotubes (CNTs) represent a relatively newly discovered allotrope of carbon that has a wide range of potential applications within nanotechnology.[33] In particular, CNTs could hold great significance for many biomedical applications in the near future.[34,35]

Individual nanotubes are hollow cylindrical tubes formed by a single wall (SWNTs) or multiple concentric walls (MWNTs) of graphite sheets, have diameters as small as 0.7 nm and lengths exceeding several micrometers.

SWNTs can be imagined as a graphene sheet rolled at a certain angle (called chiral angle) with respect to a plane perpendicular to the tube's long axis. The chiral angle can range from 0 to 30 degrees and is generally identified by a pair of indexes (*n*, *m*). These indexes define the nanotubes chirality.[36] Depending on their chirality, SWNTs can be divided into metallic or semiconducting, resulting in different electronic and optical properties.[37] For example, only semiconducting SWNTs are characterized by efficient NIR emission properties (see Chapter II, Section 1.1.2).[38] Indeed, this variety opens the use of SWNTs in many different applications.[34]

At present, SWNTs can be produced by different techniques, such as electric arc discharge, catalytic decomposition, chemical vapour deposition (CVD) and high pressure CO disproportionation process.[39] The latter (commonly referred to as HiPCO method) produces large amounts of SWNTs by combusting CO gas and iron-containing catalysts, $Fe(CO)_5$, under controlled conditions. Due to the synthetic mechanism, a high concentration of undesiderable defects, carbonaceous and metal catalyst impurities is generally present in the SWNTs material, making the toxicity of SWNTs a complex question (see Chapter 3, Section 1.2) and potentially limiting their use in biomedicine. Despite this, there is an increasing number of published studies which support the potential development of SWNTs-based biomaterials for tissue regeneration (e.g., neuronal substrates[40] and orthopaedic materials[41-43]), cancer treatment,[44] drug/vaccine delivery[45,46] and optical imaging (namely Raman spectroscopy,[47] photoacoustic tomography (PAT),[48,49] and NIR photoluminescence[10-12,50-52]). Some of these topics have been discussed in recently published reviews.[35,53-58] Most of these applications will involve the implantation and/or administration of such materials into patients; as for any

therapeutic or diagnostic agent used, the use of SWNTs must be evaluated in relation to their risk-benefit ratio.[59]

As-produced SWNTs are characterized by a lack of solubility in aqueous solutions, imposing again great limitations to their extensive use in life sciences. This effect is correlated to the SWNTs capability in forming strong van der Waals interactions between one another and the formation of aggregates and bundles that precipitate.[60] With the development of covalent and non-covalent strategies for functionalising SWNTs with various chemical moieties,[39] improved processing of SWNTs has been achieved in aqueous environment, and the application of SWNTs in the biomedical area has become possible.[61]

The following section will report the recent advances in the chemical modification of SWNTs. In particular, it will discuss a series of examples to illustrate the main methodologies in which SWNTs can be modified for their exploitation in biomedicine. A successive section will describe the various applications of SWNTs in life sciences investigated until now.

3.2. Chemical Modification of SWNTs for Biomedical Applications

Rational functionalisation can endow SWNTs with desired properties for biomedical applications and with controlled solubility and toxicity.[62] Singh *et al.* showed in fact that the toxicity profile of carbon nanotubes can be altered by functionalisation and by changes in their solubility.[63]

There are two main functionalisation protocols that have produced remarkable progress in the bio-nanotechnology field by improving the SWNTs' aqueous dispersability and, at the same time, by offering a flexible platform for derivatization[61]: (1) non-covalent supramolecular modification (based on π-π stacking, van der Waals and/or hydrophobic interactions) (Scheme 1.1a) and (2) covalent functionalisation (Scheme 1.1b).[60,64,65] Both types of chemical strategies are described in detail in the following paragraphs.

Scheme 1.1. Schematic representation of (a) non-covalent and (b) covalent functionalisation of SWNTs.

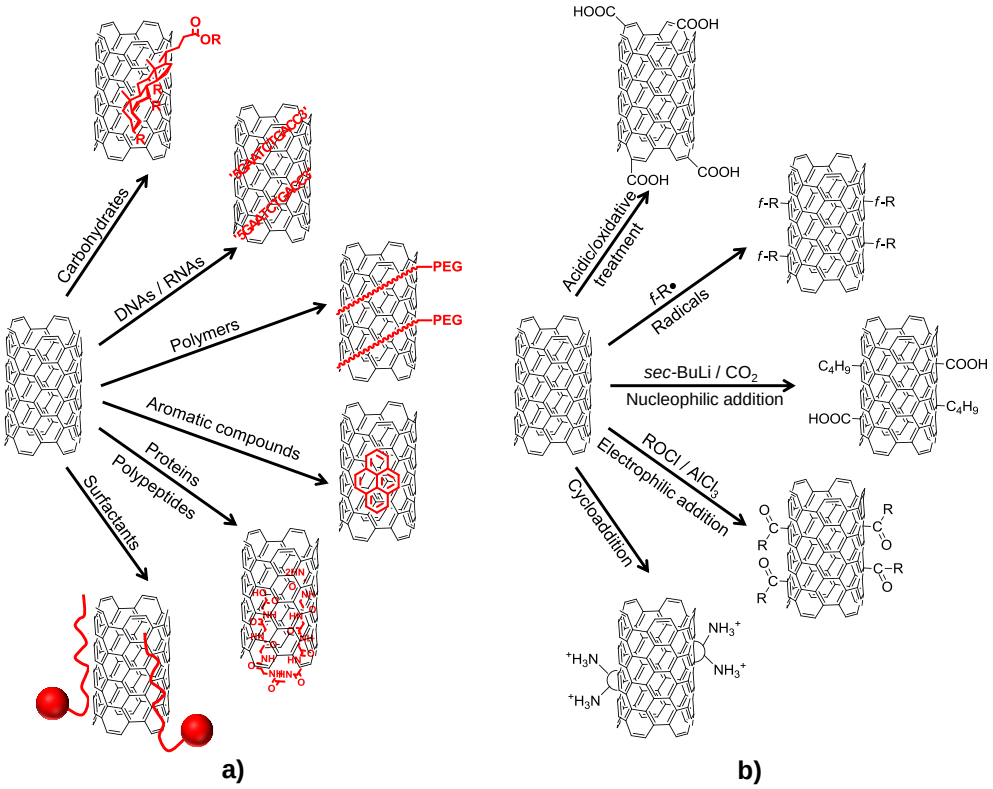

3.2.1. *Non-covalent functionalisation of SWNTs*

The non-covalent method is considered an effective approach for the preparation of functional SWNTs-based biomaterials, since such approach disaggregates the large SWNTs bundles and decorates the SWNTs surface with various bioactive molecular moieties, without strongly affecting the electronic structure of the tubes.[66]

A variety of chemical agents have been used for the non-covalent functionalisation of SWNTs. An ideal non-covalent functionalisation coating for biological applications should have the following characteristics:

- be biocompatible and non-toxic;
- be sufficiently stable to resist detachment from the nanotube surface in biological solutions (especially in biologigal fluids containing high concentrations of salts and proteins);
- have functional groups that are available for conjugation with various biomolecules.

Examples include surfactants, polymers and polynuclear aromatic compounds, as well as various biological relevant compounds such as proteins, peptides, DNA/RNA and carbohydrates.

Surfactants: Ionic surfactants are commonly used to obtain water-stable dispersions of SWNTs. Among these, sodium dodecylbenzene sulphonate (SDBS) demonstrated the highest ability in dispersing SWNTs in water with no strong diameter dependence.[67,68] Although anionic, cationic and non-ionic surfactants have shown different efficiency in suspending individual SWNTs in different environments, the exact mechanism by which CNTs and the different surfactants interact is still uncertain.[68] It has been reported that the hydrophilic part of such molecules interact with water and the hydrophobic tails are adsorbed onto the nanotubes surface.[60] In the case of charged surfactants, such as SDBS, the dispersion is stabilized by electrostatic repulsion between the micelles.[69] Typical surfactants employed in biomedical applications of SWNTs are Pluronic F127[70] and Tween 20.[71,72]

Polymers: Similarly to surfactants, amphiphilic polymeric macromolecules (such as PEG, phospholipid-PEG conjugates (PL-PEG),[73] co-polymers[70] and glycopolymers[74]) improve dramatically SWNTs dispersability by coating the nanotube surface.

While co-polymers (such as Kentera, a polymer based on polyphenylene ethynylene units) and glycopolymers have been used to modify SWNTs for cancer treatment[70] and genes transfection[74] respectively, the strategy of coating SWNTs with PL-PEG has been pioneered by Dai and co-workers.[56] According to this methodology, the distal end of the PEG chain is generally used to link bioactive molecules, such as targeting moieties (RGD sequence),[48,73] imaging radionuclides (^{64}Cu)[73] and drugs (Paclitaxel).[75]

Polynuclear aromatic compounds: Polynuclear aromatic compounds are functional molecules that exhibit π-π stacking on the sidewalls of SWNTs. Among them, pyrene moieties (commonly referred to as a "sticky label"[76,77]) are typically employed for non-covalent functionalisation of SWNTs with various bioactive molecules (such as proteins[76,77] and DNA[78]).

Proteins and Peptides: A variety of proteins can strongly bind to the nanotube exterior surface via non-covalent interactions. For example, proteins such as streptavidin and HupR (a transcriptional regulator from the photosynthetic bacterium *Rhodobacter capsulatus*), which are characterised by a helical structure, rearrange in ordered arrays onto the nanotube surface.[79] The interaction between CNTs and proteins is mainly non-

specific, *i.e.* proteins adsorb onto the SWNTs surface without any preference.[80,81] It is quite possible that the mechanism determining the protein adsorption is associated with the amino affinity of carbon nanotubes[82] and/or with π-π interactions between the aromatic amino acids constituting the biomolecule and SWNTs' π-conjugated skeleton.[83]

Common proteins, such as haemoglobin[84] and bovine serum albumin (BSA),[85,86] can be used for increasing the aqueous dispersability of the tubes. The capability of these macromolecules as dispersing agents depend on various factors, including their primary structure and the pH.[84] Proteins with more basic residues (histone and lysozyme) are for example more effective in the dispersion of SWNTs, whereas enhanced solubilisation is achieved with haemoglobin at acidic or basic pH.[84]

The attachment of proteins to SWNTs is readily transferable to numerous applications, ranging from sensors to electronic devices.[87]

DNA/RNA: Similarly to proteins, DNA and RNA can be non-covalently attached to SWNTs via helical wrapping or simple surface adsorption.[88,89] Molecular modelling showed that the nucleosides of DNA/RNA bind to the SWNT surface by π-π interactions, while their hydrophilic sugar–phosphate backbones point into the water.[90] The specific interaction between DNA sequences grafted on the CNT surface and complementary sequences present in solution can be employed for molecular biosensing applications and electronic gene sequencing;[91,92] whereas supramolecular complexes between short RNA oligomers (siRNA) and SWNTs has been exploited for gene silencing *in vivo*.[93,94]

***Carbohydrates*:** Carbohydrate ligands in the form of glycodendrimers (macromolecules that mimic N-linked glycans populating the eukaryotic cell surfaces),[95] glycolipids and polysaccharides can be non-covalently displayed on SWNTs surface.[96-100] For example, schizophyllan (a polysaccharide with a hollow triple-helix structure) can be dissociated into a single chain in DMSO and then re-constituted by simply replacing DMSO with water. Sonication of schizophyllan with SWNTs in DMSO, and then exchange of DMSO with water, results in non-covalently functionalised SWNTs.[100] Polysaccharides such as amylose, starch, gum Arabic and β-1,3-glucans are also able to solubilise SWNTs in water.[101-104] It seems that the majority of these polymers disperse SWNTs by wrapping themselves around the tubes in a helical fashion. A fascinating example of SWNTs functionalisation by polysaccharides

refers to 12-membered cyclodextrins (CDs), which are able to encapsulate SWNTs. Because of the dimensions of the CD inner cavity, CDs enable the partial separation of the tubes with respect to their diameters. [105]

Carbohydrates do not only impart significant aqueous solubility and biocompatibility to SWNTs, but they also offer the kind of bioactivity useful for various biomedical applications. For example, various studies demonstrate the capacity of sugar-bearing CNTs to engage in specific interactions with protein receptors.[106] Similarly, SWNTs non-covalently functionalised with glycolipids (pyrene-polyethylene glycol-lactose[107] or photopolymerized polydiacetylene-based glyconanorings[108]) are able to engage in specific ligand-lectin interactions. As a consequence, the potential of decorating SWNTs with carbohydrates has been carefully investigated over the past several years, with the main intent of understanding and mimicking specific cell-cell interactions[106] or the bacterial adhesion.[109-111] In particular, the identification of the bacterial infections pathways could lead to improvements in the inhibition of disease development. In addition, SWNTs coated with polysaccharides might be used to mimic the nanofibrous extracellular matrix. For example, biomimetic nanofibrous scaffolds mimicking the extracellular matrix were produced by non-covalent wrapping SWNTs with natural polysaccharides, such as amylose, sodium alginate and chitosan.[112]

3.2.2. Covalent functionalisation of SWNTs

Covalent approaches are equally important to increase the biocompatibility and bioapplication of SWNTs. There are obvious advantages related to the covalent strategy, such as control over the number of therapeutic, targeting or imaging moieties that may be attached[113] and the well-defined nature and stability of the linker that connects them to the nanotube. Molecules are therefore stably bound on the nanotube backbone and the risks of macromolecule desorption or exchange with components of biological fluids after administration is avoided. Despite the robustness of the covalent functionalisation method, care must be taken. The optical, electronic and thermal properties of SWNTs depend in fact heavily upon their highly π-conjugated skeleton,[114,115] and covalent modification can result in the complete loss of those properties.[116]

Two are the main strategies employed for covalently attaching functional molecules to the nanotube structure: (1) sidewall functionalisation and (2) oxidation.

The first strategy involves reaction of reagents or functional molecules at the sidewall of the tube and has been performed using nucleophilic, electrophilic, radical and cycloaddition approaches.[39] This methodology inherently results in loss of the sp^2 character of the sidewall carbon atoms involved in the covalent bond and subsequently in a break of the π-conjugation of the tube skeleton. Among the many sidewall functionalisation strategies available, cycloaddition reactions are the main chemical protocol employed for modifying SWNTs for biomedical applications.[35,39,55] Cycloadditions can be conducted by photochemical reaction of CNTs with azides[117,118] (Scheme 1.2a) or via the Bingel reaction[119] (Scheme 1.2b). The 1,3-dipolar cycloaddition reaction is also a commonly used reaction[120,121] (Scheme 1.2c), where an azomethine-ylide (generated by condensation of an α-amino acid and an aldehyde) is added to the graphitic surface, forming a pyrrolidine ring coupled to the CNTs sidewall. SWNTs functionalised by cycloaddition reactions find applications in biomedical imaging (functionalisation with radionuclides),[63,122,123] vaccination (using immune-activating peptides)[124,125] and cancer therapy (modification with monoclonal antibody[126] and small interfering RNA (siRNA) therapeutics[127]).

The second strategy involves the addition of functional moieties mainly at the ends of SWNTs by acidic/oxidative protocols. During this reaction, oxygenated functionalities (mostly carbonyl and carboxylic acid (COOH) groups) are introduced mainly at the ends of tubes and at defects sites generated by acidic/oxidative agents, such as nitric acid (HNO_3). Depending on both the time of reaction and the nitric acid concentration, the purification procedure may introduce varying numbers of chemically-active groups that can be further functionalised with amines and alcohols *via* amide and ester linkages.[128] Nitric acid has also the ability to remove synthetic byproducts (namely, residual catalyst particles and amorphous carbon) from as-produced SWNTs.[128-132] Small polycyclic aromatic sheets edge-terminated with carboxyl groups, called carboxylated carbonaceous fragments (CCFs), are however generated during the acidic/oxidative purification procedure by HNO_3, producing a reactive coating onto SWNTs surface and interfering with the effective further functionalisation of SWNTs.[131,133,134] The effective removal of the CCFs from acid purified samples by NaOH treatment has been demonstrated.[134-136] Debates rose however on whether previously reported procedures presenting defect-site functionalisation in the absence of NaOH treatment[137-141] were actually producing covalently functionalised materials. To

address this issue, one recent study from our group demonstrated that COOH functionality is introduced directly onto SWNTs surface and not only onto CCFs present in the sample.[142] When NaOH treatment is not employed, careful solvent washing and oxidation procedures are in fact crucial for the removal of carbonaceous material and conversion of introduced defects sites to reactive COOH groups, respectively. [142] Strong acidic/oxidative treatments have been used for producing SWNTs-based radiotracers,[143,144] and drugs for cancer therapy.[94,145] .

Scheme 1.2. Schemes of covalent functionalisation of CNTs: (a) photoinduced [1, 2] addition of azide compounds; (b) Bingel reaction on CNTs; (c) 1,3-dipolar cylcoaddition on CNTs. For biological applications, the substituent "R" is generally a hydrophilic domain (which increases the water solubility of CNTs) or a bioactive molecule.

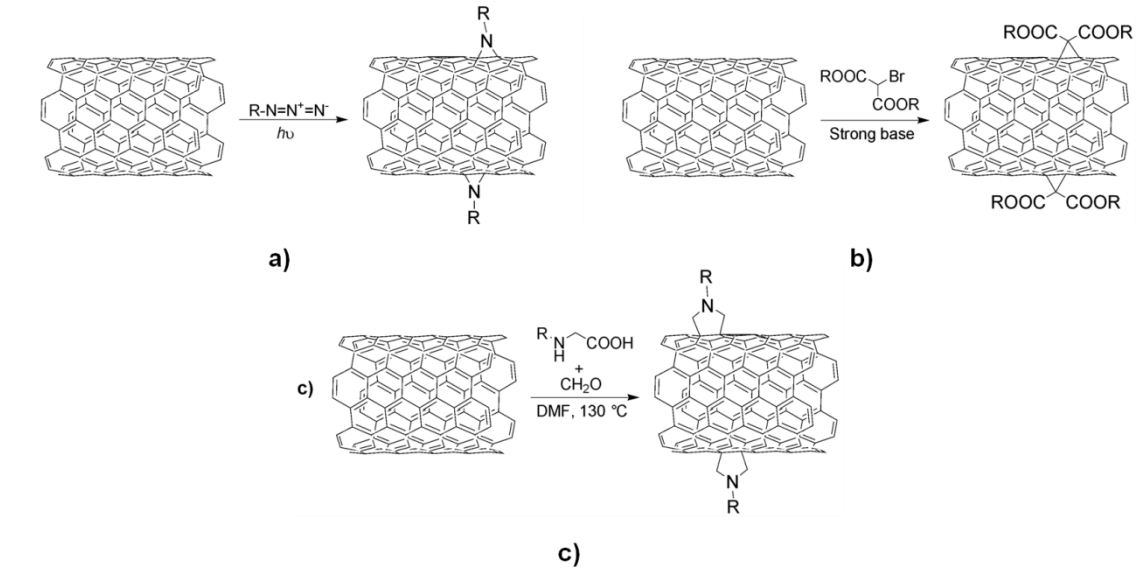

The main bioactive molecules employed in the covalent functionalisation of SWNTs for biomedical applications are proteins, peptides, DNA/RNA and carbohydrates.

Proteins and Peptides: SWNTs can be covalently functionalised with BSA or horse spleen ferritin to form SWNTs able to recognize pathogenic *Escherichia coli* (*E. coli*) cells through specific antibody-antigen interactions.[146]

DNA/RNA: Covalent functionalisation of SWNTs with DNA or RNA can be achieved by carbodiimide-activated coupling reactions either directly[147,148] or through a bifunctional linker.[149] The interaction between DNA and SWNTs largely retain the biological activities of the biological macromolecule.[150] Therefore, SWNTs decorated

with single-strand DNA (ssDNA) can be used as sensors of complementary sequences with a high degree of selectivity,[92] or as drug-delivery platforms if employing, for example, short interfering RNA (siRNA).[151] Notably, SWNTs are able to protect bounded DNA from intracellular enzymatic cleavage.[152]

Carbohydrates: Similarly to DNA/RNA, sugar ligands preserve their biological activity when covalently bound to SWNTs. As previously mentioned (Section 3.2.1), carbohydrates are major components of the cell membrane and have a key role in cell-cell recognition and communication processes, cell growth and development, pathogen binding, viral infections, inflammation, tumour metastasis and immune responses.[153] In this respect, SWNTs displaying carbohydrate moieties covalently attached on their surface were investigated as inhibitors of bacterial infections via specific adhesion-receptor interactions with the pathogenic cells. Gu *et al.* (2005) showed for example that SWNTs functionalised with galactose were able to bind to pathogenic *Escherichia coli* (*E. coli*) cells, leading to cell agglutination.[110] The high aspect ratio and surface area of SWNTs enabled the display of a large number of galactose residues, while the linear nature of SWNTs likely facilitates the binding with *E. coli* cells.[110,111] Wang *et al.* (2006) reported that SWNTs functionalised with galactose or mannose were able to bind carbohydrates on the surface of anthrax (*Bacillus anthracis*) spores in the presence of a divalent cation (Ca^{2+}), causing agglutination and almost complete inhibition of colony formation.[109] The presence of Ca^{2+} ions was crucial for the aggregation of *Bacillus anthracis* spores. According to these results, SWNTs covalently decorated with carbohydrates have potential applications in the development of potent inhibitors or effectors in pathogens detection and decontamination.

3.3. SWNTs Biomedical Applications

Functionalisation strategies as presented above suggest the feasibility and potentials of SWNTs as functional parts of biomedical systems and devices. Although the current state of the art on SWNTs in biomedicine is still at its infancy, many advantages in their application in life sciences are anticipated by the discoveries of recent years. Figure 1.3b summarises the properties that determine the advantages and the disadvantages of SWNTs in biomedicine. The aim of the following sections is to describe the main applications of SWNTs in life sciences (briefly summarised in Figure 1.3a).

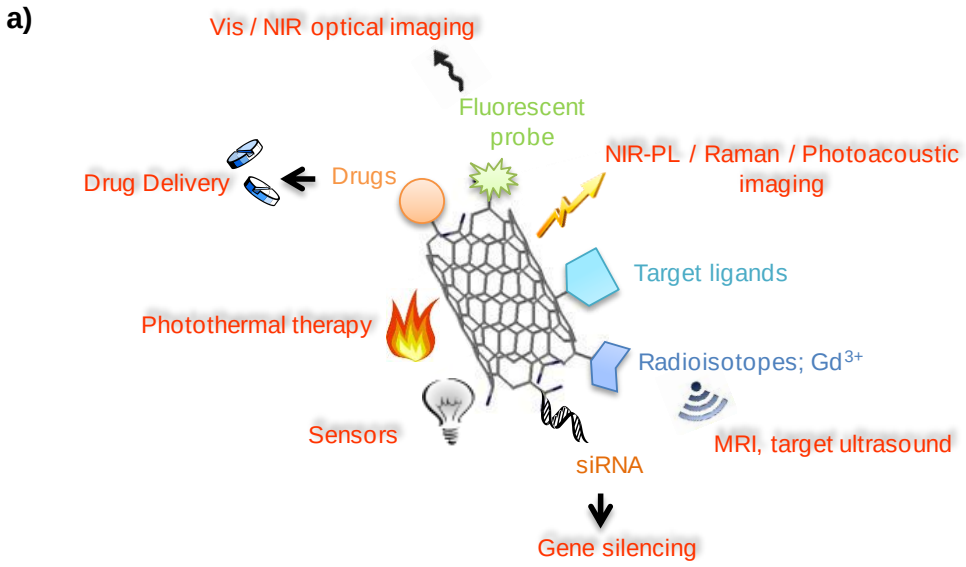

Table (b). Advantages and disadvantages of CNTs in biomedicine

SWNTs biomedical applications	
Advantages†	**Disavantages†**
Opportunity to load multiple bioactive molecules on their surface	Large, hydrophobic surface area cause protein adsorption and potential opsonisation
Potential encapsulation of therapeutics and imaging probes in their internal cavity	Limited information on their impact on human health
High stability *in vivo* due to mechanical properties	Strong tendency to aggregate
Ability of passing through biological barriers	Difficult standardisation of the materials used
Development of new diagnostic tools based on their unique electrical and optical properties	Hydrophobicity: functionalisation is required to increase their dispersability in physiological fluids

† Source: Bianco *et al.* (2008)[57] and Rosen *et al.*[62]

Figure 1.3. (a) Schematic representation of the potential applications of SWNTs in biomedicine, namely as drug/gene delivery platforms, anticancer agents for photothermal therapy, biosensors and molecular probes in various bioimaging techniques (such as Vis/NIR/Raman optical imaging and photoacoustic imaging). Targeting of a specific biomarker is possible in all these applications. (b) Advantages and disadvantages of the use of CNTs in life sciences.

3.3.1. Therapeutics

3.3.1.1. Drug delivery systems

The application of nanotechnology to drug delivery may allow (1) an improved delivery of water-insoluble drugs, (2) a tissue-targeted delivery, (3) the delivery of large macromolecule drugs to intracellular sites of action; (4) the co-delivery of drugs for

combination therapy and (5) the evaluation of drug pharmacokinetics by decorating the nanomaterial with various imaging moieties.[154] For all these reasons, CNTs have been pursued as an alternative to already available drug delivery systems.[155] Various chemiotherapeutic agents, as well as drugs for the pharmacological treatment of Alzheimer[156] and infectious diseases, have been loaded onto SWNTs surface. Here, a brief review of the main SWNTs-based drug delivery platforms developed until now is presented (Table 1.2).

Infectious diseases Infectious diseases represent a highly dynamic area where medications quickly lose their efficacy due to the emergence of resistant strains. The time required to introduce new medications is far longer than the development of resistant strains; besides, limited penetration and inadequate control to the targeted region renders current conventional treatments ineffective.[157] As a consequence, significant effort has been placed in using SWNTs as carriers for antibacterial, antifungal and antimicrobial drugs (Table 4).[54,62,158-160] For example, Wu *et al.* (2005) functionalised SWNTs with amphotericin B (AmB).[161,162] AmB is one of the most effective antimycotic agents to treat chronic fungal infections; however, AmB is poorly soluble in water, rendering it highly toxic to mammalian cells. The conjugation of SWNTs and AmB led to lower cytotoxicity of the drug and an improved efficacy of its antifungal activity.

Cancer treatment Lots of effort has been placed in the discovery of new SWNTs-based nanosystems for the delivery of chemiotherapeutic drugs, such as doxorubicin (DOX), Paclitaxel (PTX), taxoid and cisplatin.

Various groups conjugated SWNTs with DOX via non-covalent interactions.[163-167] *In vitro*, experiments showed that DOX-SWNTs induced significant cancer cell death and cell apoptosis, even if the IC_{50} (half-maximum inhibitory concentration) value for the DOX-SWNTs was higher than that of free DOX. After specific SWNTs targeting with an RGD sequence (recognizing integrin receptors up-regulated in tumours) the IC_{50} value significantly decreased.[163] The DOX 'non-covalent binding to' and 'release from' SWNTs were found to be dependent on the pH and the diameter of SWNTs: generally, lower pH and smaller diameter favoured DOX dissociation from SWNTs.[163] Similarly, DOX-SWNTs complexes targeted with an antibody (mAb) of the tumour carcinoembryonic antigen (CEA) were efficiently internalized by CEA-expressing cancer cells and DOX was rapidly released from the nanotube surface, thus exerting its

chemotherapeutic action.[165] Finally, Chaudhuri *et al.* (2010) covalently attached DOX to a pyrene moiety that adsorbed on the nanotube surface.[167] DOX-SWNTs induced cell death of melanoma cells *in vitro*. The release of the drug was presumably due to enzymatic cleavable of the carbamate linker between DOX and the pyrene by lysates of cancer cells. *In vivo*, DOX-SWNTs led to higher inhibition of tumour growth and prolonged animals survival compared to the free DOX. Recently, SWNTs coated with polysaccharides (sodium alginate and chitosan) were loaded with DOX and decorated with folic acid (also referred to as folate),[166] which is a targeting agent for many tumours (folate receptors are over-expressed on several cancer cells surface[168]). The release of DOX was pH-dependent, with better release thresholds at slightly acidic pH, which is characteristic of tumour environments. Finally, a further study showed reduction in melanoma growth after administration of DOX-SWNTs to mice, without showing detectable systemic toxic side-effects characteristic of the free DOX.[167]

The chemiotherapeutic drug PTX was conjugated to SWNTs via a cleavable ester bond to PL-PEG chains adsorbed onto SWNTs surface.[75] PTX is commercially known as Taxol® and it is clinically used. The PTX-SWNTs conjugates showed higher efficacy in suppressing tumour growth than Taxol®, due to longer blood circulation and higher drug uptake. Similar results were obtained by covalently functionalising SWNTs with taxoid via a cleavable linker (disulfide bond), and with biotin (vitamin H or vitamin B7) as targeting agent.[169]

Another potent anticancer drug that has been delivered using SWNTs is cisplatin, a widely used clinical agent. Different approaches have been attempted to conjugate this drug to SWNTs via non-covalent interactions,[170] covalent binding[145,171] or encapsulation.[172] The latest allowed protection of cisplatin from photodegradation and external reactive species, thus avoiding its decomposition. All the studies show evidence that, when cisplatin is conjugated to SWNTs, its effectiveness in killing cancer cells is higher than that of the free drug.

Table 1.2. Chemical structure of functionalised SWNTs with potential drug delivery applications. Orange boxes indicate the pharmaceutical agent employed.

Targeted disease	Therapeutic agent	Chemical structure	Ref.
		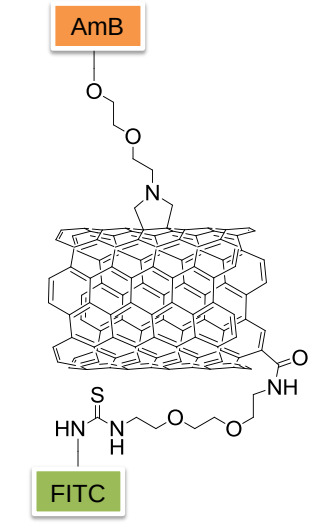	161
Fungal infection	Amphotericin B (AmB)	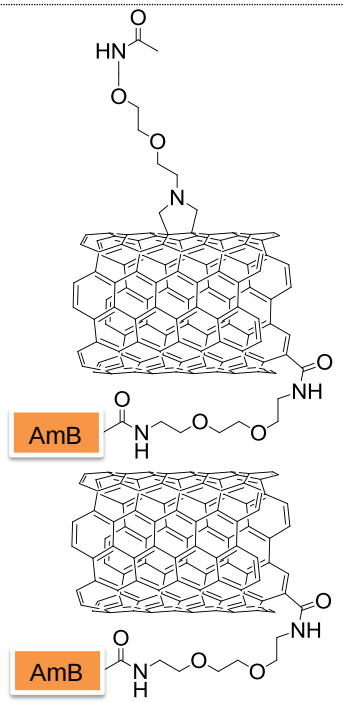	162
Cancer	Taxoid	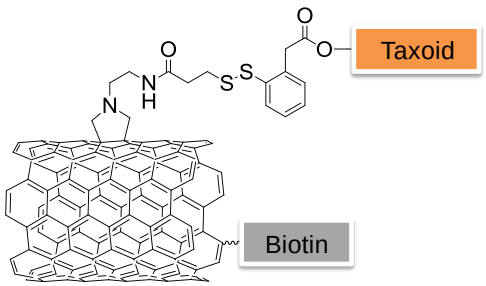	169

Targeted disease	Therapeutic agent	Chemical structure	Ref.
Cancer	Doxorubicin (DOX)	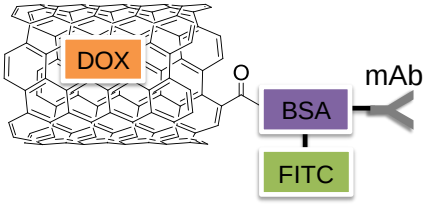	165
		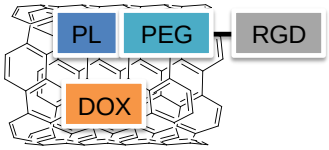	
		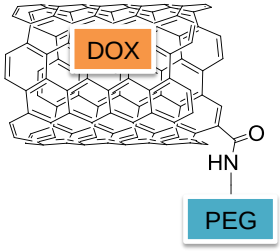	163,164
		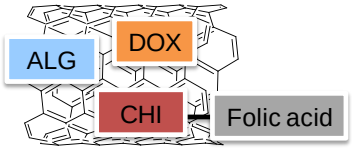	166
		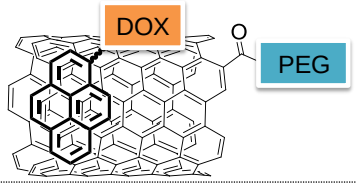	167
	Cisplatin	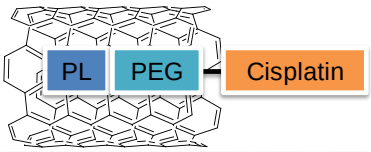	170
		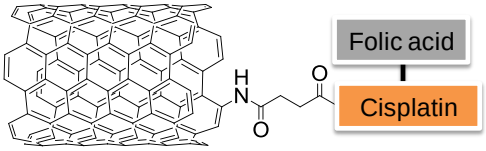	171
		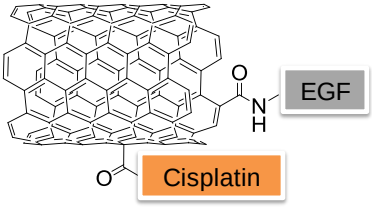	145

Targeted disease	Therapeutic agent	Chemical structure	Ref.
Cancer	Cisplatin	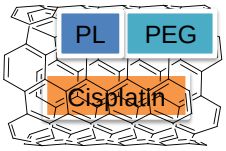	172
	Paclitaxel (PTX)	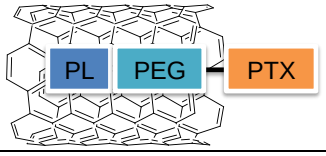	75

ALG: sodium alginate; BSA: bovine serum albumin; CHI: chitosan; EGF: epidermal growth factor; FITC: fluorescein isothiocyanate; mAb: antibody; PEG: polyethylene glycol; PL: phospholipid; RGD: arginine-glycine-aspartic acid.

3.3.1.2. Gene silencing

Beyond molecular drugs, other bioactive species such as siRNA were successfully delivered into cells by conjugating them with SWNTs (Table 1.3).[94,151,173,174] Silencing a gene using an siRNA sequence is becoming a clinically relevant option in therapy of various pathologies such as cancer and immune diseases.[175]

Different types of SWNTs decorated with ammonium groups have been used to form siRNA-SWNTs complexes. Briefly, ammonium-functionalised SWNTs were conjugated to siRNA encoding for knockdown of telomerase reverse transcriptase (TERT). Effective and specific silencing of TERT expression was achieved, resulting in decreased proliferation and growth of a tumour *in vivo*.[94] Similarly, functionalised nanotubes were complexed to a specific siRNA that targets human cyclin A_2, which plays a critical role in DNA replication, transcription and regulation of the cell cycle. The siRNA-SWNTs conjugate promoted cell apoptosis and inhibited proliferation of leukemia cells *in vitro*.[173,174] SWNTs coated with ammonium-terminated PL-PEG chains and then linked to specific siRNA silenced the gene encoding for laminin A/C protein[80] and the insulin-mediated glucose uptake in adult skeletal muscle cells,[176] while complexation with an siRNA able to block CXCR4 and CD4 receptors on human T cells and peripheral blood mononuclear cells reduced HIV infection capability.[151]

In all of the studies reported above, the conjugation of siRNA with SWNTs improved efficiently the biological activity of the siRNA sequences employed.

Table 1.3. Chemical structure of functionalised SWNTs with potential gene silencing applications. Orange boxes indicate the siRNA sequence conjugated to SWNTs.

Targeted disease	Chemical structure	Ref.
Cancer	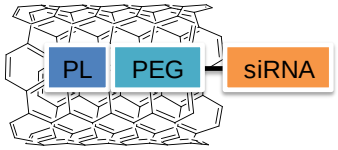	151
	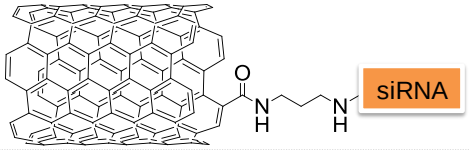	94
Leukaemia	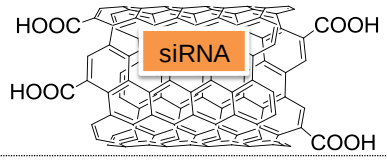	173,174
Muscular dystrophy	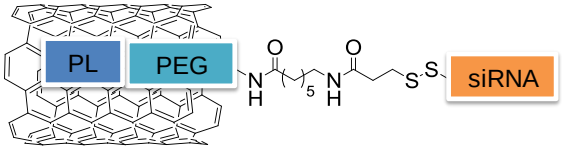 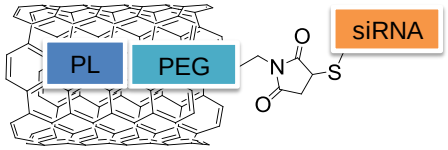	80,176
HIV infection	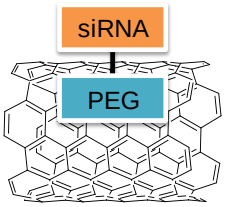	151

PEG: polyethylene glycol; PL: phospholipid.

3.3.1.3. Anticancer agents in thermal therapy

The possibility of inducing cancer cell death by heating carbon nanotubes by means of a NIR laser[177-181] or radiofrequency waves[70] has been recently reported (Table 1.4). Briefly, SWNTs were non-covalently functionalised with PL-PEG chains,[179] PL-PEG expressing a folate moiety on the side chains for selective targeting of cancer cells[177] or chitosan functionalised with folate.[180] Successful cancer cell death was triggered by irradiating the cells with NIR light[177-180] and treated mice displayed complete destruction of the tumours with no recurrence over six months.[179] No damage was detected in folate receptor-free cells.[177,180] NIR phototherapy was also applied to destroy breast cancer cells using SWNTs previously functionalised with two specific

monoclonal antibodies targeting membrane markers' insulin-like growth factor-1 receptor (IGF1R) and human endothelial receptor-2 (HER2).[178]The antibodies were conjugated to the SWNTs surface by a pyrene linker adsorbed onto the SWNTs backbone, while a coating with PEG was used to prevent undesired adsorption of other proteins onto their free surface. Finally, radiofrequency pulses killed malignant cells in direct contact with SWNTs coated with Kentera and injected directly into the liver tumour of a rabbit.[70] Minor damage was caused to the neighbouring healthy tissues.

Table 1.4. Chemical structure of functionalised SWNTs employed as thermal anticancer agents. Grey boxes indicate the molecular moiety used as targeting agent.

Heating modality	Targeting agent	Chemical structure	Ref.
NIR laser	Folate	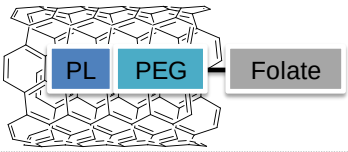	177
		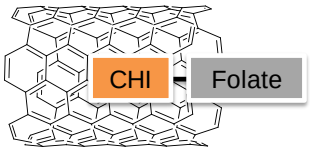	180
	IGF1R Ab, HER2 Ab	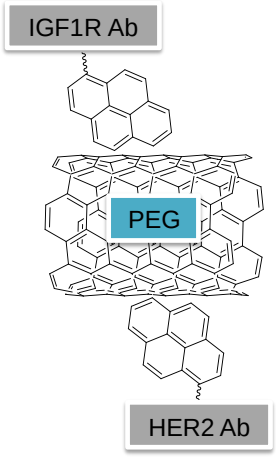	178
NIR laser	[No targeting agent]	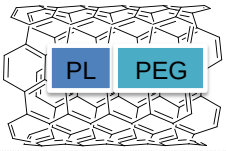	179
Radiofrequency pulses	[No targeting agent]	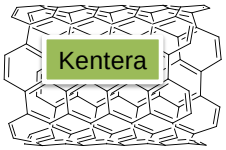	70

Ab: antibody; CHI: chitosan; HER2: human endothelial receptor-2; IGF1R: insulin-like growth factor-1; PEG: polyethylene glycol; PL: phospholipid.

The ability of SWNTs to transform NIR light into heat opens up new venues not only for direct thermal ablation of cancer cells, but also for controllable molecule transportation. Very recently, a molecular dynamics study supported the idea that optical heating of CNTs can assist in releasing encapsulated drugs,[182] and experimental investigations showed that SWNTs and double-walled carbon nanotubes (DWNTs) can function as NIR photoresponsive carriers of molecules for controlled delivery of an indole (precursor to many cancer drugs) (Figure 1.4).[183]

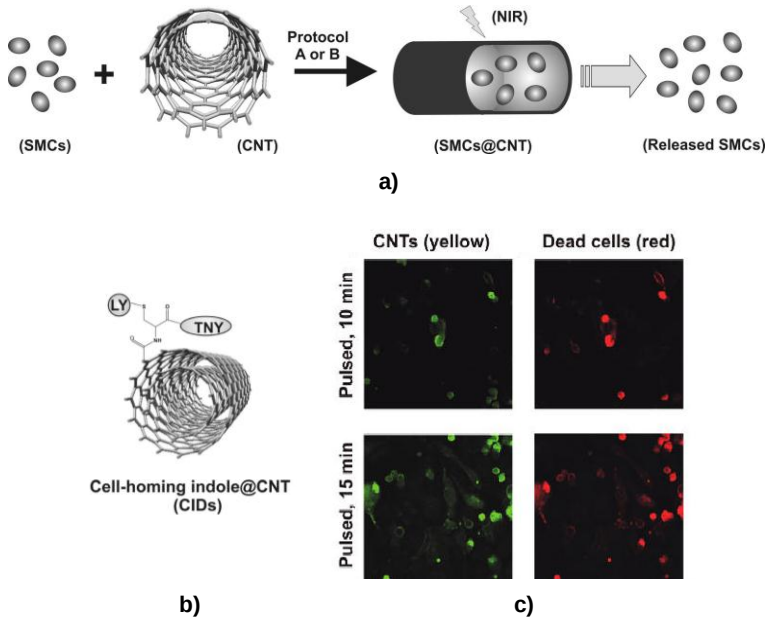

Figure 1.4. (a) Encapsulation of small molecules (SMCs) into CNTs. The SMC used was an indole. The complex thus formed (indole@CNTs) could be used as NIR-controlled molecule transporter for drug delivery. (b) Schematic representation of the complex indole@CNTs. Each complex was covalently functionalised on the surface with EphB4-binding peptide (TNY) for targeting and with Lucifer yellow (LY) for imaging purposes. The indole moieties (not shown for clarity) were encapsulated. (c) The complex indole@CNTs released the indole molecules upon NIR irradiation for 10 or 15 min, thus causing controlled and targeted cell death (adapted and modified from Su *et al.*[183]).

3.3.1.4. Antibacterial agents by direct contact

SWNTs may have the potential to be used as alternative agents to combat microbial infections of *E. coli*,[184,185] *Pseudomonas aeruginosa*,[185] *Staphilococcus aureus*[185] and *Bacillus subtilis*[185] following direct contact. Two recent articles demonstrated that the most likely antibacterial mechanism of SWNTs is cell membrane damage.[185,186] In

addition, SWNTs covalently modified with mannose and galactose interact with *Bacillus anthracis* spores, resulting in significant spore aggregation and inhibiting colony formation.[109,187]

3.3.1.5. Other therapeutic applications

SWNTs functionalised with phenolic derivatives may be attractive as antioxidant agents for medical therapeutic research,[188] whereas amine-decorated SWNTs may be useful as scaffolds in brain tissues preventing the brain from ischemic injury and enhancing the recovery of behavioural functions after a stroke.[189] There is an increasing number of published studies which support the potential development of CNTs-based biomaterials for tissues regeneration (e.g. neuronal substrates[190] and orthopaedic materials[41-43,191]) and copious reviews on the biocompatibility of such implantable CNTs composite materials[190,192,193] are available in the scientific literature.

3.3.2. Diagnostics

3.3.2.1. Biosensors

The ultimate electrical and optical properties of SWNTs, their high sensitivity and their fast response to changes in the surrounding environment have made them ideal components in biosensors, such as nanoelectronic devices (field effect transistor (FET) sensors) and optical detectors for chemical and biological molecules.[194,195] These systems have demonstrated new opportunities for the detection and quantification of biomolecules in relevant biomedical samples, under physiological conditions and in real time. A number of recent reviews has been published on the subject and examples will be outlined in the following.[194,195]

Carbon nanotubes field effect transistors In general, a carbon nanotubes field effect transistor (NTFET) is formed by a substrate (gate), two microelectrodes (source and drain) and a single SWNT or a SWNTs network bridging the electrodes.[90] Upon interaction of biological macromolecules with the nanotubes surface, a change in the charge state perturbs the current flow in the nanotube, thus producing detectable signals for the sensing. The integration of one-dimensional (1D) nanomaterials, such as SWNTs, into electrical devices offers substantial advantages over conventional optical biodetection, mainly associated with sensitivity and ‘size compatibility’. The current

flow in NTFETs is in fact extremely sensitive to the substances adsorption (i. e., even small changes in the charge environment can cause drastic changes to their electrical properties), thus making possible the development of label-free biosensors. Additionally, electronic circuits in which the components are comparable in size to biological entities ensure appropriate analytes detection.[196]

Only semiconducting SWNTs are used in NTFETs.[195,197] However, as-produced SWNTs are mixtures of semiconducting and metallic nanotubes. Protocols for the selective removal of metallic SWNTs developed in the recent years are therefore highly beneficial in the development of these nanoelectronic devices.

The majority of research on NTFETs involves the detection of proteins with carbon nanotubes (Table 1.5).[71,198,199] For example, unmodified SWNTs were employed in NTFETs for detecting cytochrome C (Cyt C).[200] Adsorption of Cyt C onto SWNTs caused changes in the electron transport properties of the transistors.[200] NTFETs have also been explored for the detection of DNA hybridization,[201-203] in antibody-antigen assays[72,204] and in enzymatic reactions[205] (Table 1.5). Specific sensitivity and chemical selectivity can be achieved by employing recognition molecules attached on SWNTs.[90] Star *et al.* (2003) fabricated for example NTFETs sensitive to streptavidin by using biotin-functionalised SWNTs coated with a mixture of two polymers: poly(ethylene imine) (PEI) and PEG.[206] While PEI provided amino groups for the covalent binding of the biotin moieties, PEG chains prevented the non-specific adsorption of proteins on the NTFET. Specific binding of streptavidin occurred only at the biotinylated interface.

Antibodies are often used as specific targeting agents, achieving highly selective biosensing[71,204,207] by antigen-antibody interactions[72] (for example in detecting prostate-specific antigen[204]). Alternatively, synthetic oligonuleotides (*i.e.*, aptamers or ssDNA) have demonstrated specific detection of amino acids, drugs and proteins.[198] Aptamer-modified CNTs have been used for the detection of immunoglobulin E (IgE),[198] while NTFETs modified with ssDNA were used to study DNA hybridization[201] as well as for the chemical detection of a range of substances (such as water, propionic acid, trimethylamine, methanol, dimethyl methylphosphonate and dinitrotoluene).[208] In addition, DNA-NTFETs based on nucleic acid recognition processes were developed for the rapid, simple and label-free testing of genetic and infectious diseases.[203,209] These fascinating systems allowed to distinguishing between mutant (mut) and wild type (wt) alleles[209] or to target the H63D polymorphism in the human HFE gene, which

is associated with hereditary hemochromatosis, a common disease of iron metabolism.[210]

NTFETs formed by glycosylated SWNTs were also interfaced with living cells to electronically detect dynamic secretion of biomolecules from living cells.[211] The solid network of SWNTs was non-covalently functionalised with N-acetyl-D-glucosamine (GlcNAc), thus conferring biocompatibility to SWNTs and allowing adhesion and growth of neuronal cells, without modifying SWNTs electronic properties. Since D-glucosamine-functionalised SWNTs are capable of binding lectins, helix pomatia agglutinin (HPA) and concanavalin A (Con A), the device could be used for the real-time monitoring of biomolecule exocytosis. For example, the exocytosis of catecholamine from neuronal cells induced significant changes in nanotube current flow.[211]

Finally, the potential use of NTFETs in diagnosis and management of *diabetes mellitus* have been explored and demonstrated by numerous studies.[205,212] The glucose detection relies on the production of hydrogen peroxide during the enzymatic oxidation of glucose by the enzyme glucose oxidase (GOx) adsorbed onto SWNTs surface.[90] Similarly, SWNTs wrapped with amylose (linear component of starch) can be used in NTFETs for monitoring the enzymatic activity of α-amylase, an enzyme present in saliva that breaks amylose down into smaller carbohydrate fragments, finally resulting in the formation of glucose.[101]

Table 1.5. Chemical structure of functionalised SWNTs employed in the development of NTFETs for biosensing applications.

Analyte family	Analyte detected	Targeting agent	Chemical structure	Ref.
Oligonucleotides	DNA	Single-strand DNA (ssDNA)	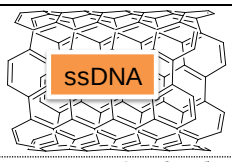	201, 202
Proteins	Cyt C	[No targeting agent]	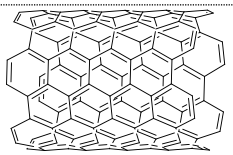	200
	BSA, HSA, hCG, α-hCG, hIgG, avidin	[No targeting agent]	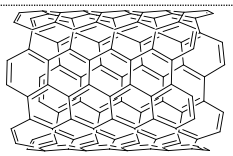	71

Analyte family	Analyte detected	Targeting agent	Chemical structure	Ref.
Proteins	Streptavin	Biotin	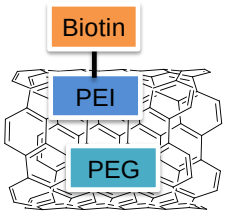	206
	Catecholamine	N-acetyl-D-glucosamine (GlcNAc)	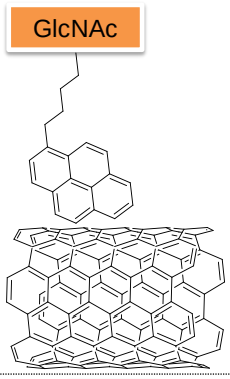	211
	Streptavidin	Biotin	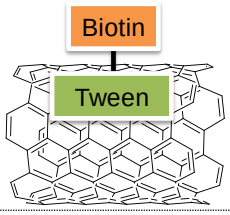	72
	IgG	Staphylococcal protein A (SpA)	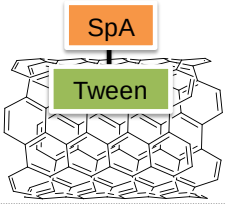	
	10E3 antibody (mAb)	U1A antigen	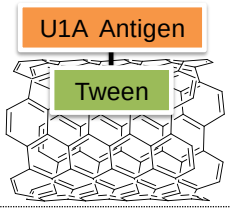	
	Prostate-specific antigen (PSA)	PSA Ab	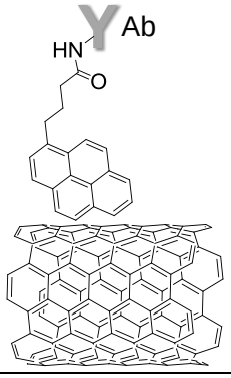	204

Analyte family	Analyte detected	Targeting agent	Chemical structure	Ref.
Proteins	IgE	DNA aptamer	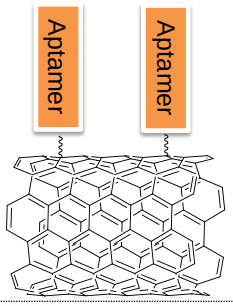	198
Saccharides	Glucose	Glucose oxidase (GOx)	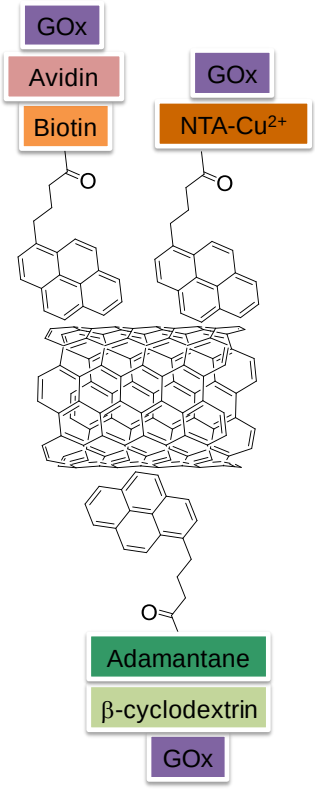	212
		Glucose oxidase (GOx)	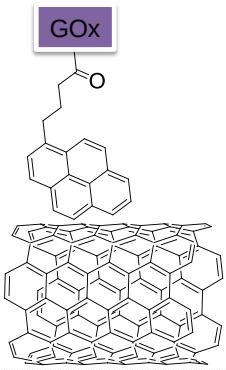	205
Enzymes	α-Amylase	Amylose	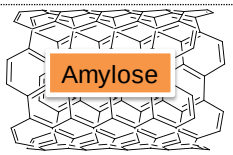	101

Analyte family	Analyte detected	Targeting agent	Chemical structure	Ref.
Chemicals	H_2O, propionic acid, TMA, methanol, DMMP, DNT	DNA	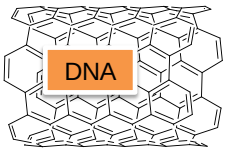	208

Ab: antidody; α-hCG: monoclonal antibody of hCG; BSA: Bovine serum albumin; Cyt C: cytochrome C; DMMP: dimethyl methylphosphonate; DNT: dinitrotoluene; hCG: Human chorionic gonadotropin; hIgG: polyclonal human IgG; HSA: Human serum albumin; IgE: Immunoglobulin E; IgG: Immunoglobulin G; NTA: nitrilotriacetic acid; PEG: poly(ethylene glycol); PEI: poly(ethylene imine); TMA: trimethylamine.

Optical biosensors Exploiting the optical properties of SWNTs, rather than monitoring their conductance in transistor devices, opens another route for sensitive and selective biomolecule detection using this material.

NIR optical biosensors Semiconducting SWNTs are able to emit in the NIR region (see Chapter II, Section 1.1.2) and such NIR emission responds to changes in the local dielectric properties of the environment or of the tubes structure.[213] Adsorption of molecules on the nanotubes surface can therefore be translated into an optical signal by perturbing the electronic structure of the nanotubes.[52] Additionally, the interference of tissues fluorescence is minimal in the NIR range; as a result, NIR SWNTs biosensors (Table 1.6) have great potential for *in vivo* use.[52]

Detection of analytes by NIR biosensors is based on two main strategies: (1) reversible quenching of SWNTs fluorescence or (2) detection of the polymorphism or hybridization of DNA immobilized onto SWNTs surface in response to the presence of an analyte.

The first strategy, which is based on the reversible fluorescence quenching of SWNTs, was used in several works.[51,199,214,215] Barone *et al.* (2005 and 2006) developed NIR optical sensors for long-term β-D-glucose detection by monitoring SWNTs emission changes in response to glucose adsorption[51] or to SWNTs aggregation.[215] In the latest, SWNTs were first coated with phenoxy dextran (to form stable colloidal suspensions) and then SWNTs aggregation was induced by addition of a lectin (Con A), thus quenching their photoluminescence. In the presence of glucose, nanotube disaggregated and their ability to emit in the NIR was restored.[215] In a different study, a dye-ligand conjugate (biotinylated anthracene) was immobilized on the nanotube surface, resulting in quenching of the nanotube fluorescence.[214] Target analytes, bearing an avidin

receptor, induced the recovery of fluorescence by removing the dye-ligand conjugate from the nanotube surface. The reversibility and versatility of this approach allowed sensitive and selective detection of selected analytes at the nanomolar level. Finally, a protein microarray for label-free single-protein detection has been recently developed by Strano and co-workers (2011) by exploiting the NIR emission of SWNTs.[199] In this work, SWNTs were non-covalently modified with chitosan bearing an NTA chelator chelated to Ni^{2+}. Native or *in situ* synthesised proteins expressing a C-terminal His-tag ("capture protein") were then bound to NTA-Ni^{2+} by non-covalent interactions. The binding event was transduced by a decrease in NIR-PL intensity of SWNTs. This was due to changes in the intermolecular distance between SWNTs and Ni^{2+} ions, which act as NIR-PL quenchers when in proximity to the SWNTs surface. Binding of an "analyte protein" to the "capture protein" resulted in NIR-PL recovering, thus showing that microarrays formed by SWNTs functionalised in such a manner can be used as NIR label-free detection platforms of proteins.

In the second strategy, analyte detection is allowed by DNA polymorphism[13,216] (*i.e.*, the conformational rearrangement of the DNA from the right handed B form to the left handed Z form) or hybridization.[217] When immobilised on SWNTs surface, DNA strands form charge transfer interactions with SWNTs. Consequently, binding of complementary DNA sequences or DNA conformational changes induce a shift of the SWNTs NIR emission. DNA-SWNTs sensors are photobleaching-resistant, remaining functional in live cells for up to three months.[13] Since Hg^{2+} can specifically generate DNA conformational transition, such SWNTs biosensors are promising for the detection of Hg^{2+} levels in blood.[216] Recently, DNA-SWNTs biosensors capable to detect cell signalling molecules (insulin) in real time[217] or various important biological analytes at the same time[218] were proposed. In particular, the latter allowed rapid detection of six genotoxins (including chemotherapeutic drugs and reactive oxygen species) inside living cells, with no need of sample processing and with single-molecule sensitivity in detecting hydrogen peroxide (H_2O_2).[218] Alkylating drugs and reactive oxygen species are important biological analytes and their concentrations are difficult to measure in real time *in vivo* due to their fast degradation in the body. However, in this system each genotoxic molecule induced specific NIR-PL shifts/intensity changes, thus allowing not only molecular detection but also compound identification.

Table 1.6. Chemical structure of functionalised SWNTs employed as NIR optical biosensors.

Mechanism	Targeting agent	Analyte detected	Chemical structure	Ref.
NIR-PL quenching	Glucose oxidase (GOx)	Glucose	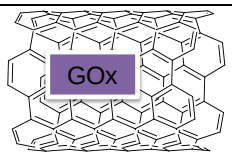	51
NIR-PL recovery	Con A	Glucose	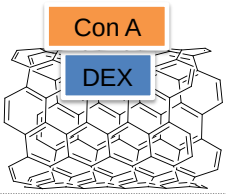	215
	Biotin	Avidin	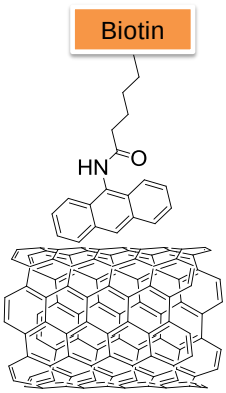	214
			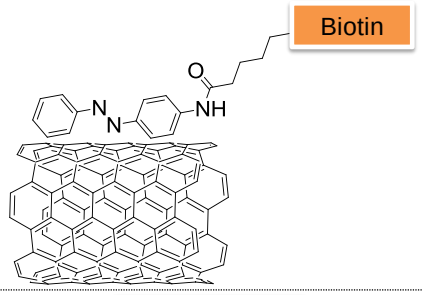	
	His-tag protein	Label-free proteins	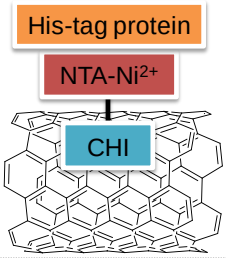	199
DNA polymorfism	DNA	Hg^{2+}	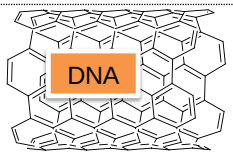	13,216
		Anticancer drugs, ROS	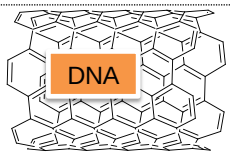	218

Mechanism	Targeting agent	Analyte detected	Chemical structure	Ref.
DNA hybridization	Insulin-binding aptamer (IBA)	Insulin	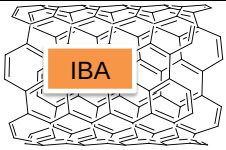	217

CHI: chitosan; Con A: Concanavalin A; DEX: dextran; His: histidine; NTA: nitrilotriacetic acid; ROS: reactive oxygen species.

Vis optical biosensors Studies on the use of the intrinsic visible (Vis) fluorescence of functionalised SWNTs[219-221] for targeting chemicals and/or environmental sensing are scarce. Recently, Qian et al. (2011) employed highly-oxidised SWNTs for sensing metal ions.[221] Briefly, the presence of metal ions and transition metal ions in solution caused a decrease in Vis fluorescence intensity.

3.3.2.2. Molecular probes for bioimaging

Imaging studies using SWNTs as probes (Table 1.7) can be divided in two main categories: (1) indirect imaging of fluorescent or radioactive agents attached to SWNTs surface and (2) direct optical imaging of SWNTs.

Indirect imaging For indirect optical imaging, SWNTs exploit the function of carriers for the fluorescent/radioactive molecular label. In a study by Dai and co-workers (2007), as-produced SWNTs were sonicated in an aqueous solution of fluorescein-poly(ethylene glycol) (Fluor-PEG) to obtain Fluor-PEG functionalised SWNTs.[222] According to the bio-evaluation results, these functionalised SWNTs served as intracellular fluorescent markers, enabling the fluorescence detection inside the cells (BT474 breast cancer cells).[222] In addition to fluorescence-based imaging, radioisotope tracing has also been effective as a SWNTs-based bioimaging technique.[63,73,223] In particular, efficient tumour targeting and imaging was achieved by conjugating a RGD peptide and a radiolabel (DOTA-^{64}Cu) to PEGylated SWNTs (Figure 1.5a).[73] When DOTA-^{64}Cu-SWNTs were intravenously injected into tumour-bearing mice, their biodistribution could be monitored by micro-positron emission tomography (micro-PET) over time[73] (Figure 1.5b). An interesting example of radioemitting SWNTs probes was recently reported by Hong *et al.* (2010), who used the interior cavity of SWNTs as cage for radioactive metal halide salts (^{125}Na).[223] The advantages of this approach are

that (1) there is no accumulation of isotopes into high-affinity organs (thyroid and stomach) and (2) the SWNTs surface can be further functionalised via both covalent or non-covalent approaches, independently of the guest radioisotope chosen.[224]

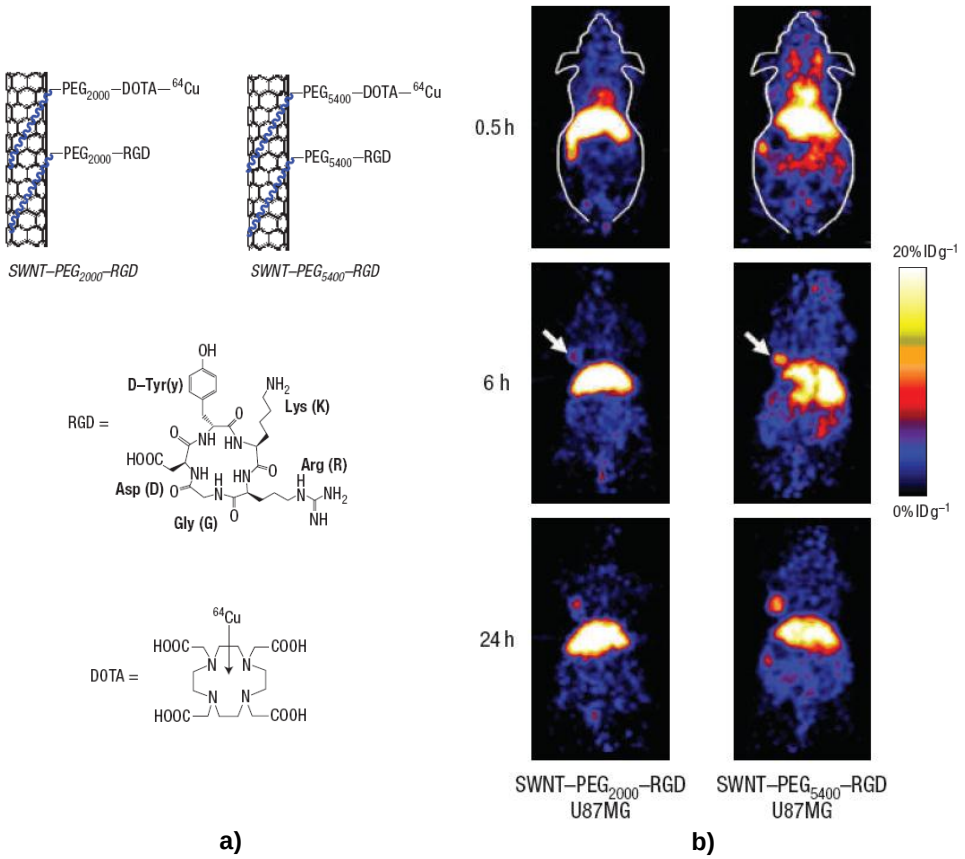

Figure 1.5. *In vivo* tumour targeting and imaging with SWNTs. (a) Scheme of PEGylated SWNTs functionalised with RGD and radiolabelled with DOTA-^{64}Cu, and chemical structure of RGD and DOTA. (b) Micro-PET images of mice overtime. Arrows point out the tumours site. High tumour uptake is observed for SWNT-PEG$_{5400}$-RGD (adapted and modified from Liu *et al.*[73]).

Direct imaging The employment of SWNTs in direct imaging techniques relies on their ability to emit in the Vis[219,225] and NIR[38] region, on their intrinsic Raman-active structure[226] or on their high optical absorption[56] (Table 1.7).

Vis fluorescent probes As SWNTs with surface defects exhibit relatively strong Vis fluorescence[225] (with brighter emission when higher functionalisation is achieved[219]), functionalised SWNTs are amenable to *in vitro* optical bioimaging. This imaging

methodology may be very useful as a widely applicable tool for elucidating the intracellular transport mechanism of carbon nanotubes. For example, Lacerda *et al.* (2007) covalently linked NH_3^+ terminated aliphatic appendages to SWNTs (SWNT-NH_3^+) and investigated the interaction of SWNT-NH_3^+ with human lung carcinoma cells by confocal laser scanning microscopy.[227] This was the first report on the visible florescence imaging of SWNTs in cells without the need for large fluorescent labels attached to SWNTs.

NIR fluorescent probes Intact SWNTs can be employed as NIR fluorescent tags. The NIR of SWNTs (often referred to as band-gap fluorescence) was discovered by the group led by Weisman and Smalley.[38] When semiconducting SWNTs were individualized by an exfoliation method involving no chemical modification or damage to the nanotubes conjugated structure, fluorescence emission was observed in the NIR spectral region (900 - 1600 nm) (see Chapter 2, Section 1.1.2). *In vitro*, Cherukuri *et al.* (2004) used NIR fluorescence imaging to study the uptake of Pluronic-dispersed SWNTs into "macrophage-like" cells, showing the localisation of nanotubes in numerous intracellular vesicles.[10] Heller *et al.* (2005) used SWNTs non-covalently functionalised with ssDNA as photobleaching-resistant markers in live fibroblast and myoblast stem cells.[13] Welsher *et al.* (2008) non-covalently functionalised SWNTs with Rituxan (an antibody recognizing the CD_{20} cell surface receptor) and Herceptin (recognizing the HER2 neureceptor expressed on breast cancer cells), showing specific binding of the antibody-conjugated SWNTs to the host cells.[12] *In vivo*, Leeuw *et al.* (2007) used NIR fluorescence microscopy to image SWNTs in organisms and biological tissues of *Drosophila melanogaster* (fruit flies),[14] while video-rate fluorescent imaging allowed *in vivo* imaging of intravenously injected SWNTs through deep tissues in mice.[4] These studies demonstrate the beneficial effects of using NIR fluorescent SWNTs as probes for diagnostic applications.

Raman active tags CNTs produce strong Raman scattering spectra characterised by unique and well-defined bands at 150-300 cm^{-1}, 1300-1400 cm^{-1} and 1500-1600 cm^{-1} away from the excitation wavelength.[226] The first band, called the radial breathing modes (RBMs), is caused by radial vibration of the carbon atoms in phase.[226] The D-band (1300-1400 cm^{-1}), also called the "disorder" band, is related to the breathing motions of the sp^2 carbon atoms in rings and reflects the amount of sp^2-hybridized carbon converted to sp^3-hybridized carbon on the nanotube surface.[226] Finally, the G-

band (1500-1600 cm^{-1}) is caused by stretching along C–C bonds of graphene.[226] Both metallic and semiconducting SWNTs demonstrate intense Raman scattering, which does not blink or quench and will not diminish under prolonged excitation.[226] This defines the great advantage of SWNTs Raman tags in lieu of traditional fluorophores in immunoassays and *in vitro*/*in vivo* imaging.[56] In immunoassays, coupling the intense Raman signal of SWNTs with surface-enhanced Raman scattering (SERS) techniques presents the opportunity to extend the limit of detection of traditional fluorescent assays from approximately 1 pmol/L[228] to the femtomolar level or below. For example, SWNTs suspended by PL-PEG and coupled to goat anti-mouse immunoglobulin G (GaM-IgG) allowed selective detection of mouse IgG at concentration of 1 fmol/L.[229] This methodology can also be extended to the detection of human immunoglobulins.[229] *In vitro* and *in vivo*, Raman microscopy was used to image SWNTs in liver cells, as well as in tissue slices, by monitoring the RBM or the G-band peaks.[13,47,230]

Photoacoustic imaging tags The high optical absorption of SWNTs can be used in photoacoustic imaging.[56] In photoacoustic imaging sounds are generated as a result of local heating by the absorption of laser light, achieving higher spatial resolution than traditional ultrasound and deeper tissue penetration than optical fluorescence imaging.[231] RGD-conjugated SWNTs were used as contrast agent for photoacoustic imaging of cancer in a mouse model[48] and recently an ICG-SWNTs conjugate targeted with RGD demonstrated a 300 times higher photoacoustic contrast in living tissues than previously reported SWNTs photoacoustic tags,[232] leading to subnanomolar sensitivity and opening up new opportunities for *in vivo* biological imaging with SWNTs.

Table 1.7. Chemical structure of functionalised SWNTs employed as optical probes in indirect and direct bioimaging.

Category	Optical region	Model	Chemical structure	Ref.
Indirect imaging	Vis	*In vitro* [BT474 cells]	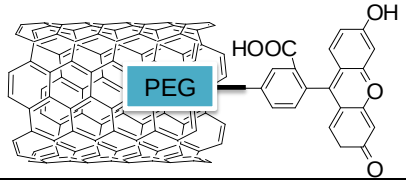	222

Category	Optical region	Model	Chemical structure	Ref.
Indirect imaging	Radioisotope tracing	*In vivo* [mice]	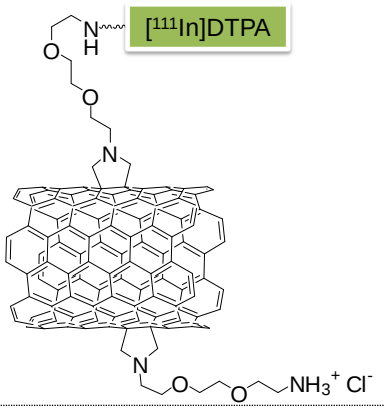	63
			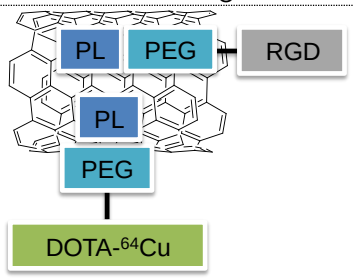	73
			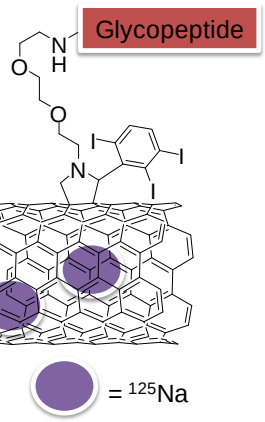	223
Direct imaging	Vis	*In vitro* [A549 cells]	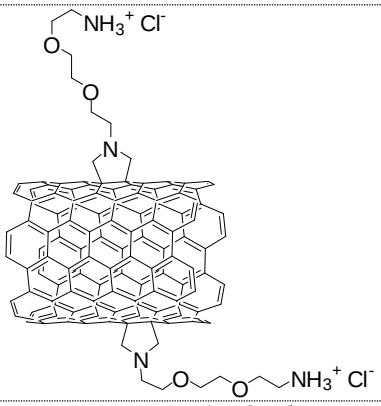	227
	NIR	*In vitro* [macrophages]	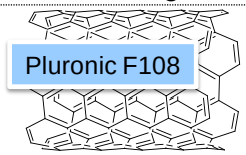	10

Category	Optical region	Model	Chemical structure	Ref.
Direct imaging	NIR	*In vitro* [Raji cells and CEM cells]	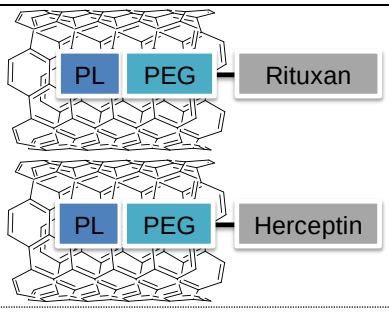	12
		In vivo [*Drosophila melanogaster*]	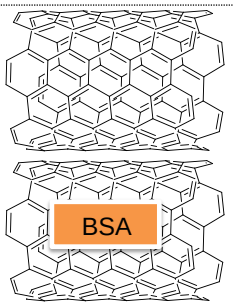	14
		In vivo [mice]	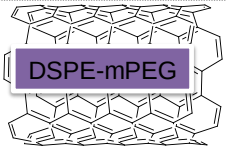	4
		In vitro [U87 MG cells] *In vivo* [mice]	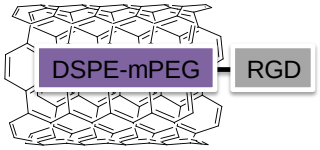	50
	Raman	*In vitro* [immunoassay]	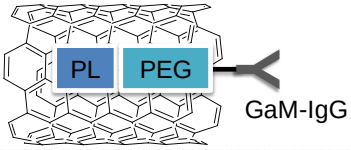	229
		In vivo [mice]	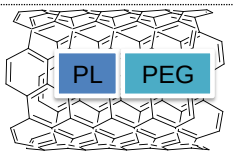	230
			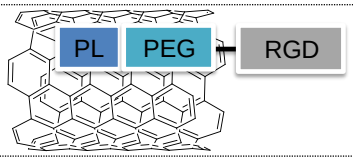	47
	Raman and NIR	*In vitro* [fibroblast and myoblast stem cells]		13
	Photoacoustic imaging	*In vivo* [mice]	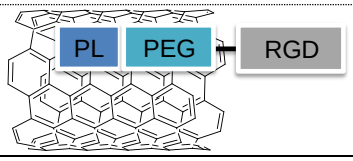	48

Category	Optical region	Model	Chemical structure	Ref.
Direct imaging	Photoacoustic imaging	*In vivo* [mice]	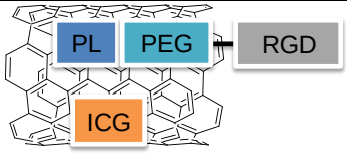	232

A549 cells: human lung carcinoma cells; BSA: bovine serum albumin; BT474 cells: human breast tumour cells; DSPE-mPEG: 1,2-distearoyl-phosphatidylethanolamine-methyl-polyethyleneglycol conjugate; DTPA: diethylentriaminepentaacetic; GaM-IgG: goat anti-mouse immunoglobulin G; HER2 cells: breast cancer cells; ICG: indocyanine green; PEG: poly(ethylene glycol); PL: phospholipid; U87 MG cells: human malignant glioma cells.

3.4. Bioavailability of SWNTs

The biodistribution and translocation of CNTs are key factors for their intended *in vivo* biomedical functions[233] and they rely largely on their physical-chemical characteristics.[143,234-236] The findings summarised in the following have implications on the understanding of the ability of CNTs to translocate biological barriers; this has an important impact on the design of drug delivery systems and optical imaging probes based on SWNTs.

3.4.1. *Biodistribution of SWNTs*

Several studies concerning the biodistribution and clearance of CNTs have been reported so far.[122,143,230,236-240] Most of them investigate the biokinetics of covalently functionalised CNTs, whereas only a few evaluate the distribution of non-covalently modified CNTs in the body.

Covalently modified SWNTs Wang *et al.* (2004) firstly radiotraced the distribution of ^{125}Iodine-labeled hydroxylated SWNTs (^{125}I-SWNT-OH) in mice after intraperitoneal administration.[143] ^{125}I-SWNT-OH distributed quickly throughout the whole body.[143] The preferred organs for CNTs accumulation were the stomach, kidneys and bone, while they were excreted into the urine (94%) and in the faeces (6%).[143] More recently the biodistribution and blood circulation half-life of SWNTs covalently radiolabeled with [^{111}In]DTPA was studied.[237] The biodistribution profiles showed that [^{111}In]DTPA-SWNTs were distributed in kidneys, muscle, skin and bone within 30 minutes after their intravenous administration in mice. DTPA-SWNTs were rapidly cleared from all tissues and a maximum blood circulation half-life of 3 h was determined.[237] In contrast, as-produced/raw SWNTs suspended in an aqueous solution of Pluronic F108 showed a

much shorter half-life (1 h).[240] [^{111}In]DTPA-SWNTs were excreted intact through the renal route into the bladder and urine,[237] indicating that no biodegradation of CNTs occurred *in vivo*. Later studies clarified that DTPA-CNTs began to permeate through the renal glomerular filtration system within 5 min post intravenous administration,[122] and terminated in a few hours. The authors stated that the mechanism of CNTs filtration "involves the acquisition of a spatial conformation in which the longitudinal CNT dimension is perpendicular to the endothelial fenestrations, since only the traverse dimension of CNT (cross section is between 20 – 30 nm) is small enough to allow permeation".[236] According to this study, the CNTs length would not be a key parameter in determining renal clearance of these nanostructures. Aggregates or bundles would not be able though to cross the glomerular membrane[241] and may accumulate in the liver, spleen, or lungs. Similar mechanisms of elimination of SWNTs was recently reported by Ruggiero *et al.* (2010).[239] The renal clearance of SWNTs covalently functionalised with various ligands (DOTA, AF488 and AF680) was monitored in mice by means of three different imaging techniques (dynamic positron emission tomography, near-infrared fluorescence imaging and microscopy). According to the experimental data, SWNTs were rapidly cleared by glomerular filtration in the kidneys with only partial tubular re-adsorption. No active secretion was involved in the process. This means that the elimination of a major fraction (85% of the injected dose) of the SWNTs tested (average length: 200-300 nm; molecular weight: ca. 350-500 kDa) followed the rapid, "first-pass" pharmacokinetics, similarly to the clearance of small molecules (molecular weight: ca. 30-50 kDa). According to the theoretical explanations offered in this study, SWNTs have a great tendency to align with the blood flow and they are therefore rapidly excreted through the renal filter.

Non-covalently modified SWNTs The biodistribution of non-covalently modified CNTs was investigated following intravenous administration in mice.[230] Raman spectroscopy was used to monitor the blood concentration and tissues accumulation of PEGylated over a period of several months.[230] The results indicated that PEG coating increased the blood half-life up to 24 h and near-complete clearance of PEG-SWNTs was achieved after two months with no changes in the health conditions of the animals exposed. PEGylation of CNTs is known to decrease significantly their cytotoxicity[242] (see Chapter III, Section 1.2.4). Since PEG-SWNTs were seen accumulating in the

intestines, faeces, kidneys, and bladder of mice, the authors concluded that the main excretion route of PEG-SWNTs were via billiard and renal pathways.

3.4.2. *Translocation of SWNTs*

The translocation properties of SWNTs through cellular membranes may also be a key factor in determining the efficacy of the designed SWNTs-based drug delivery system or imaging probe.

It is commonly accepted that the cellular uptake of CNTs depends on their length, surface chemistry and aggregation. Becker *et al.* (2007) demonstrated in fact a length-selective cellular uptake of DNA-wrapped SWNTs in cultured human fibroblast (IMR90) cells.[243] The approximate uptake threshold was 189 ± 17 nm; whereas Jin *et al.* (2009) reported an uptake threshold from 130 to 660 nm in fibroblast (NIH-3T3) cells.[244] Functionalised CNTs by covalent or non-covalent approaches can penetrate the mammalian cells membrane.[240,245,246] For example, water-soluble functionalised CNTs were able to translocate into cell cytoplasm,[247] and carbon nanotubes condensed with plasmid DNA were able to deliver it intracellularly thus enhancing marker gene expression.[248] Dumortier *et al.* (2006) showed however that only well-dispersed SWNTs were internalized by lymphocytes and macrophages.[249]

Determination of the exact mechanism leading to CNTs cellular internalisation is of great importance,[190] but discrepancies in the reported mechanisms are evident in the literature. Some researchers proposed an energy-dependent endocytosis mechanism,[158,170,250-253] while other studies demonstrated that functionalised CNTs are able to penetrate cells in a passive way.[245,247,254] Indeed, both mechanisms may occur. Kostarelos *et al.* (2007) studied extensively the uptake of a range of functionalised CNTs (SWNTs, MWNTs) in a variety of cells,[245] including adherent mammalian cells monolayers (A549, HeLa, and MOD-K cells), mammalian cells suspensions (Jurkat), fungal cells (*Cryptococcus neoformans*), yeast (*Saccharomyces cerevisiae*) and bacteria (*E. coli*). Cellular internalisation was reported for all CNTs samples, in all cell types, even in those cells lacking the capability for endocytosis or after inhibition of endocytosis. The nature of the functionalisation group did not influence the internalisation; in particular, both negatively or neutrally charged CNTs were uptaken by cells. Kam *et al.* (2005) observed, however, considerable reduction in the cellular uptake of CNTs labelled with a fluorescent macromolecule under endocytosis-inhibiting

conditions.[158] According to the scientific literature, such discrepancies could be attributed to the differences between the CNTs studied.[190]

Another important question is whether exocytosis occurs after CNTs internalisation. Evidence of exocytosis of DNA-coated SWNTs in fibroblast (NIH-3T3) cells was recently presented.[253] The exocytosis rate was close to that of endocytosis after a minor temporary offset, thus keeping the SWNTs accumulation inside the cell below the cytotoxic levels.

Finally, the subcellular localisation of CNTs is still controversial. Some reports showed that CNTs enter the cells without reaching the nucleus,[246] while other works demonstrated that CNTs can enter the nucleus.[247,255,256] Recently, Zhou *et al.* (2010) demonstrated the possibility of manipulating the intracellular localization of non-covalently modified SWNTs by varying the conjugated molecule.[257]

4. AIMS OF THE STUDY

As largely demonstrated in Section 3.3, a vast number of SWNTs-based materials with potential biomedical applications have emerged since the discovery of SWNTs. In particular, great interest has been raised by the possibility of realizing versatile platforms for biomedical imaging. This novel bioimaging technology is very exciting; it requires, however, considerable development and precaution before it can be translated into a clinically realistic diagnostic tool as all the studies are at a very early, proof-of-concept stage, lacking systematic preclinical therapeutic data.

The interest of this research project lies in the development of novel SWNTs-based NIR fluorescent probes for bioimaging with reduced toxicological impact on human health. In this context, the aims of this study are:

(1) to develop a covalent functionalisation protocol for improving the biocompatibility of SWNTs while preserving their NIR fluorescent properties;

(2) to test the toxicity of the newly-engineered NIR fluorescent probes in a novel nanotoxicology testing system that integrates the old set of testing protocols with modern technologies.

In the first part of this thesis (Chapter II), purification and oxidation are used to process SWNTs. Oxidation reactions are extensively used for purifying SWNTs material from the large amount of impurities that come from their synthesis (such as metal catalysts and fullerenes). Simultaneously, these procedures generate carboxylic acid (COOH) groups on the nanotube sidewalls, thus increasing the dispersability of SWNTs in aqueous solutions and allowing potential further functionalisation with various organic biological targeting agents. A systematic investigation of the effect of this procedure on the optical properties of SWNTs, with particular emphasis on the NIR-PL, is reported in Chapter II. The results show for the first time that purified (p-SWNTs) and oxidized (o-SWNTs) samples display bright, well-structured emission features in the NIR. These results establish covalently modified SWNTs as potential novel NIR fluorophores for *in vitro* (and potentially *in vivo*) imaging.

In the second part of the thesis (Chapter III), three-dimensional (3D) tissue-mimetic models (that better represent the organization of physiological tissues) are integrated for the first time in the cytotoxicity assessment of p- and o-SWNTs. An established ultrasound standing wave trap (USWT) was used to generate the 3D cell aggregates and a comparison with traditional two-dimensional (2D) cell culture models was carried out. The results show that SWNTs toxicity is significantly reduced in the 3D cellular model when compared to the 2D toxicity data, thus indicating the importance of employing 3D cell culture models in the assessment of SWNTs toxicity. Our results clearly indicate that 3D cell aggregates can serve as alternative *in vitro* models providing guidance on nanomaterial toxicity, in a tissue-mimetic manner, thus offering future cost-effective solutions for toxicity screening assays.

The results summarised in this thesis could open the way towards the translation of nanotechnology and nanomedicine from the laboratory bench to the patients' bedside, for the treatment of you and I.

5. REFERENCES

(1) Pysz, M. A.; Gambhir, S. S.; Willmann, J. K. *Clin. Radiol.* **2010**, *65*, 500.

(2) Licha, K.; Olbrich, C. *Adv. Drug Delivery Rev.* **2005**, *57*, 1087.

(3) Klohs, J.; Wunder, A.; Licha, K. *Basic Res. Cardiol.* **2008**, *103*, 144.

(4) Welsher, K.; Sherlock, S. P.; Dai, H. *PNAS* **2011**, *108*, 8943.

(5) Ghoroghchian, P. P.; Therien, M. J.; Hammer, D. A. *Wiley Interdiscip. Rev.: Nanomed. Nanobiotechnol.* **2009**, *1*, 156.

(6) Sakudo, A.; Suganuma, Y.; Kobayashi, T.; Onodera, T.; Ikuta, K. *Biochem. Biophys. Res. Commun.* **2006**, *341*, 279.

(7) Irani, F.; Platek, S. M.; Bunce, S.; Ruocco, A. C.; Chute, D. *Clin. Neuropsychol.* **2007**, *21*, 9.

(8) Bornhop, D. J.; Contag, C. H.; Licha, K.; Murphy, C. J. *J. Biomed. Opt.* **2001**, *6*, 106.

(9) Ghoroghchian, P. P.; Frail, P. R.; Susumu, K.; Blessington, D.; Brannan, A. K.; Bates, F. S.; Chance, B.; Hammer, D. A.; Therien, M. J. *PNAS* **2005**, *102*, 2922.

(10) Cherukuri, P.; Bachilo, S. M.; Litovsky, S. H.; Weisman, R. B. *J. Am. Chem. Soc.* **2004**, *126*, 15638.

(11) Cherukuri, P.; Gannon, C. J.; Leeuw, T. K.; Schmidt, H. K.; Smalley, R. E.; Curley, S. A.; Weisman, R. B. *PNAS* **2006**, *103*, 18882.

(12) Welsher, K.; Liu, Z.; Daranciang, D.; Dai, H. *Nano Lett.* **2008**, *8*, 586.

(13) Heller, D. A.; Baik, S.; Eurell, T. E.; Strano, M. S. *Adv. Mater.* **2005**, *17*, 2793.

(14) Leeuw, T. K.; Reith, R. M.; Simonette, R. A.; Harden, M. E.; Cherukuri, P.; Tsyboulski, D. A.; Beckingham, K. M.; Weisman, R. B. *Nano Lett.* **2007**, *7*, 2650.

(15) *Nature* **2011**, *476*, 251.

(16) *The Project on Emerging Nanotechnologies*, http://www.nanotechproject.org/.

(17) *Nanotechnologies for the Life Sciences*; WILEY-VCH: Weinheim, 2007; Vol. 7, 10.

(18) Bhaskar, S.; Tian, F. R.; Stoeger, T.; Kreyling, W.; de la Fuente, J. M.; Grazu, V.; Borm, P.; Estrada, G.; Ntziachristos, V.; Razansky, D. *Part. Fibre Toxicol.* **2010**, *7*.

(19) Godin, B.; Tasciotti, E.; Liu, X.; Serda, R. E.; Ferrari, M. *Accounts Chem. Res.* **2011**, DOI: 10.1021/ar200077p.

(20) *CrystalplexWest, Sunnyvale, CA, USA*, http://www.crystalplex.com/.

(21) *InvitrogenCorporation*, http://www.invitrogen.com/site/us/en/home/brands/Molecular-Probes/Key-Molecular-Probes-Products/Qdot/Technology-Overview.html.

(22) Barreto, J. A.; O'Malley, W.; Kubeil, M.; Graham, B.; Stephan, H.; Spiccia, L. *Adv. Mater.* **2011**, *23*, H18.

(23) Cheon, J.; Lee, J. H. *Acc. Chem. Res.* **2008**, *41*, 1630.

(24) Sunderland, C. J.; Steiert, M.; Talmadge, J. E.; Derfus, A. M.; Barry, S. E. *Drug Develop. Res.* **2006**, *67*, 70.

(25) Bawarski, W. E.; Chidlowsky, E.; Bharali, D. J.; Mousa, S. A. *Nanomedicine - Nanotechnology Biology and Medicine* **2008**, *4*, 273.

(26) Neuberger, T.; Schopf, B.; Hofmann, H.; Hofmann, M.; von Rechenberg, B. *J. Magn. Magn. Mater.* **2005**, *293*, 483.

(27) Owens, D. E.; Peppas, N. A. *Int. J. Pharm.* **2006**, *307*, 93.

(28) Moghimi, S. M.; Hunter, A. C.; Murray, J. C. *Pharmacol. Rev.* **2001**, *53*, 283.

(29) Aggarwal, P.; Hall, J. B.; McLeland, C. B.; Dobrovolskaia, M. A.; McNeil, S. E. *Adv. Drug Delivery Rev.* **2009**, *61*, 428.

(30) Carstensen, H.; Muller, R. H.; Muller, B. W. *Clin. Nutr.* **1992**, *11*, 289.

(31) Knop, K.; Hoogenboom, R.; Fischer, D.; Schubert, U. S. *Angew. Chem. Int. Ed.* **2010**, *49*, 6288.

(32) Choi, H. S.; Ipe, B. I.; Misra, P.; Lee, J. H.; Bawendi, M. G.; Frangioni, J. V. *Nano Lett.* **2009**, *9*, 2354.

(33) Hirsch, A. *Nat. Mater.* **2010**, *9*, 868.

(34) Schnorr, J. M.; Swager, T. M. *Chem. Mater.* **2011**, *23*, 646.

(35) Bianco, A.; Sainz, R.; Li, S.; Dumortier, H.; Lacerda, L.; Kostarelos, K.; Giordani, S.; Prato, M. In *Medicinal Chemistry and Pharmacological Potential of Fullerenes and Carbon Nanotubes*; Cataldo, F., Ros, T., Eds.; Springer Netherlands: Dordrecht, 2008; Vol. 1, p 23.

(36) Tasis, D.; Tagmatarchis, N.; Bianco, A.; Prato, M. *Chem. Rev.* **2006**, *106*, 1105.

(37) Bachilo, S. M.; Strano, M. S.; Kittrell, C.; Hauge, R. H.; Smalley, R. E.; Weisman, R. B. *Science* **2002**, *298*, 2361

(38) O'Connell, M. J.; Bachilo, S. M.; Huffman, C. B.; Moore, V. C.; Strano, M. S.; Haroz, E. H.; Rialon, K. L.; Boul, P. J.; Noon, W. H.; Kittrell, C.; Ma, J. P.; Hauge, R. H.; Weisman, R. B.; Smalley, R. E. *Science* **2002**, *297*, 593.

(39) Tasis, D.; Tagmatarchis, N.; Bianco, A.; Prato, M. *Chem. Rev.* **2006**, *106*, 1105.

(40) Cui, H.-F.; Vashist, S. K.; Al-Rubeaan, K.; Luong, J. H. T.; Sheu, F.-S. *Chem. Res. Toxicol.* **2010**, *23*, 1131.

(41) Chlopek, J.; Czajkowska, B.; Szaraniec, B.; Frackowiak, E.; Szostak, K.; Beguin, F. *Carbon* **2006**, *44*, 1106.

(42) Nayak, T. R.; Jian, L.; Phua, L. C.; Ho, H. K.; Ren, Y.; Pastorin, G. *ACS Nano* **2010**, *4*, 7717.

(43) Tutak, W.; Park, K. H.; Vasilov, A.; Starovoytov, V.; Fanchini, G.; Cai, S. Q.; Partridge, N. C.; Sesti, F.; Chhowalla, M. *Nanotechnology* **2009**, *20*.

(44) Burke, A.; Ding, X. F.; Singh, R.; Kraft, R. A.; Levi-Polyachenko, N.; Rylander, M. N.; Szot, C.; Buchanan, C.; Whitney, J.; Fisher, J.; Hatcher, H. C.; D'Agostino, R.; Kock, N. D.; Ajayan, P. M.; Carroll, D. L.; Akman, S.; Torti, F. M.; Torti, S. V. *PNAS* **2009**, *106*, 12897.

(45) Moghimi, S. M.; Kissel, T. *Adv. Drug Delivery Rev.* **2006**, *58*, 1451.

(46) Crinelli, R.; Carloni, E.; Menotta, M.; Giacomini, E.; Bianchi, M.; Ambrosi, G.; Giorgi, L.; Magnani, M. *ACS Nano* **2010**, *4*, 2791.

(47) Zavaleta, C.; de la Zerda, A.; Liu, Z.; Keren, S.; Cheng, Z.; Schipper, M.; Chen, X.; Dai, H.; Gambhir, S. S. *Nano Lett.* **2008**, *8*, 2800.

(48) De La Zerda, A.; Zavaleta, C.; Keren, S.; Vaithilingam, S.; Bodapati, S.; Liu, Z.; Levi, J.; Smith, B. R.; Ma, T. J.; Oralkan, O.; Cheng, Z.; Chen, X. Y.; Dai, H. J.; Khuri-Yakub, B. T.; Gambhir, S. S. *Nat. Nanotechnol.* **2008**, *3*, 557.

(49) Galanzha, E. I.; Shashkov, E. V.; Kelly, T.; Kim, J.-W.; Yang, L.; Zharov, V. P. *Nat. Nanotechnol.* **2009**, *4*, 855.

(50) Welsher, K.; Liu, Z.; Sherlock, S. P.; Robinson, J. T.; Chen, Z.; Daranciang, D.; Dai, H. *Nat. Nanotechnol.* **2009**, *4*, 773.

(51) Barone, P. W.; Baik, S.; Heller, D. A.; Strano, M. S. *Nat. Mater.* **2005**, *4*, 86.

(52) Barone, P. W.; Parker, R. S.; Strano, M. S. *Anal Chem* **2005**, *77*, 7556.

(53) Lu, F. S.; Gu, L. R.; Meziani, M. J.; Wang, X.; Luo, P. G.; Veca, L. M.; Cao, L.; Sun, Y. P. *Adv. Mater.* **2009**, *21*, 139.

(54) Menard-Moyon, C.; Venturelli, E.; Fabbro, C.; Samori, C.; Da Ros, T.; Kostarelos, K.; Prato, M.; Bianco, A. *Expert Opin Drug Dis* **2010**, *5*, 691.

(55) Kostarelos, K.; Bianco, A.; Prato, M. *Nat. Nanotechnol.* **2009**, *4*, 627.

(56) Liu, Z.; Tabakman, S.; Welsher, K.; Dai, H. J. *Nano Res.* **2009**, *2*, 85.

(57) Bianco, A.; Kostarelos, K.; Prato, M. *Expert Opin. Drug Deliv.* **2008**, *5*, 331.

(58) Harrison, B. S.; Atala, A. *Biomaterials* **2007**, *28*, 344.

(59) Kostarelos, K. *Nat. Biotechnol.* **2008**, *26*, 774.

(60) Britz, D. A.; Khlobystov, A. N. *Chemical Society Reviews* **2006**, *35*, 637.

(61) Bianco, A.; Sainz, R.; Li, S.; Dumortier, H.; Lacerda, L.; Kostarelos, K.; Giordani, S.; Prato, M. *Carbon Materials: Chemistry and Physics, Springer* **2008**, *1*, 23.

(62) Rosen, Y.; Elman, N. M. *Expert Opin Drug Del* **2009**, *6*, 517.

(63) Singh, R.; Pantarotto, D.; Lacerda, L.; Pastorin, G.; Klumpp, C.; Prato, M.; Bianco, A.; Kostarelos, K. *PNAS* **2006**, *103*, 3357.

(64) Campidelli, S.; Klumpp, C.; Bianco, A.; Guldi, D. M.; Prato, M. *Journal of Physical Organic Chemistry* **2006**, *19*, 531.

(65) Singh, P.; Campidelli, S.; Giordani, S.; Bonifazi, D.; Bianco, A.; Prato, M. *Chem. Soc. Rev.* **2009**, *38*, 2214

(66) Fernando, K. A. S.; Lin, Y.; Wang, W.; Kumar, S.; Zhou, B.; Xie, S. Y.; Cureton, L. T.; Sun, Y. P. *J. Am. Chem. Soc.* **2004**, *126*, 10234.

(67) Moore, V. C.; Strano, M. S.; Haroz, E. H.; Hauge, R. H.; Smalley, R. E.; Schmidt, J.; Talmon, Y. *Nano Letters* **2003**, *3*, 1379.

(68) Suttipong, M.; Tummala, N. R.; Kitiyanan, B.; Striolo, A. *J. Phys. Chem. C* **2011**, 17286.

(69) O'Connell, M. J.; Bachilo, S. M.; Huffman, C. B.; Moore, V. C.; Strano, M. S.; Haroz, E. H.; Rialon, K. L.; Boul, P. J.; Noon, W. H.; Kittrell, C.; Ma, J.; Hauge, R. H.; Weisman, R. B.; Smalley, R. E. *Science* **2002**, *297*, 593.

(70) Gannon, C. J.; Cherukuri, P.; Yakobson, B. I.; Cognet, L.; Kanzius, J. S.; Kittrell, C.; Weisman, R. B.; Pasquali, M.; Schmidt, H. K.; Smalley, R. E.; Curley, S. A. *Cancer* **2007**, *110*, 2654.

(71) Chen, R. J.; Choi, H. C.; Bangsaruntip, S.; Yenilmez, E.; Tang, X.; Wang, Q.; Chang, Y. L.; Dai, H. *J. Am. Chem. Soc.* **2004**, *126*, 1563.

(72) Chen, R. J.; Bangsaruntip, S.; Drouvalakis, K. A.; Kam, N. W.; Shim, M.; Li, Y.; Kim, W.; Utz, P. J.; Dai, H. *PNAS* **2003**, *100*, 4984.

(73) Liu, Z.; Cai, W.; He, L.; Nakayama, N.; Chen, K.; Sun, X.; Chen, X.; Dai, H. *Nat. Nanotechnol.* **2007**, *2*, 47.

(74) Ahmed, M.; Jiang, X. Z.; Deng, Z. C.; Narain, R. *Bioconjugate Chem.* **2009**, *20*, 2017.

(75) Liu, Z.; Chen, K.; Davis, C.; Sherlock, S.; Cao, Q. Z.; Chen, X. Y.; Dai, H. J. *Cancer Res.* **2008**, *68*, 6652.

(76) Chen, R. J.; Zhang, Y.; Wang, D.; Dai, H. *J. Am. Chem. Soc.* **2001**, *123*, 3838.

(77) Wu, P.; Chen, X.; Hu, N.; Tam, U. C.; Blixt, O.; Zettl, A.; Bertozzi, C. R. *Angew. Chem. Int. Ed.* **2008**, *47*, 5022.

(78) Chung, C. L.; Gautier, C.; Campidelli, S.; Filoramo, A. *Chem. Commun.* **2010**, *46*, 6539.

(79) Balavoine, F.; Schultz, P.; Richard, C.; Mallouh, V.; Ebbesen, T. W.; Mioskowski, C. *Angew. Chem. Int. Ed.* **1999**, *38*, 1912.

(80) Kam, N. W.; Liu, Z.; Dai, H. *J. Am. Chem. Soc.* **2005**, *127*, 12492.

(81) Zanello, L. P.; Zhao, B.; Hu, H.; Haddon, R. C. *Nano Lett.* **2006**, *6*, 562.

(82) Bradley, K.; Briman, M.; Star, A.; Gruner, G. *Nano Lett.* **2004**, *4*, 253.

(83) Wang, S.; Humphreys, E. S.; Chung, S. Y.; Delduco, D. F.; Lustig, S. R.; Wang, H.; Parker, K. N.; Rizzo, N. W.; Subramoney, S.; Chiang, Y. M.; Jagota, A. *Nat. Mater.* **2003**, *2*, 196.

(84) Nepal, D.; Geckeler, K. E. *Small* **2007**, *3*, 1259.

(85) Valenti, L. E.; Fiorito, P. A.; Garcia, C. D.; Giacomelli, C. E. *J. Colloid Interf. Sci.* **2007**, *307*, 349.

(86) Matsuura, K.; Saito, T.; Okazaki, T.; Ohshima, S.; Yumura, M.; Iijima, S. *Chem. Phys. Lett.* **2006**, *429*, 497.

(87) Fahmy, T. M.; Fadel, T. R.; Steenblock, E. R.; Stern, E.; Li, N.; Wang, X. M.; Haller, G. L.; Pfefferle, L. D. *Nano Lett.* **2008**, *8*, 2070.

(88) Zheng, M.; Jagota, A.; Semke, E. D.; Diner, B. A.; Mclean, R. S.; Lustig, S. R.; Richardson, R. E.; Tassi, N. G. *Nat. Mater.* **2003**, *2*, 338.

(89) Zheng, M.; Jagota, A.; Strano, M. S.; Santos, A. P.; Barone, P.; Chou, S. G.; Diner, B. A.; Dresselhaus, M. S.; McLean, R. S.; Onoa, G. B.; Samsonidze, G. G.; Semke, E. D.; Usrey, M.; Walls, D. J. *Science* **2003**, *302*, 1545.

(90) Allen, B. L.; Kichambare, P. D.; Star, A. *Adv. Mater.* **2007**, *19*, 1439.

(91) Chen, Y.; Liu, H.; Ye, T.; Kim, J.; Mao, C. *J. Am. Chem. Soc.* **2007**, *129*, 8696.

(92) Sanchez-Pomales, G.; Santiago-Rodriguez, L.; Cabrera, C. R. *J. Nanosci. Nanotechnol.* **2009**, *9*, 2175.

(93) Yang, R. H.; Wang, H.; Yang, L.; Tan, W. H. *ACS Nano* **2009**, *3*, 2451.

(94) Zhang, Z.; Yang, X.; Zhang, Y.; Zeng, B.; Wang, S.; Zhu, T.; Roden, R. B.; Chen, Y.; Yang, R. *Clin. Cancer Res.* **2006**, *12*, 4933.

(95) Cloninger, M. J. *Curr. Opin. Chem. Biol.* **2002**, *6*, 742.

(96) Chen, X.; Lee, G. S.; Zettl, A.; Bertozzi, C. R. *Angew Chem Int Ed Engl* **2004**, *43*, 6111.

(97) Liu, Y.; Liang, P.; Zhang, H. Y.; Guo, D. S. *Small* **2006**, *2*, 874.

(98) Hasegawa, T.; Fujisawa, T.; Numata, M.; Umeda, M.; Matsumoto, T.; Kimura, T.; Okumura, S.; Sakurai, K.; Shinkai, S. *Chem. Commun.* **2004**, 2150.

(99) Numata, M.; Asai, M.; Kaneko, K.; Bae, A. H.; Hasegawa, T.; Sakurai, K.; Shinkai, S. *J. Am. Chem. Soc.* **2005**, *127*, 5875.

(100) Numata, M.; Sugikawa, K.; Kaneko, K.; Shinkai, S. *Chemistry* **2008**, *14*, 2398.

(101) Star, A.; Joshi, V.; Han, T. R.; Altoe, M. V. P.; Gruner, G.; Stoddart, J. F. *Org. Lett.* **2004**, *6*, 2089.

(102) Star, A.; Steuerman, D. W.; Heath, J. R.; Stoddart, J. F. *Angew. Chem. Int. Ed.* **2002**, *41*, 2508.

(103) Bandyopadhyaya, R.; Nativ-Roth, E.; Regev, O.; Yerushalmi-Rozen, R. *Nano Lett.* **2002**, *2*, 25.

(104) Kim, O. K.; Je, J. T.; Baldwin, J. W.; Kooi, S.; Pehrsson, P. E.; Buckley, L. J. *J. Am. Chem. Soc.* **2003**, *125*, 4426.

(105) Dodziuk, H.; Ejchart, A.; Anczewski, W.; Ueda, H.; Krinichnaya, E.; Dolgonos, G.; Kutner, W. *Chem. Commun.* **2003**, 986.

(106) Chen, X.; Lee, G. S.; Zettl, A.; Bertozzi, C. R. *Angew. Chem. Int. Ed.* **2004**, *43*, 6111.

(107) Khiar, N.; Assali, M.; Leal, M. P.; Fernandez, I.; Baati, R.; Mioskowski, C. *Soft Matter* **2009**, *5*, 948.

(108) Khiar, N.; Leal, M. P.; Baati, R.; Ruhlmann, C.; Mioskowski, C.; Schultz, P.; Fernandez, I. *Chem. Commun.* **2009**, 4121.

(109) Wang, H.; Gu, L.; Lin, Y.; Lu, F.; Meziani, M. J.; Luo, P. G.; Wang, W.; Cao, L.; Sun, Y. P. *J. Am. Chem. Soc.* **2006**, *128*, 13364.

(110) Gu, L.; Elkin, T.; Jiang, X.; Li, H.; Lin, Y.; Qu, L.; Tzeng, T. R.; Joseph, R.; Sun, Y. P. *Chem. Commun.* **2005**, 874.

(111) Gu, L.; Lin, Y.; Qu, L.; Sun, Y. P. *Biomacromolecules* **2006**, *7*, 400.

(112) Zhang, X.; Meng, L.; Lu, Q. *ACS Nano* **2009**, *3*, 3200.

(113) Prato, M. *Nature* **2010**, *465*, 172.

(114) Itkis, M. E.; Niyogi, S.; Meng, M. E.; Hamon, M. A.; Hu, H.; Haddon, R. C. *Nano Lett.* **2002**, *2*, 155.

(115) Niyogi, S.; Hamon, M. A.; Hu, H.; Zhao, B.; Bhowmik, P.; Sen, R.; Itkis, M. E.; Haddon, R. C. *Acc. Chem. Res.* **2002**, *35*, 1105.

(116) Strano, M. S.; Dyke, C. A.; Usrey, M. L.; Barone, P. W.; Allen, M. J.; Shan, H. W.; Kittrell, C.; Hauge, R. H.; Tour, J. M.; Smalley, R. E. *Science* **2003**, *301*, 1519.

(117) Lee, K. M.; Li, L. C.; Dai, L. M. *J. Am. Chem. Soc.* **2005**, *127*, 4122.

(118) Moghaddam, M. J.; Taylor, S.; Gao, M.; Huang, S. M.; Dai, L. M.; McCall, M. J. *Nano Lett.* **2004**, *4*, 89.

(119) Coleman, K. S.; Bailey, S. R.; Fogden, S.; Green, M. L. H. *J. Am. Chem. Soc.* **2003**, *125*, 8722.

(120) Georgakilas, V.; Kordatos, K.; Prato, M.; Guldi, D. M.; Holzinger, M.; Hirsch, A. *J. Am. Chem. Soc.* **2002**, *124*, 760.

(121) Tagmatarchis, N.; Prato, M. *J. Mater. Chem.* **2004**, *14*, 437.

(122) Lacerda, L.; Soundararajan, A.; Singh, R.; Pastorin, G.; Al-Jamal, K. T.; Turton, J.; Frederik, P.; Herrero, M. A.; Bao, S. L. A.; Emfietzoglou, D.; Mather, S.; Phillips, W. T.; Prato, M.; Bianco, A.; Goins, B.; Kostarelos, K. *Adv. Mater.* **2008**, *20*, 225.

(123) McDevitt, M. R.; Chattopadhyay, D.; Jaggi, J. S.; Finn, R. D.; Zanzonico, P. B.; Villa, C.; Rey, D.; Mendenhall, J.; Batt, C. A.; Njardarson, J. T.; Scheinberg, D. A. *PLoS One* **2007**, *2*.

(124) Yandar, N.; Pastorin, G.; Prato, M.; Bianco, A.; Patarroyo, M. E.; Manuel Lozano, J. *Vaccine* **2008**, *26*, 5864.

(125) Pantarotto, D.; Partidos, C. D.; Hoebeke, J.; Brown, F.; Kramer, E.; Briand, J. P.; Muller, S.; Prato, M.; Bianco, A. *Chem. Biol.* **2003**, *10*, 961.

(126) McDevitt, M. R.; Chattopadhyay, D.; Kappel, B. J.; Jaggi, J. S.; Schiffman, S. R.; Antczak, C.; Njardarson, J. T.; Brentjens, R.; Scheinberg, D. A. *J. Nucl. Med.* **2007**, *48*, 1180.

(127) Podesta, J. E.; Al-Jamal, K. T.; Herrero, M. A.; Tian, B.; Ali-Boucetta, H.; Hegde, V.; Bianco, A.; Prato, M.; Kostarelos, K. *Small* **2009**, *5*, 1176.

(128) Hu, H.; Zhao, B.; Itkis, M. E.; Haddon, R. C. *J. Phys. Chem. B* **2003**, *107*, 13838.

(129) Haddon, R. C. *Science* **1993**, *261*, 1545.

(130) Tohji, K.; Goto, T.; Takahashi, H.; Shinoda, Y.; Shimizu, N.; Jeyadevan, B.; Matsuoka, I.; Saito, Y.; Kasuya, A.; Ohsuna, T.; Hiraga, H.; Nishina, Y. *Nature* **1996**, *383*, 679.

(131) Dillon, A. C.; Gennett, T.; Jones, K. M.; Alleman, J. L.; Parilla, P. A.; Heben, M. J. *Adv. Mater.* **1999**, *11*, 1354.

(132) Giordani, S.; Colomer, J. F.; Cattaruzza, F.; Alfonsi, J.; Meneghetti, M.; Prato, M.; Bonifazi, D. *Carbon* **2009**, *47*, 578.

(133) Rinzler, A. G.; Liu, J.; Dai, H.; Nikolaev, P.; Huffman, C. B.; Rodriguez-Macias, F. J.; Boul, P. J.; Lu, A. H.; Heymann, D.; Colbert, D. T.; Lee, R. S.; Fischer, J. E.; Rao, A. M.; Eklund, P. C.; Smalley, R. E. *Appl. Phys. A: Mater. Sci. Process.* **1998**, *67*, 29.

(134) Salzmann, C. G.; Llewellyn, S. A.; Tobias, G.; Ward, M. A. H.; Huh, Y.; Green, M. L. H. *Adv. Mater.* **2007**, *19*, 883.

(135) Shao, L.; Tobias, G.; Salzmann, C. G.; Ballesteros, B.; Hong, S. Y.; Crossley, A.; Davis, B. G.; Green, M. L. H. *Chem. Commun.* **2007**, 5090.

(136) Price, B. K.; Lomeda, J. R.; Tour, J. M. *Chem. Mater.* **2009**, *21*, 3917.

(137) Chen, J.; Hamon, M. A.; Hu, H.; Chen, Y. S.; Rao, A. M.; Eklund, P. C.; Haddon, R. C. *Science* **1998**, *282*, 95.

(138) Hamon, M. A.; Chen, J.; Hu, H.; Chen, Y. S.; Itkis, M. E.; Rao, A. M.; Eklund, P. C.; Haddon, R. C. *Adv. Mater.* **1999**, *11*, 834.

(139) Kahn, M. G. C.; Banerjee, S.; Wong, S. S. *Nano Lett.* **2002**, *2*, 1215.

(140) Hu, H.; Zhao, B.; Hamon, M. A.; Kamaras, K.; Itkis, M. E.; Haddon, R. C. *J. Am. Chem. Soc.* **2003**, *125*, 14893.

(141) Kostarelos, K.; Lacerda, L.; Pastorin, G.; Wu, W.; Wieckowski, S.; Luangsivilay, J.; Godefroy, S.; Pantarotto, D.; Briand, J. P.; Muller, S.; Prato, M.; Bianco, A. *Nat. Nanotechnol.* **2007**, *2*, 108.

(142) Del Canto, E.; Flavin, K.; Movia, D.; Navio, C.; Bittencourt, C.; Giordani, S. *Chem. Mater.* **2011**, *23*, 67.

(143) Wang, H. F.; Wang, J.; Deng, X. Y.; Sun, H. F.; Shi, Z. J.; Gu, Z. N.; Liu, Y. F.; Zhao, Y. L. *J. Nanosci. Nanotechnol.* **2004**, *4*, 1019.

(144) Yang, S. T.; Guo, W.; Lin, Y.; Deng, X. Y.; Wang, H. F.; Sun, H. F.; Liu, Y. F.; Wang, X.; Wang, W.; Chen, M.; Huang, Y. P.; Sun, Y. P. *J. Phys. Chem. C* **2007**, *111*, 17761.

(145) Bhirde, A. A.; Patel, V.; Gavard, J.; Zhang, G.; Sousa, A. A.; Masedunskas, A.; Leapman, R. D.; Weigert, R.; Gutkind, J. S.; Rusling, J. F. *ACS Nano* **2009**, *3*, 307.

(146) Elkin, T.; Jiang, X. P.; Taylor, S.; Lin, Y.; Gu, L. R.; Yang, H.; Brown, J.; Collins, S.; Sun, Y. P. *Chembiochem* **2005**, *6*, 640.

(147) Li, S.; He, P.; Dong, J.; Guo, Z.; Dai, L. *J. Am. Chem. Soc.* **2005**, *127*, 14.

(148) Wang, X.; Liu, F.; Andavan, G. T. S.; Jing, X. Y.; Singh, K.; Yazdanpanah, V. R.; Bruque, N.; Pandey, R. R.; Lake, R.; Ozkan, M.; Wang, K. L.; Ozkan, C. S. *Small* **2006**, *2*, 1356.

(149) Lee, C. S.; Baker, S. E.; Marcus, M. S.; Yang, W. S.; Eriksson, M. A.; Hamers, R. J. *Nano Lett.* **2004**, *4*, 1713.

(150) Rege, K.; Viswanathan, G.; Zhu, G. Y.; Vijayaraghavan, A.; Ajayan, P. M.; Dordick, J. S. *Small* **2006**, *2*, 718.

(151) Liu, Z.; Winters, M.; Holodniy, M.; Dai, H. *Angew. Chem. Int. Ed.* **2007**, *46*, 2023.

(152) Tan, W. H.; Wu, Y. R.; Phillips, J. A.; Liu, H. P.; Yang, R. H. *ACS Nano* **2008**, *2*, 2023.

(153) Bertozzi, C. R.; Kiessling, L. L. *Science* **2001**, *291*, 2357.

(154) Farokhzad, O. C.; Langer, R. *ACS Nano* **2009**, *3*, 16.

(155) Vashist, S. K.; Zheng, D.; Pastorin, G.; Al-Rubeaan, K.; Luong, J. H. T.; Sheu, F.-S. *Carbon* **2011**, *49*, 4077.

(156) Zhang, Y. G.; Yang, Z.; Yang, Y. L. A.; Sun, L.; Han, D.; Li, H.; Wang, C. *Nanomedicine - Nanotechnology Biology and Medicine* **2010**, *6*, 427.

(157) *Principles and Practice of Infectious Diseases*; 6th ed.; Mandell, G. L.; Bennett, J. E.; Dolin, R., Eds.; Churchill Livingstone, 2004.

(158) Kam, N. W. S.; Dai, H. J. *J. Am. Chem. Soc.* **2005**, *127*, 6021.

(159) Lacerda, L.; Raffa, S.; Prato, M.; Bianco, A.; Kostarelos, K. *Nano Today* **2007**, *2*, 38.

(160) Pantarotto, D.; Briand, J.-P.; Prato, M.; Bianco, A. *Chem. Commun.* **2004**, 16.

(161) Wu, W.; Wieckowski, S.; Pastorin, G.; Benincasa, M.; Klumpp, C.; Briand, J. P.; Gennaro, R.; Prato, M.; Bianco, A. *Angew. Chem. Int. Ed.* **2005**, *44*, 6358.

(162) Benincasa, M.; Pacor, S.; Wu, W.; Prato, M.; Bianco, A.; Gennaro, R. *ACS Nano* **2011**, *5*, 199.

(163) Liu, Z.; Sun, X. M.; Nakayama-Ratchford, N.; Dai, H. J. *ACS Nano* **2007**, *1*, 50.

(164) Liu, Z.; Fan, A. C.; Rakhra, K.; Sherlock, S.; Goodwin, A.; Chen, X. Y.; Yang, Q. W.; Felsher, D. W.; Dai, H. J. *Angew. Chem. Int. Ed.* **2009**, *48*, 7668.

(165) Heister, E.; Neves, V.; Tilmaciu, C.; Lipert, K.; Beltran, V. S.; Coley, H. M.; Silva, S. R. P.; McFadden, J. *Carbon* **2009**, *47*, 2152.

(166) Zhang, X.; Meng, L.; Lu, Q.; Fei, Z.; Dyson, P. J. *Biomaterials* **2009**, *30*, 6041.

(167) Chaudhuri, P.; Soni, S.; Sengupta, S. *Nanotechnology* **2010**, *21*, 025102.

(168) Sudimack, J.; Lee, R. J. *Adv. Drug Delivery Rev.* **2000**, *41*, 147.

(169) Chen, J.; Chen, S.; Zhao, X.; Kuznetsova, L. V.; Wong, S. S.; Ojima, I. *J. Am. Chem. Soc.* **2008**, *130*, 16778.

(170) Feazell, R. P.; Nakayama-Ratchford, N.; Dai, H.; Lippard, S. J. *J. Am. Chem. Soc.* **2007**, *129*, 8438.

(171) Dhar, S.; Liu, Z.; Thomale, J.; Lippard, S. J.; Dai, H. J. *J. Am. Chem. Soc.* **2008**, *130*, 11467.

(172) Tripisciano, C.; Kraemer, K.; Taylor, A.; Borowiak-Palen, E. *Chem. Phys. Lett.* **2009**, *478*, 200.

(173) Wang, X.; Ren, J.; Qu, X. *ChemMedChem* **2008**, *3*, 940.

(174) Wang, X.; Song, Y.; Ren, J.; Qu, X. *PLoS One* **2009**, *4*, e6665.

(175) Nguyen, T.; Menocal, E. M.; Harborth, J.; Fruehauf, J. H. *Curr. Opin. Mol. Ther.* **2008**, *10*, 158.

(176) Lanner, J. T.; Bruton, J. D.; Assefaw-Redda, Y.; Andronache, Z.; Zhang, S. J.; Severa, D.; Zhang, Z. B.; Melzer, W.; Zhang, S. L.; Katz, A.; Westerblad, H. *Faseb J.* **2009**, *23*, 1728.

(177) Kam, N. W. S.; O'Connell, M.; Wisdom, J. A.; Dai, H. J. *PNAS* **2005**, *102*, 11600.

(178) Shao, N.; Lu, S.; Wickstrom, E.; Panchapakesan, B. *Nanotechnology* **2007**, *18*.

(179) Moon, H. K.; Lee, S. H.; Choi, H. C. *ACS Nano* **2009**.

(180) Kang, B.; Yu, D. C.; Dai, Y. D.; Chang, S. Q.; Chen, D.; Ding, Y. T. *Small* **2009**, *5*, 1292.

(181) Biris, A. R.; Ardelean, S.; Lupu, D.; Misan, I.; Iancu, C.; Bartos, D. M.; Ilie, I. R.; Dervishi, E.; Xu, Y.; Biswas, A.; Biris, A. S. *Carbon* **2011**, *49*, 4403.

(182) Chaban, V. V.; Savchenko, T. I.; Kovalenko, S. M.; Prezhdo, O. V. *J. Phys. Chem. B* **2010**, *114*, 13481.

(183) Su, Z. D.; Zhu, S. H.; Donkor, A. D.; Tzoganakis, C.; Honek, J. F. *J. Am. Chem. Soc.* **2011**, *133*, 6874.

(184) Kang, S.; Pinault, M.; Pfefferle, L. D.; Elimelech, M. *Langmuir* **2007**, *23*, 8670.

(185) Liu, S.; Wei, L.; Hao, L.; Fang, N.; Chang, M. W.; Xu, R.; Yang, Y.; Chen, Y. *ACS Nano* **2009**, *3*, 3891.

(186) Elimelech, M. *Mater. Technol.* **2007**, *22*, 179.

(187) Luo, P. G.; Wang, H.; Gu, L.; Lu, F.; Lin, Y.; Christensen, K. A.; Yang, S. T.; Sun, Y. P. *ACS Nano* **2009**, *3*, 3909.

(188) Lucente-Schultz, R. M.; Moore, V. C.; Leonard, A. D.; Price, B. K.; Kosynkin, D. V.; Lu, M.; Partha, R.; Conyers, J. L.; Tour, J. M. *J. Am. Chem. Soc.* **2009**, *131*, 3934.

(189) Lee, H. J.; Park, J.; Yoon, O. J.; Kim, H. W.; Lee, D. Y.; Kim, D. H.; Lee, W. B.; Lee, N. E.; Bonventre, J. V.; Kim, S. S. *Nat. Nanotechnol.* **2011**, *6*, 120.

(190) Cui, H. F.; Vashist, S. K.; Al-Rubeaan, K.; Luong, J. H. T.; Sheu, F. S. *Chemical Research in Toxicology* **2010**, *23*, 1131.

(191) Namgung, S.; Baik, K. Y.; Park, J.; Hong, S. *ACS Nano* **2011**, DOI: 10.1021/nn2023057.

(192) Smart, S. K.; Cassady, A. I.; Lu, G. Q.; Martin, D. J. *Carbon* **2006**, *44*, 1034.

(193) Lacerda, L.; Bianco, A.; Prato, M.; Kostarelos, K. *Adv Drug Deliver Rev* **2006**, *58*, 1460.

(194) Yun, Y.; Dong, Z.; Shanov, V.; Heineman, W. R.; Halsall, H. B.; Bhattacharya, A.; Conforti, L.; Narayan, R. K.; Ball, W. S.; Schulz, M. J. *Nano Today* **2007**, *2*, 30.

(195) Avouris, P.; Chen, Z. H.; Perebeinos, V. *Nat. Nanotechnol.* **2007**, *2*, 605.

(196) Gruner, G. *Anal. Bioanal. Chem.* **2006**, *384*, 322.

(197) Kong, J.; Franklin, N. R.; Zhou, C.; Chapline, M. G.; Peng, S.; Cho, K.; Dai, H. *Science* **2000**, *287*, 622.

(198) Maehashi, K.; Katsura, T.; Kerman, K.; Takamura, Y.; Matsumoto, K.; Tamiya, E. *Anal Chem* **2007**, *79*, 782.

(199) Ahn, J. H.; Kim, J. H.; Reuel, N. F.; Barone, P. W.; Boghossian, A. A.; Zhang, J.; Yoon, H.; Chang, A. C.; Hilmer, A. J.; Strano, M. S. *Nano Lett.* **2011**.

(200) Boussaad, S.; Tao, N. J.; Zhang, R.; Hopson, T.; Nagahara, L. A. *Chem. Commun.* **2003**, 1502.

(201) Gui, E. L.; Li, L. J.; Zhang, K.; Xu, Y.; Dong, X.; Ho, X.; Lee, P. S.; Kasim, J.; Shen, Z. X.; Rogers, J. A.; Mhaisalkar, S. G. *J. Am. Chem. Soc.* **2007**, *129*, 14427.

(202) Star, A.; Tu, E.; Niemann, J.; Gabriel, J. C.; Joiner, C. S.; Valcke, C. *PNAS* **2006**, *103*, 921.

(203) Martinez, M. T.; Tseng, Y. C.; Ormategui, N.; Loinaz, I.; Eritja, R.; Bokor, J. *Nano Lett.* **2009**, *9*, 530.

(204) Li, C.; Curreli, M.; Lin, H.; Lei, B.; Ishikawa, F. N.; Datar, R.; Cote, R. J.; Thompson, M. E.; Zhou, C. *J. Am. Chem. Soc.* **2005**, *127*, 12484.

(205) Besteman, K.; Lee, J. O.; Wiertz, F. G. M.; Heering, H. A.; Dekker, C. *Nano Lett.* **2003**, *3*, 727.

(206) Star, A.; Gabriel, J. C. P.; Bradley, K.; Gruner, G. *Nano Lett.* **2003**, *3*, 459.

(207) Byon, H. R.; Choi, H. C. *J. Am. Chem. Soc.* **2006**, *128*, 2188.

(208) Staii, C.; Johnson, A. T.; Chen, M.; Gelperin, A. *Nano Lett.* **2005**, *5*, 1774.

(209) Franchini, M.; Veneri, D. *Ann. Hematol.* **2005**, *84*, 347.

(210) Limdi, J. K.; Crampton, J. R. *QJM* **2004**, *97*, 315.

(211) Liu, X. W.; Sudibya, H. G.; Ma, J. M.; Dong, X. C.; Ng, S.; Li, L. J.; Chen, P. *Angew. Chem. Int. Ed.* **2009**, *48*, 2723.

(212) Holzinger, M.; Baur, J.; Haddad, R.; Wang, X.; Cosnier, S. *Chem. Commun.* **2011**, *47*, 2450.

(213) Weisman, R. B.; Bachilo, S. M.; Tsyboulski, D. *Appl. Phys. A: Mater. Sci. Process.* **2004**, *78*, 1111.

(214) Satishkumar, B. C.; Brown, L. O.; Gao, Y.; Wang, C. C.; Wang, H. L.; Doorn, S. K. *Nat. Nanotechnol.* **2007**, *2*, 560.

(215) Barone, P. W.; Strano, M. S. *Angew. Chem. Int. Ed.* **2006**, *45*, 8138.

(216) Heller, D. A.; Jeng, E. S.; Yeung, T. K.; Martinez, B. M.; Moll, A. E.; Gastala, J. B.; Strano, M. S. *Science* **2006**, *311*, 508.

(217) Cha, T. G.; Baker, B. A.; Sauffer, M. D.; Salgado, J.; Jaroch, D.; Rickus, J. L.; Porterfield, D. M.; Choi, J. H. *ACS Nano* **2011**, *5*, 4236.

(218) Heller, D. A.; Jin, H.; Martinez, B. M.; Patel, D.; Miller, B. M.; Yeung, T. K.; Jena, P. V.; Hobartner, C.; Ha, T.; Silverman, S. K.; Strano, M. S. *Nat. Nanotechnol.* **2009**, *4*, 114.

(219) Lin, Y.; Zhou, B.; Martin, R. B.; Henbest, K. B.; Harruff, B. A.; Riggs, J. E.; Guo, Z. X.; Allard, L. F.; Sun, Y. P. *J. Phys. Chem. B* **2005**, *109*, 14779.

(220) Guldi, D. M.; Holzinger, M.; Hirsch, A.; Georgakilas, V.; Prato, M. *Journal of Chemical Communications* **2003**, 1130.

(221) Qian, Z.; Wang, C.; Feng, H.; Chen, C.; Zhou, J.; Chen, J. *Chem. Commun.* **2011**, *47*, 7167.

(222) Nakayama-Ratchford, N.; Bangsaruntip, S.; Sun, X.; Welsher, K.; Dai, H. *J. Am. Chem. Soc.* **2007**, *129*, 2448.

(223) Hong, S. Y.; Tobias, G.; Al-Jamal, K. T.; Ballesteros, B.; Ali-Boucetta, H.; Lozano-Perez, S.; Nellist, P. D.; Sim, R. B.; Finucane, C.; Mather, S. J.; Green, M. L. H.; Kostarelos, K.; Davis, B. G. *Nat. Mater.* **2010**, *9*, 485.

(224) Strano, M. S. *Nat. Mater.* **2010**, *9*, 467.

(225) Riggs, J. E.; Guo, Z. X.; Carroll, D. L.; Sun, Y. P. *J. Am. Chem. Soc.* **2000**, *122*, 5879.

(226) Ferrari, A. C.; Robertson, J. *Phys. Rev. B* **2000**, *61*, 14095.

(227) Lacerda, L.; Pastorin, G.; Gathercole, D.; Buddle, J.; Prato, M.; Bianco, A.; Kostarelos, K. *Adv. Mater.* **2007**, *19*, 1480.

(228) Espina, V.; Woodhouse, E. C.; Wulfkuhle, J.; Asmussen, H. D.; Petricoin, E. F.; Liotta, L. A. *J. Immunol. Methods* **2004**, *290*, 121.

(229) Chen, Z.; Tabakman, S. M.; Goodwin, A. P.; Kattah, M. G.; Daranciang, D.; Wang, X. R.; Zhang, G. Y.; Li, X. L.; Liu, Z.; Utz, P. J.; Jiang, K. L.; Fan, S. S.; Dai, H. J. *Nat. Biotechnol.* **2008**, *26*, 1285.

(230) Liu, Z.; Davis, C.; Cai, W. B.; He, L.; Chen, X. Y.; Dai, H. J. *PNAS* **2008**, *105*, 1410.

(231) Xu, M. H.; Wang, L. H. V. *Rev. Sci. Instrum.* **2006**, *77*.

(232) de la Zerda, A.; Liu, Z.; Bodapati, S.; Teed, R.; Vaithilingam, S.; Khuri-Yakub, B. T.; Chen, X.; Dai, H.; Gambhir, S. S. *Nano Lett.* **2010**, *10*, 2168.

(233) Torchilin, V. P. *Adv. Drug Delivery Rev.* **2006**, *58*, 1532.

(234) Nel, A.; Xia, T.; Madler, L.; Li, N. *Science* **2006**, *311*, 622.

(235) Kostarelos, K. *Adv. Colloid Interface Sci.* **2003**, *106*, 147.

(236) Lacerda, L.; Herrero, M. A.; Venner, K.; Bianco, A.; Prato, M.; Kostarelos, K. *Small* **2008**, *4*, 1130.

(237) Singh, R.; Pantarotto, D.; Lacerda, L.; Pastorin, G.; Klumpp, C.; Prato, M.; Bianco, A.; Kostarelos, K. *P Natl Acad Sci USA* **2006**, *103*, 3357.

(238) Lacerda, L.; Ali-Boucettal, H.; Herrero, M. A.; Pastorin, G.; Bianco, A.; Prato, M.; Kostarelos, K. *Nanomedicine* **2008**, *3*, 149.

(239) Ruggiero, A.; Villa, C. H.; Bander, E.; Rey, D. A.; Bergkvist, M.; Batt, C. A.; Manova-Todorova, K.; Deen, W. M.; Scheinberg, D. A.; McDevitt, M. R. *PNAS* **2010**, *107*, 12369.

(240) Cherukuri, P.; Gannon, C. J.; Leeuw, T. K.; Schmidt, H. K.; Smalley, R. E.; Curley, S. A.; Weisman, R. B. *P Natl Acad Sci USA* **2006**, *103*, 18882.

(241) Kostarelos, K. *Nat. Mater.* **2010**, *9*, 793.

(242) Heister, E.; Lamprecht, C.; Neves, V.; Tilmaciu, C.; Datas, L.; Flahaut, E.; Soula, B.; Hinterdorfer, P.; Coley, H. M.; Silva, S. R. P.; McFadden, J. *ACS Nano* **2010**, *4*, 2615.

(243) Becker, M. L.; Fagan, J. A.; Gallant, N. D.; Bauer, B. J.; Bajpai, V.; Hobbie, E. K.; Lacerda, S. H.; Migler, K. B.; Jakupciak, J. P. *Adv. Mater.* **2007**, *19*, 939.

(244) Jin, H.; Heller, D. A.; Sharma, R.; Strano, M. S. *ACS Nano* **2009**, *3*, 149.

(245) Kostarelos, K.; Lacerda, L.; Pastorin, G.; Wu, W.; Wieckowski, S.; Luangsivilay, J.; Godefroy, S.; Pantarotto, D.; Briand, J. P.; Muller, S.; Prato, M.; Bianco, A. *Nat Nanotechnol* **2007**, *2*, 108.

(246) Lacerda, L.; Pastorin, G.; Gathercole, D.; Buddle, J.; Prato, M.; Bianco, A.; Kostarelos, K. *Advanced Materials* **2007**, *19*, 1480.

(247) Pantarotto, D.; Briand, J. P.; Prato, M.; Bianco, A. *Chem. Commun.* **2004**, 16.

(248) Pantarotto, D.; Singh, R.; McCarthy, D.; Erhardt, M.; Briand, J. P.; Prato, M.; Kostarelos, K.; Bianco, A. *Angew. Chem., Int. Ed.* **2004**, *43*, 5242.

(249) Dumortier, H.; Lacotte, S.; Pastorin, G.; Marega, R.; Wu, W.; Bonifazi, D.; Briand, J. P.; Prato, M.; Muller, S.; Bianco, A. *Nano Letters* **2006**, *6*, 1522.

(250) Kisin, E. R.; Murray, A. R.; Keane, M. J.; Shi, X. C.; Schwegler-Berry, D.; Gorelik, O.; Arepalli, S.; Castranova, V.; Wallace, W. E.; Kagan, V. E.; Shvedova, A. A. *J. Toxicol. Environ. Health, Part A* **2007**, *70*, 2071.

(251) Heller, D. A.; Baik, S.; Eurell, T. E.; Strano, M. S. *Advanced Materials* **2005**, *17*, 2793.

(252) Kam, N. W. S.; O'Connell, M.; Wisdom, J. A.; Dai, H. J. *P Natl Acad Sci USA* **2005**, *102*, 11600.

(253) Jin, H.; Heller, D. A.; Strano, M. S. *Nano Letters* **2008**, *8*, 1577.

(254) Van den Bossche, J.; Al-Jamal, W. T.; Tian, B.; Nunes, A.; Fabbro, C.; Bianco, A.; Prato, M.; Kostarelos, K. *Chem. Commun.* **2010**, *46*, 7379.

(255) Mu, Q. X.; Broughton, D. L.; Yan, B. *Nano Lett.* **2009**, *9*, 4370.

(256) Porter, A. E.; Gass, M.; Bendall, J. S.; Muller, K.; Goode, A.; Skepper, J. N.; Midgley, P. A.; Welland, M. *ACS Nano* **2009**, *3*, 1485.

(257) Zhou, F. F.; Xing, D.; Wu, B. Y.; Wu, S. N.; Ou, Z. M.; Chen, W. R. *Nano Lett.* **2010**, *10*, 1677.

CHAPTER II.
PURIFIED AND COVALENTLY FUNCTIONALISED SWNTS AS ROBUST NEAR-IR FLUORESCENT PROBES FOR MOLECULAR IMAGING

CONTENTS

1. INTRODUCTION

Over the last years the application of SWNTs in various imaging techniques with clinical relevance[1] (such as molecular magnetic resonance imaging (MRI),[2-4] optical fluorescence,[5] photoacoustic tomography (PAT)[6-8] and positron emission tomography (PET)[9]) has been extensively explored. To exploit such techniques, radioactive and fluorescent moieties were bound onto the carbon nanotubes' surface both covalently and non-covalently.

Thanks to their unique, intrinsic optical properties, SWNTs have also been investigated as molecular probes in four other imaging techniques, namely Raman spectroscopy,[10] Vis optical imaging,[5] photoacoustic imaging[6] and NIR photoluminescence (PL).[11-16]

1.1. OPTICAL PROPERTIES OF SWNTS

The optical properties of SWNTs refer specifically to those detected by means of absorption and emission spectroscopies and derive from the electronic transitions within density of states (DOS). One-dimensional (1D) nanomaterials (such as CNTs) are characterized by non-continuous DOS that generates discontinuous spikes in the electronic transitions (Figure 2.1a, b). These sharp peaks are called van Hove (vH) singularities and the energies between them are strictly correlated to the nanotube structure.

The optical transitions that occur between the v_1-c_1 and v_2-c_2, states are traditionally labeled as S_{11} and S_{22} for semiconducting SWNTs (Figure 2.1a), and M_{11} for metallic SWNTs (Figure 2.1b). If the conductivity properties of SWNTs are not taken into account, these optical transitions can also be referred to as E_{11} and E_{22}, respectively.

1.1.1. Absorption properties of SWNTs

Absorption spectra of non-functionalised SWNTs exhibit well-resolved bands (Figure 2.1c) which arise from transitions between symmetrical vH singularities (namely, v_1-c_1 or v_2-c_2) in the electronic DOS of the tube (Figure 2.1a, b). As the band gap energy of SWNTs is related to their chirality and diameter,[17] each (*n*,*m*) SWNT species is identified by a different set of vH transitions. In detail, the absorption bands in the range 400-600 nm correspond to the first vH transitions of metallic tubes (M_{11}), those within the 550-900 nm range are due to the second vH transitions of semiconducting tubes

(S_{22}), while the bands within the 900-1100 nm range originate from the first vH transitions (S_{11}) of the semiconducting nanotubes with small diameters (Figure 2.1c). Finally, semiconducting nanotubes with large diameters show a S_{11} transition in the optical window 1100-1600 nm (Figure 2.1c).[18] Dispersions dominated by individual tubes show spectra with sharp, well-resolved transitions, while an enrichment in bundles results in the overlapping of the transitions of the different SWNTs species and subsequently in the broadening of the absorption bands.[18] Covalent functionalisation methods, which modify SWNTs electronic structure by introducing defects on their π-conjugated skeleton, cause partial quenching or complete loss of their M_{11}, S_{11} and S_{22} absorption features.[18]

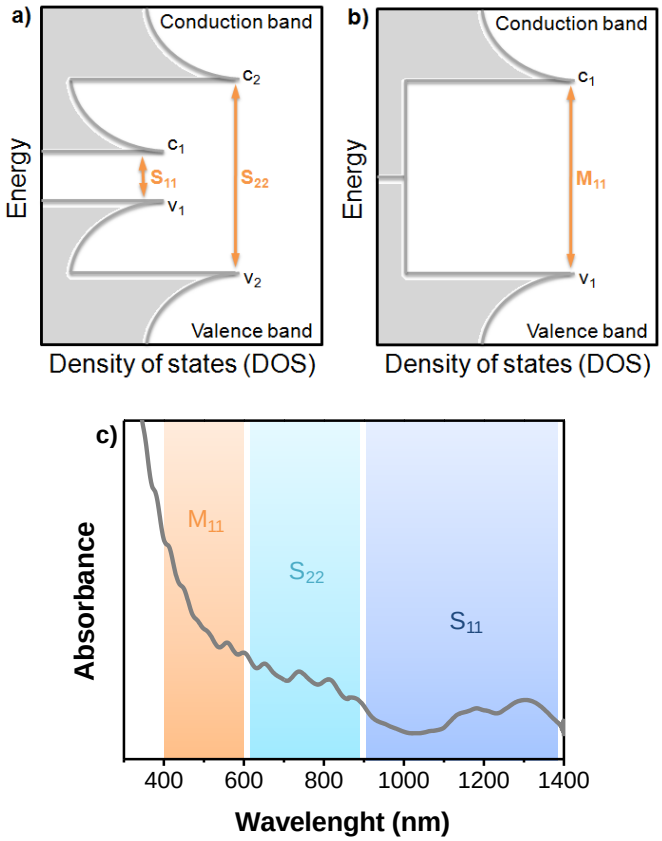

Figure 2.1. Diagram of the density of electronic states (DOS) of (a) semiconducting and (b) metallic SWNTs. Allowed absorption transitions are illustrated as vertical arrows. (c) Typical absorption spectra of raw HiPCO SWNTs dispersed in an aqueous solution of sodium dodecylbenzene sulphonate (SDBS).

1.1.2. Emission properties of SWNTs

It is documented that individual SWNTs with intact electronic structure exhibit efficient NIR photoluminescence (NIR-PL) (Figure 2.2a),[19] while functionalised SWNTs show significant emission in the visible range when excited at shorter wavelengths.[20-22]

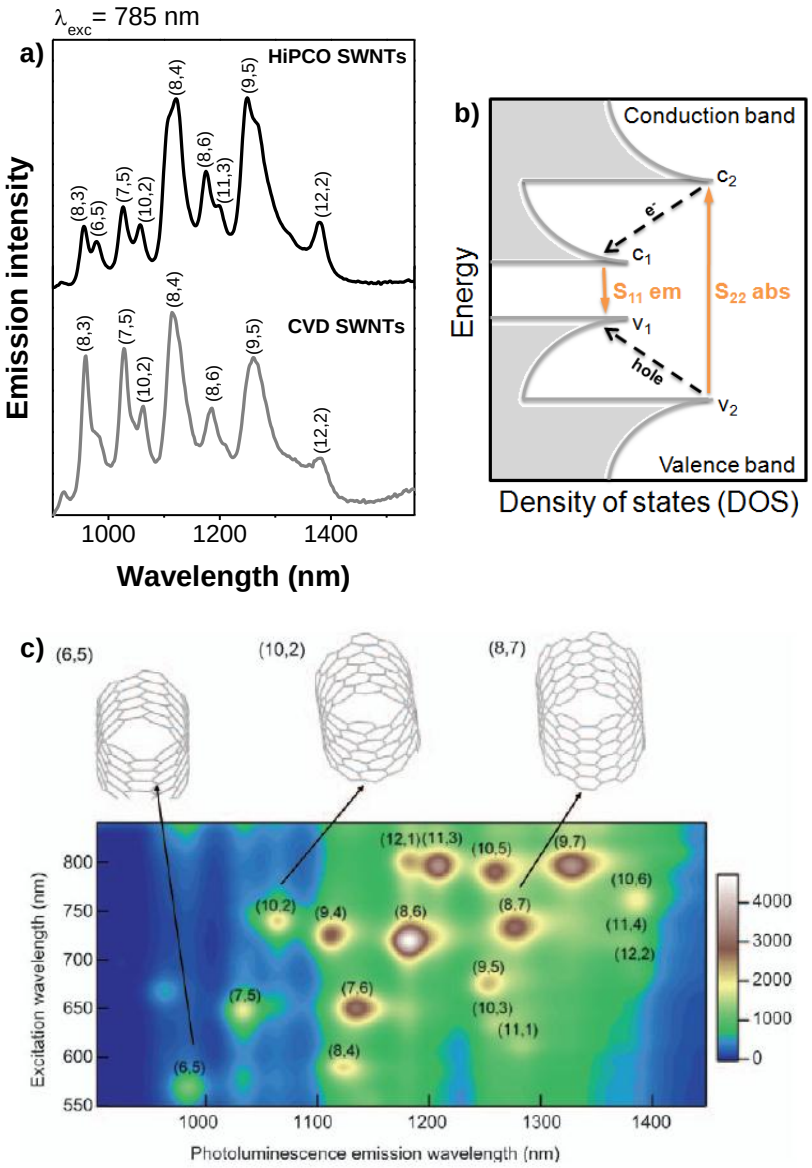

Figure 2.2. (a) NIR-PL spectra of unmodified SWNTs produced by HiPCO or CVD methods in a SDBS aqueous solution at excitation wavelength (λ_{exc}) of 785 nm. Identification of the (*n*,*m*) indexes for each optical transition have been carried out according to the Kataura plot.[17] (b) DOS diagram showing the electronic transitions contributing to the NIR emission of semiconducting SWNTs. (c) PL excitation and emission spectra of HiPCO SWNTs. SWNTs chiralities are assigned. Partial reproduction of an image from Liu *et al.*[23]

NIR-PL phenomena occur when an electron in a nanotube absorbs excitation light via E_{22} transition, creating an electron-hole pair (called exciton). Both electron and hole rapidly relax from c_2 to c_1 and from v_2 to v_1 states, respectively. Finally, they recombine through a c_1-v_1 transition, resulting in light emission in the NIR region (Figure 2.2b).[19] The relaxation time is typically quite short (within 100 ps),[24] while the spectral range in which SWNTs emit is rather wide, stretching between 900 and 1600 nm.[19] According to the mechanism described above, NIR-PL is observed only for semiconducting SWNTs. In metallic tubes electrons can in fact be excited, thus resulting in optical absorption, but the hole is immediately filled by another electron, thus quenching the light emission.

Much effort has been exerted on the spectroscopic assignment and prediction of optical transition frequencies for the different (*n,m*) species of semiconducting SWNTs (Figure 2.2c). Recently, fluorescent band-gap transitions from a variety of (*n,m*) SWNTs species have been calculated, and a theoretical graph based on this calculations has been designed by Hiromichi Kataura to rationalize the experimental findings.[17] The Kataura plot relates the *(n, m)* indexes, the diameter and the band-gap energy of each nanotube species. This plot illustrates the strong dependence of SWNTs properties on their *(n, m)* indexes rather than on their diameter. For example, SWNTs with indexes equal to (10,0) and (8,3) have almost the same diameter, but very different properties: the former is metallic, but the latter is semiconducting.

NIR fluorescence appears to be the SWNTs optical property that is most sensitive to sample aggregation,[25,26] environment[27,28] and surface chemistry.[29-31]

Aggregation The negative effect of SWNTs aggregation on their NIR-PL efficiency is due to the presence of metallic nanotubes within bundles; metallic SWNTs quench the relaxation of the electron-hole pair on an adjacent semiconducting tube, thus preventing its luminescence.[19,32] A necessary condition to improve the emission efficiency of SWNTs is therefore to achieve well-dispersed suspensions.[20] Surfactants are commonly used to obtain stable dispersions of individual SWNTs in water (see Chapter I, Section 3.2.1). Among these, sodium dodecylbenzene sulphonate (SDBS) has demonstrated the highest ability in dispersing SWNTs with no strong diameter dependence.[33,34] Typically, a nanotube/surfactant dispersion is produced by sonication and subsequent centrifugation (up to 122,000 ×*g*) in order to remove the residual bundles.[25,35] This results in a high mass loss. Another approach recently developed by Hasan *et al.* (2007)

stabilizes SWNTs dispersions in N-methyl-2-pyrrolidone (NMP) by addition of polyvinylpyrrolidone (PVP), a polymeric moiety.[32]

Environment The NIR-PL efficiency is also sensitive to the chemical environment. Changes in temperature[27] and/or addition of an acid[28] to the SWNTs suspension can cause fluorescence quenching. Acid quenching is reversible by addition of a base to restore a neutral or alkaline pH,[28] or it can be prevented by employing as dispersing agent a mixture of SDBS and biocompatible PVP.[36] Furthermore, changes in the dispersing agent employed produce spectral shifts of E_{11} and E_{22} transitions.[17]

Surface chemistry NIR-PL of SWNTs is very sensitive to surface chemistry and a partial or complete quenching of NIR-PL has been reported upon covalent functionalisation of SWNTs.[29]

1.2. SWNTs as NIR Fluorescent Probes for Molecular Imaging

The ability of SWNTs to emit efficiently in the NIR makes them promising candidates as NIR contrast agents[37] (see Chapter I, Section 3.3.2.2).

There are several parameters that define the effectiveness of a probe employed in molecular imaging. Among them, the photophysical properties of the dye (such as persistent photoluminescence and wide Stokes shifts), its biocompatibility, targeting and pharmacokinetics are the main important features.[38] Few NIR imaging probes have clinical use:[38] aqueous insolubility, aggregate formation and small Stokes shifts are the main limits encountered in the development of such dyes.[39] Although the modification of the skeleton of existing NIR dyes with appropriate functional groups has improved the properties of these molecules, the increasing molecular weight of the newly designed dyes has created new issues, such as precipitation and modification of the pharmacokinetics profiles.[39] The majority of recent attempts in NIR probe design have focused therefore on nanomaterial-based probes[1] that (1) offer the possibility of imaging molecular markers not only on the surface[13] but also inside the cells[11,40] thanks to the nanoscale-size of the probe, (2) allow the combination of NIR fluorescence imaging with other imaging modalities[41,42] and (3) permit the efficient incorporation of multiple targeting groups, allowing for example the generation of targeted imaging agents coupled with drug/gene delivery[43-45] or anticancer[46,47] potential.

Thus far, non-covalently functionalised SWNTs[48] have been used as NIR imaging agents *in vitro*,[11-13,40] in *Drosophila melanogaster* (fruit flies)[49] and in mice[14,50] (see

Chapter I, Section 3.3.2.2). NIR probes based on SWNTs have shown low photobleaching,[40] long-term fluorescence in the NIR II region[51] and reduced background from autofluorescence thanks to the large separation between the SWNTs excitation (550-800 nm) and emission bands (900-1600 nm).[23]

While various covalent functionalisation reactions (such as oxidation and 1,3-dipolar cycloaddition) have been applied on carbon nanotubes surface to develop drug delivery nanosystems (see Chapter 1, Section 3.3.1.1),[52-54] no examples of NIR probes based on covalently targeted SWNTs have been reported in the literature to the best of the author's knowledge. Although covalent modification allows a more controlled chemistry on the nanotubes surface, when compared to non-covalent approaches,[55] this is not the ideal protocol for NIR imaging applications. SWNTs optical properties are in fact largely compromised when defects are introduced on the nanotube surface.[29-31]

Since NIR-PL is also sensitive to tubes aggregation, non-covalent functionalisation is considered the best approach in order to (1) individualise semiconducting SWNTs, and (2) decorate their surface with bioactive molecules without affecting their NIR-PL efficiency. So far, carbohydrates,[56] DNA and polyethyleneglycol[6,57,58] have been used to develop SWNTs NIR probes with high biocompatibility. Nevertheless, the toxicological profile of such nanomaterial is still the primary concern for the effective application of SWNTs in molecular imaging.[59] Recent studies have indicated the manufacturing impurities,[60] as well as the tubes aggregation and their high aspect ratio,[61] as main sources of the *in vitro* and *in vivo* SWNTs toxicity. It has been reported in fact that the catalytic metals used in the production of the carbon nanomaterials, such as iron and nickel, induce oxidative stress, thus influencing the real toxic effect of SWNTs.[62,63] Besides, as-produced SWNTs are inherently hydrophobic and have a high aspect ratio. Therefore, they easily aggregate in biopersistent fibers that cause *in vivo* granuloma formation.[61] In contrast, covalently functionalised SWNTs have demonstrated good biocompatibility *in vitro*[64-66] and *in vivo.*[60] The functionalisation of SWNTs reduces in fact their aggregation, thus permitting their rapid renal clearance from the systemic blood circulation.[67-70] Furthermore, it has been reported that acid-treated[66] and functionalised[45,71] SWNTs are internalized by mammalian and prokaryotic cells even under endocytosis-inhibiting conditions and they are able to pass efficiently through various cellular barriers. The results briefly summarized above strongly suggest that purification, decreased aspect ratio and covalent functionalisation of SWNTs are the

three prerequisites towards the successful conversion of these materials into non-harmful imaging contrast agents.

1.3. AIMS OF THIS STUDY

In this study the use of purified and covalently modified SWNTs as NIR fluorescent probes for molecular imaging is explored. To purify and reduce the length of as-produced SWNTs (r-SWNTs), a well-known two-step procedure,[72-74] in which purification by nitric acid (HNO_3) is followed by an oxidative treatment with H_2SO_4 and H_2O_2 (Scheme 2.1), is applied While the HNO_3 treatment is known to reduce the amount of metal impurities of the r-SWNTs, the oxidative treatment decreases the SWNT aspect ratio by cutting the nanotubes.[75] The oxidation procedure results also in the covalent functionalisation of the carbon nanotube surface by introducing covalently attached oxygenated functionalities mainly at the nanotube tips or in correspondence with pre-existing defects.[76]

Scheme 2.1. Purification and oxidation of as-produced HiPCO SWNTs (r-SWNTs)[77]: (a) HNO_3 2.6 M, 100 °C, 48 h; (b) H_2SO_4•H_2O_2 (4:1), 35 °C, 1 h.

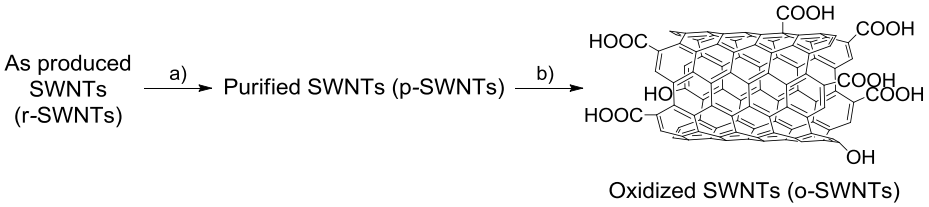

Different purification methods have been employed in the literature depending on the starting material and on the grade of purity needed, and many examples of purification procedures are available today based on oxidation with strong acids.[78] In our study, the catalyst (Fe) particles were annihilated by HNO_3 following the redox reaction described below (Eq. 1):

$$Fe^0 + 3\ NO_3^- + 6\ H^+ \rightleftharpoons Fe^{3+} + 3\ NO_2 + 3\ H_2O \qquad \textbf{Eq. 1}$$

This purification/oxidation approach was preferred to other methods as it results in the introduction of covalently attached oxygenated functionalities that provide the template

for potential further functionalisation *via* amidation and esterification,[79] thus enabling the future development of a multifunctional SWNT-based nanoplatform.

Since the presence of defect-sites on SWNTs surface is known to quench the optical properties of carbon nanotubes, the effect that these two chemical treatments have on the NIR-PL of the tubes is investigated. The results show that purified (p-SWNTs) and oxidized (o-SWNTs) SWNTs samples still display structured emission features in the NIR when dispersed in surfactant aqueous solution, with a residual emission efficiency of 30%. 2D Fluorescence Lifetime Imaging (FLIM) of aggregates of p- and o-SWNTs in DMF showed average lifetime of 1.3 ns and 1.2 ns, respectively.

The positive NIR-PL results obtained in this study can facilitate the practical transformation of p- and o-SWNTs into NIR fluorescent probes for molecular imaging.

2. RESULTS

r-SWNTs were purified and oxidized through a two-step procedure following a previously reported protocol[74,80] briefly summarized in Scheme 2.1. The first step consisted of refluxing the r-SWNTs in HNO_3 in order to eliminate the iron catalyst as soluble species. The second step consisted of oxidizing the tubes with a mixture of H_2SO_4 and H_2O_2 (piranha solution) to introduce oxygenated functionalities (hydroxyl and carboxylic acid groups) that can be further functionalised.[74,79]

The elimination of the metal catalyst was confirmed by Thermal Gravimetric Analysis (TGA) and High Resolution Transmission Electron Microscopy (HR-TEM) (Figure 2.3). TGA analysis (Figure 2.3a, b) showed that p-SWNTs had a reduced residue at 900 ºC (4 %wt) as compared to r-SWNTs (25 %wt), thus demonstrating that the amount of impurities was effectively decreased with the nitric acid treatment. The subsequent treatment with piranha solution further decreased the content of impurities from the 4 % wt of the p-SWNTs to 0 % wt in the o-SWNTs sample. HR-TEM images of r-SWNTs (Figure 2.3c) showed a high content of iron catalyst (visible as black particles thanks to the high diffraction contrast of metals), while images of p- and o-SWNTs show a clean material composed mainly of bundles of SWNTs (Figure 2.3d and 2.3e, respectively).

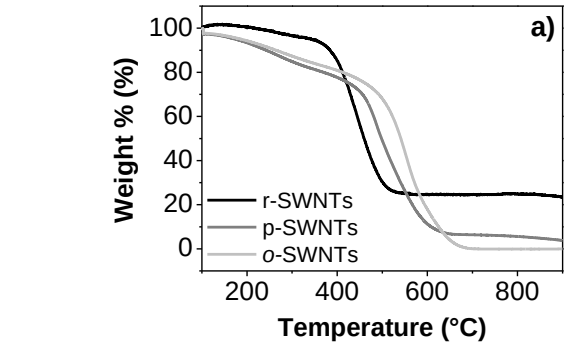

b)

Sample	TGA (air) Residue at 900 C
r-SWNTs	25 % wt
p-SWNTs	4 % wt
o-SWNTs	0 % wt

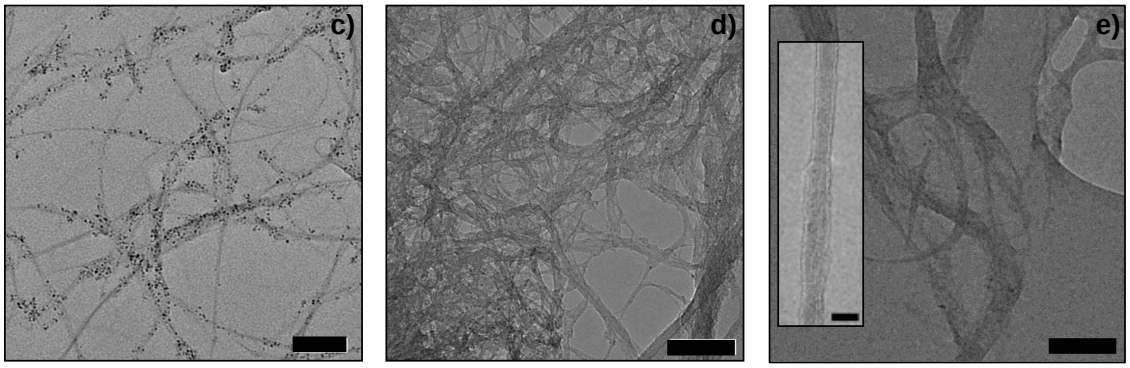

Figure 2.3. (a) TGA traces in air flow of r-, p- and o-SWNTs. (b) Weight (wt) loss % at 900 ºC of r-, p- and o-SWNTs. TGA analysis was carried out by Elisa Del Canto. (c-e) HR-TEM images of (c) r-SWNTs, (d) p-SWNTs, and (e) o-SWNTs on 200 mesh Cu holey carbon grids demonstrating the removal of the metal impurities (black particles) by purification and oxidation procedures. Scale bar: 100 nm. The inset in Figure C shows a detail of a small bundle of o-SWNTs with a diameter of 20 nm circa (scale bar: 20 nm).

Atomic Force Microscopy (AFM) showed the shortening of the tubes to an average length of 260 ± 120 nm after the oxidative treatment (Figure 2.4c, d), while r-SWNTs were characterized by different length nanotubes and impurities (associated with carbonaceous material and catalyst particles) (Figure 2.4a).

Raman analysis clearly showed that the I_D/I_G ratio increases going from r-SWNTs to p- and o-SWNTs (Figure 2.5a). These results were indicative of the increase of disorder on the graphitic surface of chemically treated nanotubes.[81] The oxidation with HNO_3 and piranha solution led to small changes also in the radial breathing mode (RBM) bands of the samples (Figure 2.5b): small bands resonant at higher Raman shifts in fact disappeared as an indication of the partial loss of small diameter SWNTs.[82]

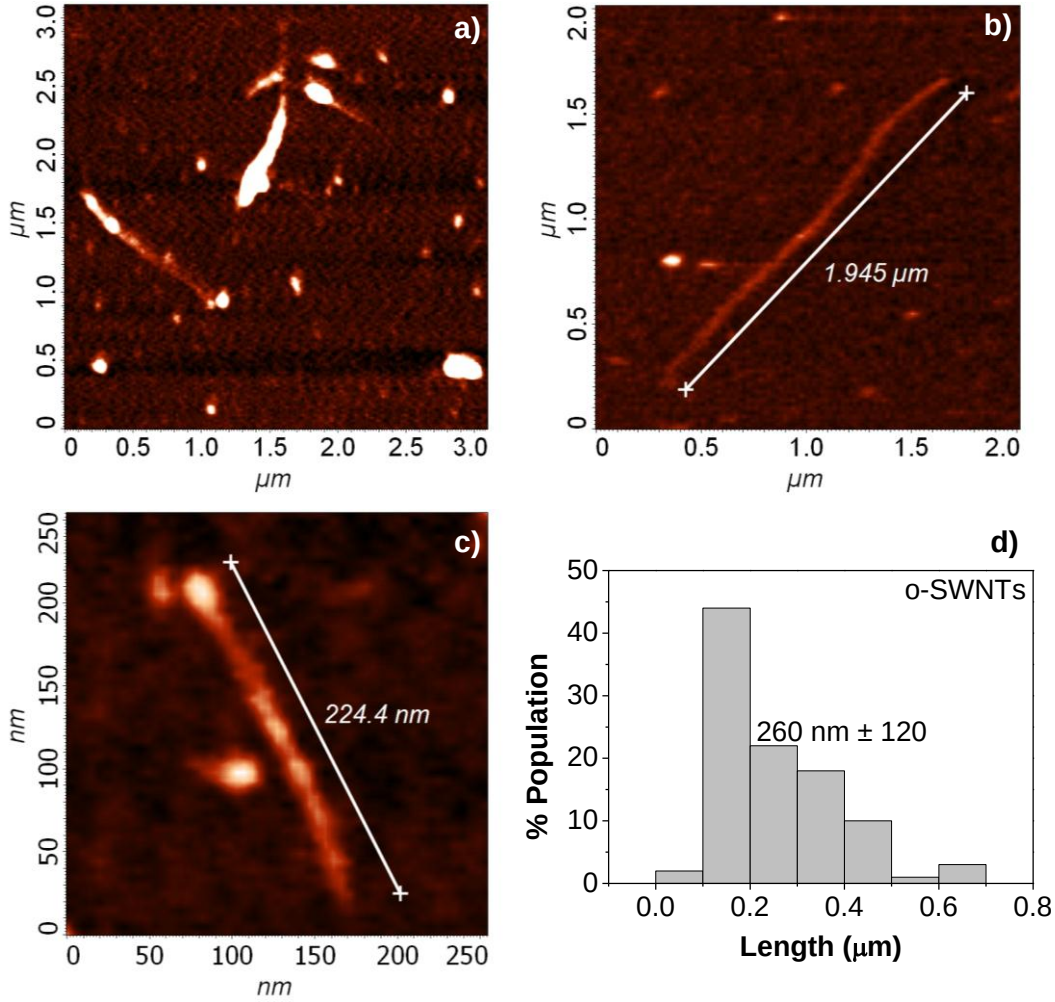

Figure 2.4. Selection of AFM topographic images of (a) r-, (b) p- and (c) o-SWNTs deposited on freshly cleaved mica. Image size: (a) 3.1 μm × 3.1 μm; (b) 2 μm × 2 μm; (c) 250 nm × 250 nm. Z-slide: 0 – 2.2 nm for all the images. d) Histogram of length distribution of o-SWNTs. The calculated average length is 260 ± 120 nm. AFM measurements were carried out by Elisa Del Canto.

The FT-IR data (Figure 2.5c) showed that the nanotubes treated with piranha solution (o-SWNTs) had an intense band at 1662 cm^{-1} and a broad band in the 3200-3500 cm^{-1} region, which were not present in r- and p-SWNTs. These bands may be assigned to the C=O and to the O-H stretching transitions of the carboxylic acid (COOH) functions on SWNTs surface, respectively.[83]

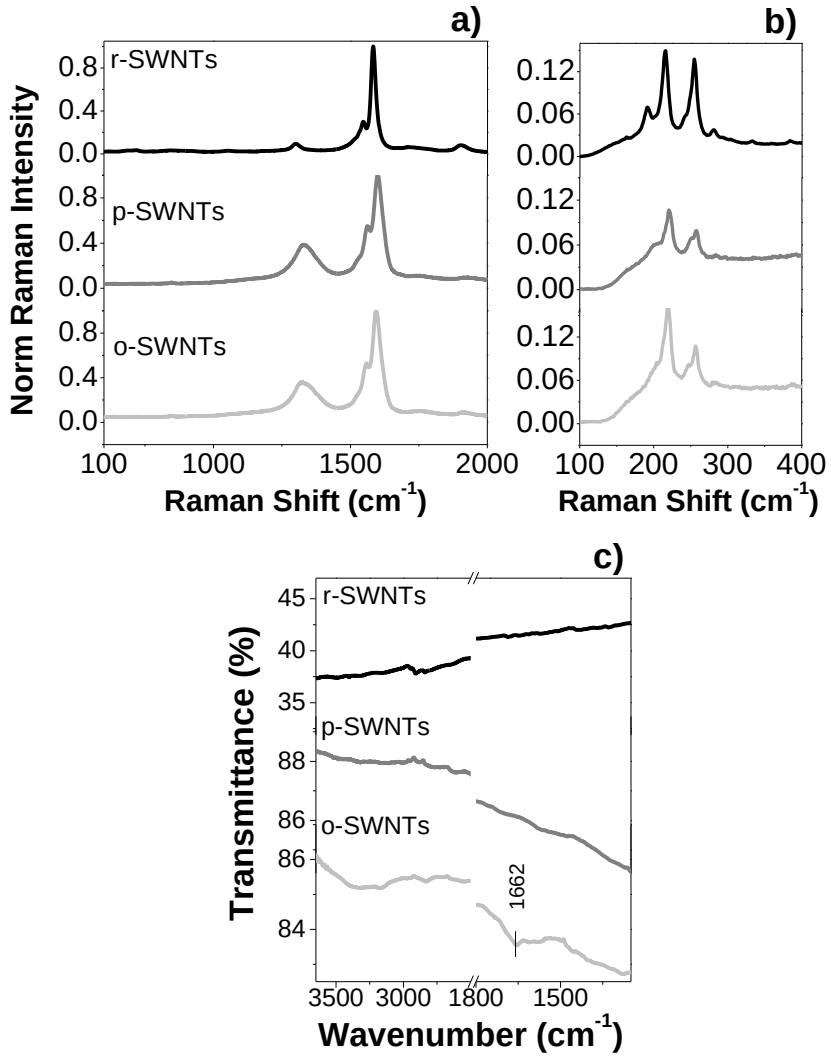

Figure 2.5. (a) Raman spectra of r- (black line), p- (grey line) and o-SWNTs (light grey line) (λ_{exc} = 633 nm) normalized on the G-band. (b) Radial breathing modes (RBMs) of r- (black line), p- (grey line), and o-SWNTs (light grey line). (c) ATR/Fourier transform IR (ATR/FT-IR) spectra of r- (black line), p- (grey line) and o-SWNTs (light grey line). Raman and ATR/FT-IR measurements were carried out by Elisa Del Canto.

Since the tubes shortening and the introduction of defect-sites on SWNTs surface can adversely affect the optical properties that make SWNTs attractive (affecting in particular the quantum yield of their NIR-photoluminescence[29-31,84]) the NIR-PL properties of p- and o-SWNTs dispersed in an aqueous solution of sodium dodecylbenzene sulphonate (SDBS) were investigated (Figure 2.6a-c). The NIR-PL results evidently showed that p- and o-SWNTs, as well as r-SWNTs, displayed a structured emission in the NIR. No significant shifts were evidenced in the position of the NIR-PL bands of the short, oxidised tubes when compared to those of r-SWNTs.

This concurred with the results previously reported by Dai and co. workers,[85] in which blue-shifts were shown in the SWNTs optical spectra only when analyzing tubes with lengths below 50 nm. By evaluating the average efficiency of NIR emission of the three samples (Figure 2.6d), the NIR-PL of p- and o-SWNTs resulted quenched, however, of the 70% when compared to the emission efficiency of r-SWNTs. It should be noted that, due to the nature of the calculations performed (see Chapter IV, Section 2.3), the emission efficiencies here reported for r-, p- and o-SWNTs did not take into consideration the substantial interference from the absorption background of SWNTs. Absorption measurements of SWNTs suspended in organic solvents and/or water are subject in fact to significant absorption backgrounds, and an accurate determination of its contributions is very difficult.[86] This background has been previously attributed to scattering of light by nanotube bundles and carbonaceous impurities in dispersion, near-ultraviolet plasmon resonances of nanotubes and overlap of optical transitions of different (*n*,*m*) SWNTs species.[87] It has been recently reported that absorption background is also influenced by sidewall functionalization and SWNTs length.[88] In this study, the emission efficiency calculations rely on the assumption that the absorption background contributions were length independent and therefore comparable among r-, p- and o-SWNTs samples. Homogeneous solutions of SWNTs samples enriched in a specific semiconducting (*n*,*m*) species obtained by nonlinear density gradient ultracentrifugation (DGU) would be required to perform a quantitative evaluation of the emission efficiency parameters of r-, p- and o-SWNTs.[88]

The reproducibility of the NIR-PL properties of p- and o-SWNTs was also proved by recording the NIR-PL spectra with a different spectrofluorometer at excitation wavelengths of 683 (Figure 2.7a-c) and 785 nm (Figure 2.7d-f). A correspondence in the optical frequency was demonstrated among the NIR transitions recorded with the two different instruments.

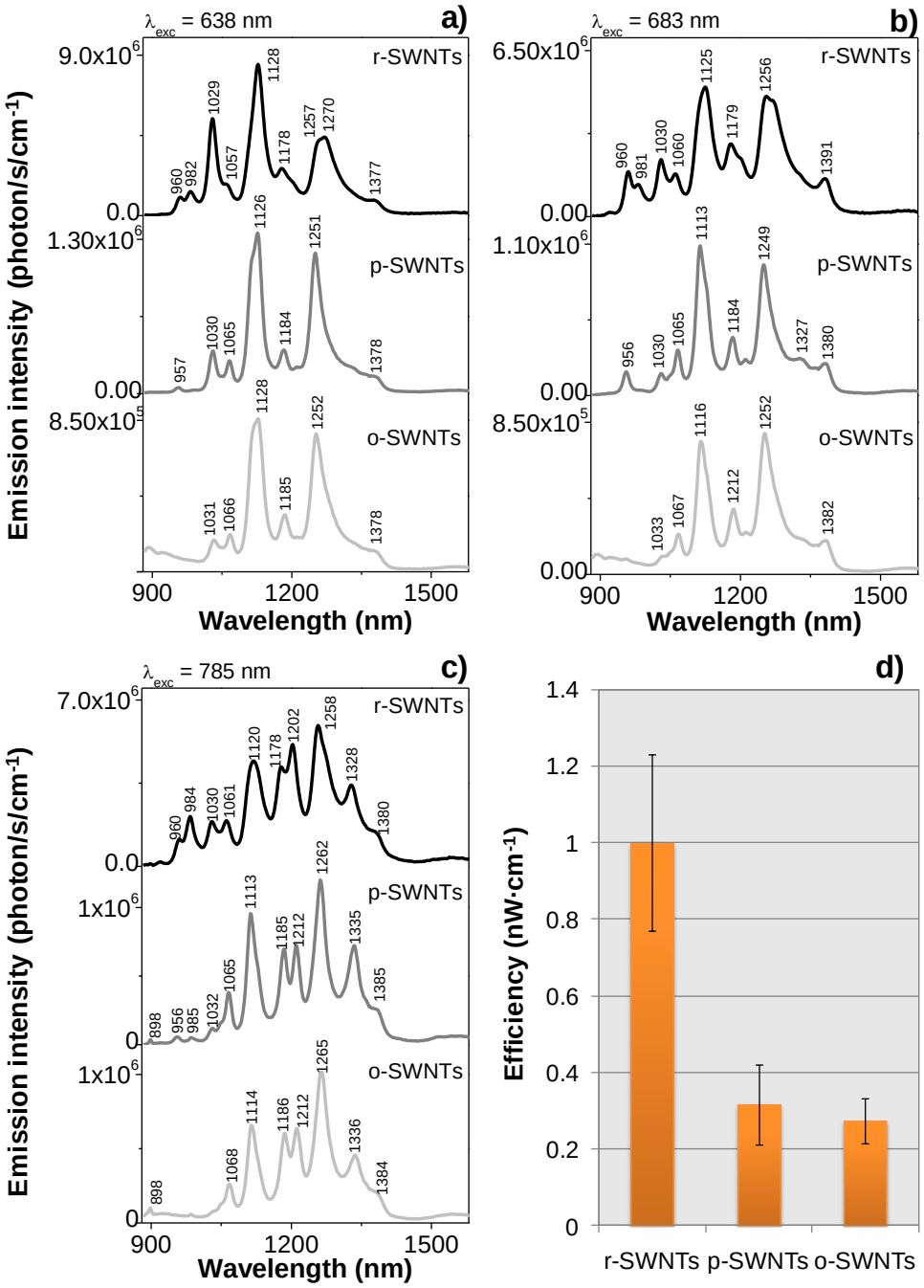

Figure 2.6. (a-c) NIR-PL spectra of r- (black line), p- (grey line) and o-SWNTs (light grey line) dispersed in SDBS aqueous solution at λ_{exc} of (a) 638 nm, (b) 683 nm and (c) 785 nm. $[SWNTs]_i = 8\times10^{-2}$ mg/mL; SWNTs:SDBS weight ratio = 1:25. (d) Histogram of the average NIR-PL efficiency of r-, p- and o-SWNTs dispersed in SDBS aqueous solution. $[SWNTs]_i = 8\times10^{-2}$ mg/mL; SWNTs:SDBS weight ratio = 1:25. The data are expressed as average ($n_{\lambda exc} = 3$; $n_{measurements} = 3$) ± standard deviation and normalized to the NIR-PL efficiency of r-SWNTs.

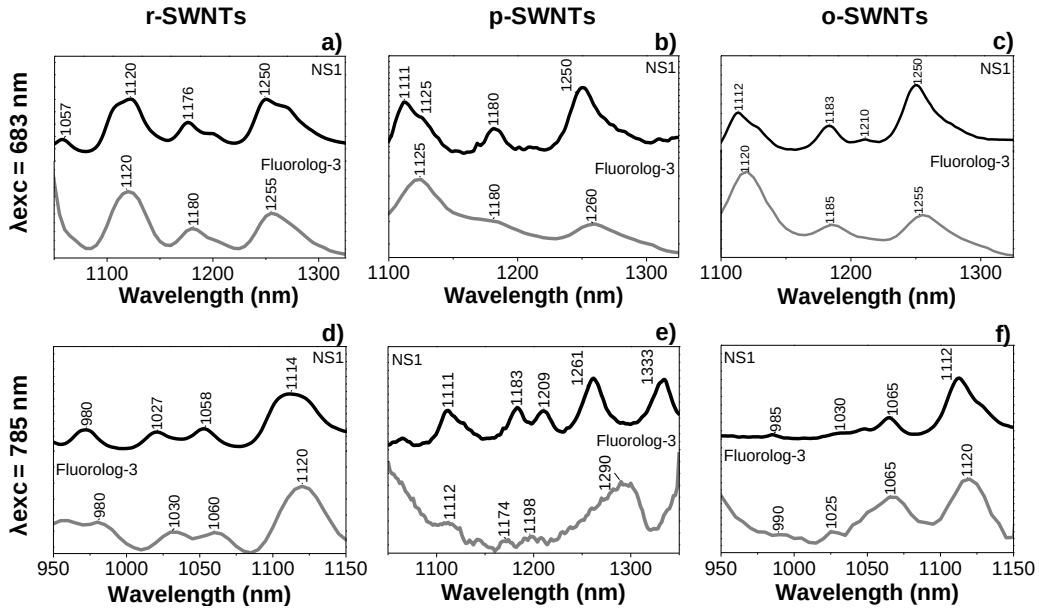

Figure 2.7. (a-f) Comparison of the NIR-PL spectra of (a, d) r-, (b, e) p- and (c, f) o-SWNTs collected with the NS1 NanoSpectralyzer® (black line) and the Fluorolog-3 (grey line) at (a-c) 683 nm and (d-f) 785 nm excitation wavelength. The emission intensities of the spectra are not compared. $[SWNTs]_i = 4.2\times10^{-2}$ mg/mL; SWNTs:SDBS weight ratio of 1:25.

The o-SWNTs sample showed a characteristic emission in the region 880-1000 nm (Figure 2.6a-c), as earlier reported by Lebedkin *et al.* for SWNTs prepared by laser vaporization method and purified with HNO_3.[89] It is suggested that this effect was due to the introduction of defects on the nanotubes surface with piranha solution,[77] which was translated into a stronger emission of o-SWNTs in proximity of the visible region.[20,21] In order to investigate this effect, Vis emission studies were carried out on r-, p- and o-SWNTs dispersed in SDBS aqueous solution (Figure 2.8a-c). The results clearly showed that p- and o-SWNTs were able to emit in the visible region when excited at 638 nm (Figure 2.8a), at 683 nm (Figure 2.8b) and at 785 nm (Figure 2.8c). In particular, the emission intensity of o-SWNTs was higher than that of p-SWNTs. In contrast, no emission was registered for r-SWNTs in the same optical range. The optical properties of p- and o-SWNTs in the visible range and the absence of Vis fluorescence for r-SWNTs were also validated by applying an λ_{exc} (420 nm) that is included in the range typically adopted to detect the nanotubes' fluorescence in such an optical region (Figure 2.8d).[20,21]

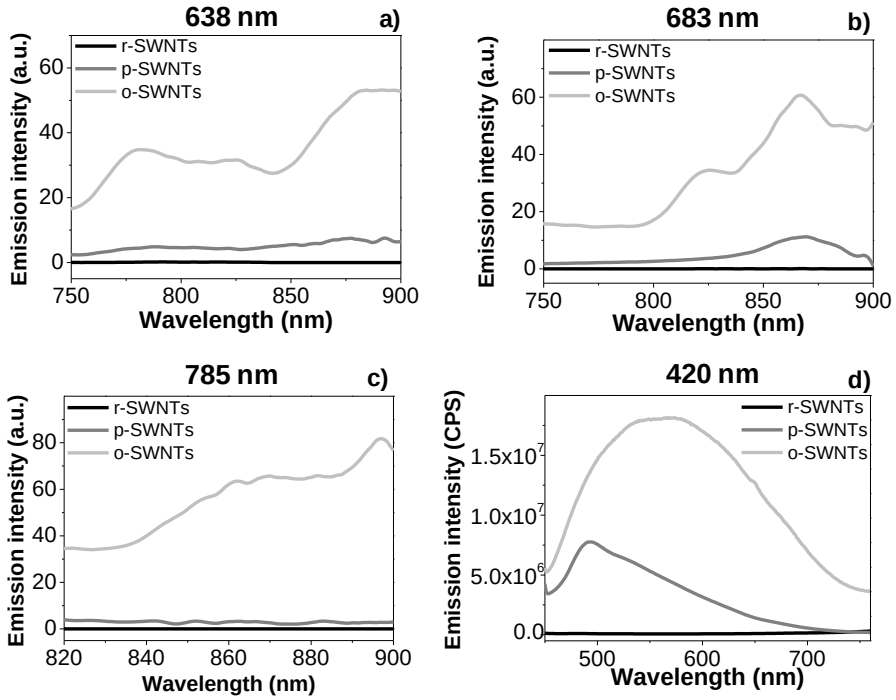

Figure 2.8. Vis emission spectra of r- (black line), p- (grey line) and o-SWNTs (light grey line) dispersed in SDBS aqueous solution at λ_{exc} of (a) 638 nm, (b) 683 nm, (c) 785 nm and (d) 420 nm. $[SWNTs]_i = 8\times10^{-2}$ mg/mL; SWNTs:SDBS weight ratio = 1:25.

The optical properties of p- and o-SWNTs dispersed in SDBS aqueous solution were also detectable by UV-Vis/NIR absorption spectroscopy (Figure 2.9). The UV-Vis/NIR absorption spectrum of r-SWNTs showed well-resolved vH transitions associated with the absorption bands of metallic (M_{11}) and semiconducting (S_{22}, S_{11}) tubes.[18] The vH features were still visible in the absorption spectra of p- and o-SWNTs, but they were less resolved. Such a result, combined with the data obtained by NIR-PL spectroscopy, confirmed that the purification and oxidation procedures resulted only in the partial loss of the SWNTs optical properties.

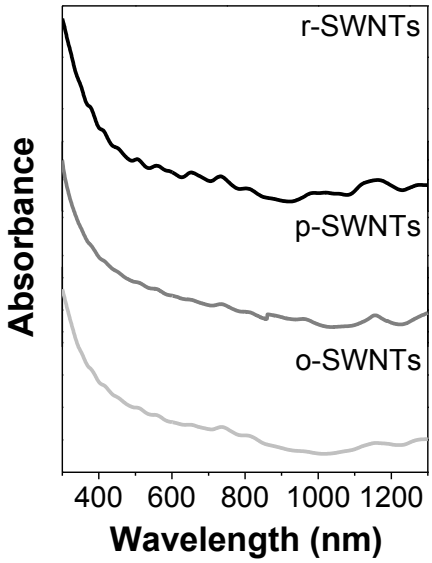

Figure 2.9. UV-Vis/NIR absorption spectra of r- (black line), p- (grey line) and o-SWNTs (light grey line) in SDBS aqueous solution. $[SWNTs]_i = 2.1\times10^{-2}$ mg/mL; SWNTs:SDBS weight ratio = 1:25.

To gain a better insight into the possibility of using *p*-SWNTs and *o*-SWNTs in molecular imaging, 2D Fluorescence Lifetime Imaging (FLIM) was finally used to evaluate the PL lifetime of p- and o-SWNTs in the form of large aggregates dispersed in dimethylformamide (DMF) (Figure 2.10). Each pixel in the FLIM images (Figure 2.10a, c) represents the lifetime of the sample at a precise 2D spatial position while monitoring the NIR-PL spectrum in the optical range from 670 nm to 1000 nm, the optical window in which the absorption coefficient of tissues is at minimum.[38] The FLIM setup enabled a defined visualization of the SWNTs aggregates with a spatial resolution of 1 nm, while the analysis of the corresponding PL lifetime histograms evidenced that p- and o-SWNTs had an average PL lifetime of 1.3 ns and 1.2 ns, respectively.

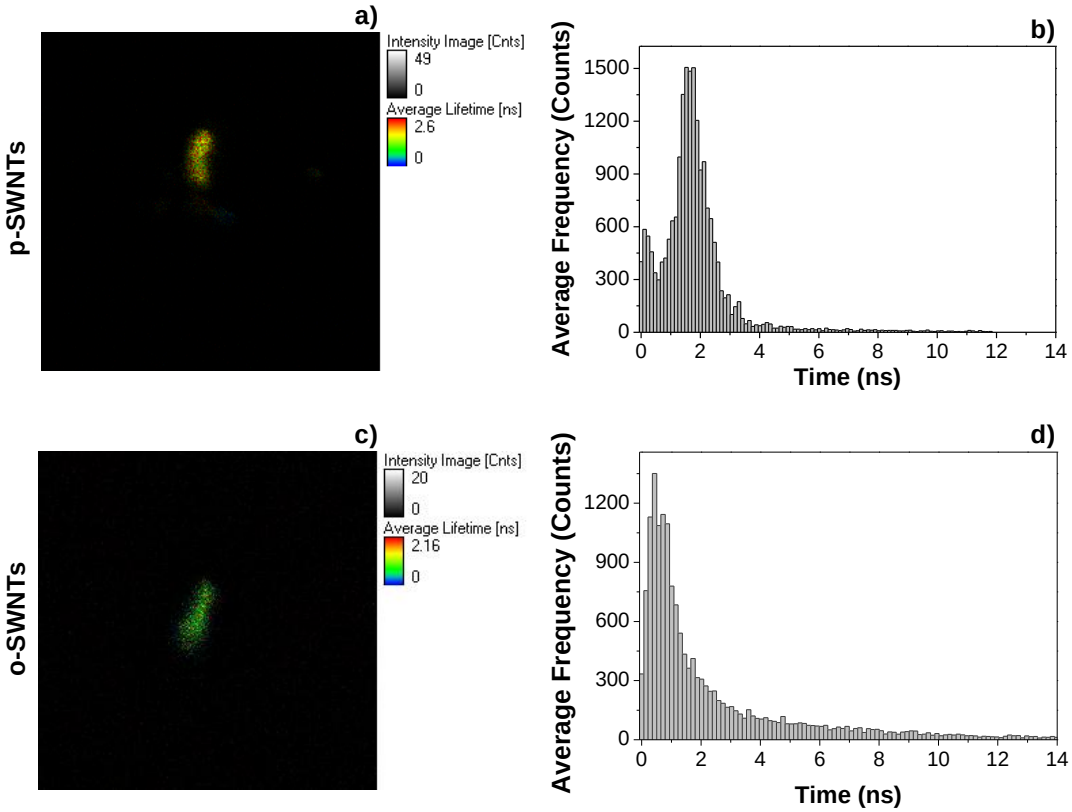

Figure 2.10. (a, c) FLIM images (80 µm × 80 µm) of large aggregates of (a) p- and (c) o-SWNTs dispersed in DMF. Optical window: 670 nm - 1000 nm; λ_{exc} = 630 nm. (b, d) Histograms of the lifetime distribution of the large aggregates of (b) p- and (d) o-SWNTs imaged.

3. DISCUSSION

In this study, a two-step oxidation procedure was employed with the aims of (1) removing the toxic metal impurities, (2) decreasing the lengths of the tubes and (3) introducing functional oxygenated groups on the SWNT surface to potentially enable future functionalisation/targeting of the SWNTs-based molecular probes for NIR imaging.

Using TGA we demonstrated conclusively that our purification procedure effectively removed the metal impurities contained in the r-SWNTs (Figure 2.3a, b). The removal of the highly diffracting metal particles following the purification step was verified also by HR-TEM (Figure 2.3c-e). As removal of metal impurities decreases significantly the direct toxicity and cytotoxicity of SWNTs,[60,61] the acidic treatment was considered crucial for the development of SWNTs-based NIR probes. AFM analysis of the length

distributions before and after chemical treatments (Figure 2.4) led to the conclusion that the oxidation procedure adopted was highly efficient in cutting the tubes, producing o-SWNTs with length in the 140-400 nanometer range. This result was in agreement with those previously reported by other groups employing similar oxidation procedures.[72,76,79] The decreased aspect ratio of the o-SWNTs is an essential property for the bioapplication of SWNTs in molecular imaging, as it reduces the toxic side-effects of *in vivo* administrations of r-SWNTs.[61] Finally, investigation of the changes in the I_D/I_G ratio after chemical treatments by Raman spectroscopy demonstrated the introduction of defect-sites on p- and o-SWNTs (Figure 2.5a). In particular, ATR/FT-IR spectroscopic studies revealed the presence of C=O stretching transitions (1660 cm^{-1} circa) in the spectra of o-SWNTs (Figure 2.5c). This was indicative of the presence of COOH functionalities in such sample and confirmed that the oxidation treatment did introduce a significant amount of carboxylic functionalities on the tubes.

NIR-PL and UV/Vis-NIR absorption spectroscopies proved that the optical properties of SWNTs were still detectable even after the purification step followed by the oxidative procedure (Figure 2.6a-c and Figure 2.9, respectively), even if a partial NIR-PL quenching of 70% was detected in p- and o-SWNTs (Figure 2.6d). The decreased NIR-PL of p- and o-SWNTs was due to the perturbation of the SWNTs surface induced by the chemical treatments,[29] and to the decreased aspect ratio of the tubes.[84,89] The assignment of the optical frequency of each NIR-PL peak evidenced that the bands at smaller wavelengths present in the r-SWNTs spectrum disappeared after the purification and oxidation procedures (Figure 2.6a-c). According to the peak assignment described in the Kataura plot,[17] this outcome may be associated with the partial loss of the small diameter SWNTs during the purification and oxidation steps. This result found correspondence in the RBM of p- and o-SWNTs (Figure 2.5b), which showed decreased intensities of the bands associated with the smaller diameter tubes resonant in the RBM region of the SWNTs Raman spectra.

Finally, FLIM imaging of large aggregates of p- and o-SWNTs was possible (Figure 2.10a, c). The main outcome of the FLIM imaging is a two-dimensional map of in-plane variations of the PL decay times. FLIM technology has already been used successfully in previous studies for imaging NIR fluorescent nanomaterials[90] and for the assessment of the physical interactions and PL lifetime changes of nanomaterials incubated in *in vitro* cell cultures.[91] The choice of imaging aggregates of SWNTs as presented here was

driven by the consideration that the hydrophobic nature of SWNTs surface would cause their aggregation *in vivo*. FLIM results distinctly assessed the potential application of p- and o-SWNTs in molecular imaging as NIR fluorescent probes. Notably, the similar lifetime decays of the two samples (p- and o-SWNTs) were much longer than those reported by previous studies for individual micelle-isolated r-SWNTs.[92,93] Since the optical window examined by FLIM was between 670 and 1000 nm, the results presented here were likely due to the contribution of the SWNTs emission in the Vis region.

4. CONCLUSIONS

In conclusion, this study shows the effective removal of metal impurities contained in r-SWNTs by HNO_3 treatment, while shortening of the tubes and introduction of defect-site oxygenated functionalities on the nanotube skeleton is registered after oxidative treatment. Using a combination of spectroscopic methods (such as NIR-PL and UV-Vis/NIR absorption spectroscopies) and microscopic techniques (FLIM), it is demonstrated that p- and o-SWNTs conserved part of their optical properties despite the employment of strong acidic and oxidative conditions that introduce defect sites on the nanotube surface. In particular, p- and o-SWNTs are able to emit efficiently in the near-infrared region when dispersed in surfactant aqueous solution, as well as in the form of large aggregates in DMF.

Given the lower toxicity of carbon nanotubes cleaned from the metal catalysts,[61] the *in vivo* clearance of SWNTs with small aspect ratio through urinal secretion,[70] and the potential targeting of oxidized SWNTs by further fuctionalisation,[74,79,94] this work establishes the potential use of less-toxic purified and oxidized SWNTs as NIR photoluminescence agents for molecular imaging.

5. REFERENCES

(1) Hong, H.; Gao, T.; Cai, W. B. *Nano Today* **2009**, *4*, 252.

(2) Sitharaman, B.; Kissell, K. R.; Hartman, K. B.; Tran, L. A.; Baikalov, A.; Rusakova, I.; Sun, Y.; Khant, H. A.; Ludtke, S. J.; Chiu, W.; Laus, S.; Toth, E.; Helm, L.; Merbach, A. E.; Wilson, L. J. *Chem. Commun.* **2005**, 3915.

(3) Richard, C.; Doan, B. T.; Beloeil, J. C.; Bessodes, M.; Toth, E.; Scherman, D. *Nano Lett.* **2008**, *8*, 232.

(4) Ananta, J. S.; Matson, M. L.; Tang, A. M.; Mandal, T.; Lin, S.; Wong, K.; Wong, S. T.; Wilson, L. J. *J. Phys. Chem. C* **2009**, *113*, 19369.

(5) Lacerda, L.; Pastorin, G.; Gathercole, D.; Buddle, J.; Prato, M.; Bianco, A.; Kostarelos, K. *Adv. Mater.* **2007**, *19*, 1480.

(6) De La Zerda, A.; Zavaleta, C.; Keren, S.; Vaithilingam, S.; Bodapati, S.; Liu, Z.; Levi, J.; Smith, B. R.; Ma, T. J.; Oralkan, O.; Cheng, Z.; Chen, X. Y.; Dai, H. J.; Khuri-Yakub, B. T.; Gambhir, S. S. *Nat. Nanotechnol.* **2008**, *3*, 557.

(7) Galanzha, E. I.; Shashkov, E. V.; Kelly, T.; Kim, J.-W.; Yang, L.; Zharov, V. P. *Nat. Nanotechnol.* **2009**, *4*, 855.

(8) Zemp, J. R. *Nat. Nanotechnol.* **2009**, *4*, 798.

(9) Liu, Z.; Cai, W.; He, L.; Nakayama, N.; Chen, K.; Sun, X.; Chen, X.; Dai, H. *Nat. Nanotechnol.* **2007**, *2*, 47.

(10) Zavaleta, C.; de la Zerda, A.; Liu, Z.; Keren, S.; Cheng, Z.; Schipper, M.; Chen, X.; Dai, H.; Gambhir, S. S. *Nano Lett.* **2008**, *8*, 2800.

(11) Cherukuri, P.; Bachilo, S. M.; Litovsky, S. H.; Weisman, R. B. *J. Am. Chem. Soc.* **2004**, *126*, 15638.

(12) Cherukuri, P.; Gannon, C. J.; Leeuw, T. K.; Schmidt, H. K.; Smalley, R. E.; Curley, S. A.; Weisman, R. B. *PNAS* **2006**, *103*, 18882.

(13) Welsher, K.; Liu, Z.; Daranciang, D.; Dai, H. *Nano Lett.* **2008**, *8*, 586.

(14) Welsher, K.; Liu, Z.; Sherlock, S. P.; Robinson, J. T.; Chen, Z.; Daranciang, D.; Dai, H. *Nat. Nanotechnol.* **2009**, *4*, 773.

(15) Barone, P. W.; Baik, S.; Heller, D. A.; Strano, M. S. *Nat. Mater.* **2005**, *4*, 86.

(16) Barone, P. W.; Parker, R. S.; Strano, M. S. *Anal Chem* **2005**, *77*, 7556.

(17) Weisman, R. B.; Bachilo, S. M. *Nano Lett.* **2003**, *3*, 1235.

(18) Paredes, J. I.; Burghard, M. *Langmuir* **2004**, *20*, 5149.

(19) O'Connell, M. J.; Bachilo, S. M.; Huffman, C. B.; Moore, V. C.; Strano, M. S.; Haroz, E. H.; Rialon, K. L.; Boul, P. J.; Noon, W. H.; Kittrell, C.; Ma, J.; Hauge, R. H.; Weisman, R. B.; Smalley, R. E. *Science* **2002**, *297*, 593.

(20) Lin, Y.; Zhou, B.; Martin, R. B.; Henbest, K. B.; Harruff, B. A.; Riggs, J. E.; Guo, Z. X.; Allard, L. F.; Sun, Y. P. *J. Phys. Chem. B* **2005**, *109*, 14779.

(21) Guldi, D. M.; Holzinger, M.; Hirsch, A.; Georgakilas, V.; Prato, M. *Chem. Commun.* **2003**, 1130.

(22) Qian, Z.; Wang, C.; Feng, H.; Chen, C.; Zhou, J.; Chen, J. *Chem. Commun.* **2011**, *47*, 7167.

(23) Liu, Z.; Tabakman, S.; Welsher, K.; Dai, H. J. *Nano Res.* **2009**, *2*, 85.

(24) Wang, F.; Dukovic, G.; Brus, L. E.; Heinz, T. F. *Phys Rev Lett* **2004**, *92*.

(25) Weisman, R. B.; Bachilo, S. M.; Tsyboulski, D. *Appl. Phys. A: Mater. Sci. Process.* **2004**, *78*, 1111.

(26) Tan, P. H.; Rozhin, A. G.; Hasan, T.; Hu, P.; Scardaci, V.; Milne, W. I.; Ferrari, A. C. *Phys. Rev. Lett.* **2007**, *99*.

(27) Arnold, K.; Lebedkin, S.; Kiowski, O.; Hennrich, F.; Kappes, M. M. *Nano Lett.* **2004**, *4*, 2349.

(28) Strano, M. S.; Huffman, C. B.; Moore, V. C.; O'Connell, M. J.; Haroz, E. H.; Hubbard, J.; Miller, M.; Rialon, K.; Kittrell, C.; Ramesh, S.; Hauge, R. H.; Smalley, R. E. *J. Phys. Chem. C* **2003**, *107*, 6979.

(29) Cognet, L.; Tsyboulski, D. A.; Rocha, J. D. R.; Doyle, C. D.; Tour, J. M.; Weisman, R. B. *Science* **2007**, *316*, 1465

(30) Aprile, C.; Martin, R.; Alvaro, M.; Scaiano, J. C.; Garcia, H. *ChemPhysChem* **2009**, *10*, 1305.

(31) Crochet, J.; Clemens, M.; Hertel, T. *J. Am. Chem. Soc.* **2007**, *129*, 8058.

(32) Hasan, T.; Scardaci, V.; Tan, P.; Rozhin, A. G.; Milne, W. I.; Ferrari, A. C. *J. Phys. Chem. C* **2007**, *111*, 12594.

(33) Moore, V. C.; Strano, M. S.; Haroz, E. H.; Hauge, R. H.; Smalley, R. E.; Schmidt, J.; Talmon, Y. *Nano Lett.* **2003**, *3*, 1379.

(34) Suttipong, M.; Tummala, N. R.; Kitiyanan, B.; Striolo, A. *J. Phys. Chem. C* **2011**, 17286.

(35) O'Connell, M. J.; Bachilo, S. M.; Huffman, C. B.; Moore, V. C.; Strano, M. S.; Haroz, E. H.; Rialon, K. L.; Boul, P. J.; Noon, W. H.; Kittrell, C.; Ma, J. P.; Hauge, R. H.; Weisman, R. B.; Smalley, R. E. *Science* **2002**, *297*, 593.

(36) Duque, J. G.; Cognet, L.; Parra-Vasquez, A. N. G.; Nicholas, N.; Schmidt, H. K.; Pasquali, M. *J. Am. Chem. Soc.* **2008**, *130*, 2626.

(37) Liu, Y. F.; Wang, H. F. *Nat. Nanotechnol.* **2007**, *2*, 20.

(38) Hilderbrand, S. A.; Weissleder, R. *Curr. Opin. Chem. Biol.* **2010**, *14*, 71.

(39) Escobedo, J. O.; Rusin, O.; Lim, S.; Strongin, R. M. *Curr. Opin. Chem. Biol.* **2010**, *14*, 64.

(40) Heller, D. A.; Baik, S.; Eurell, T. E.; Strano, M. S. *Adv. Mater.* **2005**, *17*, 2793.

(41) Jin, T.; Yoshioka, Y.; Fujii, F.; Komai, Y.; Seki, J.; Seiyama, A. *Chem. Commun.* **2008**, 5764.

(42) Choi, J. H.; Nguyen, F. T.; Barone, P. W.; Heller, D. A.; Moll, A. E.; Patel, D.; Boppart, S. A.; Strano, M. S. *Nano Lett.* **2007**, *7*, 861.

(43) Wang, H.; Chen, X. Y. *Expert Opin. Drug Deliv.* **2009**, *6*, 745.

(44) Son, S. J.; Bai, X.; Lee, S. *Drug Discov. Today* **2007**, *12*, 657.

(45) Pantarotto, D.; Singh, R.; McCarthy, D.; Erhardt, M.; Briand, J.-P.; Prato, M.; Kostarelos, K.; Bianco, A. *Angew. Chem. Int. Ed.* **2004**, *43*, 5242.

(46) Kam, N. W. S.; O'Connell, M.; Wisdom, J. A.; Dai, H. J. *PNAS* **2005**, *102*, 11600.

(47) Ferrari, M. *Nat. Rev. Cancer* **2005**, *5*, 161.

(48) Srinivasan, S.; Babu, S.; Praveen, V.; Ajayaghosh, A. *Angew. Chem. Int. Ed.* **2008**, *47*, 5746.

(49) Leeuw, T. K.; Reith, R. M.; Simonette, R. A.; Harden, M. E.; Cherukuri, P.; Tsyboulski, D. A.; Beckingham, K. M.; Weisman, R. B. *Nano Lett.* **2007**, *7*, 2650.

(50) Welsher, K.; Sherlock, S. P.; Dai, H. *PNAS* **2011**, *108*, 8943.

(51) Jin, H.; Heller, D. A.; Strano, M. S. *Nano Lett.* **2008**, *8*, 1577.

(52) Pastorin, G. *Pharm. Res.* **2009**, *26*, 746.

(53) Liu, Z.; Tabakman, S.; Welsher, K.; Dai, H. *Nano Res.* **2009**, *2*, 85.

(54) Menard-Moyon, C.; Venturelli, E.; Fabbro, C.; Samori, C.; Da Ros, T.; Kostarelos, K.; Prato, M.; Bianco, A. *Expert Opin Drug Dis* **2010**, *5*, 691.

(55) Prato, M. *Nature* **2010**, *465*, 172.

(56) Hong, S. Y.; Tobias, G.; Al-Jamal, K. T.; Ballesteros, B.; Ali-Boucetta, H.; Lozano-Perez, S.; Nellist, P. D.; Sim, R. B.; Finucane, C.; Mather, S. J.; Green, M. L. H.; Kostarelos, K.; Davis, B. G. *Nat. Mater.* **2010**, *9*, 485.

(57) Moon, H. K.; Lee, S. H.; Choi, H. C. *ACS Nano* **2009**.

(58) Liu, Z.; Tabakman, S. M.; Chen, Z.; Dai, H. J. *Nat Protoc* **2009**, *4*, 1372.

(59) Kostarelos, K.; Bianco, A.; Prato, M. *Nat. Nanotechnol.* **2009**, *4*, 627.

(60) Koyama, S.; Kim, Y. A.; Hayashi, T.; Takeuchi, K.; Fujii, C.; Kuroiwa, N.; Koyama, H.; Tsukahara, T.; Endo, M. *Carbon* **2009**, *47*, 1365.

(61) Kolosnjaj-Tabi, J.; Hartman, K. B.; Boudjemaa, S.; Ananta, J. S.; Morgant, G.; Szwarc, H.; Wilson, L. J.; Moussa, F. *ACS Nano* **2010**.

(62) Tian, F.; Cui, D.; Schwarz, H.; Estrada, G. G.; Kobayashi, H. *Toxicol. in Vitro* **2006**, *20*, 1202.

(63) Cui, H.-F.; Vashist, S. K.; Al-Rubeaan, K.; Luong, J. H. T.; Sheu, F.-S. *Chem. Res. Toxicol.* **2010**, *23*, 1131.

(64) Dumortier, H.; Lacotte, S.; Pastorin, G.; Marega, R.; Wu, W.; Bonifazi, D.; Briand, J. P.; Prato, M.; Muller, S.; Bianco, A. *Nano Lett.* **2006**, *6*, 3003.

(65) Sayes, C. M.; Liang, F.; Hudson, J. L.; Mendez, J.; Guo, W.; Beach, J. M.; Moore, V. C.; Doyle, C. D.; West, J. L.; Billups, W. E.; Ausman, K. D.; Colvin, V. L. *Toxicol. Lett.* **2006**, *161*, 135.

(66) Porter, A. E.; Gass, M.; Bendall, J. S.; Muller, K.; Goode, A.; Skepper, J. N.; Midgley, P. A.; Welland, M. *ACS Nano* **2009**, *3*, 1485.

(67) Bianco, A.; Sainz, R.; Li, S.; Dumortier, H.; Lacerda, L.; Kostarelos, K.; Giordani, S.; Prato, M. In *Medicinal Chemistry and Pharmacological Potential of Fullerenes and Carbon Nanotubes*; Cataldo, F., Ros, T., Eds.; Springer Netherlands: Dordrecht, 2008; Vol. 1, p 23.

(68) Liu, Z.; Davis, C.; Cai, W. B.; He, L.; Chen, X. Y.; Dai, H. J. *PNAS* **2008**, *105*, 1410.

(69) Schipper, M. L.; Nakayama-Ratchford, N.; Davis, C. R.; Kam, N. W. S.; Chu, P.; Liu, Z.; Sun, X.; Dai, H.; Gambhir, S. S. *Nat. Nanotechnol.* **2008**, *3*, 216.

(70) Singh, R.; Pantarotto, D.; Lacerda, L.; Pastorin, G.; Klumpp, C.; Prato, M.; Bianco, A.; Kostarelos, K. *PNAS* **2006**, *103*, 3357.

(71) Pantarotto, D.; Briand, J.-P.; Prato, M.; Bianco, A. *Chem. Commun.* **2004**, 16.

(72) Ziegler, K. J.; Gu, Z.; Peng, H.; Flor, E. L.; Hauge, R. H.; Smalley, R. E. *J. Am. Chem. Soc.* **2005**, *127*, 1541.

(73) Bonifazi, D.; Nacci, C.; Marega, R.; Campidelli, S.; Ceballos, G.; Modesti, S.; Meneghetti, M.; Prato, M. *Nano Lett.* **2006**, *6*, 1408.

(74) Del Canto, E.; Flavin, K.; Natali, M.; Perova, T.; Giordani, S. *Carbon* **2010**, *48*, 2815.

(75) Ziegler, K. J.; Gu, Z. N.; Peng, H. Q.; Flor, E. L.; Hauge, R. H.; Smalley, R. E. *J. Am. Chem. Soc.* **2005**, *127*, 1541.

(76) Liu, J.; Rinzler, A. G.; Dai, H. J.; Hafner, J. H.; Bradley, R. K.; Boul, P. J.; Lu, A.; Iverson, T.; Shelimov, K.; Huffman, C. B.; Rodriguez-Macias, F.; Shon, Y. S.; Lee, T. R.; Colbert, D. T.; Smalley, R. E. *Science* **1998**, *280*, 1253.

(77) Movia, D.; Del Canto, E.; Giordani, S. *J. Phys. Chem. C* **2010**, *114*, 18407.

(78) Holzinger, M.; Hirsch, A.; Bernier, P.; Duesberg, G. S.; Burghard, M. *Appl. Phys. A: Mater. Sci. Process.* **2000**, *70*, 599.

(79) Giordani, S.; Colomer, J. F.; Cattaruzza, F.; Alfonsi, J.; Meneghetti, M.; Prato, M.; Bonifazi, D. *Carbon* **2009**, *47*, 578.

(80) Movia, D.; Del Canto, E.; Giordani, S. *Phys. Stat. Sol. B* **2009**, *246*, 2704.

(81) Ferrari, A. C.; Robertson, J. *Phys. Rev. B* **2000**, *61*, 14095.

(82) Rao, A. M.; Richter, E.; Bandow, S.; Chase, B.; Eklund, P. C.; Williams, K. A.; Fang, S.; Subbaswamy, K. R.; Menon, M.; Thess, A.; Smalley, R. E.; Dresselhaus, G.; Dresselhaus, M. S. *Science* **1997**, *275*, 187.

(83) Kim, U. J.; Furtado, C. A.; Liu, X.; Chen, G.; Eklund, P. C. *J. Am. Chem. Soc.* **2005**, *127*, 15437.

(84) Miyauchi, Y.; Matsuda, K.; Yamamoto, Y.; Nakashima, N.; Kanemitsu, Y. *J. Phys. Chem. C* **2010**, *114*, 12905.

(85) Sun, X.; Zaric, S.; Daranciang, D.; Welsher, K.; Lu, Y.; Li, X.; Dai, H. *J. Am. Chem. Soc.* **2008**, *130*, 6551.

(86) Zhou, B.; Lin, Y.; Li, H.; Huang, W.; Connell, J. W.; Allard, L. F.; Sun, Y.-P. *J. Phys. Chem. B* **2003**, *107*, 13588.

(87) Kataura, H.; Kumazawa, Y.; Maniwa, Y.; Umezu, I.; Suzuki, S.; Ohtsuka, Y.; Achiba, Y. *Synth. Met.* **1999**, *103*, 2555.

(88) Naumov, A. V.; Ghosh, S.; Tsyboulski, D. A.; Bachilo, S. M.; Weisman, R. B. *ACS Nano* **2011**, *5*, 1639.

(89) Heller, D. A.; Mayrhofer, R. M.; Baik, S.; Grinkova, Y. V.; Usrey, M. L.; Strano, M. S. *J. Am. Chem. Soc.* **2004**, *126*, 14567.

(90) Rakovich, Y. P.; Volkov, Y.; Sapra, S.; Susha, A. S.; Doblinger, M.; Donegan, J. F.; Rogach, A. L. *J. Phys. Chem. C* **2007**, *111*, 18927.

(91) Conroy, J.; Byrne, S. J.; Gun'ko, Y. K.; Rakovich, Y. P.; Donegan, J. F.; Davies, A.; Kelleher, D.; Volkov, Y. *Small* **2008**, *4*, 2006.

(92) Lebedkin, S.; Arnold, K.; Hennrich, F.; Krupke, R.; Renker, B.; Kappes, M. M. In *Molecular Nanostructures*; Kuzmany, H., Fink, J., Mehring, M., Roth, S., Eds.; Amer Inst Physics: Melville, 2003; Vol. 685, p 230.

(93) Huang, L. B.; Krauss, T. D. *Phys. Rev. Lett.* **2006**, *96*.

(94) Pastorin, G.; Wu, W.; Wieckowski, S.; Briand, J. P.; Kostarelos, K.; Prato, M.; Bianco, A. *Chem. Commun.* **2006**, 1182.

CHAPTER III.
SCREENING THE TOXICITY OF SWNTS-BASED NIR PROBES USING 3D TISSUE-MIMETIC MODELS

CONTENTS

1. INTRODUCTION

Although SWNTs-based NIR fluorescent agents represent a growing family of fascinating probes with outstanding biomedical applications, SWNTs' unique properties (such as size, shape, and composition) raise concerns on their potential human toxicity,[1,2] while their diversity from bulk materials poses significant challenges over traditional toxicity screening approaches.[3]

The main concerns raised by toxicology experts about the potential toxicity of SWNTs are fuelled by three considerations. First, SWNTs possess a high surface area, thus enhancing the contact area with their surroundings. This could expose catalytic or reactive sites of the SWNTs surface, inducing in some cases the formation of reactive oxygen species.[4] Second, due to their small size, SWNTs may enter in many cells and organs in larger extent than bulk materials. Long-term toxic effects due to prolonged accumulation and retention in the organism need therefore to be considered. Third, the shape of SWNTs may play a crucial role in determining toxic responses. Geometric effects of CNTs have been shown, for example, in macrophage models ("frustrated phagocytosis" effects[5]). Additionally, differences in synthetic methods, impurities, coatings, and surface functionalisation can lead to thousands of possible SWNTs variants.

1.1. CHALLENGES IN THE ASSESSMENT OF NANOMATERIALS (NMS) TOXICITY

Nanotoxicology challenges include (1) the large number of substances that need to be tested, and (2) how to offer increased efficiency in test design and costs.

The test system currently employed for assessing the toxicity of chemical substances was introduced over 80 years ago.[3] Only a few changes have been incorporated over the past decades, thus leaving the screening procedures almost unchanged and the experimental protocols obsolete when testing nanomaterials.[3,6] Over the past five years, there has been an on-going debate on the most appropriate test strategies to use for evaluating the potential hazards of SWNTs and of NMs in general. Clearly, not all can be evaluated in *in vivo* studies [3], as a single *in vivo* study can cost $ 50,000:[7] traditional *in vivo* studies conducted on even those NMs currently in commerce could total a billion dollars and it could take 30-50 years to be completed. International efforts have geared towards establishing characterization schemes and consistent approaches for various NMs.[4,8-10] Currently, nanotechnology policies and regulation are encouraging

the development of new test models, the implementation of *in vitro* high throughput screening tools[1,3,7] and the assessment of the physico-chemical properties of the tested nanomaterial within the experimental test systems employed.[11-13] This is because the toxicological outputs of a specific NM may be different depending, for example, on the specific protein content of the environment, impurities concentration and methods used to "dissolve" the NMs.[13,14] Agglomeration and aggregation are for example recognized as major issues in the evaluation of the NMs effects since they may affect the "dose" of the NMs. For the same reason, what constitutes "dose" for a nanomaterial may not always be "mass" (ppm, mg/kg, mol/L) and the dose metric of concern may be related to some aspect of the NM physical structure.[8] This is well known in particle and fibre toxicology where the dose metric may be expressed as the surface area of the particle or the number of fibres of a given length.[12]

In 2005, the U.S. Environmental Protection Agency (EPA), with support from the U.S. National Toxicology Program (NTP), funded a project at the National Research Council (NRC) for developing a long-range vision for toxicity testing and a strategic plan for implementing that vision.[15] In summary, NRC proposed a largely *in vitro* approach for the evaluation of toxicity of substances of public health concern. In recent years, there have been many attempts to apply this approach to the study of NMs, and a number of paradigms have emerged in nanotoxicology: the bio-nano interface/protein corona paradigm,[16] the oxidative stress paradigm[10] and the pathogenic fibre paradigm,[17] to name a few. Such theoretical paradigms are helpful as platforms from which a large number of *in vitro* data can be interpreted. However, although this approach may have merit in accelerating the rate of gathering toxicological data on NMs by predicting their hazard potential, it does not state the *in vivo* disease outcome, which depends on a number of variables that cannot be included in *in vitro* studies. The serious limitations of *in vitro* models, including the number of co-cultured cell types and the methods of exposing cells, do not reproduce the physiological relevance of coordinated three-dimensional (3D) responses among various cell types in tissues and organs, and the delivery of NMs in one single dose does not reflect *in vivo* realistic conditions, where NMs are likely to accumulate gradually.

A three-step scheme, described in the following, has been recently proposed by Hartung as the way towards the assessment of NMs toxicity:[3] (1) define the limitations of current toxicity assessment tools; (2) combine them in a strategic way; and finally (3)

develop a new testing system that integrates the old set of testing protocols with modern technologies. Among the latest, Hartung proposed imaging techniques and robotized testing platforms (such as High Content Screening and Analysis (HCSA)), *in silico* methods (heatmaps and quantitative structure-activity relationship (QSAR)), advanced cell-culturing techniques (3D "organotypic" cell cultures) and "omics" technologies (genomics and proteomics).[3] While HCSA[7,9,18-22] and *in silico* methods[19,23] are commonly recognised and exploited as important techniques for the assessment of NMs toxicity, the use of 3D *in vitro* cell models (that can better represent the 3D organisation of tissues *in vivo* compared to the conventional 2D cell cultures[24,25]) is still at its infancy within the nanotoxicology field. 3D cell aggregates more closely resemble the *in vivo* situation with regard to cell shape and cellular environment,[26] which can in turn regulate the gene expression and hence the biological behaviour of cells.[27] To the best of the author's knowledge, only few studies used co-cultures systems[28] and/or 3D cell cultures for testing nanomaterials toxicity.[29,30] However, no "organotypic" cell culture technique has been employed to date for the assessment of CNTs toxicity.

1.2. Challenges in the Assessment of CNTs Toxicity

Several factors are associated with the difficulty in assessing the CNTs toxicity. Among them, CNTs interactions with components of the dispersing medium, the cytotoxicity assay employed, impurities, CNTs surface chemistry and dispersion state are the main parameters. Such factors may be the source of the discrepancies that can be found in the CNTs toxicity data available in the literature and described in Section 1.3.

1.2.1. Interaction with dispersing medium

Toxicological testing of CNTs typically involves their dispersion within a biological medium, followed by their addition to a cell line of interest or by administration to animal models. However, the degree of interaction between CNTs and the medium and the influence of such interactions on cellular responses are not completely exploited. Considerable interaction between carbon nanotubes and components of cell culture medium, such as for example phenol red, riboflavin and foetal bovine serum, have been evidenced as a result of physisorption through Van der Waals forces.[31] Such spontaneous accumulation of bio-compounds at the solid-liquid interface and the subsequent formation of bio-coatings on the CNTs surface is a process commonly

addressed as formation of biomolecule "corona". If a nanomaterial enters the cell, modification of the components absorbed on its surface is expected, with variations depending on the cell compartment of interest.[14] *In vivo* this may be translated in slow exchange of the protein corona depending on the organ involved or in different bioavailability thresholds in the various districts of the body. These interactions may potentially play a role in the toxicity of CNTs[32] by reducing the availability of proteins and nutrients to the cells,[31] modifying the conformational state of the components and their functionality,[13] influencing the cell recognition[13,18] or adsorbing cell-signalling immunomodulating agents on CNTs surface.[33]

1.2.2. Interaction with cytotoxicity assays

A number of *in vitro* toxicity assays have been developed to determine cell viability and/or cytotoxicity in cultured cells. These assays often use colorimetric or fluorescent dyes as markers assessing membrane integrity or cellular metabolism. While these assays have shown to provide accurate data for various molecular families, they provide less reliable results when assessing NMs cytotoxicity. In particular, CNTs interact with various commonly used cytotoxicity assays by interfering with the absorption/fluorescence properties of the dye employed, underestimating or overestimating the toxic response, providing confusing results, false positive results and conflicting reports. For this reason, Wörle-Knirsch *et al.* (2006),[34] followed by Casey *et al.* (2007)[35] and Monteiro-Riviere *et al.* (2009),[36] advised caution when performing even established toxicity assays in the presence of significant quantities of carbon nanostructures and encouraged the use of at least two or more independent test assays to validate any *in vitro* results on NMs. Table 3.1 summarises the interactions between CNTs and various cytotoxicity assays as reported in the scientific literature.

Table 3.1. Summary of cytotoxicity assays used in *in vitro* toxicity studies on CNTs and potential interactions detected.

Assay	Detection method	Target	Data reliability	Ref.
Calcein AM (CAM)	Live cells: green stained	Cell membrane	Yes*	36
Coomassie Brilliant Blue G250 dye	Binds specifically to tyrosine side chains of proteins	Cell membrane	No	35
CytoTox One™ Homogeneous	LDH released by cells with damaged membrane results	Cell membrane	No	36

Assay	Detection method	Target	Data reliability	Ref.
Membrane Integrity (CTO)	in the conversion of resazurin into a fluorescent resorufin product			
Lactate dehydrogenase (LDH)	LDH released by cells with damaged membrane results in the conversion of a tetrazolium compound into a water-soluble fluorescent formazan dye	Cell membrane	Yes	34
Trypan Blue exclusion (TB)	Dead cells: blue stained	Cell membrane	Yes*	36
Alamar Blue® (AB)	Live cells: resazurin reduction to red fluorescent dye resorufin	Cell metabolism	No	35,36
Celltiter 96® Aqueous One (96 AQ)	Live cells: tetrazolium conversion to soluble purple formazan salt	Cell metabolism	Yes	36
CellTiter-Blue® (CTB)	Kit form of Alamar Blue	Cell metabolism	Yes	36
Mitochondrial Membrane Potential (MMP)	Detection of metalloproteinase activity	Cell metabolism	Yes	34
MTT	Live cells: tetrazolium conversion to insoluble purple formazan salt	Cell metabolism	No	34-36
WST-1	Live cells: tetrazolium conversion to water-soluble purple formazan salt	Cell metabolism	Yes No	34 35
Live/Dead® (LD)	Dead cells: red stained; live cells: green stained	Cell membrane	Yes*	36
Neutral red (NR)	Live cells: red lysosomes	Lysosomal membrane	No	35,36

*Difficult interpretation due to deposition of CNTs on the cells monolayer in conventional two-dimensional (2D) cell culture models.

The knowledge gathered so far in CNTs toxicity consists of data based on a non-standardized CNTs material; all the studies listed in Table 3.1 have to be considered, therefore, as separate and not directly comparable experiments. In particular, from the divergent interpretation of the WST-1 assay output in two different studies[34,35] it is clear that a standardized CNT reference material used by all toxicologists is needed. It is also important to keep in mind that the employment of viability tests based on the evaluation of cellular metabolic activity may give false positive results, as many different conditions can increase or decrease the metabolic activity of treated cells while the number of viable cells remains constant.

1.2.3. Effect of impurities

Variation of impurities content in the different CNT preparations[37] offers additional challenges in the accurate and consistent assessment of CNTs toxicity. As-produced CNTs contain generally high amounts of catalytic metal particles, such as iron and nickel, used as precursors in their synthesis. High concentrations of these metals are cytotoxic,[38,39] mainly due to oxidative stress and induction of inflammatory processes generated by catalytic reactions at the metal particle surface.[40] Another very important contamination is amorphous carbon, which exhibits comparable biological effects as carbon black or relevant ambient air particles.

1.2.4. Effect of dispersion

The poor dispersability of CNTs in biological media can affect both the *in vitro*[41] and the *in vivo*[42] toxicity of such nanomaterials.

In vitro, cell responses seem to depend strongly on the dispersing agent employed. Decreased oxidative stress was shown in primary bronchial epithelial (NHBE) cells and in alveolar epithelial carcinoma (A549) cells when incubated with SWNTs dispersed in cell culture medium with foetal calf serum (FCS) supplement; whereas addition of dipalmitoylphosphatidylcholine (DPPC), the major constituent of lung surfactant, resulted in increasing oxidative stress.[43] Alpatova *et al.* (2010) demonstrated that SWNTs non-covalently functionalised by a range of natural (gum Arabic, amylase, Suwanee River natural organic matter) and synthetic (polyvinyl pyrrolidone, Triton X-100) surfactants did not cause any cell viability loss in cultured *E. coli* and rat liver epithelial (WB-F344) cells, when the dispersing agent itself was non-cytotoxic.[41] Similar results were previously reported by Dong *et al.* (2009),[44] showing that the cytotoxicity of SWNTs incubated with human astrocytoma cells depend on the toxicity of the surfactant employed.

In vivo, SWNTs individually dispersed by Pluronic F108 demonstrated to be non-toxic after intratracheal administration to mice, while aggregated SWNTs caused granuloma-like structures with mild fibrosis in the lungs of the treated animals.[42]

1.3. SWNTs TOXICITY

Although concern over the potential toxic impact of SWNTs on environmental and human health is recent, CNTs toxicity is one of the better-researched nanotoxicity areas. Up to 2006 there were less than ten published research studies focusing on CNTs toxicity.[37] From that year onwards, the number of reports investigating the *in vitro* and *in vivo* toxicity of CNTs has increased exponentially. Even though *in vitro* and *in vivo* studies do reveal concerns on CNTs toxicity, these two test models often provide contradictory results, thus raising more questions. Because of these divergent reports, specific pathways and mechanisms through which CNTs may exert their toxic effects *in vivo* remain unknown. The main mechanisms proposed are:

- oxidative stress due to redox features in the presence of physiologically relevant redox agents;[45,46]
- inflammatory and fibrogenic responses in lungs, accompanied by a pulmonary function decline and enhanced susceptibility to infections;[47]
- toxic effect of transition metals or other environmental contaminants present in as-produced CNTs;[48,49]
- ineffective recognition of CNTs by macrophages.[50]

CNTs may enter the human body through dermal contact, inhalation, intentional injection, or ingestion.[51] Additionally, CNTs could translocate to distant organs and tissues, such as the intraperitoneal cavity. The interaction of carbon nanotubes with the immune system, particularly macrophages, may play a significant role in such translocation processes.[52] In Table 3.2, a summary of the main *in vitro* on the toxicity of SWNTs reported in the literature to date is presented, by classifying them on the portal of entry through which they encounter the body. Similarly, the *in vivo* data are summarised in Table 3.3.

Table 3.2. Summary of SWNTs *in vitro* toxicity. The term "CNTs" indicates that the material was not identified as single- (SWNTs) or multi-walled (MWNTs) carbon nanotubes. Percentage of catalytically active transition metals in the CNTs is reported when indicated by the authors.

CNTs tested	Production method	Cellular model	Cytotoxic effect	Ref.
		Dermal cytotoxicity		
SWNTs	Arc-discharge	A549	Catalysts-dependent cytotoxicity	53
SWNTs	Arc-discharge (< 1 wt. % Ni and Y)	HaCaT	Cell proliferation reduced	49
SWNTs	HiPCO	HaCaT	Time-dependent cytotoxicity	48
SWNTs	HiPCO	HaCaT HeLa	Detectable oxidative stress (ROS production, NF-κB activation) Cell proliferation inhibited	54
SWNTs	HiPCO (30 wt. % Fe *versus* 0.23 wt. % Fe)	JB6 P+; EpiDerm FT engineered skin	Unpurified SWNTs: free radical generation, oxidative stress, inflammation	55
SWNTs	HiPCO (10 wt. % Fe)	HaCaT	Cell proliferation reduced	49
Phenyl-functionalised SWNTs	HiPCO (< 1 wt. % Fe)	HDF	Cytotoxicity as a function of chemical derivatization	56
6-aminohexanoic acid SWNTs	HiPCO	HEK	Dose-dependent cytotoxicity Time-dependent cytotoxicity Aggregation-dependent cytotoxicity	33
SWNTs	[Not specified]	HEK	Changes in gene expression in SWNTs-treated cells become closer to control cells over time	57
		Pulmonary cytotoxicity		
SWNTs	Arc-discharge (<1 wt% of Ni and Y)	A549 BEAS-2B	Cell proliferation reduced	49
SWNTs	HiPCO	A549 H1299	Cell proliferation inhibited	54
SWNTs	HiPCO (10 wt. % Fe)	A549 NHBF	Suppression of inflammatory mediators	43
SWNTs	HiPCO (10 wt.% Fe)	A549 BEAS-2B	Cell proliferation reduced	49
SWNTs	HiPCO (10 wt.% iron)	A549	Very low acute toxicity Increase in lamellar bodies	58

CNTs tested	Production method	Cellular model	Cytotoxic effect	Ref.
	In vitro inflammatory response			
Purified SWNTs	Arc-discharge	Guinea pigs alveolar macrophages	Dose-dependent inflammation	59
SWNTs	CVD (0 wt. % Co and Ni)	J774 MDMs	None	60
SWNTs	HiPCO (0.3 wt. % Fe)	RAW 264.7	No intracellular production of superoxide radicals or nitric oxide (NO) Enhancement of lipid peroxidation and GSH depletion proportional to the iron content	61
CNTs (800 nm and 200 nm length)	[Not specified]	THP-1	Detectable inflammatory response	62
	Vascular system			
SWNTs	[Not specified] (minimal purity: >90 wt. %)	Human platelets	Platelet activation and aggregation by inducing Ca^{2+} influx	63
SWNTs	[Not specified]	Human platelets	Platelet aggregation	64
CNTs	[Not specified]	Human neutrophils	Decreased cell viability Detectable inflammatory response	65
	Additional cell models			
MWNTs (50%) + SWNTs (30%)	Arc-discharge (0 wt. % catalyst)	Jurkat cells	Aggregation-dependent cytotoxicity Contaminant-dependent cytotoxicity	66
SWNTs	CVD (1 wt. % Co and Mo)	Jurkat cells	Aggregation-dependent cytotoxicity Contaminant-dependent cytotoxicity	66
SWNTs	Arc-discharge	MSTO-211H	Aggregation-dependent cytotoxicity	67

CNTs tested	Production method	Cellular model	Cytotoxic effect	Ref.
SWNTs	[Not specified]	HEK293	Cell proliferation reduced Cell adhesion reduced Dose-dependent cytotoxicity Time-dependent cytotoxicity	68

A549: human adenocarcinomic alveolar epithelial cells; BEAS-2B: human bronchial epithelial cells; H1299: human lung carcinoma cells; HaCaT: human keratinocyte cells; HDF: human dermal fibroblast; HEK: human epidermal keratinocytes; HEK293: human embryonic kidney cells; HeLa: cervical cancer cells; J774: murine macrophages cells; JB6 P+: promoter-sensitive (P+) murine epidermal cells; Jurkat cells: immortalized T lymphocyte cells; MDMs: MDMS-resistant cloned cells; MSTO-211H: lung mesothelioma cells; NHBF: normal human bronchial epithelial cells; RAW 264.7: Mouse leukaemic monocyte macrophage cells; THP-1: Human acute monocytic leukemia cells.

At first glance, the *in vitro* (Table 3.2) and *in vivo* (Table 3.3) studies on SWNTs toxicity appear to be confusing, inconclusive or contradictory, confirming that the toxicity and/or biocompatibility of SWNTs are not fully established. However, if one considers interference with dye-based viability assays, agglomeration issues and oxidative stress due to catalysts contamination, the data available to date seems to favour the conclusion that well-dispersed, purified and/or functionalised SWNTs exhibit relatively low toxicity.

Table 3.3. Summary of *in vivo* toxicity of SWNTs. The term "CNTs" indicates that the material was not identified as single- (SWNTs) or multi-walled (MWNTs) carbon nanotubes. The column "time" indicates the maximum time of treatment: in-between time points were sometimes investigated. Percentage of catalytically active transition metals in the CNTs is reported when indicated by the authors.

CNTs tested	Production method	Model	Administration	Time	Toxic outcome	Ref.
			Dermal toxicity			
CNTs	Arc-discharge	Rabbit	Eyes instillation	72 h	None	69
CNTs	Arc-discharge	Human	Patch test	96 h	None	69
SWNTs	HiPCO (30 wt. % Fe)	Mice	Topical exposure	5 d	Detectable oxidative stress Skin thickening Inflammation	55

CNTs tested	Production method	Model	Administration	Time	Toxic outcome	Ref.
SWNTs	CVD (1-1.5 wt. % Fe)	Mice	Subcutaneous implantation	90 d	Low	[70]
			Pulmonary toxicity			
SWNTs	Not specified (Sigma-Aldrich)	Mice	Pharyngeal aspiration	24 h	Pulmonary inflammatory responses	[71]
CNTs	Arc-discharge	Guinea pigs	Intratracheal instillation	28 d	None	[72]
SWNTs	HiPCO (17.7 wt. % iron)	Mice	Inhalation *versus* pharyngeal aspiration	28 d	Higher toxicity by inhalation	[73]
SWNTs	HiPCO (< 2 wt. % iron)	Mice	Pharyngeal aspiration	30 d	Higher SWNTs dispersion causes higher toxic outcomes	[74]
SWNTs	HiPCO (0.23 wt. % Fe)	Mice	Pharyngeal aspiration	60 d	Acute inflammation	[47]
SWNTs	Laser ablation (5 wt. % Ni and Co)	Rats	Intratracheal instillation	90 d	Controversial	[75,76]
SWNTs	HiPCO (unpurified: 26.9 wt. % Fe, 0.78 wt. % Ni; purified: 2.14 wt. % Fe)	Mice	Intratracheal instillation	90 d	Dose-dependent toxicity	[77]
			In vivo immune responses			
MWNTs, SWNTs	CVD (5 wt. % catalysts)	Mice	Subcutaneous injection/ Intranasal administration	26 d	Allergic responses	[78]
			Vascular system			
[^{111}In] DTPA-CNTs	MWNTs; SWNTs; method not specified	Mice	Intravenous administration	3 h	Non toxic Blood half-life: 3 h Renal clearance	[79]
Pluronic F108-SWNTs	HiPCO	Rabbits	Intravenous administration	24 h	Non toxic Blood half-life: 1 h Accumulation in the liver	[80]
SWNTs-[(DOTA)(AF488)(AF680)]	HiPCO	Mice	Intravenous administration	7 d	Non toxic Renal clearance No active secretion	[81]

CNTs tested	Production method	Model	Administration	Time	Toxic outcome	Ref.
PEG-SWNTs	HiPCO	Mice	Intravenous administration	90 d	Non toxic Blood half-life: 1 day Complete clearance after 2 months	82
			Abdominal cavity			
^{125}I-SWNT-OH	[Not specified]	Mice	Intraperitoneal administration	---	Non toxic Renal clearance	83

The results briefly summarised in Table 3.2 and Table 3.3 clearly indicate that the use of a more coordinated global approach is imperative to define and describe the toxicological responses triggered by SWNTs. Since SWNTs samples vary greatly in terms of composition depending on production and purification methods, the impact of such variability on their toxicity needs to be addressed in a controlled manner and in a cost-effective approach. Current data indicate that functionalised CNTs exhibit lower toxicity than unmodified or unrefined nanotubes. Further research needs to be conducted to confirm that this is the case. Keeping in mind the recent discovery on the biodegradability of CNTs,[84,85] it is imperative to establish the long-term stability of these conjugates *in vivo*. Furthermore, some of the unwanted (toxic) responses of carbon nanotubes may lead to desirable outcomes depending on the specific context. For instance, the controlled induction of carbon nanotube-dependent cellular toxicity could serve as a novel and effective approach for combating cancer. The success of SWNTs technology depends upon the continuation of research into the toxicology of SWNTs and SWNTs-related materials.

1.4. AIMS OF THE STUDY

The purpose of the present study is to assess the cytotoxicity of the SWNTs-based NIR fluorescent probes (p- and o-SWNTs) previously described (see Chapter II) using 3D cellular, tissue-mimetic models for the first time. An established ultrasound standing wave trap (USWT) is used to generate the 3D cell aggregates. A comparative approach with traditional 2D cell culture models is presented, determining the importance of the third dimension in cell culture. Protein-based (bovine serum albumin, BSA) and

surfactant-based (Pluronic F68) dispersions of p- and o-SWNTs were tested and compared to a reference suspension in dimethyl sulfoxide (DMSO). The THP-1 cell line, a macrophage model, was employed to represent the resident phagocytic cells (*i.e.*, monocytes and macrophages) located in the liver (Kupffer cells)[86] that have the main function of removing pathogens, senescent cells and external particles from the bloodstream.[87] Since the liver is a preferential site of nanomaterials accumulation in humans and rats[86,88] (see Chapter I, Section 2.1), THP-1 cells may be exploited as a close equivalent of key indicative phagocytic cell population responding to carbon nanotubes (CNTs). This cell line has been previously employed to gain insight into the potential effects of SWNTs in the liver.[86] The author acknowledges that macrophage responses do not provide a full indication of potential toxic effects in the body; nevertheless, this cellular model offers good cytotoxicity prediction information particularly in the early phases of investigations.[8,50]

The results showed for the first time that the cytotoxicity of p- and o-SWNTs was not detectable in the 3D cellular model following a 24 h exposure. In contrast, 2D cell cultures were significantly affected by exposure to p- and o-SWNTs after 24 h, as assessed by viability and multifluorescence-based cell assays. The different chemical modifications of the SWNTs surface (p- *versus* o-SWNTs; BSA *versus* Pluronic F68) had no detectable effect on the cytotoxicity of p- and o-SWNTs. Finally, cytokine (IL-6 and TNF-α) secretion levels were elevated in the 2D but remained essentially unchanged in the 3D cell models.

In conjunction with the previously reported study on nanoparticles cytotoxicity in 3D cell cultures,[28-30,89] our data clearly underline the importance of incorporating 3D tissue-mimetic cell models in the assessment of SWNTs toxicity and strongly advocate the pressing need for the redefinition of the established nanotoxicology protocols. 3D cell aggregates can serve in fact as alternative *in vitro* models providing guidance on nanomaterial toxicity, in a tissue-mimetic manner. Cells within a tissue interact in fact with adjacent cells and with the extracellular matrix (ECM) through biochemical and mechanical signals. Cell-cell and cell-ECM interactions form a 3D communication network and guarantee the specificity and homeostasis of tissues.[90] Key events in the cell cycle (*i.e.*, growth, proliferation, migration and apoptosis) are also regulated by these interactions,[91] which are not reproduced in standard 2D cell models. 3D cell aggregates offer therefore future cost-effective solutions for toxicity screening assays

under experimental conditions mimicking the functions of living tissues and more closely related to *in vivo* microenvironments, where cells continuously cross-talk through intracellular signaling.[24]

2. RESULTS

2.1. PHYSICO-CHEMICAL CHARACTERIZATION

SWNTs-based NIR fluorescent probes (p- and o-SWNTs) were prepared as described in Chapter II.

NIR-PL spectra showed that p- (Figure 3.1a) and o-SWNTs (Figure 3.1e) in RPMI 1640 cell media emitted more efficiently when dispersed in media supplemented with bovine serum albumin (BSA) or Pluronic F68. In addition, the NIR-PL intensity of o-SWNTs was higher than that of p-SWNTs. Interestingly, the NIR-PL intensity of Pluronic F68-stabilised dispersions decreased significantly (Figure 3.1d and 3.1h) after 24 and 72 h, whereas the NIR-PL intensity of BSA-stabilised dispersions was rather stable over 2 days (Figure 3.1c and 3.1g).

Zeta potential measurements evidenced a negative surface potential for both p- and o-SWNTs in DI water or in supplemented RPMI 1640 cell media (Table 3.4), with or without addition of dispersing agents (BSA or Pluronic F68). As previously described in the literature, the electrophoretic determination of zeta potential was calculated by assuming spherical geometry[92,93] and then applying the Smoluchowski approximation.[94] Table 3.4 shows that in DI water o-SWNTs had increased absolute values of zeta potential when compared to p-SWNTs. A decrease in the absolute values of zeta potential is registered when both p- and o-SWNTs are suspended in RPMI 1640 cell media. Notably, p-SWNTs dispersions in RPMI 1640 cell media had higher zeta potential than o-SWNTs suspensions.

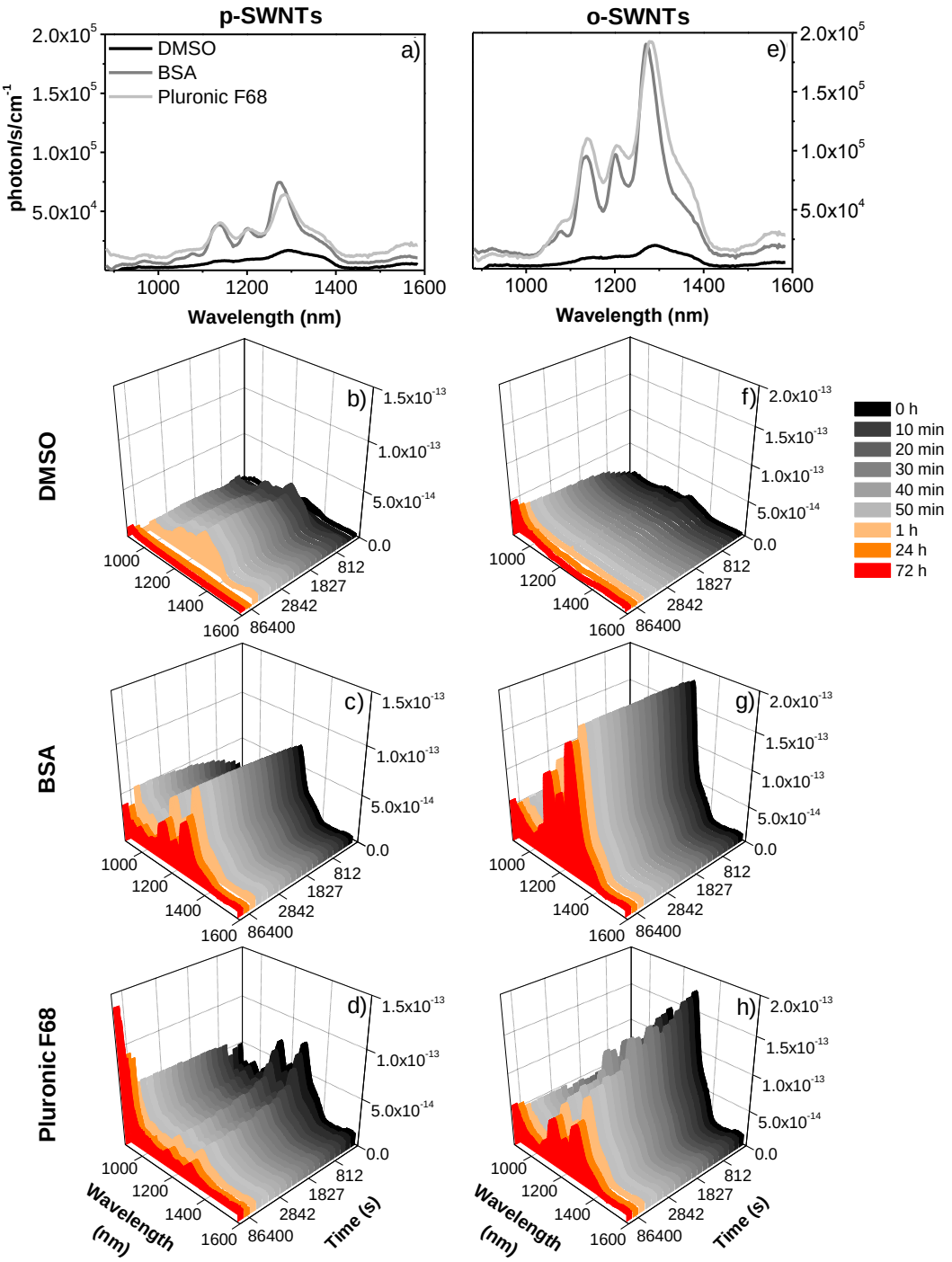

Figure 3.1. NIR-PL spectra (λ_{exc} = 683 nm) of (a-d) p- and (e-h) o-SWNTs dispersed in supplemented RPMI 1640 cell media ($[SWNTs]_i$ = 120 µg/mL) with or without the addition of a dispersing agent (BSA or Pluronic F68). Graphs (b-d; f-h) show the changes of NIR-PL of (b, f) DMSO-, (c, g) BSA- and (d, h) Pluronic F68-stabilised dispersions over 1 h (black to light orange curves), after 24 h (orange curves), and after 72 h (red curves).

Table 3.4. Surface charges of p- and o-SWNTs before and after dispersion in supplemented RPMI 1640 cell media at three different concentrations (120, 60, and 12 μg/mL). Zeta potential values are reported as average (± standard error of the mean).

SWNTs	Dose (μg/mL)	Zeta potential (mV)†					
		DMSO*		BSA*		Pluronic F68*	
		DI water	RPMI 1640	DI water	RPMI 1640	DI water	RPMI 1640
p-SWNTs	120	-23.6 (± 2.8)	-2.7 (± 0.3)	-30.3 (± 3.3)	-9.3 (± 0.9)	-14.1 (± 1.3)	-0.9 (± 0.1)
	60	-21.0 (± 5.3)	-6.5 (± 0.9)	-12.9 (± 2.0)	-11.1 (± 0.9)	-13.1 (± 1.8)	-10.6 (± 0.8)
	12	-27.8 (± 0.6)	-2.0 (± 0.4)	-33.4 (± 0.7)	-14.4 (± 0.7)	-17.0 (± 0.9)	-11.5 (± 0.9)
o-SWNTs	120	-40.2 (± 1.5)	-2.9 (± 1.0)	-9.2 (± 0.3)	-2.8 (± 0.3)	-29.8 (± 0.6)	-1.1 (± 0.2)
	60	-58.4 (± 0.7)	-4.7 (± 0.6)	-33.2 (± 0.5)	-1.2 (± 0.2)	-41.7 (± 0.8)	-1.9 (± 0.3)
	12	-38.2 (± 2.2)	-0.4 (± 0.2)	-41.3 (± 0.5)	-0.8 (± 0.2)	-43.3 (± 1.2)	-0.4 (± 0.2)

† Surface charges were measured in DI water or in RPMI 1640 cell media.
* Dispersing agent added as described in the experimental section (Chapter IV, Section 3.1).

2.2. High Content Screening and Analysis (HCSA) of 2D cell cultures

Three different concentrations (120, 60 and 12 μg/mL) of p- and o-SWNTs were tested on populations of 20,000 cells. Doses are therefore expressed as 12×10^{-4}, 6×10^{-4} and 1.2×10^{-4} μg/cell respectively. No significant changes in cellular responses were detectable when 2D cell cultures were exposed to solutions containing equivalent amounts of DMSO, BSA, or Pluronic F68 for 72 h (see Chapter IV, Section 3.4.1).

Cell viability: Results for the time and dose dependent effect of p- and o-SWNTs on the cell viability are shown in Figure 3.2 in the form of heatmap. The corresponding multiparametric HCSA data plotted as conventional graphs are reported in Chapter VI (Section 4.1). Both p- and o-SWNTs demonstrated to influence considerably the cell viability, causing a significant decrease in cell count at all doses and for all nanotube dispersions after 24 and 72 h.

Cell membrane permeability: A significant increase in the cell membrane permeability was registered after a 72 h exposure to BSA-stabilised p-SWNTs dispersions at all employed concentrations (Figure 3.2). These results indicate that the cytoplasmic membrane was compromised, while it remained unaffected after 24 h of exposure to DMSO- and Pluronic F68-stabilised dispersions of p-SWNTs at all examined timepoints. Significant changes were found in cells incubated with o-SWNTs,

irrespective of the dispersing agent used (BSA, DMSO or Pluronic F68) or the timepoint.

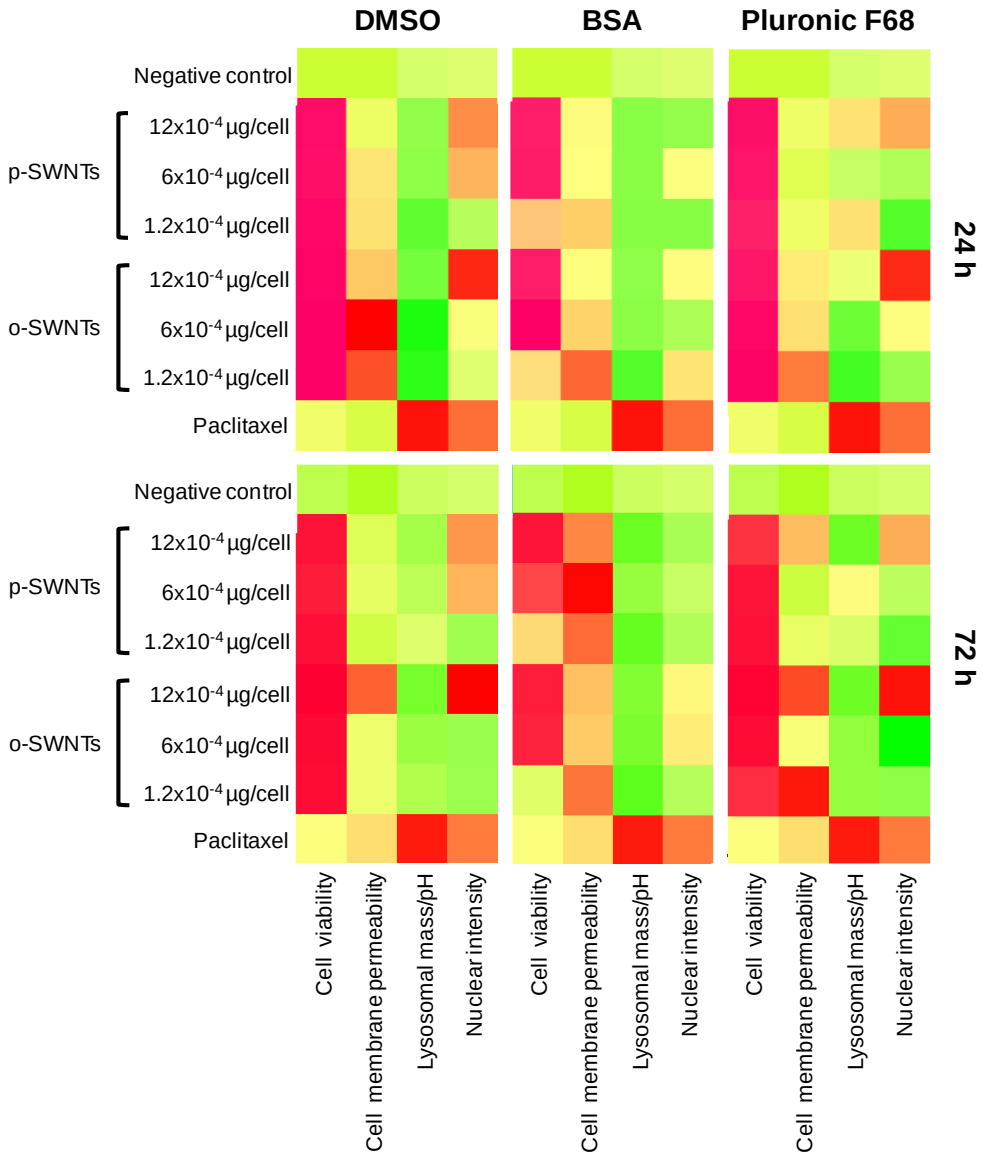

Figure 3.2. Graphical response intensity tables (heatmaps) of multiparametric HCSA data for 2D cell cultures exposed to p- and o-SWNTs for 24 h and 72 h. Colorimetric gradient tables reflect the cytoxicity evolution by showing the cell viability (left column), cell membrane permeability, lysosomal mass/pH and nuclear intensity (right column) changes. Colours range from dark green (values lower than 15% of maximum value measured) to bright green (30%), yellow (50%), bright orange (60%), dark orange (75%) and finally to red (values higher than 75% of maximum value). Heatmap values are normalised to the percentages of the positive control and Z score is calculated as described in the statistical analysis section. Data represent three independent experiments performed in triplicate samples.

Lysosomal mass/pH: No significant changes in the lysosomal mass/pH were seen in p- or o-SWNTs treated cultures (Figure 3.2).

Nuclear Intensity: As for the lysosomal mass/pH changes, marginal or non-detectable changes in the nuclear intensity were seen in any treatment with the exception of the 12×10^{-4} µg/cell dose, after 24 and 72 h exposure to p- and o-SWNTs, and of the 6×10^{-4} µg/cell dose in 2D cell cultures treated with DMSO-stabilised p-SWNTs dispersions (Figure 3.2).

2.3. Cytotoxicity assays of 3D cell culture models in situ in the USWT

Trypan Blue exclusion assay: 3D cell aggregates (non-treated, negative control) were 78 % viable over 24 h in the USWT and remained as such following exposure to p- and o-SWNTs at 1.2×10^{-4} µg/cell (Figure 3.3a-b). Significant cell death was measured only when aggregates were treated with 1.7 µM Paclitaxel (positive control) or phorbol-12-myristate-13-acetate (PMA, 0.5 mM). No differences in cell death levels were seen among the various stabilised SWNTs suspensions tested.

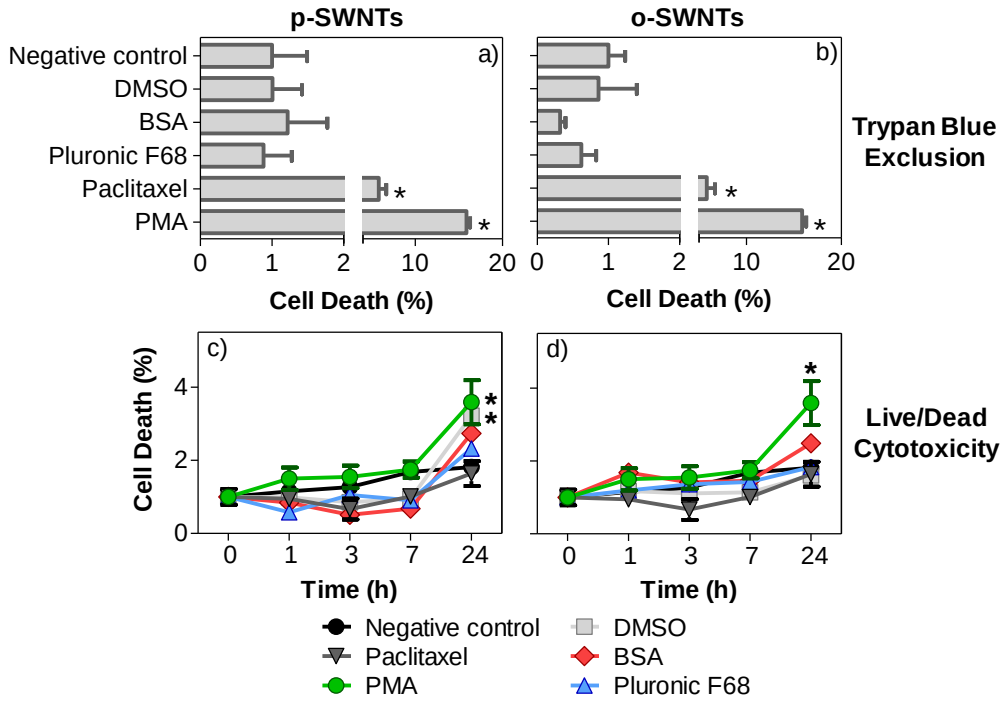

Figure 3.3. Cell death response quantified by (a, b) Trypan Blue exclusion and (c, d) Live/Dead Cytotoxicity assays after exposure of 3D cell aggregates to (a, c) p- and (b, d) o-SWNTs at 1.2×10^{-4} µg/cell for 24 h *in situ* in the USWT. DMSO-, BSA- and Pluronic F68-stabilised dispersions were tested.

Live/Dead Cytotoxity assay: The Live/Dead cytotoxicity assay was performed in order to (1) validate the data obtained by Trypan Blue exclusion assay, and (2) investigate whether the cell death was localised to the edges of the 3D aggregates, where cells were in direct contact with SWNTs. Quantification of cell death based on the epifluorescent images (Figure 3.3c-d) revealed no significant cytotoxic effects of the three differently stabilised p- and o-SWNTs dispersions when compared to the negative control (cell death ranged between 20 and 44 %). In parallel, the distribution of live and dead cells in SWNTs-treated 3D aggregates (Figure 3.4d) was similar to the negative control (Figure 3.4c) for all time points examined. Figure 3.4 shows representative results for p-SWNTs BSA-stabilised dispersion; consistent results were obtained for all the other SWNTs samples.

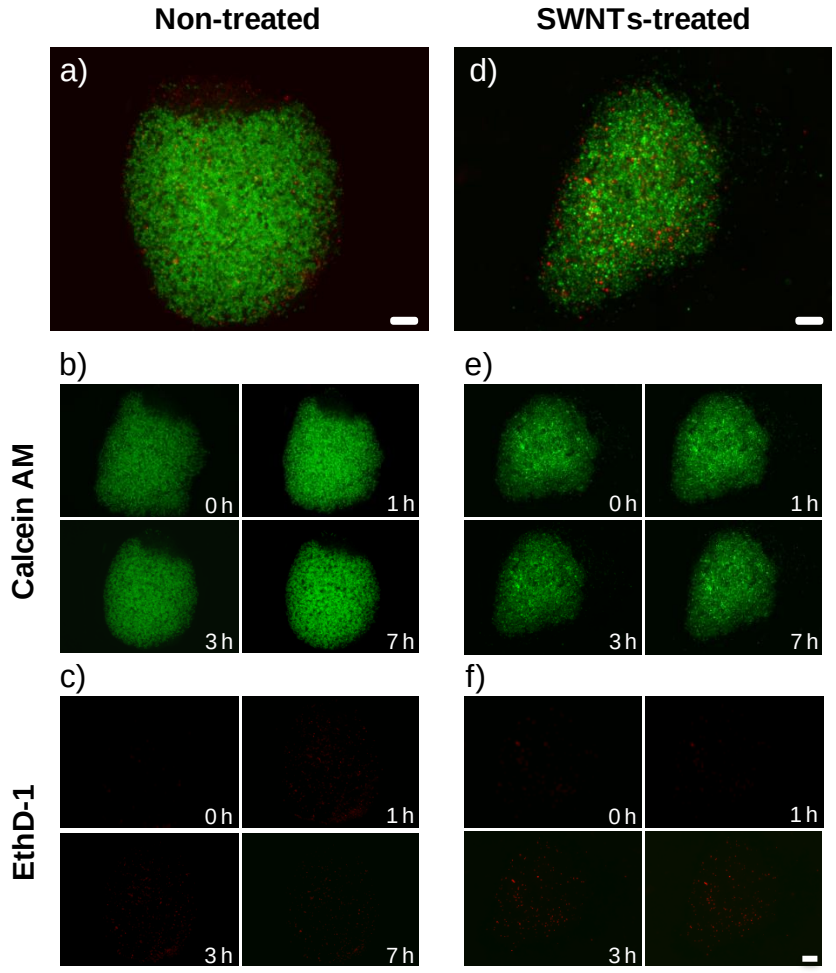

Figure 3.4. Representative epifluorescent images of (a-c) non-treated and (d-e) SWNTs-treated 3D cell aggregates *in situ* in the USWT (a, d) after 24 h and b, c, e, f) after 0, 1, 3, and 7 h, stained with Calcein AM (live cells) and EthD-1 (dead cells). SWNTs concentration: 1.2×10^{-4}

µg/cell; SWNTs sample: p-SWNTs BSA-stabilised dispersion. Scale bars: 40 µm (10× magnification).

2.4. Cytotoxicity assays in 3D cell culture models in culture

In order to determine whether the different cellular responses observed in the 2D and 3D cellular models could be somehow associated with the different activation state of the THP-1 cell models employed (adherent "macrophage-like" cells in the 2D cell model and suspended monocytes in 3D cell aggregates), 3D cell aggregates of PMA-activated THP-1 cells were initially formed in the USWT, subsequently recovered from it and exposed to p- and o-SWNTs in 24-well plates.

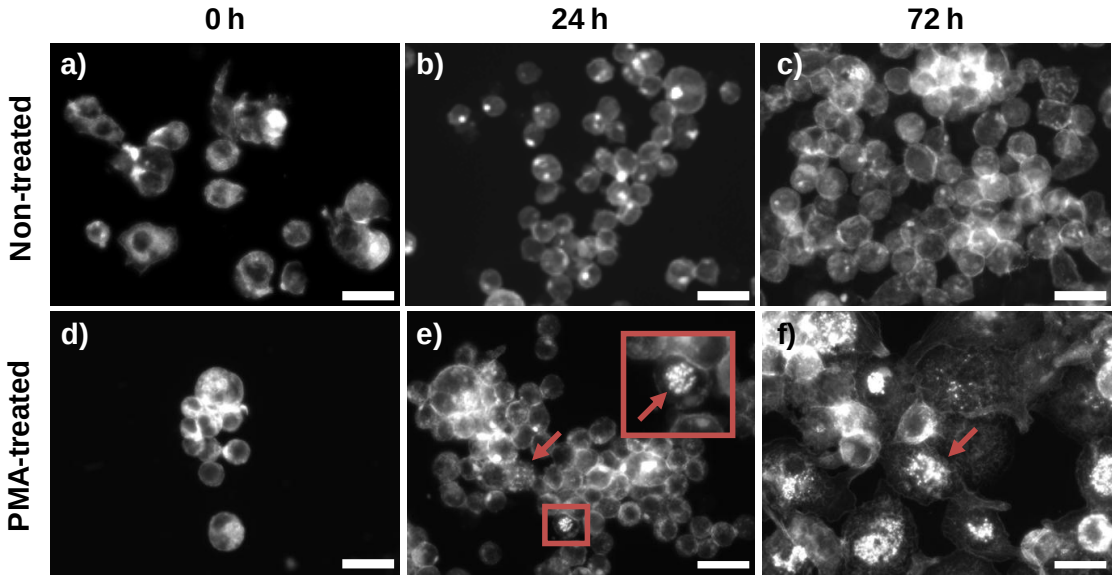

Figure 3.5. Representative epifluorescent microscopy images of (a, b, c) non-treated and (d, e, f) PMA-treated 3D cell aggregates stained with Phalloidin-Alexa 488 conjugate after: (a, d) 0 h, (b, e) 24 h, and (c, f) 72 h incubation. (e) PMA induced activation of THP-1 cells in 3D aggregates after 24 h. (e, f) Arrows point out the punctate F-actin staining. Scale bars: 20 µm (50× magnification).

Epifluorescence microscopy analysis showed that F-actin was localised at the cell periphery in non-treated and PMA-treated aggregates cells soon after plating (t = 0 h) (Figure 3.5a, d). However, in PMA-treated aggregates F-actin redistributed into intensely stained punctate foci after 24 h in culture (Figure 3.5e), thus confirming that PMA induced the activation of THP-1 cells within the 3D aggregates. The punctate F-

actin fluorescence along the cells is associated with monocyte-to-macrophage differentiation and it is indicative of adhesive structure formation.[95] The F-actin foci were restricted to the cells in direct contact with the substrate. However, since this F-actin reorganization was not highlighted in non-treated 3D aggregates (Figure 3.5b, c), an activation process due to the cell-substrate interaction was excluded. Punctate F-actin was even more visible across the entire cell surface after 72 h (Figure 3.5f), while it was absent in non-treated 3D cell aggregates at 24 and 72 h (Figure 3.5b and 3.5c respectively). Confocal microscopy analysis confirmed that PMA caused F-actin reorganization in PMA-treated 3D cell aggregates after 24 h (Figure 3.6b, c). Notably, THP-1 cells activation was achieved not only when PMA was mixed with THP-1 cells just before introducing them into the USWT, but also when PMA was introduced into the USWT after formation of the 3D cell aggregate (data not shown).

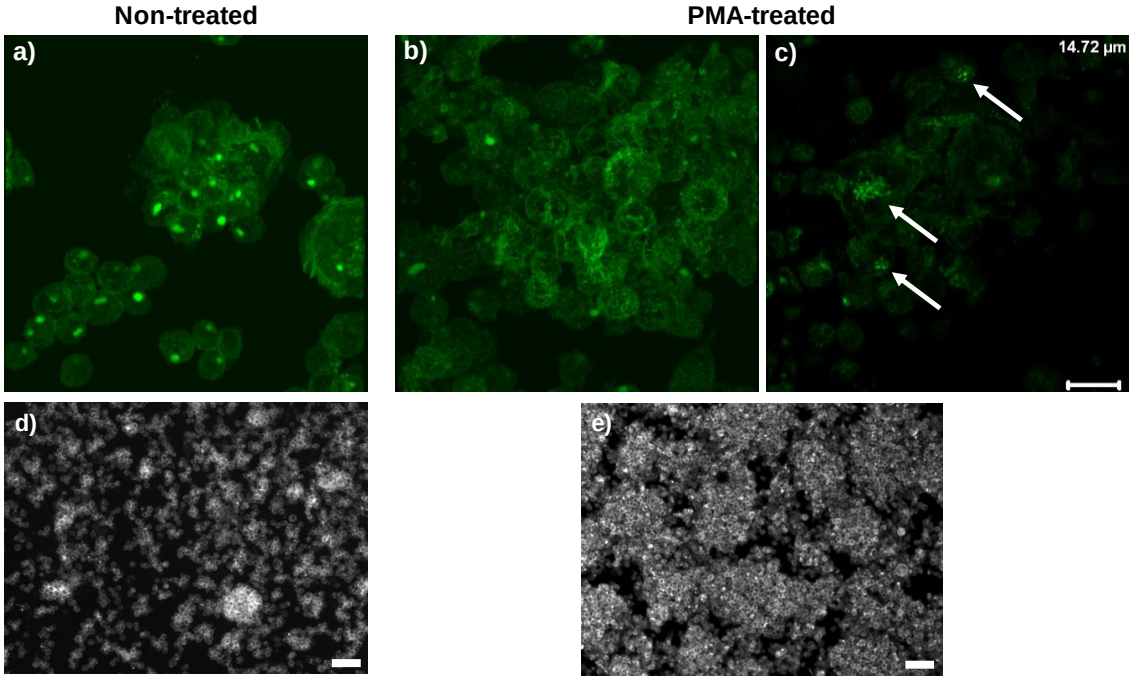

Figure 3.6. Representative (a-c) confocal and (d, e) epifluorescent microscopy images of (a, d) non-treated and (b, c, e) PMA-treated 3D cell aggregates stained with Phalloidin-Alexa 488 conjugate after 24 h incubation. (a, b) Different F-actin organization is evident between the two aggregates. (c) Z-stack image of the PMA-treated 3D cell aggregate shown in (b) illustrating the cells in direct contact with the substrate. Redistribution of F-actin into intensely staining punctate foci is evident (arrows). (e) Large cell aggregates are seen in PMA-treated samples. (a-c) Scale bar: 20 µm (63× magnification); (d, e) scale bars: 40 µm (10× magnification).

As per 3D aggregates morphology, PMA-treated 3D cell aggregates were mechanically robust, allowing for their easy handling (Figure 3.6e). In contrast, non-treated 3D cell aggregates broke easily when F-actin staining was carried out (Figure 3.6d). This result supported the F-actin staining data, suggesting the formation of adhesive structures among THP-1 cells.

Trypan Blue exclusion assay: Non-treated (negative control) 3D aggregates remained 80 % viable over 24 h (similarly to the results obtained for 3D aggregates *in situ* in the USWT). Exposure to p- and o-SWNTs did not significantly impaired cell viability, with the exception of the DMSO-stabilised p-SWNTs dispersion (Figure 3.7a, b).

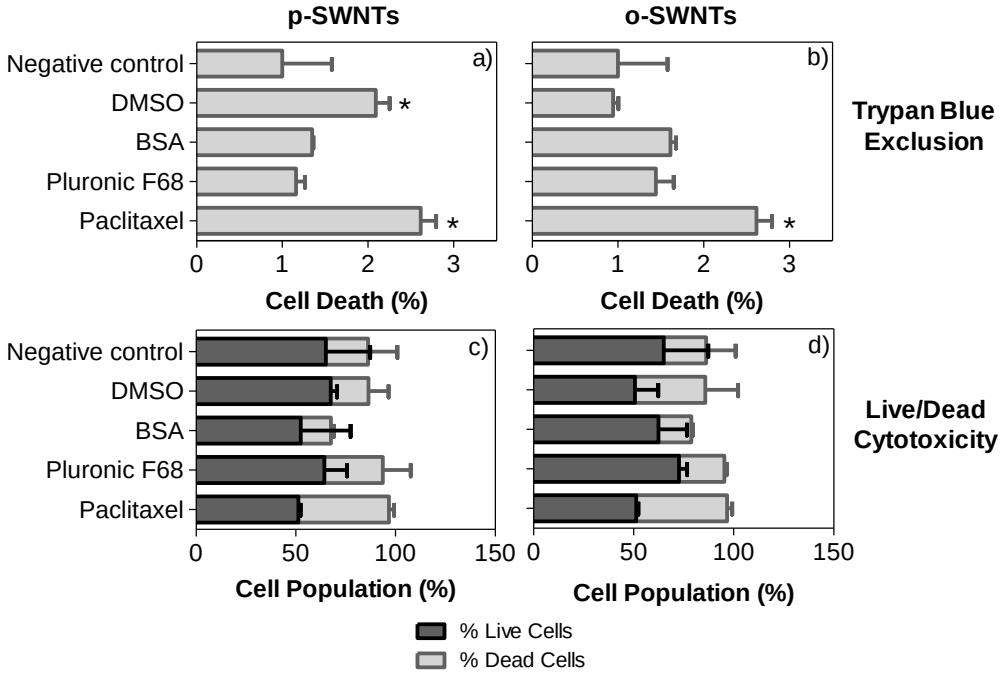

Figure 3.7. (a, b) Percentage (%) of cell death quantified by Trypan Blue exclusion assay and (c, d) % of live and dead cells detected by flow cytometry in 3D cell aggregates in culture exposed to (a, c) p- and (b, d) o-SWNTs at 1.2×10^{-4} µg/cell for 24 h.

Flow cytometry of Live/Dead cells: p- and o-SWNTs did not cause any detectable cytotoxic outcome when compared to the non-treated aggregates (Figure 3.7c, d). The accompanying representative flow cytometric graphs are shown in Figure 3.8.

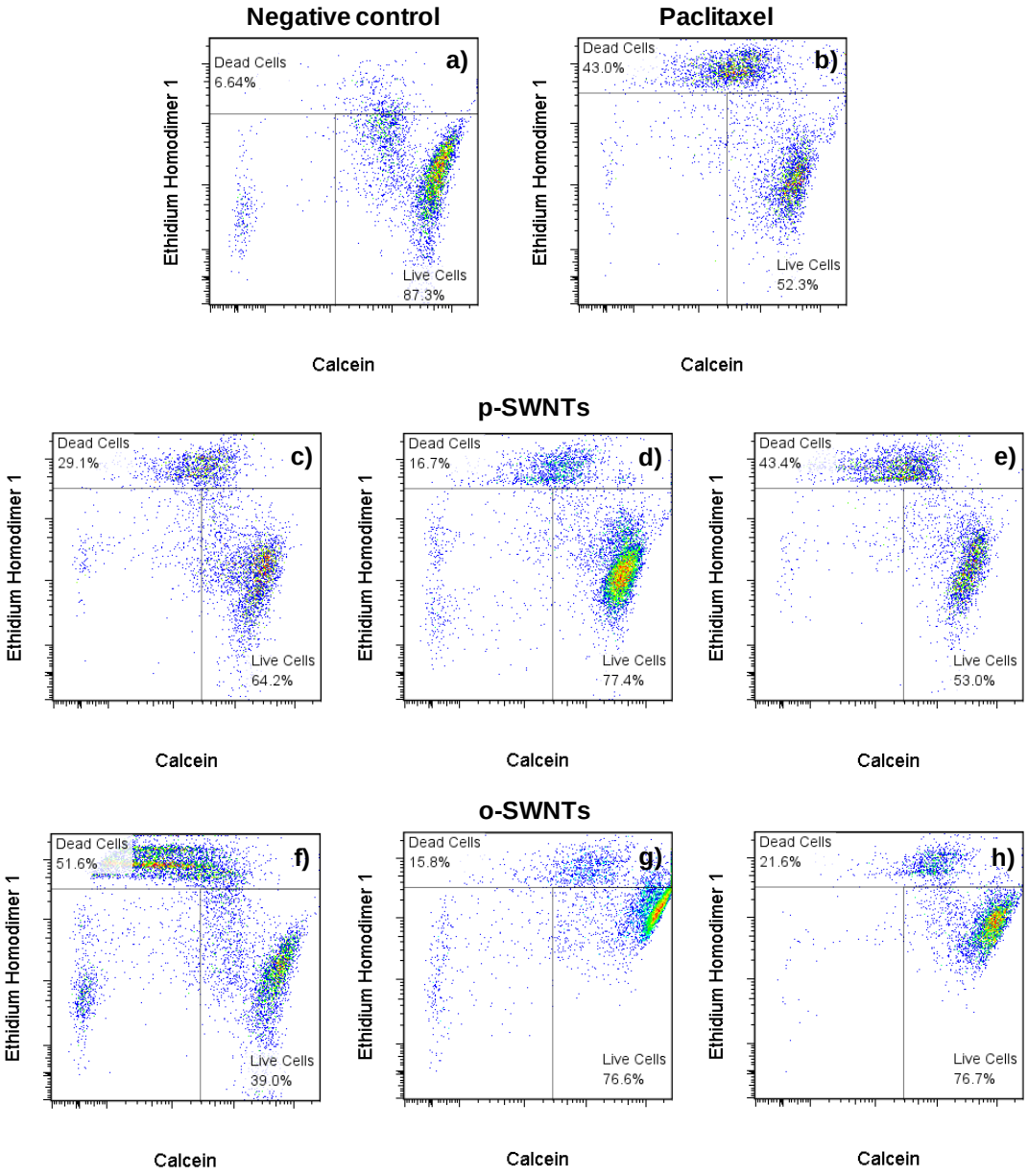

Figure 3.8. Representative flow cytometry graphs (single cells gated) of 3D aggregates in culture: (a) negative control; (b) Paclitaxel 1.7 µM; (c, d, e) exposed to p-SWNTs; (f, g, h) exposed to o-SWNTs. (c, f) DMSO-, (d, g) BSA-, and (f, h) Pluronic F68-stabilised dispersions were tested.

Live/dead staining analysis of 3D cell aggregates by confocal microscopy (Figure 3.9) further confirmed the flow cytometric data. Figure 3.9b and 3.9d are representative of all the SWNTs dispersions tested in 3D cell aggregates in culture.

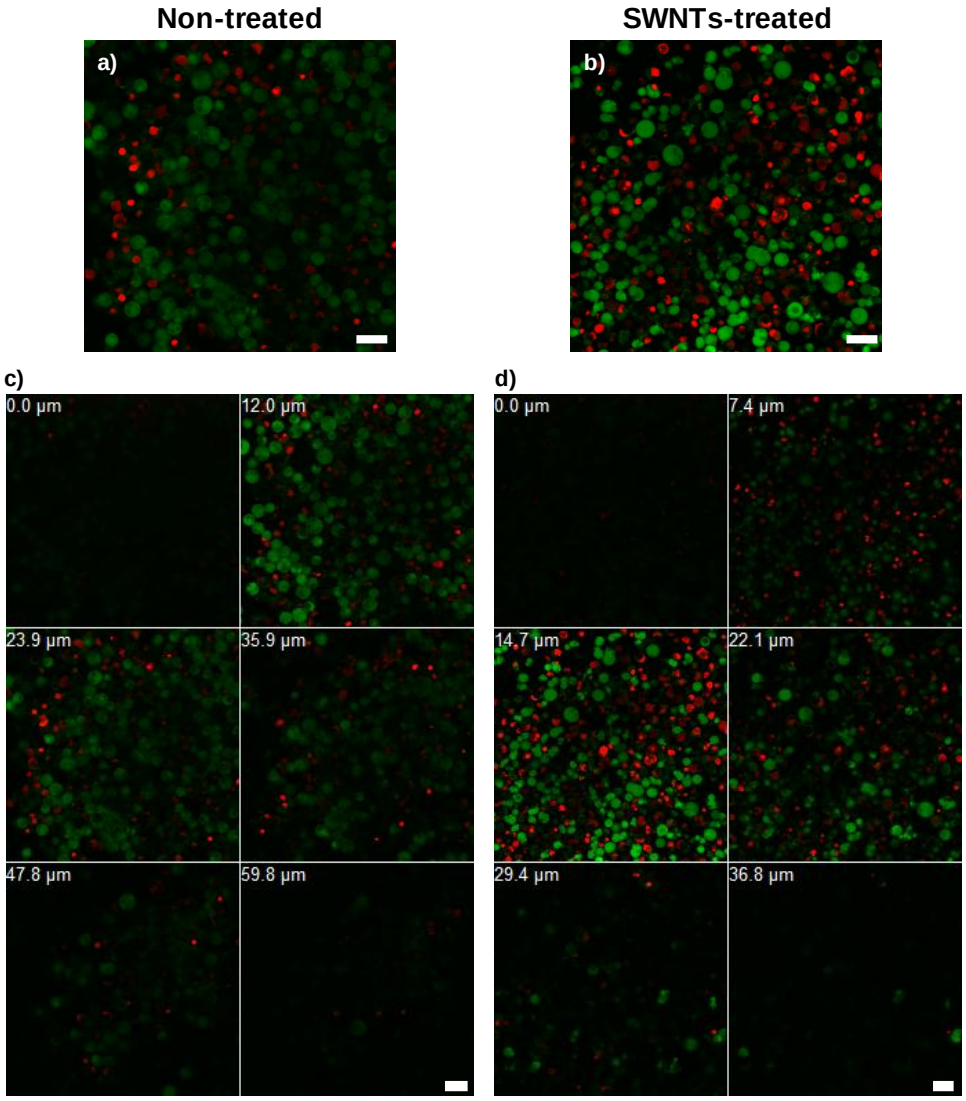

Figure 3.9. (a, b) Representative confocal images of (a) non-treated (negative control) and (b) SWNTs-treated 3D cell aggregates in culture after 24 h. (c, d) Gallery of stack images of (c) non-treated and (d) SWNTs-treated 3D cell aggregates. Micrographs in (c) and (d) are of the same 3D cell aggregate shown in (a) and (b) respectively. Live cells are seen in green, red indicates dead cells. Similar cell viability level can be seen in the two 3D cell aggregates. SWNTs sample: p-SWNTs BSA-stabilised dispersion. Scale bars: 20 µm (20× magnification).

2.5. CYTOKINES EXPRESSION

Indirect post-exposure quantification of TNF-α and IL-6 expression levels by enzyme-linked immunosorbent assay (ELISA) allowed to quantify the extent of inflammatory proteins secretion due to the cell stress-induced signalling cascade and transduction activity.

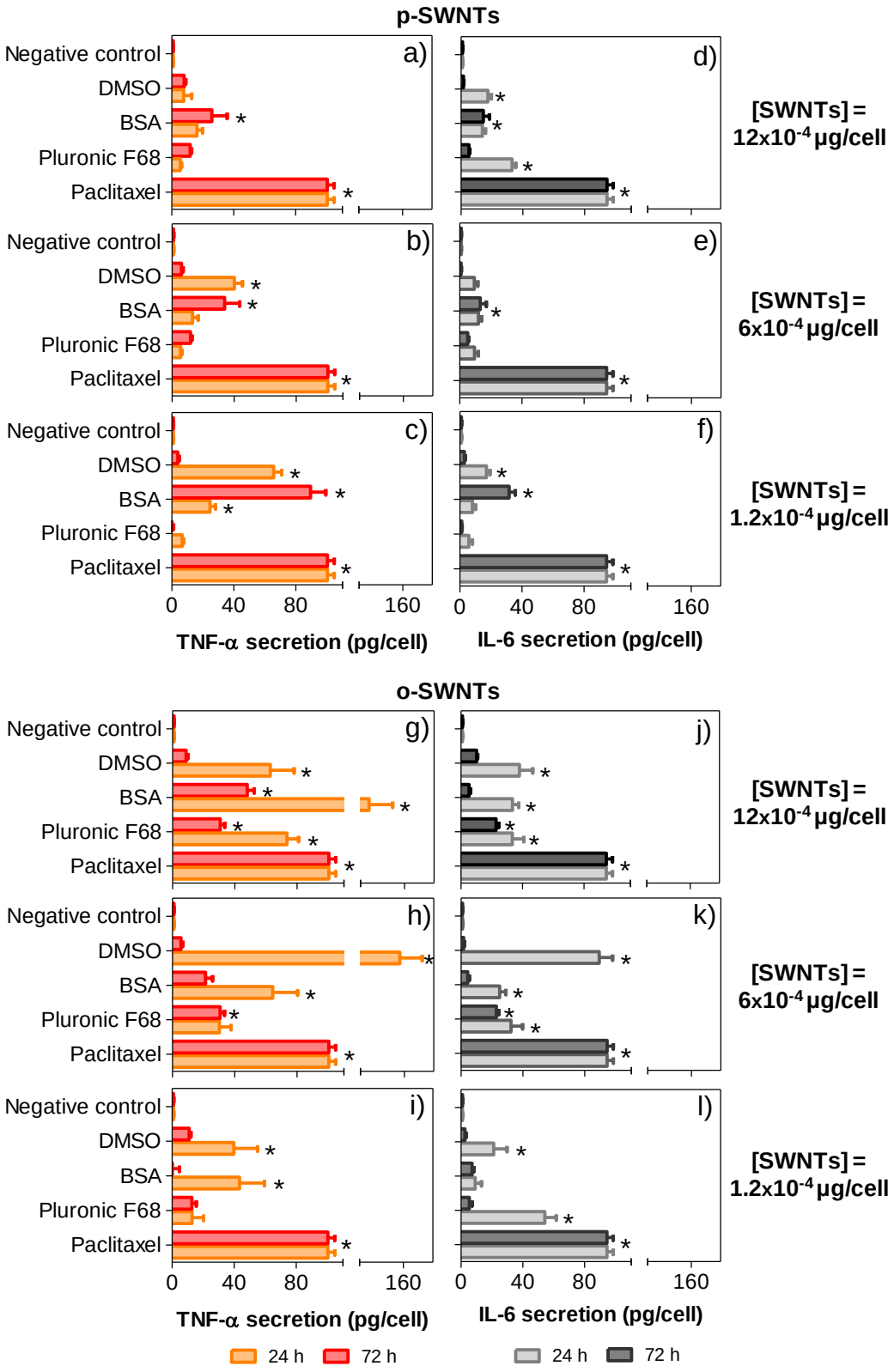

Figure 3.10. Release of (a-c, g-i) TNF-α and (d-f, j-l) IL-6 from 2D cell cultures after 24 and 72 h exposure to (a-f) p- and (g-l) o-SWNTs at various concentrations: (a, d, g, j) 12×10^{-4}, (b, e, h, k) 6×10^{-4} and (c, f, i, l) 1.2×10^{-4} µg/cell.

ELISA assays revealed high secretion of pro-inflammatory cytokines (IL-6 and TNF-α) in 2D cell cultures following exposure to p- (Figure 3.10a-f) and o-SWNTs (Figure 3.10g-l) after 24 and 72 h exposure. In contrast, no significant changes in IL-6 and TNF-α secretion were detected in 3D cell aggregates exposed to p- and o-SWNTs *in situ* in the USWT (Figure 3.11a, c, e, g) or in culture (Figure 3.11b, d, f, h) after 24 h exposure, which is in concert with the above described data on comparative SWNT cytotoxicity in 2D and 3D models

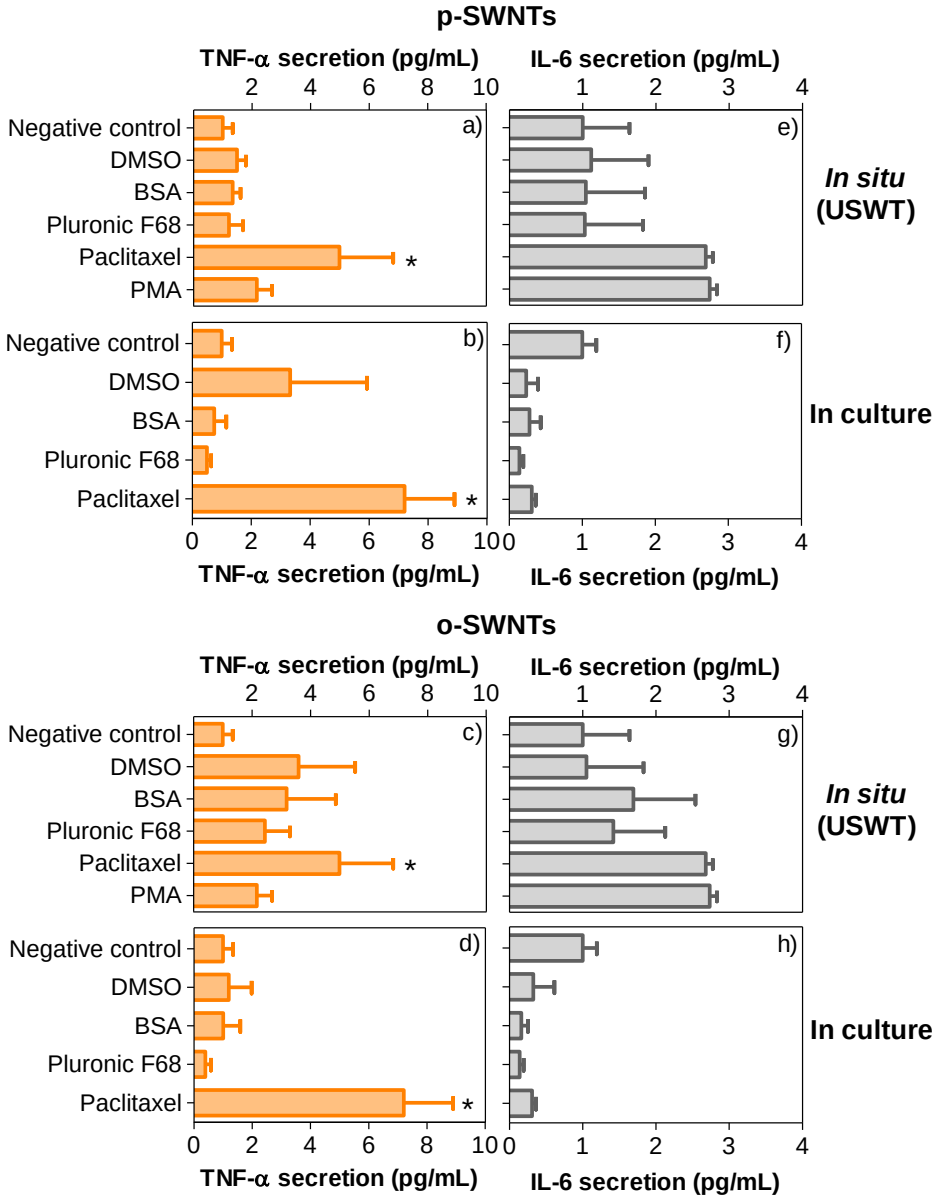

Figure 3.11. Release of (a-d) TNF-α and (d-h) IL-6 from 3D cell aggregates (a, c, e, g) *in situ* in the USWT or (eb, d, f, h) in culture after 24 h exposure to (a, b, e, f) p- and (c, d, g, h) o-SWNTs at 1.2×10^{-4} µg/cell.

3. DISCUSSION

3.1. PHYSICO-CHEMICAL CHARACTERIZATION

Complete physico-chemical characterisation of the tested material is required nowadays to enhance the validity of the performed toxicity studies.[6,11-13,51,96] A thorough characterisation of the impurities content, lengths and electronic properties of the SWNTs-based NIR probes (p- and o-SWNTs) is reported in Chapter II, showing that p- and o-SWNTs are able to emit efficiently in the NIR despite the employment of strong chemical treatments that shorten the tubes and introduce defect sites on the nanotube surface.[97] In this chapter, NIR-PL spectroscopy (Figure 3.1) and zeta potential measurements (Table 3.4) were carried out on p- and o-SWNTs dispersed in DI water or RPMI 1640 cell media. Taking into account that (1) the dispersion grade of CNTs in the biological media can affect both their *in vitro*[41] and *in vivo*[42] toxicity, (2) bundles of SWNTs can be disrupted via non-covalent functionalisation with surfactants[98,99] and (3) *in vitro* cell responses seem to depend strongly on the surfactant employed,[41,43,44] protein-based (BSA) and surfactant-based (Pluronic F68) methodologies were used for dispersing p- and o-SWNTs in an aqueous/biological environment. BSA is a water-soluble globular protein that has been shown to adsorb on CNTs surface[100,101] and to have an excellent dispersing capability[102] even in *in vitro* conditions.[103] BSA is characterised by a pH-sensitive tertiary structure,[104,105] which strongly affects its capability of stabilising CNTs dispersions at varying pH.[106] Better-dispersed SWNTs solutions are achieved at pH ranging between 4 and 8,[106] which was in agreement with this study, where all SWNTs solutions had a neutral pH (pH = 6-7). Pluronic F68 is a biocompatible,[107] linear copolymer of isopropylene glycol repeating units, with properties very similar to a non-ionic surfactant.[108] Pluronic F68 is able to stabilise aqueous dispersion of SWNTs[109] and copolymers of the Pluronic family are successfully adopted in the toxicity testing of CNTs.[42,110] SWNTs dispersions in DMSO were used as reference. For consistency both p- and o-SWNTs were dispersed in DMSO.

NIR-PL spectroscopy (Figure 3.1) was employed to clarify the stability of p- and o-SWNTs in RPMI 1640 cell media over time. As mentioned in Chapter II (Section 1.1.2), NIR fluorescence is the optical property of SWNTs that is most sensitive to sample dispersion grade. Aggregation of isolated nanotubes prevents in fact the luminescence of SWNTs[111,112] and reduces PL intensity.[112-115] Better dispersions were

achieved by addition of BSA and Pluronic F68 to the supplemented RPMI 1640 media (Figure 3.1a, e). Shifts in the position of the NIR-PL peaks were shown when BSA or Pluronic F68 was added, thus confirming the interaction of such dispersing agents with the nanotubes' surface. The higher NIR-PL intensity of o-SWNTs (Figure 3.1e) suggested that the more hydrophilic o-SWNTs were better dispersed in cell media than p-SWNTs (Figure 3.1a). Additionally, Pluronic F68 was less effective than BSA in stabilising p- and o-SWNTs dispersions over time. The NIR-PL intensity of Pluronic F68-stabilised dispersions decreased significantly after 24 and 72 h (Figure 3.1d, h), whereas BSA was capable of forming dispersions that were rather stable over 72 h (Figure 3.1c, g). This result found rationalization in the remarkable property of BSA to stabilise SWNTs aqueous solutions even in the presence of monocationic (Na^+) and dication (Ca^{2+}) ions.[116]

The zeta potential of p- and o-SWNTs was negative at neutral pH (Table 3.4), similar to previously reported findings.[92,94,116,117] In DI water, o-SWNTs showed high absolute values of zeta potential with all surfactants: this may be due to the negative surface charges associated with the dissociated carboxylic groups (COO^-) on their surface[93] or to the higher dispersability of the more hydrophilic o-SWNTs in water (dispersions with zeta potential above +30 mV or below -30 mV correspond to stable solutions[118]). Yet the co-existence of the two phenomena is possible. When RPMI 1640 cell media was added, the dispersions' stability decreased (*i.e.*, absolute values of zeta potential decreased). Similar to what is observed with aqueous colloidal particles[118] and to what is reported in previous studies on carbon nanotubes,[92,116] our results are attributed to the high ionic strength of RPMI 1640 cell media that suppressed the electrostatic repulsion among tubes. Notably, p-SWNTs dispersions in RPMI 1640 cell media had higher zeta potential than o-SWNTs suspensions. As shown by NIR-PL data, this is not associated with a higher stability of p-SWNTs dispersions in RPMI 1640 media, whereas it can be explained by the passivation of the COO^- attached onto o-SWNTs surface by the positively charged components (such as cations, proteins) of the cell media.

3.2. Cytotoxicity Analysis of 2D cell cultures

As per Hartung's guidelines,[3] we chose the HCSA system as the ideal tool in simultaneously detecting changes in many cellular properties, thus producing a comprehensive set of data that provide guidance on the toxic response of a whole

organism.[119] Cell viability, cell membrane permeability, lysosomal mass/pH and nuclear staining intensity changes are parameters commonly used for evaluating the cellular cytotoxicity of chemical compounds,[120] drugs and nanomaterials [20,121,122]. In this study, HCSA data (Figure 3.2) and cytokine secretion (Figure 3.10) consistently showed that p- and o-SWNTs can cause cell stress no matter the purity grade, the reactive groups present onto SWNTs surface, the dispersing agent used and/or the stability of the dispersion. Even though contradictory cytotoxicity results have been shown on the cellular response of macrophages in 2D cell models exposed to SWNTs,[60,61,123,124] these results were in agreement with some studies recently reported in the literature.[59,125] Additionally, although metal impurities seem to play a key role for the toxicity of SWNTs,[60,61,124,126] recent studies did identify the CNTs themselves as the principle cause of cytotoxicity in macrophages, rather than the catalysts.[125] In particular, the HCSA data indicated that SWNTs can cause cell stress no matter the purity grade and/or the dispersing agent used (Figure 3.2). Concentrations of p- and o-SWNTs used in this study (120, 60, and 12 μg/mL, equivalent to 12×10^{-4}, 6×10^{-4} and 1.2×10^{-4} μg/cell) were relatively high, but consistent with published studies. In recent *in vitro* studies on macrophages responses, SWNTs concentrations varied from 0.3 – 10 μg/mL,[126] to 1 – 50 μg/mL,[125] 15 - 60 μg/mL,[60] 3 – 150 μg/mL,[127] 50 - 200 μg/mL,[128] and finally up to 0.12 - 0.5 mg/mL.[61] Also in these above referenced reports contradictory cytotoxicity responses have been detected.

3.3. CYTOTOXICITY ASSAYS OF 3D CELL CULTURE MODELS

Cell viability analysis (Figure 3.3 and Figure 3.7) and cytokine secretion (Figure 3.11) consistently showed no detectable cytotoxic response or cell stress in 3D cell aggregates exposed to p- and o-SWNTs *in situ* in the USWT or in culture. Furthermore, epifluorescent microscopy analysis provided evidences that cell death had a random distribution within SWNTs-treated 3D aggregates *in situ* in the USWT (Figure 3.4) and in culture (Figure 3.9) and it was not localised in areas where cells were in direct contact with the SWNTs.

Using the USWT we successfully fulfilled the necessity of reproducing one of the most important features of tissues i*n vivo*, *i.e.* its three-dimensional architecture, bridging the gap between *in vitro* cell models and complex *in vivo* studies[129] and offering added value on the prediction of SWNTs toxicity. 3D cell aggregates formed

by USWT give rise to a more tissue-mimetic cell model compared to conventional 3D cellular models. The USWT avoids in fact the introduction of polymeric 3D-cell-growth substrates[130-133] while allowing intercellular adhesive interactions to occur among cells.[134,135] Additionally, it permits to monitor the cytotoxic response of cells to SWNTs without any interference by sedimentation processes.[136] To this end, the different cytotoxic responses and cytokine release between the 2D and 3D cell models (both *in situ* in the USWT and in culture) presented here, are most likely associated with the addition of the third dimension in the cell culture models and the extensive cell-cell interactions occurring in the 3D cell aggregates. It is a well-established fact that enhanced cell adhesion contacts commonly result in the increased population viability, in contrast to the loss of adhesion, or *anoikis*, leading to apoptosis.[137] In addition, some intrinsic limitations of *in vitro* models, including the methods of exposing cells, do not allow to accurately reproduce the physiologically coordinated responses among various cell types in tissues and organs, and the delivery of SWNTs in one single dose does not reflect *in vivo* realistic conditions, where SWNTs are likely to accumulate gradually and at different concentrations due to different penetration thresholds through the different cellular layers. Further studies are necessary to clarify the cellular mechanisms involved in the response of 3D cell models to nanomaterials, including SWNTs.

4. CONCLUSIONS

The study showed that the SWNTs-based NIR fluorescent probes (p- and o-SWNTs) were cytotoxic in 2D but not to the same extent in 3D cell culture models. As there is great uncertainty when conducting toxicological studies of CNTs (mainly due to the accuracy of the toxicity protocols and of the technologies employed until now), this study clearly demonstrated the importance of 3D cell culture models. The ability to rapidly and reproducibly form uniformly shaped and sized 3D aggregates by the USWT is undoubtedly of high interest and potential in the screening of the toxicity of SWNTs and other nanomaterials. In addition to the opportunities to more closely imitate realistic 3D tissue microenvironments, these 3D models can help in identifying and establishing necessary chemical modifications that are required to make such nanomaterials more biocompatible for a range of biological and medical applications, such as biomedical imaging.

5. REFERENCES

(1) Walker, N. J.; Bucher, J. R. *Toxicol. Sci.* **2009**, *110*, 251.

(2) Kipen, H. M.; Laskin, D. L. *Am. J. Physiol.-Lung Cell. Mol. Physiol.* **2005**, *289*, L696.

(3) Hartung, T. *Nature* **2009**, *460*, 208.

(4) Meng, H.; Xia, T.; George, S.; Nel, A. E. *ACS Nano* **2009**, *3*, 1620.

(5) Poland, C. A.; Duffin, R.; Kinloch, I.; Maynard, A.; Wallace, W. A. H.; Seaton, A.; Stone, V.; Brown, S.; MacNee, W.; Donaldson, K. *Nat. Nanotechnol.* **2008**, *3*, 423.

(6) Krug, H. F.; Wick, P. *Angew. Chem. Int. Ed.* **2011**, *50*, 1260.

(7) Service, R. F. *Science* **2008**, *321*, 1036.

(8) Stone, V.; Johnston, H.; Schins, R. P. F. *Crit. Rev. Toxicol.* **2009**, *39*, 613.

(9) Jones, C. F.; Grainger, D. W. *Adv. Drug Delivery Rev.* **2009**, *61*, 438.

(10) Nel, A.; Xia, T.; Madler, L.; Li, N. *Science* **2006**, *311*, 622.

(11) Rivera Gil, P.; Oberdorster, G.; Elder, A.; Puntes, V.; Parak, W. J. *ACS Nano* **2010**, *4*, 5527.

(12) Oberdorster, G.; Maynard, A.; Donaldson, K.; Castranova, V.; Fitzpatrick, J.; Ausman, K.; Carter, J.; Karn, B.; Kreyling, W.; Lai, D.; Olin, S.; Monteiro-Riviere, N.; Warheit, D.; Yang, H. *Part. Fibre Toxicol.* **2005**, *2*, 8.

(13) Nel, A. E.; Madler, L.; Velegol, D.; Xia, T.; Hoek, E. M.; Somasundaran, P.; Klaessig, F.; Castranova, V.; Thompson, M. *Nat. Mater.* **2009**, *8*, 543.

(14) Walczyk, D.; Bombelli, F. B.; Monopoli, M. P.; Lynch, I.; Dawson, K. A. *J. Am. Chem. Soc.* **2010**, *132*, 5761.

(15) Collins, F. S.; Gray, G. M.; Bucher, J. R. *Science* **2008**, *319*, 906.

(16) Lynch, I.; Cedervall, T.; Lundqvist, M.; Cabaleiro-Lago, C.; Linse, S.; Dawson, K. A. *Adv. Colloid Interface Sci.* **2007**, *134-35*, 167.

(17) Donaldson, K.; Murphy, F. A.; Duffin, R.; Poland, C. A. *Part. Fibre Toxicol.* **2010**, *7*.

(18) Feliu, N.; Fadeel, B. *Nanoscale* **2010**, *2*, 2514.

(19) Shaw, S. Y.; Westly, E. C.; Pittet, M. J.; Subramanian, A.; Schreiber, S. L.; Weissleder, R. *PNAS* **2008**, *105*, 7387.

(20) Jan, E.; Byrne, S. J.; Cuddihy, M.; Davies, A. M.; Volkov, Y.; Gun'ko, Y. K.; Kotov, N. A. *ACS Nano* **2008**, *2*, 928.

(21) George, S.; Pokhrel, S.; Xia, T.; Gilbert, B.; Ji, Z. X.; Schowalter, M.; Rosenauer, A.; Damoiseaux, R.; Bradley, K. A.; Madler, L.; Nel, A. E. *ACS Nano* **2010**, *4*, 15.

(22) Zhang, T. T.; Stilwell, J. L.; Gerion, D.; Ding, L. H.; Elboudwarej, O.; Cooke, P. A.; Gray, J. W.; Alivisatos, A. P.; Chen, F. F. *Nano Lett.* **2006**, *6*, 800.

(23) Puzyn, T.; Rasulev, B.; Gajewicz, A.; Hu, X.; Dasari, T. P.; Michalkova, A.; Hwang, H.-M.; Toropov, A.; Leszczynska, D.; Leszczynski, J. *Nat. Nanotechnol.* **2011**, *advance online publication*.

(24) Pampaloni, F.; Reynaud, E. G.; Stelzer, E. H. K. *Nat. Rev. Mol. Cell Biol.* **2007**, *8*, 839.

(25) Yamada, K. M.; Cukierman, E. *Cell* **2007**, *130*, 601.

(26) Beningo, K. A.; Dembo, M.; Wang, Y. L. *PNAS* **2004**, *101*, 18024.

(27) Zhang, X. L.; Wang, W.; Yu, W. T.; Xie, Y. B.; Zhang, X. H.; Zhang, Y.; Ma, X. J. *Biotechnol. Prog.* **2005**, *21*, 1289.

(28) Li, S.; He, P.; Dong, J.; Guo, Z.; Dai, L. *J. Am. Chem. Soc.* **2005**, *127*, 14.

(29) Lee, J.; Lilly, G. D.; Doty, R. C.; Podsiadlo, P.; Kotov, N. A. *Small* **2009**, *5*, 1213.

(30) Sanchez, V. C.; Weston, P.; Yan, A. H.; Hurt, R. H.; Kane, A. B. *Part. Fibre Toxicol.* **2011**, *8*.

(31) Casey, A.; Davoren, M.; Herzog, E.; Lyng, F. M.; Byrne, H. J.; Chambers, G. *Carbon* **2007**, *45*, 34.

(32) Monteiro-Riviere, N. A.; Inman, A. O. *Carbon* **2006**, *44*, 1070.

(33) Zhang, L. W.; Zeng, L. L.; Barron, A. R.; Monteiro-Riviere, N. A. *Int. J. Toxicol.* **2007**, *26*, 103.

(34) Worle-Knirsch, J. M.; Pulskamp, K.; Krug, H. F. *Nano Lett.* **2006**, *6*, 1261.

(35) Casey, A.; Herzog, E.; Davoren, M.; Lyng, F. M.; Byrne, H. J.; Chambers, G. *Carbon* **2007**, *45*, 1425.

(36) Monteiro-Riviere, N. A.; Inman, A. O.; Zhang, L. W. *Toxicol. Appl. Pharmacol.* **2009**, *234*, 222.

(37) Smart, S. K.; Cassady, A. I.; Lu, G. Q.; Martin, D. J. *Carbon* **2006**, *44*, 1034.

(38) Donaldson, K.; Brown, D. M.; Mitchell, C.; Dineva, M.; Beswick, P. H.; Gilmour, P.; MacNee, W. *Environ. Health Perspect.* **1997**, *105*, 1285.

(39) Gilmour, P. S.; Brown, D. M.; Beswick, P. H.; MacNee, W.; Rahman, I.; Donaldson, K. *Environ. Health Perspect.* **1997**, *105*, 1313.

(40) Voinov, M. A.; Pagán, J. O. S.; Morrison, E.; Smirnova, T. I.; Smirnov, A. I. *J. Am. Chem. Soc.* **2010**, DOI 10.1021/ja104683w.

(41) Alpatova, A. L.; Shan, W. Q.; Babica, P.; Upham, B. L.; Rogensues, A. R.; Masten, S. J.; Drown, E.; Mohanty, A. K.; Alocilja, E. C.; Tarabara, V. V. *Water Res* **2010**, *44*, 505.

(42) Mutlu, G. M.; Budinger, G. R. S.; Green, A. A.; Urich, D.; Soberanes, S.; Chiarella, S. E.; Alheid, G. F.; McCrimmon, D. R.; Szleifer, I.; Hersam, M. C. *Nano Lett.* **2010**, *10*, 1664.

(43) Herzog, E.; Byrne, H. J.; Davoren, M.; Casey, A.; Duschl, A.; Oostingh, G. J. *Toxicol. Appl. Pharmacol.* **2009**, *236*, 276.

(44) Dong, L. F.; Witkowski, C. M.; Craig, M. M.; Greenwade, M. M.; Joseph, K. L. *Nanoscale Res. Lett.* **2009**, *4*, 1517.

(45) Zheng, M.; Diner, B. A. *J. Am. Chem. Soc.* **2004**, *126*, 15490.

(46) Donaldson, K.; Beswick, P. H.; Gilmour, P. S. *Toxicol. Lett.* **1996**, *88*, 293.

(47) Shvedova, A. A.; Kisin, E. R.; Mercer, R.; Murray, A. R.; Johnson, V. J.; Potapovich, A. I.; Tyurina, Y. Y.; Gorelik, O.; Arepalli, S.; Schwegler-Berry, D.; Hubbs, A. F.; Antonini, J.; Evans, D. E.; Ku, B. K.; Ramsey, D.; Maynard, A.; Kagan, V. E.; Castranova, V.; Baron, P. *Am. J. Physiol.-Lung Cell. Mol. Physiol.* **2005**, *289*, L698.

(48) Shvedova, A. A.; Castranova, V.; Kisin, E. R.; Schwegler-Berry, D.; Murray, A. R.; Gandelsman, V. Z.; Maynard, A.; Baron, P. *J. Toxicol. Environ. Health, Part A* **2003**, *66*, 1909.

(49) Herzog, E.; Casey, A.; Lyng, F. M.; Chambers, G.; Byrne, H. J.; Davoren, M. *Toxicol. Lett.* **2007**, *174*, 49.

(50) Kagan, V. E.; Bayir, H.; Shvedova, A. A. *Nanomedicine* **2005**, *1*, 313.

(51) Hurt, R. H.; Monthioux, M.; Kane, A. *Carbon* **2006**, *44*, 1028.

(52) Shvedova, A. A.; Kagan, V. E. *J. Intern. Med.* **2010**, *267*, 106.

(53) Bruinink, A.; Manser, P.; Hasler, S. *Phys. Status Solidi B* **2009**, *246*, 2423.

(54) Manna, S. K.; Sarkar, S.; Barr, J.; Wise, K.; Barrera, E. V.; Jejelowo, O.; Rice-Ficht, A. C.; Ramesh, G. T. *Nano Lett.* **2005**, *5*, 1676.

(55) Murray, A. R.; Kisin, E.; Leonard, S. S.; Young, S. H.; Kommineni, C.; Kagan, V. E.; Castranova, V.; Shvedova, A. A. *Toxicology* **2009**, *257*, 161.

(56) Sayes, C. M.; Liang, F.; Hudson, J. L.; Mendez, J.; Guo, W. H.; Beach, J. M.; Moore, V. C.; Doyle, C. D.; West, J. L.; Billups, W. E.; Ausman, K. D.; Colvin, V. L. *Toxicol Lett* **2006**, *161*, 135.

(57) Zollanvari, A.; Cunningham, M. J.; Braga-Neto, U.; Dougherty, E. *BMC Bioinformatics* **2009**, *10*, S10.

(58) Davoren, M.; Herzog, E.; Casey, A.; Cottineau, B.; Chambers, G.; Byrne, H. J.; Lyng, F. M. *Toxicol. in Vitro* **2007**, *21*, 438.

(59) Jia, G.; Wang, H. F.; Yan, L.; Wang, X.; Pei, R. J.; Yan, T.; Zhao, Y. L.; Guo, X. B. *Environ. Sci. Technol.* **2005**, *39*, 1378.

(60) Fiorito, S.; Serafino, A.; Andreola, F.; Bernier, P. *Carbon* **2006**, *44*, 1100.

(61) Kagan, V. E.; Tyurina, Y. Y.; Tyurin, V. A.; Konduru, N. V.; Potapovich, A. I.; Osipov, A. N.; Kisin, E. R.; Schwegler-Berry, D.; Mercer, R.; Castranova, V.; Shvedova, A. A. *Toxicol. Lett.* **2006**, *165*, 88.

(62) Sato, Y.; Yokoyama, A.; Shibata, K.; Akimoto, Y.; Ogino, S.; Nodasaka, Y.; Kohgo, T.; Tamura, K.; Akasaka, T.; Uo, M.; Motomiya, K.; Jeyadevan, B.; Ishiguro, M.; Hatakeyama, R.; Watari, F.; Tohji, K. *Mol. Biosyst.* **2005**, *1*, 176.

(63) Semberova, J.; Lacerda, S. H. D. P.; Simakova, O.; Holada, K.; Gelderman, M. P.; Simak, J. *Nano Lett.* **2009**, *9*, 3312.

(64) Radomski, A.; Jurasz, P.; Alonso-Escolano, D.; Drews, M.; Morandi, M.; Malinski, T.; Radomski, M. W. *Br. J. Pharmacol.* **2005**, *146*, 882.

(65) Tamura, K.; Takashi, N.; Akasaka, T.; Roska, I. D.; Uo, M.; Totsuka, Y.; Watari, F. In *Bioceramics*; Barbosa, M. A., Monteiro, F. J., Correia, R., Leon, B., Eds.; Trans Tech Publications Ltd: Zurich-Uetikon, 2004; Vol. 254-2, p 919.

(66) De Nicola, M.; Bellucci, S.; Traversa, E.; De Bellis, G.; Micciulla, F.; Ghibelli, L. *Journal of Physics-Condensed Matter* **2008**, *20*.

(67) Wick, P.; Manser, P.; Limbach, L. K.; Dettlaff-Weglikowska, U.; Krumeich, F.; Roth, S.; Stark, W. J.; Bruinink, A. *Toxicol. Lett.* **2007**, *168*, 121.

(68) Cui, D. X.; Tian, F. R.; Ozkan, C. S.; Wang, M.; Gao, H. J. *Toxicol. Lett.* **2005**, *155*, 73.

(69) Huczko, A.; Lange, H. *Fullerene Sci. Technol.* **2001**, *9*, 247.

(70) Koyama, S.; Endo, M.; Kim, Y. A.; Hayashi, T.; Yanagisawa, T.; Osaka, K.; Koyama, H.; Haniu, H.; Kuroiwa, N. *Carbon* **2006**, *44*, 1079.

(71) Tong, H.; McGee, J. K.; Saxena, R. K.; Kodavanti, U. P.; Devlin, R. B.; Gilmour, M. I. *Toxicol. Appl. Pharmacol.* **2009**, *239*, 224.

(72) Huczko, A.; Lange, H.; Calko, E.; Grubek-Jaworska, H.; Droszcz, P. *Fullerene Sci. Technol.* **2001**, *9*, 251.

(73) Shvedova, A. A.; Kisin, E.; Murray, A. R.; Johnson, V. J.; Gorelik, O.; Arepalli, S.; Hubbs, A. F.; Mercer, R. R.; Keohavong, P.; Sussman, N.; Jin, J.; Yin, J.; Stone, S.; Chen, B. T.; Deye, G.; Maynard, A.; Castranova, V.; Baron, P. A.; Kagan, V. E. *Am. J. Physiol.-Lung Cell. Mol. Physiol.* **2008**, *295*, L552.

(74) Mercer, R. R.; Scabilloni, J.; Wang, L.; Kisin, E.; Murray, A. R.; Schwegler-Berry, D.; Shvedova, A. A.; Castranova, V. *Am. J. Physiol.-Lung Cell. Mol. Physiol.* **2008**, *294*, L87.

(75) Warheit, D. B.; Laurence, B. R.; Reed, K. L.; Roach, D. H.; Reynolds, G. A. M.; Webb, T. R. *Toxicol. Sci.* **2004**, *77*, 117.

(76) Warheit, D. B. *Carbon* **2006**, *44*, 1064.

(77) Lam, C. W.; James, J. T.; McCluskey, R.; Hunter, R. L. *Toxicol. Sci.* **2004**, *77*, 126.

(78) Nygaard, U. C.; Hansen, J. S.; Samuelsen, M.; Alberg, T.; Marioara, C. D.; Lovik, M. *Toxicol. Sci.* **2009**, *109*, 113.

(79) Singh, R.; Pantarotto, D.; Lacerda, L.; Pastorin, G.; Klumpp, C.; Prato, M.; Bianco, A.; Kostarelos, K. *P Natl Acad Sci USA* **2006**, *103*, 3357.

(80) Cherukuri, P.; Gannon, C. J.; Leeuw, T. K.; Schmidt, H. K.; Smalley, R. E.; Curley, S. A.; Weisman, R. B. *P Natl Acad Sci USA* **2006**, *103*, 18882.

(81) Ruggiero, A.; Villa, C. H.; Bander, E.; Rey, D. A.; Bergkvist, M.; Batt, C. A.; Manova-Todorova, K.; Deen, W. M.; Scheinberg, D. A.; McDevitt, M. R. *P Natl Acad Sci USA* **2010**, *107*, 12369.

(82) Liu, Z.; Davis, C.; Cai, W. B.; He, L.; Chen, X. Y.; Dai, H. J. *P Natl Acad Sci USA* **2008**, *105*, 1410.

(83) Wang, H. F.; Wang, J.; Deng, X. Y.; Sun, H. F.; Shi, Z. J.; Gu, Z. N.; Liu, Y. F.; Zhao, Y. L. *Journal of Nanoscience and Nanotechnology* **2004**, *4*, 1019.

(84) Allen, B. L.; Kotchey, G. P.; Chen, Y.; Yanamala, N. V. K.; Klein-Seetharaman, J.; Kagan, V. E.; Star, A. *J. Am. Chem. Soc.* **2009**, *131*, 17194.

(85) Kagan, V. E.; Konduru, N. V.; Feng, W. H.; Allen, B. L.; Conroy, J.; Volkov, Y.; Vlasova, II; Belikova, N. A.; Yanamala, N.; Kapralov, A.; Tyurina, Y. Y.; Shi, J. W.; Kisin, E. R.; Murray, A. R.; Franks, J.; Stolz, D.; Gou, P. P.; Klein-Seetharaman, J.; Fadeel, B.; Star, A.; Shvedova, A. A. *Nat. Nanotechnol.* **2010**, *5*, 354.

(86) Elkin, T.; Jiang, X. P.; Taylor, S.; Lin, Y.; Gu, L. R.; Yang, H.; Brown, J.; Collins, S.; Sun, Y. P. *Chembiochem* **2005**, *6*, 640.

(87) Plowden, J.; Renshaw-Hoelscher, M.; Engleman, C.; Katz, J.; Sambhara, S. *Aging Cell* **2004**, *3*, 161.

(88) Oberdorster, G.; Sharp, Z.; Atudorei, V.; Elder, A.; Gelein, R.; Lunts, A.; Kreyling, W.; Cox, C. *J. Toxicol. Environ. Health A* **2002**, *65*, 1531.

(89) Lee, C. S.; Baker, S. E.; Marcus, M. S.; Yang, W. S.; Eriksson, M. A.; Hamers, R. J. *Nano Lett.* **2004**, *4*, 1713.

(90) Kleinman, H. K.; Philp, D.; Hoffman, M. P. *Curr. Opin. Biotech.* **2003**, *14*, 526.

(91) Bissell, M. J.; Radisky, D. C.; Rizki, A.; Weaver, V. M.; Petersen, O. W. *Differentiation; research in biological diversity* **2002**, *70*, 537.

(92) Sano, M.; Okamura, J.; Shinkai, S. *Langmuir* **2001**, *17*, 7172.

(93) Smith, B.; Wepasnick, K.; Schrote, K. E.; Bertele, A. H.; Ball, W. P.; O'Melia, C.; Fairbrother, D. H. *Environ. Sci. Technol.* **2009**, *43*, 819.

(94) Hu, H.; Yu, A. P.; Kim, E.; Zhao, B.; Itkis, M. E.; Bekyarova, E.; Haddon, R. C. *J. Phys. Chem. B* **2005**, *109*, 11520.

(95) DeFife, K. M.; Jenney, C. R.; Colton, E.; Anderson, J. M. *Journal of Histochemistry & Cytochemistry* **1999**, *47*, 65.

(96) Hankin, S. M.; Boraschi, D.; Duschl, A.; Lehr, C. M.; Lichtenbeld, H. *Nano Today* **2011**.

(97) Movia, D.; Del Canto, E.; Giordani, S. *J. Phys. Chem. C* **2010**, *114*, 18407.

(98) Singh, P.; Campidelli, S.; Giordani, S.; Bonifazi, D.; Bianco, A.; Prato, M. *Chem. Soc. Rev.* **2009**, *38*, 2214.

(99) Britz, D. A.; Khlobystov, A. N. *Chem. Soc. Rev.* **2006**, *35*, 637.

(100) Valenti, L. E.; Fiorito, P. A.; Garcia, C. D.; Giacomelli, C. E. *J. Colloid Interf. Sci.* **2007**, *307*, 349.

(101) Zhao, X. C.; Liu, R. T.; Chi, Z. X.; Teng, Y.; Qin, P. F. *J. Phys. Chem. B* **2010**, *114*, 5625.

(102) Matsuura, K.; Saito, T.; Okazaki, T.; Ohshima, S.; Yumura, M.; Iijima, S. *Chem. Phys. Lett.* **2006**, *429*, 497.

(103) Wang, X.; Xia, T.; Ntim, S. A.; Ji, Z.; George, S.; Meng, H.; Zhang, H.; Castranova, V.; Mitra, S.; Nel, A. E. *ACS Nano* **2010**, *4*, 7241.

(104) Carter, D. C.; Ho, J. X. *Adv. Protein Chem.* **1994**, *45*, 153.

(105) Peter, T. In *All about albumin: Biochemistry, genetics, and medical applications*; Academic Press: San Diego, 1996, p 432.

(106) Edri, E.; Regev, O. *Anal Chem* **2008**, *80*, 4049.

(107) Parnaud, G.; Tache, S.; Peiffer, G.; Corpet, D. E. *Br. J. Cancer* **2001**, *84*, 90.

(108) Anson-Casaos, A.; Gonzalez-Dominguez, J. M.; Martinez, M. T. *Carbon* **2010**, *48*, 2917.

(109) Moore, V. C.; Strano, M. S.; Haroz, E. H.; Hauge, R. H.; Smalley, R. E.; Schmidt, J.; Talmon, Y. *Nano Lett.* **2003**, *3*, 1379.

(110) Bardi, G.; Tognini, P.; Ciofani, G.; Raffa, V.; Costa, M.; Pizzorusso, T. *Nanomedicine* **2009**, *5*, 96.

(111) O'Connell, M. J.; Bachilo, S. M.; Huffman, C. B.; Moore, V. C.; Strano, M. S.; Haroz, E. H.; Rialon, K. L.; Boul, P. J.; Noon, W. H.; Kittrell, C.; Ma, J. P.; Hauge, R. H.; Weisman, R. B.; Smalley, R. E. *Science* **2002**, *297*, 593.

(112) Hasan, T.; Scardaci, V.; Tan, P. H.; Rozhin, A. G.; Milne, W. I.; Ferrari, A. C. *J Phys Chem C* **2007**, *111*, 12594.

(113) Weisman, R. B.; Bachilo, S. M.; Tsyboulski, D. *Appl. Phys. A: Mater. Sci. Process.* **2004**, *78*, 1111.

(114) Tan, P. H.; Rozhin, A. G.; Hasan, T.; Hu, P.; Scardaci, V.; Milne, W. I.; Ferrari, A. C. *Phys. Rev. Lett.* **2007**, *99*.

(115) Paredes, J. I.; Burghard, M. *Langmuir* **2004**, *20*, 5149.

(116) Saleh, N. B.; Pfefferle, L. D.; Elimelech, M. *Environ. Sci. Technol.* **2010**, *44*, 2412.

(117) Mamedov, A. A.; Kotov, N. A.; Prato, M.; Guldi, D. M.; Wicksted, J. P.; Hirsch, A. *Nat. Mater.* **2002**, *1*, 190.

(118) American Society for Testing and Materials: 1985; Vol. ASTM D4187-82.

(119) Abraham, V. C.; Taylor, D. L.; Haskins, J. R. *Trends Biotechnol.* **2004**, *22*, 15.

(120) Movia, D.; Prina-Mello, A.; Volkov, Y.; Giordani, S. *Chem. Res. Toxicol.* **2010**, *23*, 1459.

(121) Byrne, F.; Prina-Mello, A.; Whelan, A.; Mohamed, B. M.; Davies, A.; Gun'ko, Y. K.; Coey, J. M. D.; Volkov, Y. *J. Magn. Magn. Mater.* **2009**, *321*, 1341.

(122) Williams, Y.; Sukhanova, A.; Nowostawska, M.; Davies, A. M.; Mitchell, S.; Oleinikov, V.; Gun'ko, Y.; Nabiev, I.; Kelleher, D.; Volkov, Y. *Small* **2009**, *5*, 2581.

(123) Dutta, D.; Sundaram, S. K.; Teeguarden, J. G.; Riley, B. J.; Fifield, L. S.; Jacobs, J. M.; Addleman, S. R.; Kaysen, G. A.; Moudgil, B. M.; Weber, T. J. *Toxicol. Sci.* **2007**, *100*, 303.

(124) Pulskamp, K.; Diabate, S.; Krug, H. F. *Toxicol. Lett.* **2007**, *168*, 58.

(125) Dong, P. X.; Wan, B.; Guo, L. H. *Nanotoxicology* **2011**.

(126) Porter, A. E.; Gass, M.; Bendall, J. S.; Muller, K.; Goode, A.; Skepper, J. N.; Midgley, P. A.; Welland, M. *ACS Nano* **2009**, *3*, 1485.

(127) Wang, G.; Dewilde, A. H.; Zhang, J. P.; Pal, A.; Vashist, M.; Bello, D.; Marx, K. A.; Braunhut, S. J.; Therrien, J. M. *Part. Fibre Toxicol.* **2011**, *8*.

(128) Hamilton, R. F.; Buford, M. C.; Wood, M. B.; Arnone, B.; Morandi, M.; Holian, A. *Nanotoxicology* **2007**, *1*, 104.

(129) Schnorr, J. M.; Swager, T. M. *Chem. Mater.* **2011**, *23*, 646.

(130) Bazou, D.; Foster, G. A.; Ralphs, J. R.; Coakley, W. T. *Mol. Membr. Biol.* **2005**, *22*, 229.

(131) Bazou, D.; Dowthwaite, G. P.; Khan, I. M.; Archer, C. W.; Ralphs, J. R.; Coakley, W. T. *Mol. Membr. Biol.* **2006**, *23*, 195.

(132) Coakley, W. T.; Bazou, D.; Morgan, J.; Foster, G. A.; Archer, C. W.; Powell, K.; Borthwick, K. A. J.; Twomey, C.; Bishop, J. *Colloids Surf., B* **2004**, *34*, 221.

(133) Liu, R.; Kwok, Y. L.; Li, Y.; Lao, T. T.; Zhang, X.; Dai, X. Q. *Fibers Polym.* **2006**, *7*, 389.

(134) Edwards, G. O.; Bazou, D.; Kuznetsova, L. A.; Coakley, W. T. *Cell Communication and Adhesion* **2007**, *14*, 9.

(135) Kuznetsova, L. A.; Bazou, D.; Edwards, G. O.; Coakley, W. T. *Biotechnol. Prog.* **2009**, *25*, 834.

(136) Cho, E. C.; Zhang, Q.; Xia, Y. *Nat. Nanotechnol.* **2011**.

(137) Wang, X.; Liu, F.; Andavan, G. T. S.; Jing, X. Y.; Singh, K.; Yazdanpanah, V. R.; Bruque, N.; Pandey, R. R.; Lake, R.; Ozkan, M.; Wang, K. L.; Ozkan, C. S. *Small* **2006**, *2*, 1356.

CHAPTER IV.
EXPERIMENTAL PROCEDURES

CONTENTS

1. GENERAL PROCEDURES

Chemicals and solvents were purchased from commercial sources (Sigma-Aldrich and Fisher Scientific) and used as received. Raw HiPCO SWNTs (r-SWNTs) were purchased from Unidym® (Lot. R0546). r-SWNTs were purified and oxidized by Elisa Del Canto (Trinity College Dublin) according to the procedure previously reported in the literature.[1,2] Raman and ATR/FT-IR analysis, as well as AFM measurements, were also carried out by Elisa Del Canto.

1.1. *PURIFICATION PROCEDURE OF SWNTS*

r-SWNTs were stirred in 2.6 M HNO_3 (1 mL HNO_3 solution/1 mg nanotubes ratio) under reflux at 100 °C for 48 h. The suspension was then cooled down to room temperature, filtered through 0.2 μm Millipore® isopore filters and washed with distilled water until the pH of the filtrate was neutral. The obtained purified SWNTs (p-SWNTs) were then carefully washed with organic solvents of increasing polarity (NMP, DMF and MeOH) and dried under vacuum at 60 °C overnight.

1.2. *OXIDATIVE PROCEDURE OF SWNTS*

p-SWNTs were dispersed in a small amount of distilled water by means of sonication for 10 min and piranha solution (H_2SO_4·H_2O_2 30%, ratio 4:1) was then added (1 mL piranha/1 mg of nanotubes ratio). The reaction was stirred at 35 °C for 1 h. The oxidation reaction was quenched by diluting the nanotubes suspension with ice. The oxidized SWNTs (o-SWNTs) were then filtered through 0.2 μm Millipore® isopore membranes. The product was collected as a black solid and washed with distilled water until the pH of the filtrate was neutral. The o-SWNTs were finally carefully washed with increasing polarity organic solvents (NMP, DMF and MeOH) and dried under vacuum at 60 °C overnight.

2. MATERIALS AND METHODS OF CHAPTER II

2.1. *THERMAL GRAVIMETRIC ANALYSIS*

Thermal Gravimetric Analysis was carried out on SWNTs powders on a PerkinElmer Thermogravimetric Analyzer Pyris 1 TGA. The method used for recording the TGA measurements in air flow was: (1) hold for 5 min at 30 °C; (2) heat from 30 °C to 100 °C at 10 °C/min; (3) hold for 20 min at 100 °C; (4) heat from 100 °C to 900 °C at 10 °C/min.

2.2. *SPECTROSCOPIC CHARACTERISATION*

Optical measurements were carried out in a 1 cm quartz cells on dispersions of r-, p- and o-SWNTs in aqueous sodium dodecylbenzene sulphonate (SDBS) at a SWNTs:SDBS weight ratio of 1:25. The dispersions were obtained by sonication (sonic tip, 2 min; sonic bath, 7 h) and the final pH of the dispersions was neutral. The dispersions were then centrifuged at 4,000 RPM (corresponding to 900 ×*g*) for 90 min. NIR-PL studies were carried out in triplicate on supernatants in a LOT. ORIEL NS1 NanoSpectralyzer® (Applied Nanofluorescence, USA) at three different excitation wavelengths (diode lasers at 638 nm, 683 nm and 785 nm) with an integration time of 1 s and 5 accumulations. Further NIR spectroscopic characterization was carried out on a HORIBA Jobin Yvon Fluorolog-3 Spectrofluorometer equipped with a liquid N_2 cooled InGaAs detector (λ_{exc} = 683 nm and 785 nm). NIR-PL spectra on HORIBA Jobin Yvon Fluorolog-3 Spectrofluorometer were collected after 1 cycle with 5 nm steps, 10 s of exposure time and 14.7 nm slit width. Vis emission studies were carried out on a PerkinElmer UV-Vis LS 55 Emission Spectrophotometer (λ_{exc} = 420 nm, 638 nm, 683 nm, and 785 nm). Vis emission spectra were acquired with 1 accumulation, 15.0 nm slit width and scan speed of 100 nm/min. Absorption spectroscopy was carried out on a PerkinElmer UV-Vis/NIR Lambda 1050 Absorption Spectrophotometer. All the data were recorded on supernatants after 1 cycle, with an interval of 1 nm, slit width 2 nm and scan speed of 240 nm/min.

Raman spectra were obtained on SWNTs powders at room temperature in the backscattering geometry using a RENISHAW 1000 MicroRaman system equipped with a CCD camera and a Leica Microscope. As an excitation source, a laser at 633 nm was used. The spectra were recorded after 4 accumulations with 10 s of exposure time.

Infrared spectra were collected in the solid state on a PerkinElmer FT-IR Spectrometer Spectrum 100 equipped with a universal ATR (Attenuated Total Reflection) sampling accessory (diamond/ZnSe crystal). The spectra were recorded after 256 scans with a 4 cm^{-1} resolution.

2.3. *NIR-PL EFFICIENCY CALCULATIONS*

The NIR-PL transitions of SWNTs are strictly correlated with the specific (*n,m*) nanotube structure.[3,4] Therefore, a quantitative comparison of the NIR emission based on the intensity of a specific NIR-PL band was not possible among SWNTs samples treated with different chemical procedures, which introduce defects on the nanotubes surface and may influence the sample (*n,m*) composition and cause doping effects. To allow a simple quantitative comparison of the NIR-PL intensity of the various SWNTs samples, their emission efficiency was therefore estimated. This value represents the spectrally integrated emission values adjusted to the fraction of excitation light absorbed by the sample. The emission efficiency was determined for the three λ_{exc} as follows (Eq. 4.1):

$$\text{Emission efficiency} = \text{total emission power/ absorption at } \lambda_{exc} \qquad \textbf{Eq. 4.1}$$

where the total emission power value corresponds to the integer of the total NIR emission spectrum. The term referring to the absorption at the selected λ_{exc} was included to avoid interference due to small differences in the SWNTs concentration of the samples. NIR-PL spectra were acquired three times for each sample to increase the significance of the estimation. The emission intensity was then calculated as average value (n_{exp} = 3) ± standard deviation. The results are normalised on the emission efficiency of r-SWNTs.

2.4. *MICROSCOPIC CHARACTERISATION*

For High Resolution Transmission Electron Microscopy (HR-TEM) SWNTs powders were dispersed in high purity DMF ($[SWNTs]_i$ = 0.1 mg/mL) by sonic tip and sonic bath. The samples were prepared by dropping an aliquot (10 μL c.a.) of the dispersions on 200-mesh Cu holey carbon grids. After incubation for 5 min, the grids were drained,

dried for 1 day at 37 °C and visualized under a Jeol 2100 operating at 200 kV with a Lanthanum Hexaborise emission source.

Atomic Force Microscopy (AFM) topographic images were recorded in semi-contact mode with an NT-MDT inverted configuration system. The r-, p- and o-SWNTs samples were prepared by dispersing the nanotubes in high purity DMF by sonication (sonic bath), spray-coating onto freshly cleaved mica substrates and drying overnight in an oven at 90° C. The average length value was calculated on a sample population of 100 nanotubes.

2D Fluorescence Lifetime Imaging Microscopy was carried out with the Microtime200 time-resolved confocal microscope system (PicoQuant) equipped with an Olympus IX71 inverted microscope. An aliquot of the nanotubes dispersions in high purity DMF ($[SWNTs]_i$ = 0.1 mg/mL) was dropped on a glass microslide (Corning, USA), covered with a glass coverslip and sealed. The samples were excited with a picosecond diode laser at 634 nm using an emission filter at 670 nm. The FLIM image consisted of 250 × 250 pixels (80 × 80 μm) with acquisition range 670-1000 nm. Lifetime maps were calculated on a pixel-by-pixel basis by fitting the lifetime of each pixel to the logarithm of the intensity.

3. MATERIALS AND METHODS OF CHAPTER III

3.1. *PREPARATION OF p- AND o-SWNTS DISPERSIONS*

NIR-photoluminescence (PL) spectroscopy, zeta potential measurements and toxicity tests were carried out on dispersions of p- and o-SWNTs in RPMI 1640 cell media (GIBCO, Bio Sciences Ltd., Ireland), with or without 100% bovine serum albumin (BSA) (#A9647, Sigma-Aldrich) or 10% Pluronic F68 (SAFC Biosciences). Dry powder p-SWNTs and o-SWNTs were weighted and added to a 1:1 mixture of sterile DMSO and sterile DI water at a concentration of 2 mg/mL (stock solutions). Stock solutions were sonicated (sonic bath, 4 h) and aliquoted in three vials of 100 μL to prepare the working solutions as follows: (1) 5 μL of sterile BSA was added (BSA-stabilised dispersion); (2) 5 μL of Pluronic F68 was added (Pluronic F68-stabilised dispersion); (3) the stock solution was left unchanged (DMSO-stabilised dispersion). 1.9 mL of RPMI 1640 cell media (supplemented with 2 mM L-glutamine, 10% foetal bovine serum (FBS) and 10 mg/mL penicillin- streptomycin) was mixed to solutions 1, 2, and 3, thus obtaining a final SWNTs concentration of 120 μg/mL. Serial dilutions in supplemented RPMI 1640 cell media produced dispersions with concentration of 60 and 12 μg/mL of neutral pH. A schematic representation of the dispersions preparation is shown in Figure 4.1, together with the percentage composition of each solution obtained. Dispersions of p- and o-SWNTs in DI water for zeta potential measurements were prepared following the same protocol.

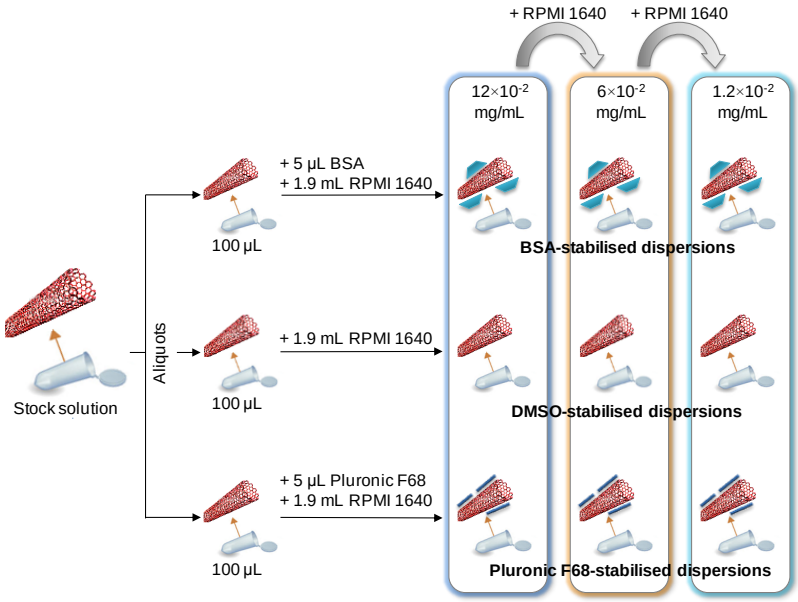

$[SWNTs]_i$ (mg/mL)	DMSO	BSA
12×10^{-2}	2.5 vol. %	0.25 vol. %
6×10^{-2}	1.2 vol. %	0.12 vol. %
1.2×10^{-2}	0.6 vol. %	0.6 vol. %

$[SWNTs]_i$ (mg/mL)	DMSO	BSA/Pluronic F68
12×10^{-2}	2.5 vol. %	0 vol. %
6×10^{-2}	1.2 vol. %	0 vol. %
1.2×10^{-2}	0.6 vol. %	0 vol. %

$[SWNTs]_i$ (mg/mL)	DMSO	Pluronic F68
12×10^{-2}	2.5 vol. %	0.25 vol. %
6×10^{-2}	1.2 vol. %	0.12 vol. %
1.2×10^{-2}	0.6 vol. %	0.6 vol. %

Figure 4.1. Preparation method of p- and o-SWNTs dispersions in RPMI 1640 cell media. Schematic of the suspensions obtained and relative percentages of DMSO, BSA and Pluronic F68 within each dispersion.

3.2. *Physico-Chemical Characterization*

NIR-PL studies were carried out on p- and o-SWNTs dispersions in supplemented RPMI 1640 cell media ($[SWNTs]_i$ = 120 µg/mL) in a LOT ORIEL NS1 NanoSpectralyzer (Applied Nanofluorescence, USA) at excitation wavelength (λ_{exc}) of 683 nm over a period of 1 h with an interval of 3.6 min. Measurements were also carried out at λ_{exc} of 638 and 785 nm with similar results (data not shown). Zeta potential measurements were performed on p- and o-SWNTs solutions in DI water or in supplemented RPMI 1640 cell media by Zetasizer Nanoseries Nano-ZS (Malvern Instruments, UK). Measurements were carried out in six replicates for each solution. Data are reported as average.

3.3. *Cell Culture*

Human monocytic leukemia (THP-1) cells were obtained from the American Tissue Culture Collection (ATCC, USA). Briefly, THP-1 cells were cultured in suspension in modified RPMI 1640 media (supplemented with 2 mM L-glutamine, 10% foetal bovine serum (FBS) and 10 mg/mL penicillin- streptomycin) and incubated at 37 °C and 5% CO_2. At 60% confluence, cells were diluted in modified RPMI 1640 media at

concentrations appropriate for each experimental procedure. The passage number was restricted between five and fifteen.

3.4. *2D CELL CULTURE MODEL*

THP-1 cells were seeded in 96-well plates at concentration of 20,000 cells/well (final volume: 200 μL/well) using a Matrix WellMate (ThermoFisher Scientific, USA) and activated with PMA (Sigma-Aldrich) for 72 h to induce differentiation into adherent macrophages and stop their natural proliferation. After removing the cell media, adherent THP-1 cells were exposed to p- and o-SWNTs dispersions. The final volume of solution added was 200 μL/well. Three different doses of p- and o-SWNTs were tested: 120, 60 and 12 μg/mL, corresponding to 12×10^{-4}, 6×10^{-4} and 1.2×10^{-4} μg/cell respectively. The anticancer agent Paclitaxel (1.7 μM) (Sigma-Aldrich) was used as positive control. Cells were exposed to SWNTs for 24 and 72 h.

3.4.1. *Cytotoxicity analysis of 2D cell culture*

Fluorescent staining: Supernatants were collected from each well for post-exposure assays, and multiple washings with phosphate-buffered saline (PBS) were carried out in order to completely remove SWNTs from wells and avoid any potential interaction with the staining dyes. The multiparameter Cytotoxicity 1 HitKit HCSA Reagent Kit (ThermoFisher, USA) was used[5,6] and staining was performed accordingly to previously reported protocols.[6,7] Cytotoxicity 1 HitKit is formed by a cocktail of three fluorescent dyes (MPCT1 Fluor Cocktail), which contain the following established fluorescent biomarkers[5,6]: (1) Hoechst Dye (blue dye) for labelling nuclei; (2) cell permeability indicator (green dye) for labelling permeabilized cells; and (3) fluorescent weak base (red dye) for labelling acidic organelles and measuring their pH and mass. A typical HCSA output image of cells stained with the Cytotoxicity 1 HitKit is shown in Figure 4.2a. This kit allows the detection of changes in many cellular properties,[6,7] as described in Figure 4.2b. Briefly: changes in cell viability are directly correlated to the toxic effects of the material tested. Following a toxic insult, cells may also respond with changes in nuclear intensity, and an increased nuclear intensity is generally associated with the cell nuclei collapse and cell stress.[8] Changes in the cell membrane permeability are often associated with an ongoing toxic or apoptotic responses and the loss of cell membrane integrity is a common feature of marked cytotoxicity.[9] Finally, external

agents can interfere with the normal cell physiology by affecting the mass, the number or the function of organelles such as lysosomes.[10]

a)

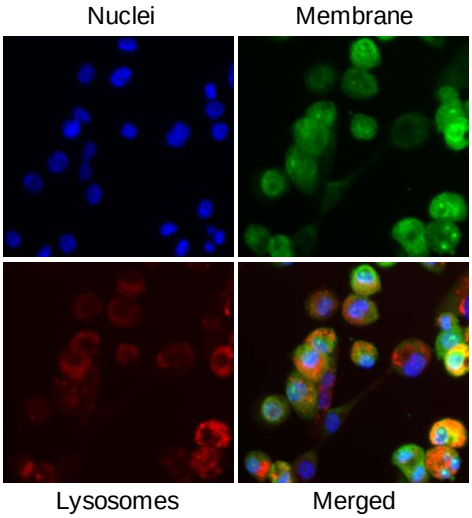

b)

Summary of the HCSA assay

Fluorescent channel	Cell parameter assessed	Assessment method
Blue channel	Cell growth/viability	• Number of nuclei identified per well • Equivalent to number of cells per well
	Nuclear intensity	• Average fluorescence intensity of pixels within nucleus
Green channel	Cell membrane permeability	• Average fluorescence intensity of pixels within the cytoplasm • Cell membrane is permeable when compromised
Red channel	Lysosomal mass/pH changes	• Average fluorescence intensity of pixels within the cytoplasm • Increase fluorescence corresponds to decreased pH or increased lysosomes number

Figure 4.2. (a) A typical HCSA output image of cells stained for nuclei, cell membrane and lysosomes with the Cytotoxicity 1 HitKit. (b) Table summarising the HCSA cytotoxicity assay.

Imaging and HCSA Analysis: Measurements were carried out using the IN-Cell 1000 automated fluorescent microscope system (GE Healthcare, USA) and its associated analysis software (In Cell Analyzer System, GE Healthcare, USA). 96-well plates were read on IN-Cell Analyzer 1000 using three detection channels (461, 509 and 599 nm) with three different excitation filters (λ<503 nm, λ>509 nm and λ>599 nm). Ten random microscopic fields were sequentially acquired by the IN-Cell 1000 automated fluorescent microscope system at a magnification of 10×. Acquired images for each

exposure time and dose were then analyzed by the IN-Cell Analyzer software accordingly to previously reported procedures.[6,11] No changes in cellular responses were detectable when 2D cell cultures were exposed to solutions containing equivalent amounts of DMSO, BSA or Pluronic F68 for 72 h (Figure 4.3).

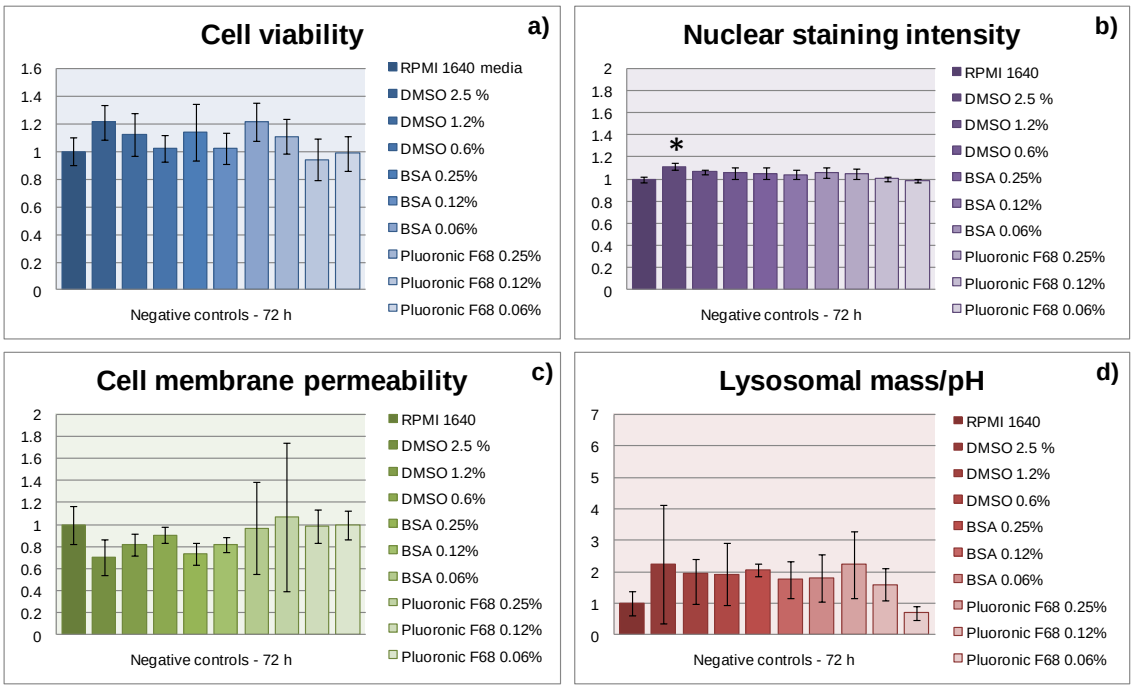

Figure 4.3. Cytotoxicity control for 2D cell cultures of activated, "macrophage-like" THP-1 exposed to RPMI 1640 cell media supplemented with DMSO, BSA or Pluronic F68 (at the working concentrations employed in the SWNTs toxicity testing). HCSA quantitative data for the changes in (a) cell viability, (b) nuclear staining intensity, (c) cell membrane permeability and (d) lysosomal mass/pH. No significant changes in these cellular parameters were detected.

Heatmaps: Multiparameter HCSA data are presented as cluster heatmaps graphical tables to highlight the potential differences in cellular responses among SWNTs dispersions, concentrations and exposure times.[12] For each SWNTs solution, the changes in cytotoxicity-associated parameters are presented in colorimetric gradients at the three different concentrations tested.

3.5. *3D CELL CULTURE MODEL*

1 mL non-activated THP-1 cells were transferred to an eppendorf, centrifuged and re-suspended in supplemented, fresh RPMI 1640 cell media to a final concentration of 1×10^6 cells/mL.

3.5.1. *Ultrasound standing wave trap (USWT) and optical system*

USWT consists of three features: a transducer (Ferroperm, Kvistgard, Denmark) in a housing of radial symmetry, an aqueous phase, and a reflector that provided optical access from the top as previously described[13,14] (Figure 4.4a). The trap was driven with a function generator (Hewlett–Packard 33120A, UK). A fast, high-resolution XM10 camera (Soft Imaging System, SIS, GmbH, Munster, Germany) mounted on an Olympus BX51M reflection epi-fluorescence microscope allowed observation in the direction of sound propagation (negative z-axis)[14] (Figure 4.4b). Images were captured by a standard PC equipped with the Cell-D image acquisition and processing software (Soft Imaging System, SIS, GmbH).

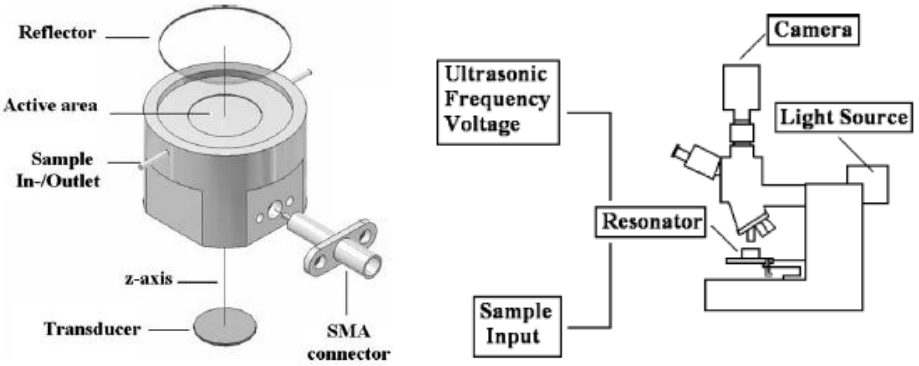

Figure 4.4. (a) Ultrasound standing wave cell manipulation device (USWT). (b) Schematic of the experimental setup for sample loading, ultrasound generation and image capturing by epi-fluorescence microscope (adapted from images by Coakley *et al.*[15] and Bazou *et al.*[13]).

3.5.2. *3D cells aggregates in situ in the USWT*

Cells were introduced into the USWT, the ultrasound was switched on for 10 min at 0.85 MPa (at which point the aggregate was mechanically robust[16]), and a 3D aggregate was formed (Figure 4.5a) as previously described.[13] In this work, aggregates consisted

of approximately 36,000 THP-1 cells, while their size was 1.5 mm circa in diameter (Figure 4.5a). p- or o-SWNTs dispersions (DMSO-, BSA- and Pluronic F68-stabilised suspensions) at concentration of 120 μg/mL, corresponding to approximately 1.2×10^{-4} μg/cell, were introduced into the USWT and surrounded completely the 3D aggregate (Figure 4.5c). After 24 h, 3D THP-1 cell aggregates had a closely packed morphology with few small empty spaces (Figure 4.5b and 4.5d). 3D cell aggregates were exposed to SWNTs samples for 24 h *in situ* in the USWT and monitored by microscopy. Aggregates perfused with fresh, supplemented RPMI 1640 cell media or Paclitaxel served as negative and positive controls, respectively.

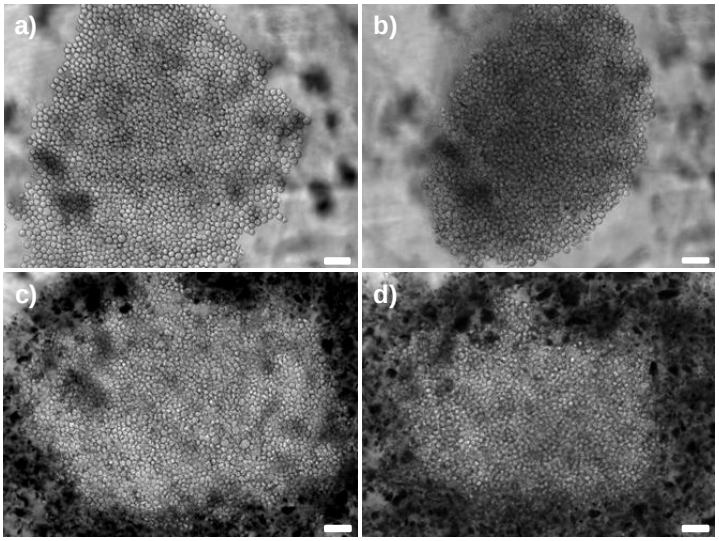

Figure 4.5. Typical 3D cell aggregates levitated in the USWT for (a) 5 min and (b) 24 h. After 24 h (b) the aggregate morphology was more closely packed. (c, d) SWNTs are visible as black agglomerates encapsulating the cell aggregate. Cell concentration: 10^6 cells/mL; SWNTs concentration: 1.2×10^{-4} μg/cell. Scale bar: 40 μm (10× magnification).

3.5.3. *3D cells aggregates in culture*

In these series of experiments, THP-1 cells were treated with 2 μL PMA (0.5 mM) to induce their differentiation into adherent macrophages. Following this, formation of 3D cell aggregates in the USWT proceeded as described above. However, aggregates were recovered from the trap after the 10 min period with a sterile 2-mL syringe (Plastipak, Becton Dickinson, UK), plated in 24-well plates (one 3D aggregate/well) and subsequently exposed to p- and o-SWNTs as described above. PMA-activated 3D aggregates had an average height of 25-30 μm.

3.5.4. *Characterisation of 3D cells aggregates in culture*

Non-treated and PMA-treated 3D cell aggregates were formed in the USWT as described in Paragraph 3.5.3. 3D cell aggregates were subsequently recovered and deposited on glass coverslips in 24-well plates. After 0, 24 and 72 h of incubation 3D aggregates were carefully recovered from the wells and placed on a HistoBond microscope slides (RA Lamb, UK). Samples were then fixed with 90% ethanol and subsequently rinsed with saline. F-actin was labelled by adding 2U/mL of Phalloidin-Alexa 488 conjugate (Invitrogen, UK). The slides were incubated at room temperature in the dark for 30 min, rinsed with saline and mounted in Vectashield (Vector, UK) prior to epifluorescence and confocal microscopy. Specimens were examined with an (1) Olympus BX51M reflection epi-fluorescence microscope equipped with standard PC and the Cell-D image acquisition/processing software (Soft Imaging System, SIS, GmbH), and (2) ZEISS 510 Meta confocal microscope (Carl Zeiss, Axiovert, Germany) equipped with Zeiss LSM Image Browser. One channel qualitative confocal imaging was carried out by acquiring a series of Z-stack images to verify the extent of cell-to-cell interaction and binding as a function of exposure time.

3.5.5. *Cytotoxicity Analysis of 3D cell cultures*

All SWNTs dispersions were tested on 3D aggregates in duplicate in both *in situ* in the USWT and in culture.

Trypan Blue exclusion assay: 3D aggregates were collected from the USWT and from the wells after exposure to p- or o-SWNTs, centrifuged and re-suspended in 10 μL of fresh RPMI 1640 cell media. 10 μL of 0.4% Trypan Blue solution (Invitrogen, Molecular probes, Oregon, USA) was then added. Blue-stained/dead cells and viable cells were counted and percentage cell death was calculated as follows (Eq. 4.2):

$$\%\ cell\ death = \frac{dead\ cells}{(viable\ cells + dead\ cells)} \times 100 \qquad \textbf{Eq. 4.2}$$

It is important to note that Trypan Blue exclusion assay does not interact with SWNTs.[17]

Live/Dead Cytotoxity assay: The Live⁄Dead Cytotoxicity Kit for mammalian cells (Invitrogen, Molecular probes, Oregon, USA) was used. The kit is formed by two

components: Calcein AM and ethidium homodimer-1 (EthD-1). SWNTs do not interact with the Live/Dead cytotoxicity assay.[17]

For 3D cells aggregates *in situ* in the USWT, 2 µL of EthD-1 (2mM) and 200 µL Calcein AM (20 µM) were added to 800 µL of non-activated THP-1 cells (10^6 cells/mL). After incubation at 37 °C/5% CO_2 for 30 min, 3D cell aggregate formation and perfusion of SWNTs proceeded as described above. 3D aggregates were examined at low magnification (5×) at 1, 3, 7 and 24 h. Quantification of live/death cells within each 3D cell aggregate was carried out using Image Pro7 software (Media Cybernetics Inc., USA) by applying advanced image filtering, object recognition and counting algorithms on the collected fluorescent images.

For 3D aggregates in culture, aggregates were collected from the wells, centrifuged, and re-suspended in 800 µL RPMI 1640 cell media. 2 µL of EthD-1 (2mM) and 200 µL Calcein AM (20 µM) were added. After incubation at 37 °C/5% CO_2 for 30 min, cells were washed by multiple steps of centrifugation and the percentages of live/dead cells was quantified by flow cytometry (Facs Canto™ II, BD, USA).

Confocal Microscopy of 3D aggregates in culture: 3D cell aggregates (PMA-activated) were formed in the USWT as described before, subsequently recovered and deposited in a 8-well glass-borosilicate chamber slide and incubated for 24 h at 37 °C with or without p-/o-SWNTs. After 1 day in culture, 300 µL of staining solution (EthD-1 2mM, Calcein AM 20 µM) was added to each well. After incubation in the dark for 45 min, aggregates were washed with sterile PBS. Specimens were immediately analyzed with a ZEISS 510 Meta confocal microscope (Carl Zeiss, Axiovert, Germany) equipped with Zeiss LSM Image Browser. Two channel qualitative confocal imaging was carried out by acquiring a series of Z-stack images.

3.6. *Cytokines Secretion of 2D and 3D Cell Models*

The concentrations of natural human Interleukin-6 (IL-6) and human Tumour Necrosis Factor-alpha (TNF-α) secreted by the exposed THP-1 cells were measured by ELISA assays (DuoSet ELISA Development kit, R&D Systems: human TNF-α/TNFSF1A; human IL-6) and compared to the relevant controls. The assays were repeated in duplicate. The optical density of each well at 450 nm was determined by means of a Epoch microplate reader (Biotek, USA), calibrated against standards, and corrected by subtracting the optical aberration of the 96-well plastic plate. The cell count for 2D and

3D cell cultures was carried out by HCSA and Trypan Blue exclusion assay respectively, in order to quantify the cytokine production as picograms per cell (pg/cell) or pictograms per mL (pg/mL) at the different concentrations and timepoints.

3.7. *STATISTICAL ANALYSIS*

A two-way analysis of variance (ANOVA) followed by a Bonferroni post-test analysis were carried out for all HCSA and cytokine assays (Prism; Graph-Pad Software Inc., USA). $p < 0.05$ was considered statistically significant and was denoted with (*) in the graphs. *p* values are reported in Chapter VI (Section 4). HCSA and ELISA data, as well as the results obtained by Trypan Blue exclusion and Live/Dead assays, are presented as mean values ($n_{test}=2$) ± standard error of the mean and normalized to the negative control. Due to the large amount of information acquired by HCSA, a data mining and exploration platform was used (KNIME (http://KNIME.org, 2.0.3) in combination with a screening module HiTS (http://code.google.com/p/hits, 0.3.0) in order to screen and normalise all parameters under investigation as previously reported.[12] All measured parameters were normalised using the percentages of the positive control. Z score was used for scoring the normalised values. These scores were summarised using the mean function as Z score = (x-mean)/StDev, as previously reported.[18] Heatmaps (*i.e.*, graphical illustration in a colorimetric gradient table format) were adopted as the most suitable schematic representation to report on any statistical significance and variation from normalised controls based on their Z score value. Heatmap tables illustrate the range of variation of each quantified parameter from the minimum (green), through the mean (yellow), to the maximum (red) value.

4. REFERENCES

(1) Movia, D.; Del Canto, E.; Giordani, S. *J. Phys. Chem. C* **2010**, *114*, 18407.

(2) Movia, D.; Del Canto, E.; Giordani, S. *Phys Status Solidi B* **2009**, *246*, 2704.

(3) Bachilo, S. M.; Strano, M. S.; Kittrell, C.; Hauge, R. H.; Smalley, R. E.; Weisman, R. B. *Science* **2002**, *298*, 2361.

(4) Weisman, R. B.; Bachilo, S. M. *Nano Lett.* **2003**, *3*, 1235.

(5) Abraham, V. C.; Taylor, D. L.; Haskins, J. R. *Trends Biotechnol.* **2004**, *22*, 15.

(6) Movia, D.; Prina-Mello, A.; Volkov, Y.; Giordani, S. *Chem. Res. Toxicol.* **2010**, *23*, 1459.

(7) Jan, E.; Byrne, S. J.; Cuddihy, M.; Davies, A. M.; Volkov, Y.; Gun'ko, Y. K.; Kotov, N. A. *ACS Nano* **2008**, *2*, 928.

(8) Majno, G.; Joris, I. *Am J Pathol* **1995**, *146*, 3.

(9) Mingeotleclercq, M. P.; Brasseur, R.; Schanck, A. *J Toxicol Env Health* **1995**, *44*, 263.

(10) Reasor, M. J. *Toxicol Appl Pharm* **1989**, *97*, 47.

(11) Byrne, F.; Prina-Mello, A.; Whelan, A.; Mohamed, B. M.; Davies, A.; Gun'ko, Y. K.; Coey, J. M. D.; Volkov, Y. *J. Magn. Magn. Mater.* **2009**, *321*, 1341.

(12) Lu, F. S.; Gu, L. R.; Meziani, M. J.; Wang, X.; Luo, P. G.; Veca, L. M.; Cao, L.; Sun, Y. P. *Adv. Mater.* **2009**, *21*, 139.

(13) Bazou, D.; Foster, G. A.; Ralphs, J. R.; Coakley, W. T. *Mol. Membr. Biol.* **2005**, *22*, 229.

(14) Bazou, D.; Kuznetsova, L. A.; Coakley, W. T. *Ultrasound in Medicine and Biology* **2005**, *31*, 423.

(15) Coakley, W. T.; Bazou, D.; Morgan, J.; Foster, G. A.; Archer, C. W.; Powell, K.; Borthwick, K. A. J.; Twomey, C.; Bishop, J. *Colloids Surf., B* **2004**, *34*, 221.

(16) *The Project on Emerging Nanotechnologies*, http://www.nanotechproject.org/.

(17) Monteiro-Riviere, N. A.; Inman, A. O.; Zhang, L. W. *Toxicol. Appl. Pharmacol.* **2009**, *234*, 222.

(18) Birmingham, A.; Selfors, L. M.; Forster, T.; Wrobel, D.; Kennedy, C. J.; Shanks, E.; Santoyo-Lopez, J.; Dunican, D. J.; Long, A.; Kelleher, D.; Smith, Q.; Beijersbergen, R. L.; Ghazal, P.; Shamu, C. E. *Nat Methods* **2009**, *6*, 569.

CHAPTER V.
CONCLUSIONS AND FUTURE WORK

CONTENTS

1. CONCLUSIONS

This study shows for the first time that covalently modified SWNTs (p- and o-SWNTs) emit efficiently in the near-infrared region, despite the introduction of defects on their surface. The possible employment of p- and o-SWNTs as NIR fluorescent imaging probes was validated *in vitro* by FLIM analysis, thus proving the potential employment of SWNTs bioimaging agents that, thanks to the chemical treatments, have biological advantages in terms of biocompatibility and "ease of use" as compared to conventional, non-covalently modified SWNTs. In particular, the main advantages of the covalently modified SWNTs-based NIR fluorescent probes are (1) the controlled removal of the synthetic by-products[1-5] (namely, residual catalyst particles and amorphous carbon) that are cytotoxic at high concentrations[6,7] and (2) a more controlled chemistry on the nanotubes surface,[8] *i.e.* control over the number of functional molecules that may be attached for targeting and the well-defined stability of the linker that connects them to the nanotube (the risk of macromolecule desorption or exchange with components of biological fluids is avoided). Upon definition of a novel toxicology testing protocol, based on robotised testing platforms (HCSA), *in silico* methods (heatmaps) and for the first time on 3D tissue-mimetic cell models, the toxicological impact related to the use of such structures as NIR-fluorescent probes was tested, demonstrating conclusively the potential use of less-toxic, purified and covalently-functionalised SWNTs as NIR photoluminescence agents for molecular imaging. Additionally, this study clearly underlines the importance of incorporating 3D tissue-mimetic cell models in the assessment of SWNTs toxicity and strongly advocates the pressing need for the redefinition of the established nanotoxicology protocols.

2. FUTURE WORK

Future studies will employ covalently functionalised SWNTs-based imaging probes in *in vitro* and *in vivo* systems for real-time NIR bioimaging, while further experiments will further explore the use of 3D tissue-mimetic cell models as a novel, cost-effective technique to evaluate the toxicity of nanomaterials, bridging the gap between *in vitro* and *in vivo* studies.

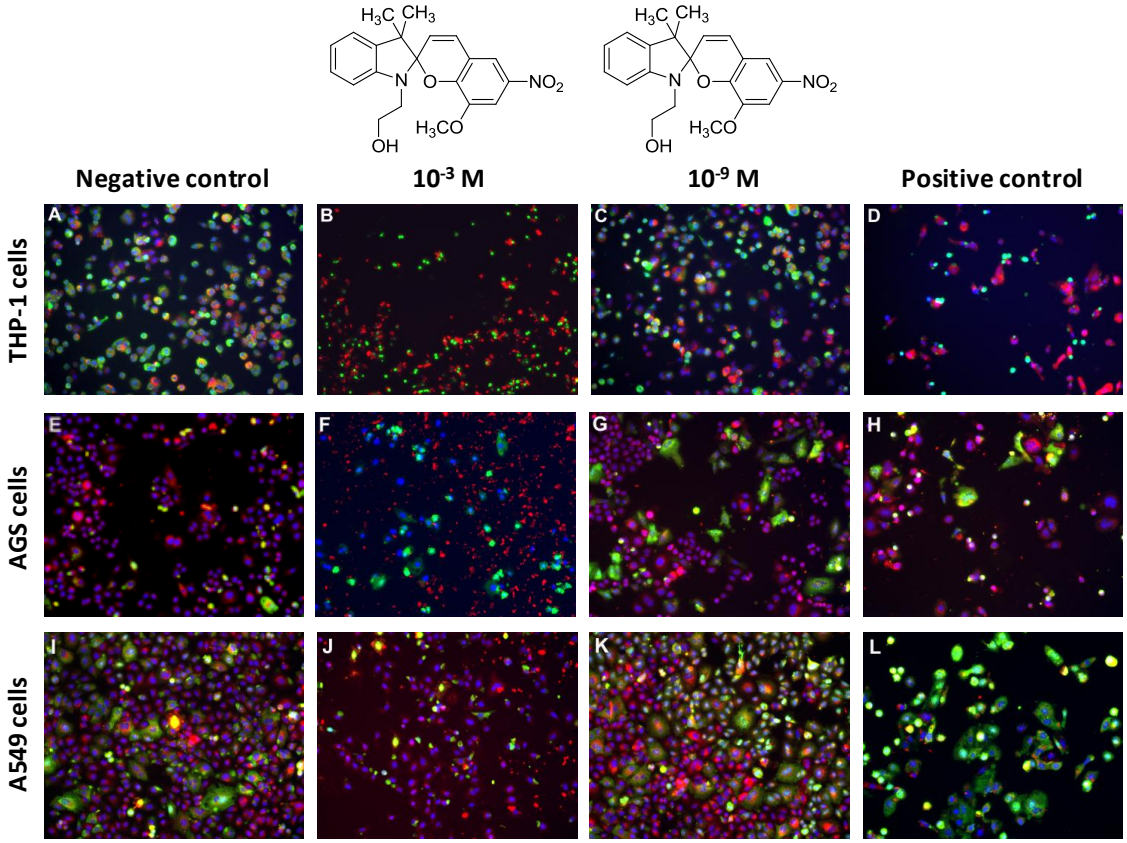

Figure 5.1. HCSA qualitative results for (a-d) macrophages, (e-h) gastric cells and (i-l) epithelial cells exposed to 8-methoxy-6-nitro-BIPS for 24 h. The composite images show the cells stained for: (i) nuclei (in blue); (ii) cell membrane (in green); and (iii) lysosomes (in red). The results for two representative concentrations (10^{-3} M and 10^{-9} M) are reported. (b, f, g) Significant image fields showing decreased cell viability and increased cell membrane permeability at 10^{-3} M. (c, g, k) The cell viability results comparable to the negative controls at 10^{-9} M. Image size: 0.897mm × 0.671 mm (10× objective).

Additionally, the potential development of light-responsive SWNTs-based Vis imaging probes will be considered. Our group has recently reported novel smart multifunctional nanodevices formed by SWNTs covalently functionalised with spiropyrans,[9] while a label-free colorimetric assay for detecting lysozyme was developed by functionalizing MWNTs with spiropyrans.[10] Spiropyrans are molecular switches that can be reversibly converted between two or more stable states in response to stimuli.[11] They may exist in three different forms: the colourless closed or spiro form (SP), the highly conjugated coloured open form referred to as merocyanine (ME) and the protonated open form (MEH). Switching among these three states is possible upon irradiation with UV and Vis light (photochromism) and by addition of an acid or a

base.[12-14] As a result of their ability to alter their structural conformation in response to various photochemical stimuli, researchers have investigated these compounds for various applications, such as imaging in living cells by optical lock-in detection (OLID) approach[15,16] and stimulated emission depletion (STED) microscopy.[17] Recently, these molecules have been integrated in nanometre-sized molecular machines,[18,19] showing that such compounds have also considerable potential for biological applications as light-controlled nanosensors and drug delivery nanosystems.[20] Our group has shown that spiropyrans preserve their photochromism when the molecule is anchored to the nanotube scaffold,[9] while our cytotoxic results clearly show that strong toxic effects on macrophages (THP-1 cells), gastric (AGS) and epithelial (A549) cells are unlikely as a result of continuous exposure to the spiropyran at micromolar concentrations (Figure 5.1) over a 72 h exposure period.[21] These results demonstrate that spiropyrans have considerable promise as integral and active components in biologically relevant nanosensors or nano-sized Vis imaging probes. Future studies will examine the relevance of spiropyran-SWNTs conjugates as Vis imaging probes and their potential toxic impact on human health.

3. REFERENCES

(1) Haddon, R. C. *Science* **1993**, *261*, 1545.

(2) Tohji, K.; Goto, T.; Takahashi, H.; Shinoda, Y.; Shimizu, N.; Jeyadevan, B.; Matsuoka, I.; Saito, Y.; Kasuya, A.; Ohsuna, T.; Hiraga, H.; Nishina, Y. *Nature* **1996**, *383*, 679.

(3) Dillon, A. C.; Gennett, T.; Jones, K. M.; Alleman, J. L.; Parilla, P. A.; Heben, M. J. *Adv. Mater.* **1999**, *11*, 1354.

(4) Giordani, S.; Colomer, J. F.; Cattaruzza, F.; Alfonsi, J.; Meneghetti, M.; Prato, M.; Bonifazi, D. *Carbon* **2009**, *47*, 578.

(5) Hu, H.; Zhao, B.; Itkis, M. E.; Haddon, R. C. *J. Phys. Chem. B* **2003**, *107*, 13838.

(6) Donaldson, K.; Brown, D. M.; Mitchell, C.; Dineva, M.; Beswick, P. H.; Gilmour, P.; MacNee, W. *Environ. Health Perspect.* **1997**, *105*, 1285.

(7) Gilmour, P. S.; Brown, D. M.; Beswick, P. H.; MacNee, W.; Rahman, I.; Donaldson, K. *Environ. Health Perspect.* **1997**, *105*, 1313.

(8) Prato, M. *Nature* **2010**, *465*, 172.

(9) Del Canto, E.; Flavin, K.; Natali, M.; Perova, T.; Giordani, S. *Carbon* **2010**, *48*, 2815.

(10) Song, Y.; Xu, C.; Wei, W.; Ren, J.; Qu, X. *Chem. Commun.* **2011**, *47*, 9083.

(11) Reitz, A. W.; Kalafawy, T. *Experientia* **1953**, *9*, 289.

(12) Raymo, F. M.; Giordani, S. *J. Am. Chem. Soc.* **2001**, *123*, 4651.

(13) Raymo, F. M.; Giordani, S.; White, A. J. P.; Williams, D. J. *J. Org. Chem.* **2003**, *68*, 4158.

(14) Giordani, S.; Raymo, F. M. *Org. Lett.* **2003**, *5*, 3559.

(15) Marriott, G.; Mao, S.; Sakata, T.; Ran, J.; Jackson, D. K.; Petchprayoon, C.; Gomez, T. J.; Warp, E.; Tulyathan, O.; Aaron, H. L.; Isacoff, E. Y.; Yan, Y. L. *PNAS* **2008**, *105*, 17789.

(16) Mao, S.; Benninger, R. K. P.; Yan, Y. L.; Petchprayoon, C.; Jackson, D.; Easley, C. J.; Piston, D. W.; Marriott, G. *Biophys. J.* **2008**, *94*, 4515.

(17) Seefeldt, B.; Kasper, R.; Beining, M.; Mattay, J.; Arden-Jacob, J.; Kemnitzer, N.; Drexhage, K. H.; Heilemann, M.; Sauer, M. *Photochem. Photobiol. Sci.* **2010**, *9*, 213.

(18) Astier, Y.; Bayley, H.; Howorka, S. *Curr. Opin. Chem. Biol.* **2005**, *9*, 576.

(19) Kocer, A.; Walko, M.; Meijberg, W.; Feringa, B. L. *Science* **2005**, *309*, 755.

(20) Yoshida, M.; Lahann, J. *ACS Nano* **2008**, *2*, 1101.

(21) Movia, D.; Prina-Mello, A.; Volkov, Y.; Giordani, S. *Chem. Res. Toxicol.* **2010**, *23*, 1459.

CHAPTER VI.

APPENDIX

CONTENTS

1. SUPPLEMENTAL INFORMATION OF CHAPTER III

1.1. HIGH CONTENT SCREENING AND ANALYSIS (HCSA) DATA

In the following the HCSA data presented in Chapter III in the form of heatmap are plotted in line-symbol graphs as average value ± standard error of the mean. The data are normalised on the negative control at t = 0 h. The symbol (*) indicates significant changes ($p < 0.05$) in the cell parameter investigated as compared to the negative control.

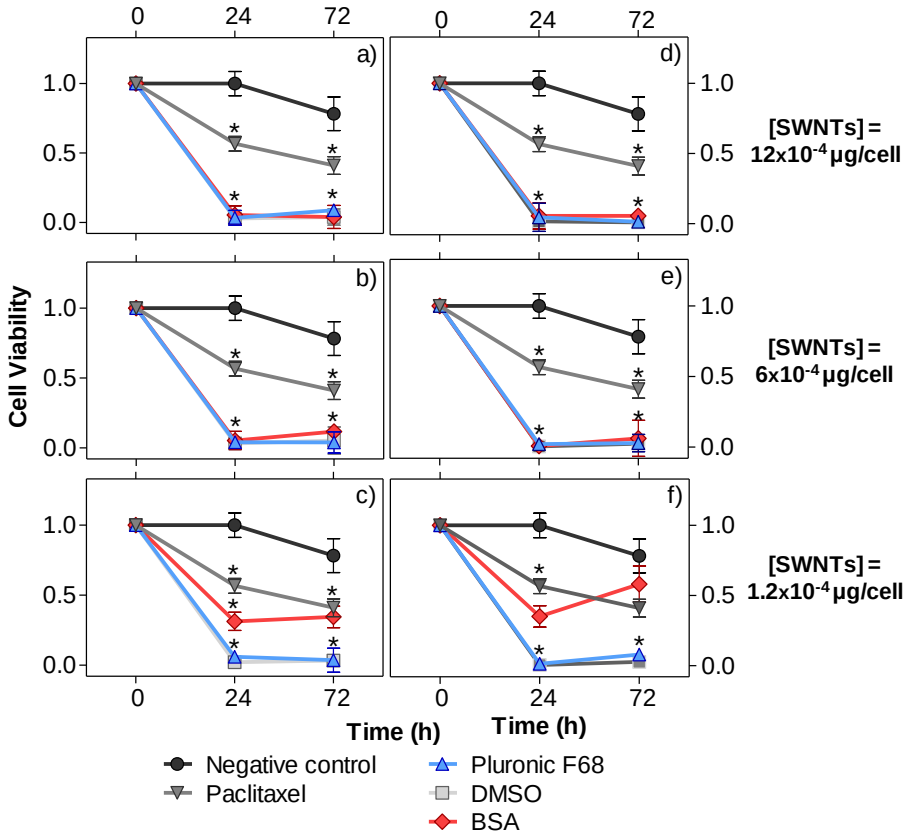

Figure 6.1. Changes in the THP-1 cells viability after exposure to (a, b, c) p-SWNTs and (d, e, f) o-SWNTs for 24 and 72 h in 2D cell cultures. THP-1 cells were exposed to SWNTs at concentration of (a, d) 12×10^{-4} µg/cell, (b, e) 6×10^{-4} µg/cell, (c, f) 1.2×10^{-4} µg/cell. DMSO-stabilised (grey), BSA-stabilised (red), and Pluronic F68-stabilised (light blue) dispersions were tested for each concentration.

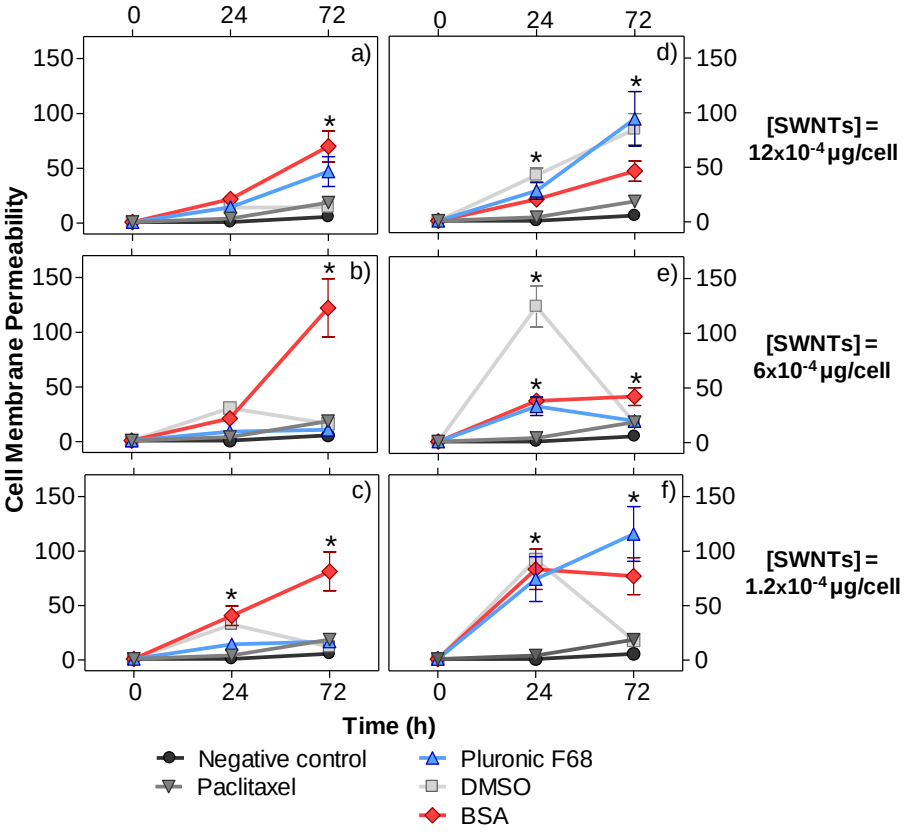

Figure 6.2. Changes in the cell membrane permeability of THP-1 cells exposed to (a, b, c) p- and (d, e, f) o-SWNTs for 24 and 72 h in 2D cell cultures. THP-1 cells were exposed to SWNTs at concentration of (a, d) 12×10^{-4} µg/cell, (b, e) 6×10^{-4} µg/cell, (c, f) 1.2×10^{-4} µg/cell. DMSO-stabilised (grey), BSA-stabilised (red), and Pluronic F68-stabilised (light blue) dispersions were tested for each concentration.

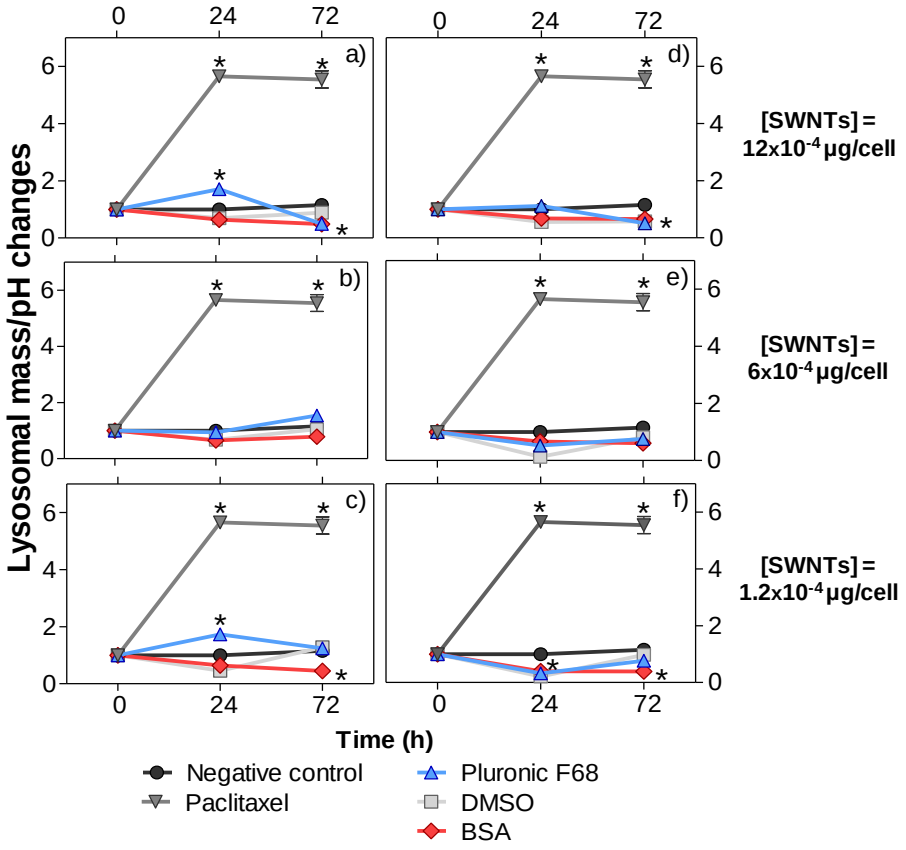

Figure 6.3. Lysosomal mass/pH changes in THP-1 cells exposed to (a, b, c) p- and (d, e, f) o-SWNTs for 24 and 72 h in 2D cell cultures. THP-1 cells were exposed to SWNTs at concentration of (a, d) 12×10^{-4} µg/cell, (b, e) 6×10^{-4} µg/cell, (c, f) 1.2×10^{-4} µg/cell. DMSO-stabilised (grey), BSA-stabilised (red), and Pluronic F68-stabilised (light blue) dispersions were tested for each concentration.

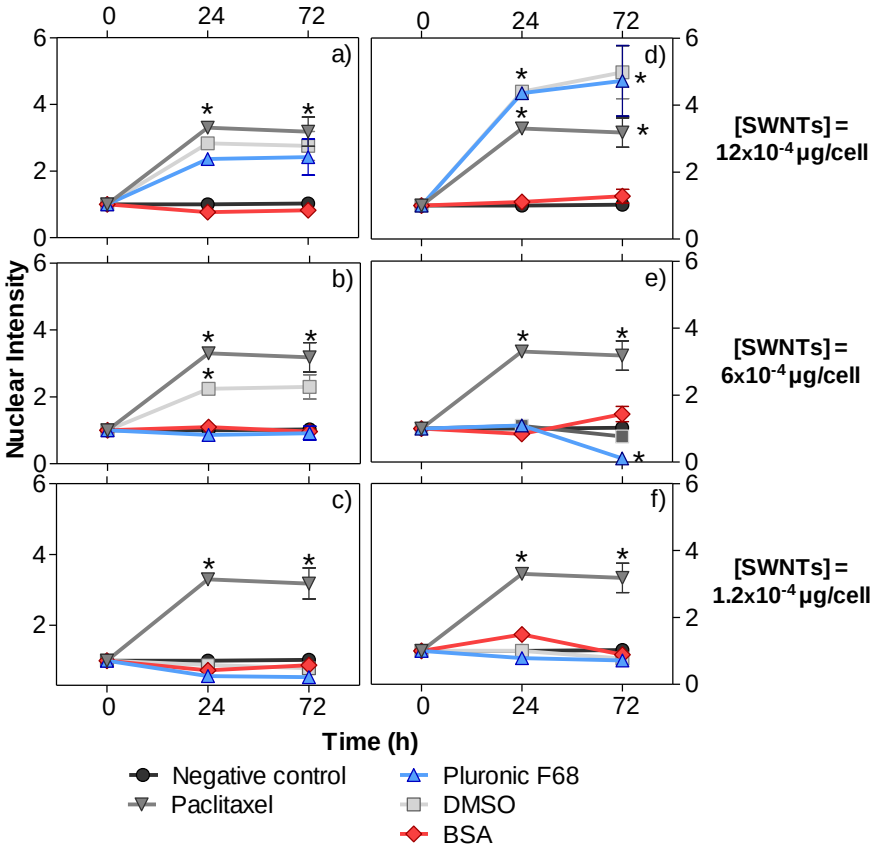

Figure 6.4. Nuclear intensity changes in THP-1 cells exposed to (a, b, c) p- and (d, e, f) o-SWNTs for 24 and 72 h in 2D cell cultures. THP-1 cells were exposed to SWNTs at concentration of (a, d) 12×10^{-4} µg/cell, (b, e) 6×10^{-4} µg/cell, (c, f) 1.2×10^{-4} µg/cell. DMSO-stabilised (grey), BSA-stabilised (red), and Pluronic F68-stabilised (light blue) dispersions were tested for each concentration.

1.2. STATISTICAL ANALYSIS – p VALUES

In the following the statistical significance (*p* values) of changes in cellular parameters (detected by HCSA in 2D cell cultures, and by Trypan Blue exclusion assay and Live/Dead Cytotoxity assay in 3D cell cultures) and cytokines secretion levels (measured by ELISA assay) in 2D and 3D cell models exposed to p- and o-SWNTs are presented.

Table 6.1. Statistical significance of the cell viability changes in 2D cell models exposed to (a) p- and (b) o-SWNTs for 24 and 72 h (ANOVA test; *ns*: $p > 0.05$).

a)

p-SWNTs	Concentration (µg/cell)	Time point (h)	*p* values
DMSO	12×10^{-4}	24 / 72	$p < 0.001$
	6×10^{-4}	24 / 72	$p < 0.001$
	1.2×10^{-4}	24 / 72	$p < 0.001$
BSA	12×10^{-4}	24 / 72	$p < 0.001$
	6×10^{-4}	72 / 72	$p < 0.001$
	1.2×10^{-4}	24	$p < 0.001$
	1.2×10^{-4}	72	$p < 0.01$
Pluronic F68	12×10^{-4}	24 / 72	$p < 0.001$
	6×10^{-4}	24 / 72	$p < 0.001$
	1.2×10^{-4}	24 / 72	$p < 0.001$

b)

o-SWNTs	Concentration (µg/cell)	Time point (h)	*p* values
DMSO	12×10^{-4}	24 / 72	$p < 0.001$
	6×10^{-4}	24 / 72	$p < 0.001$
	1.2×10^{-4}	24 / 72	$p < 0.001$
BSA	12×10^{-4}	24 / 72	$p < 0.001$
	6×10^{-4}	24 / 72	$p < 0.001$
	1.2×10^{-4}	24	$p < 0.01$
	1.2×10^{-4}	72	*ns*
Pluronic F68	12×10^{-4}	24 / 72	$p < 0.001$
	6×10^{-4}	24 / 72	$p < 0.001$
	1.2×10^{-4}	24 / 72	$p < 0.01$

Table 6.2. Statistical significance of the cell membrane permeability changes in 2D cell models exposed to (a) p- and (b) o-SWNTs for 24 and 72 h (ANOVA test; *ns*: $p > 0.05$).

a)

p-SWNTs	Concentration (µg/cell)	Time point (h)	*p* values
DMSO	12×10^{-4}	24 / 72	*ns*
	6×10^{-4}	24 / 72	*ns*
	1.2×10^{-4}	24	$p < 0.05$
	1.2×10^{-4}	72	*ns*
BSA	12×10^{-4}	24	*ns*
	12×10^{-4}	72	$p < 0.001$
	6×10^{-4}	24	*ns*
	6×10^{-4}	72	$p < 0.001$
	1.2×10^{-4}	24	*ns*
	1.2×10^{-4}	72	$p < 0.001$
Pluronic F68	12×10^{-4}	24	*ns*
	12×10^{-4}	72	$p < 0.01$
	6×10^{-4}	24 / 72	*ns*
	1.2×10^{-4}	24 / 72	*ns*

b)

o-SWNTs	Concentration (µg/cell)	Time point (h)	*p* values
DMSO	12×10^{-4}	24	$p < 0.05$
	12×10^{-4}	72	$p < 0.001$
	6×10^{-4}	24	$p < 0.001$
	6×10^{-4}	72	*ns*
	1.2×10^{-4}	24 / 72	$p < 0.001$
BSA	12×10^{-4}	24	$p < 0.001$
	12×10^{-4}	72	*ns*
	6×10^{-4}	24 / 72	$p < 0.001$
	1.2×10^{-4}	24 / 72	$p < 0.01$
Pluronic F68	12×10^{-4}	24	*ns*
	12×10^{-4}	72	$p < 0.001$
	6×10^{-4}	24	$p < 0.05$
	6×10^{-4}	72	*ns*
	1.2×10^{-4}	24	$p < 0.01$
	1.2×10^{-4}	72	$p < 0.001$

Table 6.3. Statistical significance of the lysosomal mass/pH changes in 2D cell models exposed to (a) p- and (b) o-SWNTs for 24 and 72 h (ANOVA test; *ns*: $p > 0.05$).

a)

p-SWNTs	Concentration (µg/cell)	Time point (h)	*p* values
DMSO	12×10^{-4}	24 / 72	*ns*
	6×10^{-4}	24 / 72	*ns*
	1.2×10^{-4}	24 / 72	*ns*
BSA	12×10^{-4}	24	*ns*
	12×10^{-4}	72	$p < 0.05$
	6×10^{-4}	24 / 72	*ns*
	1.2×10^{-4}	24	*ns*
	1.2×10^{-4}	72	$p < 0.05$
Pluronic F68	12×10^{-4}	24 / 72	$p < 0.05$
	6×10^{-4}	24 / 72	*ns*
	1.2×10^{-4}	24	$p < 0.01$
	1.2×10^{-4}	72	*ns*

b)

o-SWNTs	Concentration (µg/cell)	Time point (h)	*p* values
DMSO	12×10^{-4}	24	*ns*
	12×10^{-4}	72	$p < 0.05$
	6×10^{-4}	24	$p < 0.01$
	6×10^{-4}	72	*ns*
	1.2×10^{-4}	24	$p < 0.01$
	1.2×10^{-4}	72	*ns*
BSA	12×10^{-4}	24	*ns*
	12×10^{-4}	72	$p < 0.05$
	6×10^{-4}	24	*ns*
	6×10^{-4}	72	$p < 0.05$
	1.2×10^{-4}	24	$p < 0.05$
	1.2×10^{-4}	72	$p < 0.01$
Pluronic F68	12×10^{-4}	24	*ns*
	12×10^{-4}	72	$p < 0.05$
	6×10^{-4}	24 / 72	*ns*
	1.2×10^{-4}	24	$p < 0.05$
	1.2×10^{-4}	72	*ns*

Table 6.4. Statistical significance of the nuclear intensity changes in 2D cell models exposed to (a) p- and (b) o-SWNTs for 24 and 72 h (ANOVA test; *ns*: $p > 0.05$).

a)

p-SWNTs	Concentration (µg/cell)	Time point (h)	*p* values
DMSO	12×10^{-4}	24 / 72	$p < 0.01$
	6×10^{-4}	24 / 72	$p < 0.01$
	1.2×10^{-4}	24 / 72	*ns*
BSA	12×10^{-4}	24 / 72	*ns*
	6×10^{-4}	24 / 72	*ns*
	1.2×10^{-4}	24 / 72	*ns*
Pluronic F68	12×10^{-4}	24 / 72	$p < 0.05$
	6×10^{-4}	24 / 72	*ns*
	1.2×10^{-4}	24 / 72	*ns*

b)

o-SWNTs	Concentration (µg/cell)	Time point (h)	*p* values
DMSO	12×10^{-4}	24 / 72	$p < 0.001$
	6×10^{-4}	24 / 72	*ns*
	1.2×10^{-4}	24 / 72	*ns*
BSA	12×10^{-4}	24 / 72	*ns*
	6×10^{-4}	24 / 72	*ns*
	1.2×10^{-4}	24 / 72	*ns*
Pluronic F68	12×10^{-4}	24	$p < 0.01$
	12×10^{-4}	72	$p < 0.001$
	6×10^{-4}	24	*ns*
	6×10^{-4}	72	$p < 0.05$
	1.2×10^{-4}	24 / 72	*ns*

Table 6.5. Statistical significance of the cell death detected by Trypan Blue exclusion assay in 3D cell aggregates exposed to (a, c) p- and (b, d) o-SWNTs for 24 h (a, b) *in situ* in the USWT and (c, d) in culture (ANOVA test; *ns*: $p > 0.05$).

a)

p-SWNTs	*p* values
DMSO	*ns*
BSA	*ns*
Pluronic F68	*ns*

c)

p-SWNTs	*p* values
DMSO	$p < 0.05$
BSA	*ns*
Pluronic F68	*ns*

b)

o-SWNTs	*p* values
DMSO	*ns*
BSA	*ns*
Pluronic F68	*ns*

d)

o-SWNTs	*p* values
DMSO	*ns*
BSA	*ns*
Pluronic F68	*ns*

Table 6.6. Statistical significance of the cell death detected by Live/Dead Cytotoxicity assay in 3D cell cultures exposed to (a, c) p- and (b, d) o-SWNTs for 24 h (a, b) *in situ* in the USWT or (c, d) in culture (ANOVA test; *ns*: $p > 0.05$).

a)

p-SWNTs	Time point (h)	*p* values
DMSO	1 – 7	*ns*
	24	$p < 0.001$
BSA	1 – 3	*ns*
	7	$p < 0.01$
	24	$p < 0.05$
Pluronic F68	1 – 3	*ns*
	7	$p < 0.05$
	24	*ns*

b)

o-SWNTs	Time point (h)	*p* values
DMSO	1 – 24	*ns*
BSA	1 – 24	*ns*
Pluronic F68	1 – 24	*ns*

c)

p-SWNTs	*p* values
DMSO	$p < 0.05$
BSA	*ns*
Pluronic F68	*ns*

d)

o-SWNTs	*p* values
DMSO	*ns*
BSA	*ns*
Pluronic F68	*ns*

Table 6.7. Statistical significance of the (a) TNF-α and (b) IL-6 expression levels detected by ELISA assay in 2D cell cultures exposed to p-SWNTs for 24 and 72 h (ANOVA test; *ns*: $p > 0.05$).

a)

p-SWNTs	Concentration (µg/cell)	Time point (h)	*p* values
DMSO	12×10^{-4}	24 / 72	*ns*
	6×10^{-4}	24	$p < 0.001$
	6×10^{-4}	72	*ns*
	1.2×10^{-4}	24	$p < 0.001$
	1.2×10^{-4}	72	*ns*
BSA	12×10^{-4}	24	*ns*
	12×10^{-4}	72	$p < 0.01$
	6×10^{-4}	24	*ns*
	6×10^{-4}	72	$p < 0.001$
	1.2×10^{-4}	24	$p < 0.01$
	1.2×10^{-4}	72	$p < 0.001$
Pluronic F68	12×10^{-4}	24 / 72	*ns*
	6×10^{-4}	24 / 72	*ns*
	1.2×10^{-4}	24 / 72	*ns*

b)

p-SWNTs	Concentration (µg/cell)	Time point (h)	*p* values
DMSO	12×10^{-4}	24	$p < 0.01$
	12×10^{-4}	72	*ns*
	6×10^{-4}	24 / 72	*ns*
	1.2×10^{-4}	24	$p < 0.01$
	1.2×10^{-4}	72	*ns*
BSA	12×10^{-4}	24 / 72	$p < 0.01$
	6×10^{-4}	72 / 72	$p < 0.05$
	1.2×10^{-4}	24	*ns*
	1.2×10^{-4}	72	$p < 0.001$
Pluronic F68	12×10^{-4}	24	$p < 0.001$
	12×10^{-4}	72	*ns*
	6×10^{-4}	24 / 72	*ns*
	1.2×10^{-4}	24 / 72	*ns*

Table 6.8. Statistical significance of the (a) TNF-α and (b) IL-6 expression levels detected by ELISA assay in 2D cell cultures exposed to o-SWNTs for 24 and 72 h (ANOVA test; *ns*: $p > 0.05$).

a)

o-SWNTs	Concentration (µg/cell)	Time point (h)	*p* values
DMSO	12×10^{-4}	24	$p < 0.001$
	12×10^{-4}	72	*ns*
	6×10^{-4}	24	$p < 0.001$
	6×10^{-4}	72	*ns*
	1.2×10^{-4}	24	$p < 0.05$
	1.2×10^{-4}	72	*ns*
BSA	12×10^{-4}	24	$p < 0.001$
	12×10^{-4}	72	$p < 0.01$
	6×10^{-4}	24	$p < 0.001$
	6×10^{-4}	72	*ns*
	1.2×10^{-4}	24	$p < 0.01$
	1.2×10^{-4}	72	*ns*
Pluronic F68	12×10^{-4}	24	$p < 0.001$
	12×10^{-4}	72	$p < 0.05$
	6×10^{-4}	24	*ns*
	6×10^{-4}	72	$p < 0.05$
	1.2×10^{-4}	24 / 72	*ns*

b)

o-SWNTs	Concentration (µg/cell)	Time point (h)	*p* values
DMSO	12×10^{-4}	24	$p < 0.001$
	12×10^{-4}	72	*ns*
	6×10^{-4}	24	$p < 0.001$
	6×10^{-4}	72	*ns*
	1.2×10^{-4}	24	$p < 0.05$
	1.2×10^{-4}	72	*ns*
BSA	12×10^{-4}	24	$p < 0.001$
	12×10^{-4}	72	*ns*
	6×10^{-4}	24	$p < 0.01$
	6×10^{-4}	24	*ns*
	1.2×10^{-4}	24 / 72	*ns*
Pluronic F68	12×10^{-4}	24	$p < 0.001$
	12×10^{-4}	72	$p < 0.01$
	6×10^{-4}	24 / 72	$p < 0.001$
	6×10^{-4}	24 / 72	$p < 0.01$
	1.2×10^{-4}	24	$p < 0.001$
	1.2×10^{-4}	72	*ns*

Table 6.9. Statistical significance of the (a, b) TNF-α and (c, d) IL-6 expression levels in 3D cell cultures exposed to (a, c) p- and (b, d) o-SWNTs *in situ* in the USWT (ANOVA test; *ns*: $p > 0.05$).

a)

p-SWNTs	*p* values
DMSO	*ns*
BSA	*ns*
Pluronic F68	*ns*

c)

p-SWNTs	*p* values
DMSO	*ns*
BSA	*ns*
Pluronic F68	*ns*

b)

o-SWNTs	*p* values
DMSO	*ns*
BSA	*ns*
Pluronic F68	*ns*

d)

o-SWNTs	*p* values
DMSO	*ns*
BSA	*ns*
Pluronic F68	*ns*

Table 6.10. Statistical significance of the (a, b) TNF-α and (c, d) IL-6 expression levels in 3D cell aggregates exposed to (a, c) p- and (b, d) o-SWNTs in culture (ANOVA test; *ns*: $p > 0.05$).

a)

p-SWNTs	*p* values
DMSO	*ns*
BSA	*ns*
Pluronic F68	*ns*

c)

p-SWNTs	*p* values
DMSO	*ns*
BSA	*ns*
Pluronic F68	*ns*

b)

o-SWNTs	*p* values
DMSO	*ns*
BSA	*ns*
Pluronic F68	*ns*

d)

o-SWNTs	*p* values
DMSO	*ns*
BSA	*ns*
Pluronic F68	*ns*